MATHEMATICAL MODELING OF FOETAL ARTERIAL BLOOD FLOW

by

LANCE JONATHAN MYERS

MATHEMATICAL MODELLING OF FOETAL ARTERIAL BLOOD FLOW

by

LANCE JONATHAN MYERS

(BSc (Elec Eng), MSc (Elec Eng)

Thesis submitted for the degree of

DOCTOR OF PHILOSOPHY

UNIVERSITY OF CAPE TOWN

SOUTH AFRICA

August 2001

DECLARATION

I, Lance Jonathan Myers, hereby declare that the work presented in this thesis is my original work except where acknowledgements indicate otherwise. Neither the whole work, nor any part thereof, is being submitted for another degree in this or any other university.

Signed by candidate

Signed : - L.J. Myers

23/11/2001

Date

Abstract

The aim of this thesis was to develop an accurate and comprehensive computer model of the foetal circulatory system and to use this model to investigate influences of various haemodynamic variables on common Doppler blood flow velocity waveform indices.

The foetal model consists of a number of vascular compartments, cascaded together using electrical transmission line analogies. The model operates in the frequency domain and is driven by the heart which is modeled as a pulsatile flow source. Each compartment consists of fundamental arterial building blocks that are solutions to the two-dimensional Navier-Stokes equations for both oscillatory flow and steady, laminar viscous fluid flow in orthotropic viscoelastic tubes with thick walls. Three separate fundamental models obtained from the literature were compared to determine the most appropriate model for foetal physiological and anatomical parameters. These models were developed by Dinnar, Atabek and Womersley respectively. This comparison demonstrated that anisotropy may be neglected and that each model produces similar results, with Dinnar's being the most accurate.

Geometric and elastic taper are present in foetal arteries and an exact solution to account for the effects of this taper was formulated. This solution is expressed in terms of input impedances or reflection coefficients along an artery and allows flow velocity waveforms at any point along a tapered artery to be constructed. Previous solutions to this problem do not simultaneously account for both geometric and elastic taper, nor do they express the flow velocities at any point along the artery and are often time consuming numerical approaches. Thus, this theoretical solution represents a significant step forward in the modeling of flow waveforms along tapered arterial segments. The results of the theoretical model compare favourably well with those of cascaded transmission line solutions. These two methods produce identical results in the foetal descending aorta, provided that a minimum of 60 cascaded segments are utilised.

The umbilical arteries are coiled around the umbilical vein and adverse foetal outcome is associated with hyper or hypo-coiling of the umbilical arteries. In order to assess the effects of umbilical coiling on Doppler flow velocity waveforms, it was necessary to develop a theoretical model that includes the effects of coiling on arterial flow. A solution to the non-linear Navier-Stokes equations for flow in a torroidal co-ordinate system was presented in a form that may easily be incorporated into existing transmission line based flow models. The solution indicated that the effects of curvature on the steady flow component dominate over those due to the unsteady harmonics. Curvature exerts an increasing effect on the Doppler indices as the foetus ages, with the greatest increase due to curvature of around 8.4% in the umbilical arteries.

In order to effectively investigate placental pathology and to simulate foetal compromise, the peripheral vasculature required a level of detail not considered in earlier models. In this thesis,

these vascular beds were assumed to be networks of dichotomously branching compliant vessels, with self-similar properties of individual vessel elements. A fractal model was developed which allowed the morphology of the vascular trees to be specified by a reduced set of parameters. This model generates more accurate input impedance spectra than lumped models and links network input resistance, input impedance and morphology together. Thus the effects of peripheral vaso-constriction or dilation and irregular growth may be modeled accurately. The peripheral model was adapted to include the effects of tapering of the individual vessels comprising the arterial network. A comparison of the tapered network model with that of a non-tapered model indicated that the tapered model was significantly more accurate in predicting Doppler indices that agreed with those reported in the literature.

The model was adapted to be valid for all gestational ages between 28 weeks and term. Irregular growth rates of different foetal organs were considered and included into the growth model. The growth model demonstrated that the Doppler indices decreased with increasing growth and that the difference between indices obtained at either end of the umbilcial arteries decreased with increasing growth. This was shown to be due to increasing arterial dimensions and decreasing peripheral resistances.

Model simulations demonstrated that the most important determinants of the Doppler indices are placental resistance or impedance, umbilical arterial radius and length and the heart rate. The indices were shown to be relatively insensitive to alterations in pressure, cardiac output, blood viscosity, acute blood flow redistribution, umbilical coiling and umbilical and placental arterial wall properties.

Elevated placental impedance was simulated in a variety of ways. The model demonstrated that so long as an overall reduction in the placental vessel radii are present, the level at which this occurs is unimportant. The net effect of this is an increased placental input resistance and impedance, which increases the reflected waveform at the umbilico-placental interface and thus the Doppler indices measured upstream of the placenta.

The effects of changes to umbilical arterial radius are influenced by associated changes to mean arterial pressure, cardiac output, heart rate and blood flow redistribution. However, provided these cardiovascular parameters do not significantly vary from reference mean values, the net effect of a decreasing umbilical radius is to decrease the umbilical Doppler indices.

Statistical variations in umbilical arterial radius and length and heart rate are possible and the results of the model suggest that these may be responsible for normal Doppler indices being present in the face of elevated placental impedances. Therefore, it is indicated that further clinical trials should be conducted so that corrections for these variations may be applied and the Doppler indices standardised for these parameters. Alternatively, the model may be configured for use in clinical applications to provide multiple regression equations accounting for these parameters.

The model showed that the difference in indices between opposite ends of the umbilical arteries was sensitive to changes in placental impedance, umbilical radius, umbilical length and umbilical wall properties. Structural changes to the arterial wall are frequently associated with adverse foetal conditions and thus further clinical use of these differences may prove to be a reliable indicator of foetal risk.

The model simulations had a systolic notch when the umbilical radius was significantly decreased and this has also been reported in isolated clinical situations. Therefore, occurences of a systolic notch in the umbilical arterial flow velocity waveforms may be used to alert clinicians to changes in umbilical radii and potentially reduce the incidence of false Doppler findings.

This thesis presents important new theoretical contributions and extensions to standard haemodynamic modeling tools. These were combined with existing modeling tools to develop a functional model of the foetal circulatory system that was utilised to investigate determinants of common Doppler indices and flow velocity waveforms. It is hoped that both further implementations of this model and these preliminary discoveries will eventually contribute towards an increase in the number of successful pregnancies.

Acknowledgements

I am deeply indebted to many people for their kind help, friendship and support which they so readily showed me throughout my time spent working on this thesis. I wish to express my gratitude and appreciation to the following people whose roles were seminal in my commencing and completing this work :

My parents, who loyally supported me throughout the many years of my academic studies. I owe the opportunities I obtained to study so extensively to their generosity, and I am infinitely indebted to them for their love, warmth, caring, understanding and encouragement, which they at all times showed towards me. They enabled me to realize my full potential.

My aunt and uncle Maureen and Cyril Prisman, who graciously took me in and offered me a second home away from home. I wish to sincerely thank them for all the warmth, love and caring that they showed me throughout the time that I stayed with them. I appreciate their hospitality and affection deeply and without their drive and encouragement I would not be where I am today.

My aunt Glenda Myers, who has been paramount in many formative aspects of shaping and developing my intellectual capability. I wish to thank her for both her love and support and furthermore for her kind assistance in the role of the chief medical librarian of the University of the Witwatersrand.

My supervisor at the university of Cape Town - Dr Wayne Capper - who so willingly helped me with the development and preparation of this thesis. He has ungrudgingly placed his knowledge at my disposal. He has spent countless hours, and shown uncomplaining dedication in guiding me in my research. He has helped me immeasurably and has at all times been a source of encouragement to me. I am forever grateful for his expertise and insights.

To Dr John Anthony, who kindly made himself available to provide important medical advice and knowledge crucial to my understanding of the foetal cardiovascular system.

To Dr Helen Wainwright who assisted with important placental examinations and discussions fundamental to discoveries made in this thesis.

To the staff and students at the department of biomedical engineering at the University of Cape Town who have provided assistance where necessary and have frequently been a source of ideas and exchange of knowledge.

My brother Andrew, who has encouraged and supported me and provided me with countless advice and solutions to many frustrating computer-related problems. He has been both a wonderful brother and friend.

To Claire Winson, for her unique love, support and encouragement throughout most of the time spent working on this thesis. She truly is a special person and a source of inspiration.

My close friends, Assaf Mizan, Dudley Tabakin and Uwe Wilkenhoener, who helped me maintain perspective throughout trying times and who accompanied me on numerous exciting, surfing and mountain adventures fundamental for stress relief.

My many other close and special friends, Daniel, David, Michael, Naama, Max and Bronwyn and others too numerous to mention, who have been there when I needed friendship and companionship and who each in their unique way have provided moral and emotional support throughout trying times of this research.

To the National Research Fund and the Medical Research Council of South Africa for their generous financial support that made this work possible.

Glossary

Abbreviations

RI	Resistance Index
PI	Pulsatility Index
S/D	Systolic/Diastolic ratio
FVW	Flow velocity waveform
IUGR	Interuterine Growth Retardation
AEDFV	Absent End Diastolic Flow Velocity
EPH	Edema, Proteinuria, Hypertension
HIE	Hypoxic ischaemic encephalopathy
GA	Gestational Age
HAH	Head and Heart
FFT	Fast Fourier Transform
IFFT	Inverse Fast Fourier Transform
CO	Cardiac Output
HR	Heart Rate
UCI	Umbilical Coiling Index
CPI	Chronic Placental Insufficiency

Anatomical, physiological and co-ordinate variables

u	Radial velocity component
v	Tangential velocity component
w	Axial velocity component
p	Pressure
t	Time
r	Radial co-ordinate
θ	Tangential co-ordinate
z	Axial co-ordinate
ν	Kinematic Viscosity

μ	Viscosity
ρ	Density
h	Wall thickness
E	Young's modulus
σ	Poisson's ratio
ω	Angular frequency ($= 2\pi f$)
a_0	Unstressed tube radius
α	Frequency parameter $a_0 (\omega/\nu)^{1/2}$
c	Complex wave speed
m	Parameter for use with all three models (Dinnar, Atabek and Womersley)
R_s	Steady Streaming Reynolds number
ϕ_0	Visco-elastic angle

Variables for Womersely's, Atabek's and Dinnar's models

$J_x(z)$	Bessel function of order x and argument z
α_0	$\sqrt{i^3}\alpha$
M	Natural frequency of constraint for Womersley's model
E_θ	Circumferential Young's modulus
E_t	Longitudinal Young's modulus
c_0	Moens Koertweg wave velocity
σ_θ	Circumferential Poisson's ratio
σ_t	Longitudinal Poisson's ratio
γ_1	Ratio of Longitudinal to circumferential Young's moduli
γ_2	Ratio of Longitudinal to circumferential Poisson's ratios
T_{t_0}	Initial longitudinal stress
T_{θ_0}	Initial circumferential stress
K_l	Spring coefficient of tethering model
C_l	Frictional coefficent of dashpot of tethering model
M_a	Additional mass of longitudinal tethering
g	Ratio of complex viscoelastic Young's modulus of tissue to vessel wall

Transmission line variables

Q	Volumetric flow rate
Z_L	Longitudinal impedance
Z_W	Transverse or wall impedance
Z_0	Characteristic impedance
γ	Propagation constant
P_f	Forward travelling pressure harmonic
P_r	Reverse travelling pressure harmonic
Q_f	Forward travelling flow harmonic
Q_r	Reverse travelling flow harmonic
Γ_t	Terminal reflection coefficient
Z_{in}	Input impedance
Z_t	Terminal or load impedance
L	Arterial segment length

Tapering

P_s	Total source pressure
Q_s	Total source flow
Z_s	Source characteristic impedance
γ_s	Source propagation constant
h	Characteristic impedance tapering constant
q	Propagation constant tapering constant
$I_x(z)$	Modified Bessel function of the first kind of order x and argument z
$K_x(z)$	Modified Bessel function of the second kind of order x and argument z
p	Geometric radial tapering constant

Curvature

D_n	Dean number
Re	Reynolds number
R	Radius of curvature
r'	Radial co-ordinate
θ, ψ	Orthogonal tangential co-ordinates
λ	Radius to radius of curvature ratio
Q_s	Flow in a straight tube
Q_c	Flow in a curved tube
$\mathrm{H}_x(z)$	Struve function of order x and argument z
h	Pitch
R_s	Resistance in straight tube
R_c	Resistance in curved tube

Fractal model of peripheral arterial networks

r_i	Radius of i^{th} level of branching
k	Ratio of parent vessel radius to daughter vessel radius
l_r	Ratio of length to radius
K	Power law or branching ratio
n	No. of levels of branching
R_0	Input resistance of peripheral arterial network
r_x	Final (distal) radius of a tapered peripheral vessel
θ	Branching angle
x	Ratio of final radius of taperent parent vessel to initial radius of daughter vessel

Gestational age model

M_{G_A}	Mass at a particular gestational age
M_O	Organ mass
M_F	Overall foetal mass
M_{28}	Mass at 28 weeks
r_{G_A}	Radius at a particular gestational age
r_{28}	Radius at 28 weeks
V_{a28}	Arterial volume of vascular tree at 28 weeks
V_{aG}	Arterial volume of vascular tree at particular gestational age
N_p	Number of arterial trees in parallel
m	Fractional rate at which the length to radius ratio must grow

Simulation of acute and chronic changes

ϵ	Ratio of acutely altered radius to original radius
r_{new}	New radius after actute vasconstriction or dilation
r_{old}	Original radius before vasoconstriction or dilation
δ	Reduced fraction of original number of levels of branches for chronic changes
n_{new}	Number of levels of branching due to chronic change
n_{old}	Original or reference number of levels of branching
Q_{u+p}	Flow to umbilical arteries and placenta
R_u	Resistance of umbilical arteries
R_p	Resistance of placenta
P_A	Mean arterial pressure
k	Factor by which umbilical arterial resistance is increased
y	Factor by which placental resistance is decreased
z	Factor by which mean arterial pressure is increased

Q_{VB}	Flow to a particular vascular bed
R_{VB}	Resistance of a particular vascular bed
x	Factor by which flow to vascular beds increases
Z_{0c}	Characteristic impedance in a curved artery
Z_{0s}	Characteristic impedance in a straight artery
Z_{plac}	Impedance of placenta
Z_{umb}	Impedance of umbilical arteries

Contents

Chapter 1

Introduction

The foetal circulatory system is responsible for transporting nutrients to all areas of the foetus to ensure normal development. Problems in this system can result in severe complications that compromise foetal health. Thus, understanding and careful monitoring of the foetal circulatory system are essential in order to prevent undesirable outcomes.

The foetal circulatory system exhibits important anatomical and haemodynamic differences to that of the adult, due to the foetus having to adapt to a developmental environment within the uterus. The most significant difference is that of the developing placenta, the union of foetal and maternal tissues for the purpose of physiological exchange. The placenta is the organ responsible for all foetal requirements and encompasses respiration, transport of gases and metabolites, supply of nutrients and elimination of waste products. Thus the foetus is dependent on both the mother and the integrity of the placenta for its well-being.

Placental pathology resulting in suboptimal placental function will directly affect the foetus. The foetus responds by adjusting physiological variables such as heart rate, total cardiovascular output, arterial pressure, blood flow distribution (peripheral resistances), growth rate and arterial dilation, in an attempt to minimise adverse effects. It is reasonable to expect that both impaired placental function and the foetal response will be reflected in many haemodynamic changes. These alterations in the haemodynamic status of the foetus are the key to early diagnosis and treatment of placental impairment.

The unique closed environment in which the foetus exists necessitates the usage of non-invasive investigative procedures. Modern advances in Doppler ultrasound provide an important tool for detecting and measuring moving blood, thus allowing non-invasive investigation of the foetal circulatory system. The earliest application of Doppler ultrasound to the foetal circulatory system was reported in 1977 by Fitzgerald and Drumm (1977) who conducted measurements in

the umbilical arteries. Umbilical flow investigations using Doppler ultrasound appeared to be an ideal screening test due to its technical simplicity and comparatively low-cost. This prompted the need for subsequent research into the umbilical arterial blood flow velocity waveform (FVW), its changes during the course of pregnancy and its changes in response to haemodynamic variations as a result of foetal, placental or maternal pathology.

Much of the early research quantified Doppler measurements of FVW's through the introduction of simple probe angle independent indices, the most common being the Pulsatility index (PI) (Gosling and King, 1974), the Systolic-Diastolic ratio (S/D ratio) (Stuart et al. 1980) and the Resistance index (RI) (Pourcelot, 1974). However despite the widespread utility of Doppler recording of umbilical arterial flow, its place in routine clinical management remains uncertain. (Johnstone et al. 1993). Recent meta-analyses concluded that the methodical application of Doppler investigations to 'high-risk' pregnancies is of benefit to foetal outcome, whilst employment to so-called 'low-risk' pregnancies does not lead to any statistically significant improvement in the health of the women or their infants. (Goffinet et al. 1997; Alfirevic and Neilson, 1995; Johnstone et al. 1993). Furthermore, a meta-review conducted by Dornan and Beattie (1992) demonstrated that independent from the outcome measure used, the sensitivity, specificity and positive and negative predictive values of common umbilical arterial Doppler indices could be significantly improved. Currently therefore, Doppler diagnostic measures frequently fail to identify foetuses at risk of adverse neonatal outcome and may incorrectly associate healthy foetuses with those at risk.

Interpretations of Doppler measurements are usually viewed with regard to their ability to predict resistance to flow in the placental villous vascular bed and Giles et al.(1985) demonstrated that abnormal umbilical artery flow waveforms are associated with vascular sclerosis and obliteration of the small placental villous bed arteries. However, this fails to explain why some foetuses with poor Doppler indices can survive for over a month without any evidence of severe compromise, whilst others deteriorate rapidly (Kingdom et al. 1997). The foremost determinant of the FVW indices is assumed to be the downstream impedance, yet Griffin et al. (1983) demonstrated that input pressure, cardiac contractility, distance of sampling site from the heart, vessel wall compliance and wave reflections all play a role in determining the shape of the FVW. This identifies a crucial need for more in-depth and sophisticated analysis of haemodynamic data obtained by Doppler ultrasound.

The quantitative analysis of the FVW's in the clinical setting has been more reliant upon statistical correlations with outcome than on sound theoretical analyses. These difficulties with investigations in the human foetus have led to several animal studies which sought to assess the role of Doppler indices in the prediction of foetal compromise. These were frequently performed

on foetal sheep, due to their umbilical arterial waveform indices changing at approximately the same rate as those reported for human foetuses (Hasaart et al. 1993). Whilst such studies have certainly added value to clinical interpretations, their results should be interpreted with caution, due to differences that arise as a result of species characteristics and the role of anaesthetics and surgery on inhibiting cardiovascular reflex responses (Hasaart et al. 1993). Furthermore, pharmacologically induced haemodynamic alterations simultaneously influence many variables, rendering it difficult to separate out individual responses.

Therefore a mathematical model would be a useful tool to help elucidate the various haemodynamic factors that determine the FVW shape and thus the derived indices. The utility of such models are that they eliminate factors of acquisition and processing of the Doppler data, they allow control of variables which are difficult to measure and unknown parameters may be estimated by observing and correlating results with measured data. Several flow models have been proposed in the past by various authors which have contributed to the understanding of various influences of the FVW.

1.1 Modelling the FVW's

The simplest functional unit of any flow model are the equations that determine the flow in a short unterminated arterial segment subject to a driving pressure gradient. Complete circulatory system models are the result of the expansion and concatenation of these single arterial segment models and thus detail and accuracy of these basic models is of utmost importance. The mathematical description of pressure wave propagation along an artery has engaged the attention of many biomedical researchers over the last few decades and remains a problem of considerable interest.

An analysis of blood flow in an artery requires that the physical properties of blood and of the blood vessels be known. Equations describing the mechanics of the motion of the blood, as well as that of the arterial wall, necessitate a complete formulation on the basis of certain assumptions. In addition, selection of appropriate methods to solve these equations depends on the purpose of the analyses and the degree of sophistication desired and often demands further simplifying assumptions.

The purpose of a foetal circulatory system model is to determine the relationships between physical variables and the resultant FVW's. Thus to develop such a model, it is initially important to identify potential physical factors that may contribute to the determination of the FVW's, and then choose an appropriate model that would allow for investigation of each of these factors. The importance of this basic model selection should not be underestimated.

Chapter 4 deals with a careful analysis of those elements that are deemed essential for a complete investigation and upon which the choice of a model to give optimum results is based.

Common assumptions in arterial modelling regarding the fluid and flow are :

- whether the flow is laminar or turbulent,
- whether the fluid is Newtonian and,
- those which concern the nature of the fluid density.

Those assumptions governing the arterial wall consider compressibility, isotropy, visco-elasticity, wall thickness, wall loading or constraints and densities of the material. Additional geometrical or anatomical considerations are considered and pertain to non-uniform physical variables such as arterial tapering and curvature of the arterial vessels. These assumptions determine systems of equations which may be formulated into one or two-dimensional descriptions of flow and may further be categorised into linear and non-linear versions. The solutions to these equations may be numerical or exact and time or frequency domain solutions.

Following selection of the particular fluid and wall assumptions, equation formulation and solution procedures for the basic arterial unit, further consideration must be given to the construction of the overall circulatory model. The development of a mathematical model describing the foetal circulation requires further simplifying assumptions regarding the level of detail necessary to achieve the desired goals of the model. These assumptions must be carefully considered in order to obtain as accurate a model as is possible, within the constraints of computational resources. Furthermore, it is necessary to define those areas of the foetal circulatory system subject to variation across the foetal population in both health and disease as these may directly impact on the measured FVW's and therefore on the resultant clinical decisions.

These potential sources of variability and their subclassifications include :

- The foetal heart : Cardiac output, blood pressure, stroke volume, heart rate and contractibility.
- The foetal blood : Viscosity and density.
- Blood flow distribution to foetal organs : Includes redistribution as a response to distress.
- Physical dimensions of each of the arteries : Radius and length.
- Arterial wall properties : Viscoelasticity, wall thickness and anisotropy.
- Arterial tapering : Geometric and elastic tapering.

- The effects of surrounding tissue : Specifically this is important in the umbilical artery as the quantity of Wharton's Jelly is known to be variable (Bruch et al. 1997).
- The coiling of the umbilical arteries : It is known that the number of coils varies amongst the foetal population and high or low degrees of coiling are associated with adverse foetal outcome.
- The placenta : Morphological structure and vessel properties.
- The peripheral organs : Reflection properties from these terminal vascular beds require realistic modelling
- Relative changes with foetal growth.

The above quantities will vary to some degree around a mean value within a normal, healthy foetal population, as well as varying in response to foetal growth and disease. The effect of these sources of variation should be examined on flow within those arteries that are frequently the sites of clinical investigation : the thoracic and abdominal aorta and the umbilical artery. Furthermore, as a result of a gradient of Doppler indices along the umbilical artery (Forouzan et al. 1991; Vieyres et al. 1991; Abramowicz et al. 1989; Kay et al. 1989; Mehalek et al. 1989; Bruner et al. 1994), it is necessary to examine the effects of the sources of variability at positions situated along the length of the artery.

Steady state pressure and flow waveforms are composed of forward travelling waves and retrograde travelling waves. The forward traveling wave, running from the heart to the periphery, mainly contains information about the heart itself, whilst the backward traveling wave carries the information about the reflection sites and the periphery of the arterial system (Pythoud et al. 1996). It is instructive to further examine the effects of sources of variability on both forward and reverse travelling waves, and a useful model ought to be able to decompose flow waveforms into these two constitutive components. An additional, and practical, requirement for a blood flow model would be that of easy implementation and short runtime.

Such a model should therefore permit the sensitivity of the quantitative indices to each source of variation to be determined. Clinically useful indices ought to be able to discriminate between normal physiological or anatomical variation and variation as a result of pathology. Obviously, an index that can further distinguish the various types and locations of pathologies would be more preferable. The model should be useful in both determining such indices and re-evaluating existing indices in terms of these criteria. Thus far no existing foetal model is able to adequately accomplish all of these goals for each listed source of variation.

1.2 Thesis aims and contributions

The aim of this thesis was to develop an accurate model of the foetal-placental circulatory system that allows investigation in terms of the above stated criteria. This model should then be utilised to determine the sensitivities of Doppler indices to changes in various physical variables. Achievement of this goal required the development of a full foetal model that differs from existing foetal models in many respects. In particular :

- The development of useful fundamental haemodynamical modelling tools. These are equations that include non-linear effects of tapering and curvature into flow models. These models have been designed in such a manner that permits convenient implementation and incorporation into existing transmission line flow models, although they may be applied to non-transmission line formulations. In this thesis the models are applied to the foetal system, however, these equations have widespread use beyond this scenario. Their development forms a significant theoretical contribution that further extends the available set of tools used to investigate axial flow velocity variations in mammalian circulatory systems.

- The model equations are based upon solutions to the two-dimensional Navier-Stokes equations for pulsatile, laminar viscous fluid flow in an anisotropic visco-elastic tube with thick walls, constrained by surrounding tissues. This allows the model to investigate the effects of possible wall anisotropy and the effects of surrounding tissues in addition to other commonly investigated blood and arterial wall properties.

- The model implements exact solutions to the fundamental equations in the frequency domain and thus requires significantly less computational time than a complex numerical time domain iterative solution.

- The model equations are connected together using transmission line analogies which have the important feature of allowing the flow at any point in the system to be measured and decomposed into forward and retrograde components. The manner in which the heart is modelled differs from other formulations in that the heart ejects a flow rather than pressure pulse.

- The fractal method of modelling the peripheral vascular beds contains increased detail and levels of control over previous models and this facilitates investigation of detailed morphological changes within the placenta. The fraction of cardiac output distributed to the peripheral regions is derived from the literature rather than computed and thus the resistance of the vascular beds are specified. This specification dictates the subsequent morphology of the networks and thus their impedance spectra. The nature of the equations

for the vascular beds allows the vascular structure to be manipulated in an appropriate manner in response to imposed alterations of pressure, cardiac output or resistance of the vascular networks. The method of modelling these peripheral networks may be used in applications alternate to the foetal model to obtain a more accurate representation of impedance spectra than is possible by single lumped components or windkessel models.

- Foetal growth, and in particular placental growth, is considered in a unique manner. The growth model allows various foetal organs to grow at different rates and facilitates investigation of the foetal condition at any gestational age.

The model is used to assess the effects of important physiological and pathological changes on flow velocity waveforms. It must be stressed that a large variety of simulations may be performed subject to the particular nature of conducted investigations. However, in this thesis a reduced number of simulations that are regarded as informative and relevant have been selected. These results are not the principal objective of this thesis but are produced to both validate the model and to further elucidate a number of common concerns regarding the utility of Doppler measurements. They are intended to offer a glimpse into the value of the completed foetal model and not to provide a comprehensive analysis of all conceivable simulations.

1.3 Scope and structure of thesis

A brief summary of the content of each chapter in this thesis, emphasisng the new contributions and how they add to the final goal is listed below.

- Chapter 2 - **Overview of foetal physiology and pathology** : This chapter initially describes the normal anatomy and physiology of the foetal circulatory system. Foetal pathology, with particular emphasis on foetal hypoxia is subsequently discussed. A summary of experimental investigations on foetal sheep that highlights the studied effects of various forms of hypoxia and pathology is presented. An understanding of both the physiology and pathology is essential in order to develop an accurate model to simulate these scenarios.

- Chapter 3 - **Overview of the foetal model** : This chapter begins with a background section reviewing previous foetal models that have been developed. The shortcomings of a number of these models are discussed and an overview of the model to be constructed in this thesis is presented. This focuses on general design methodology and does not focus on specific detail. A model for the output flow from the foetal heart is developed.

- Chapter 4 - **Fundamental arterial model** : This chapter deals with the formulation and selection of an appropriate flow model to use as the basic building block for an arterial segment. Included in this chapter is a background and revision of arterial models and a discussion of which of these arterial models is most appropriate to account for necessary requirements and physiological values encountered in the human foetus. A transmission line analogy of the basic arterial model is developed so that arterial segments may be connected together to form the complete model. This also offers the advantage of being able to measure and decompose the FVW's at any point in the arterial tree into forward and reverse travelling waves.

- Chapter 5 - **Arterial tapering** : This chapter deals with the development of the necessary tools to include both geometric and elastic tapering of arteries. The equations are developed to be compatible with the basic arterial model and with a transmission line analogy. Both geometric and elastic tapering are known to occur in the aorta, and in addition, chapter 7 demonstrates that tapering may also occur in the peripheral arterial trees. Furthermore, the development of a set of easy to implement equations that considers the effect of tapering on flow velocities has widespread use beyond the development of a foetal model, as indicated in the chapter.

- Chapter 6 - **Umbilical arterial coiling** : This chapter deals with the background to the equations for and the development of the necessary tools to incorporate the effect of umbilical arterial coiling into the basic flow model. Once again, equations which determine the effect of arterial curvature (or coiling) on flow velocities has potential use in other modelling applications.

- Chapter 7 - **Peripheral arterial beds and placental model**: A fractal model of the peripheral arterial tree networks is developed. This model is organised so that it can easily be incorporated into the existing structure of the full foetal model. Placental pathology may subsequently be examined in terms of the placental model.

- Chapter 8 - **Gestational age dependency of the model**: This chapter shows how the full model is adapted for foetal growth between 28 weeks and term. Non-uniform growth of the foetal organs is taken into account.

- Chapter 9 - **Foetal model**: This chapter places all the building blocks developed in the previous chapters together to construct the full foetal model. Selections of normal or reference anatomical and physiological parameters are discussed. The overall simulation algorithm is described, along with a brief description of the computer coding methodology.

- Chapter 10 - **Simulation and validation for normal foetuses** : This chapter deals with the validation of the foetal model by correlating model generated indices with actual

clinical indices reported in the literature. Additional validation is performed based upon foetal growth, the shape of the FVW's and impedance measurements in foetal sheep.

- Chapter 11 - **Determinants of Doppler indices:** The validated model is now used to develop insights into the interpretations of FVW's. The procedure and mathematical equations necessary to simulate changes is developed. Simulations are conducted to assess the sensitivity of individual variables on the Doppler indices and the FVW's. Further examinations of the indices and their variation along the umbilical artery are considered, as well as the decomposition into forward and reflected waveforms. Detailed discussions of each simulations results are presented and where possible, these are correlated with clinical or experimental work previously performed.

- Chapter 12 - **Conclusions:** The important findings of this work are highlighted and presented and future recommendations are also discussed.

- Chapter 13 - **Appendices**

Chapter 2

Overview of foetal physiology and pathology

2.1 Introduction

By the eighth week of foetal development, the major organ systems are operational (Sparks and Cetin, 1992). However, flow waveforms to these organs continue to change as further foetal development takes place. Prior to 18 weeks gestational age, blood flow to the placenta is extremely pulsatile in nature, and umbilical arterial end diastolic flow is always absent (Fisk et al. 1988; Hendricks et al. 1989). As the foetus ages, the umbilical flow waveform becomes less pulsatile, and typically by 18 weeks, end diastolic flow can be measured in the normal foetus. By 28 weeks, end diastolic flow in the normal foetus is well established. However, in cases of placental insufficiency and foetal compromise, absent end diastolic flow may occur beyond 18 weeks and in these cases the prognosis is often poor and intervention may be necessary. In severe cases a caesarian section can be performed after 28 weeks in order to extricate the foetus from a suboptimal environment. Large clinical studies have identified normal ranges for the various Doppler indices, and a particular measurement that falls outside of these ranges for a particular gestational age is regarded as an early warning. Many of these trials are only conducted from 28 weeks onwards (Dornan and Beattie, 1992) and thus both further physiological discussions and the model developed in this thesis will consider only those foetuses that are post 28 weeks gestational age. However, factors other than gestational age may affect the interpretation of Doppler recordings and these require further investigation.

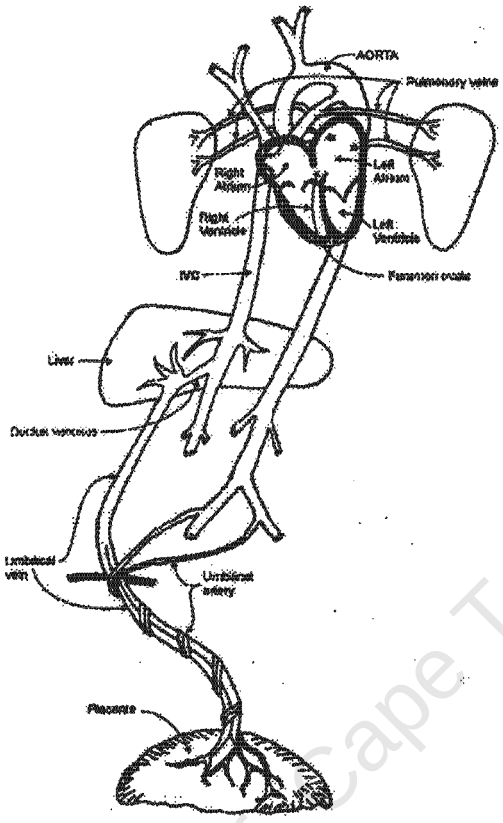

Figure 2.1: Normal circulation of the human foetus.

2.2 Foetal circulatory system anatomy and physiology

A number of unique distinctions occur between the foetal and postnatal circulatory systems and these will briefly be discussed in order that an anatomically accurate foetal cardiovascular model may be developed. During the course of gestation, the foetal lungs are largely non-functional and the liver only partially functional and thus it is unessential for blood to be pumped through either of these organs. However, as the placenta now serves as the primary site of gaseous and nutrient exchange, the foetal heart is required to pump large quantities of blood through the placenta. Several special anatomical arrangements facilitate these requirements, specifically the presence of three vascular shunts, namely the *ductus venosus*, the *foramen ovale* and the *ductus arteriosus*. Figure (2.1) depicts the circulatory system of a normal human foetus.

Oxygenated blood returns from the placenta through the umbilical vein. (See figure (2.2)). A large percentage of this blood is shunted through the ductus venosus, in order to by-pass the liver. The ductus venosus is a narrow vessel which directly connects the umbilical vein to the inferior vena cava (IVC). The blood from the IVC enters the right atrium (RA) of the foetal

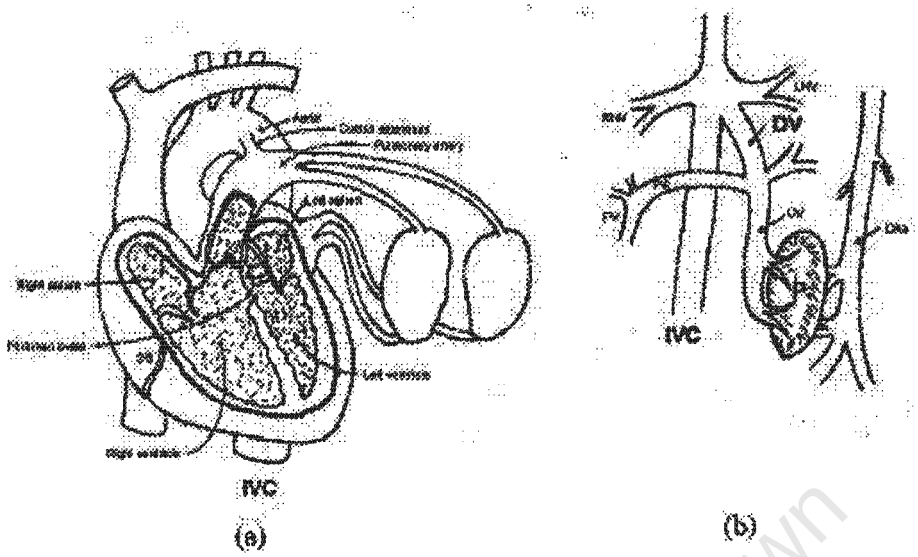

Figure 2.2: (a) Circulation in the foetal heart and cardiac vessels. (b) Circulation in the umbilical, inferior vena cava and hepatic venous drainage.

heart. A large portion of the blood entering the RA is preferentially channelled through the foramen ovale and into the left atrium (LA). The foramen ovale is a hole through the inter-atrial septum which is covered by a small flap. Approximately 45 % of the blood is shunted through this foramen (Dawes, 1968), and is distributed almost exclusively to the upper body (Rudolph, 1974). The foramen ovale therefore accentuates the difference in oxygen content between the blood distributed to the heart and brain and that distributed to the lower body. Venous blood from the upper body also drains into the right atrium via the superior vena cava (SVC). This blood is predominantly channeled to the right ventricle into the pulmonary artery, where most of it (70%) is shunted into the descending aorta via the ductus arteriosus. The anatomical structure of the vessels branching from the aorta are identical to that of the adult. The paired umbilical arteries each branch from an internal iliac artery and after passing through the foetal umbilicos, they spiral in a helical course around the umbilical vein before anastomosing with the placental vessels, where substrate transfer takes place.

2.3 Placental anatomy

The placenta is responsible for performing many functions essential for foetal survival and development and may be subject to mal-development and disease. The placenta is a temporary organ attached to the uterine wall during the course of the pregnancy. It is disk shaped and composed of blood vessels and connective tissue. The human placenta weighs about 0.5 kg at

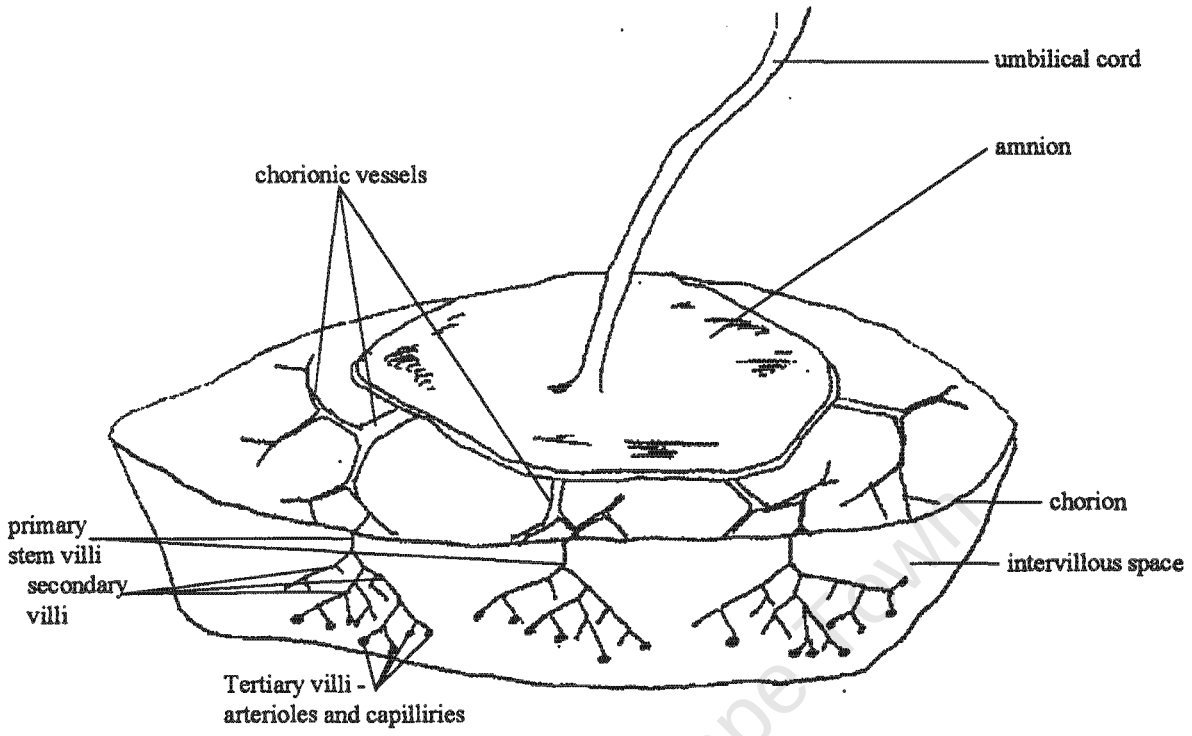

Figure 2.3: A schematic drawing of the placenta adapted from Bergman and Ullberg (1998). The placental arterial tree extends from the umbilical cord. Firstly it branches within the chorion before diving into the intervillous space to become primary stem villi. The primary stem villi further branch in a tree like manner to become secondary villous trees and finally tertiary villi. The tertiary or terminal villi represent the microvasculature of arteriole and capillary networks and are diagramatically represented as a single lumped unit, although they continue to branch as an arterial tree network.

term, and measures approximately 3cm in thickness and 20 cm in diameter (Bergman et al., 1998). It consists of both foetal and maternal compartments. The foetal portion of the placenta compromises of two membranes (the amnion and the chorion), the umbilical cord and a tree like network of blood vessels termed chorionic vessels, stem, secondary and terminal villi. See figure (2.3).

Foetal blood passes to the placenta through paired umbilical arteries which spiral around the umbilical vein. These arteries usually anastomose before inserting into the placenta. The site of insertion may vary but commonly occurs at the centre of the placenta. On reaching the placenta, the veins and the arteries initially run along the plane of the chorion. They branch during this chorionic course and a proportion of the branches perforate the chorion to dive into the placental substance. In addition a number of perforating branches are given off directly from the undersurface of the main arteries (Fox, 1978). Usually about 4 levels of branching takes place

within the chorionic surface before the placenta is entered (Bergman et al., 1998). Once the *chorionic vessels* enter the placenta, they are known as *primary stem villi* and continue to branch in a tree like manner, progressively becoming smaller in diameter, until they reach the arterioles and capillaries. It is generally estimated that there are about 200 primary villous stems arising from the chorionic plate (Wigglesworth, 1969; Hamilton, 1972). In the term foetus, the vessels between the 1000-600μm diameter range are termed *mature intermediate or secondary villi* and the vessels below the 600 μm diameter range are termed *terminal or tertiary villi* (Bernischke, 1990). The majority of gaseous exchange takes place at the level of the capillaries.

2.4 Foetal distress and pathology

The term *foetal distress* has been used to describe those situations in which oxygen delivery to the foetus is decreased (Mead, 1996). The Royal College of Obstetricians and Gynaecologists (RCOG) recommended that the term foetal distress be abandoned due to its imprecision as it is usually a description of foetal hypoxia rather than a diagnosis (RCOG 1994). *Hypoxia* is defined as a reduction of a tissue's oxygen supply to below physiological levels, despite adequate perfusion of the tissue by blood. Alternatively, the term *hypoxemia* is often used in the literature and it is defined as below normal oxygen content in arterial blood due to deficient oxygenation of the blood. Hypoxemia results in hypoxia, which eventually restricts the foetus from normal growth and development. Hypoxia may lead to a reduction in either uterine or umbilical flow, which in turn will interfere with CO_2 removal from the foetus, resulting in foetal respiratory acidemia. Foetal asphyxia is defined as the combination of hypoxia with acidosis.

Foetal hypoxia has a variety of causes which may be divided into categories of maternal, uterine, placental and foetal origin. Decreasing the oxygen content of the maternal blood will decrease oxygen delivery to the foetus. Thus, possible maternal factors are exposure to high altitude, lung disease, anemia, haemoglobin binding with carbon monoxide, hypertension, preeclampsia and decreased blood flow to the uterus from heart failure or shock. Uterine factors may be tetany or vascular disease. Placental factors are placental disease, infection, abruption or lack of development. Foetal factors could arise from complications of the umbilical cord in the case of nuchal cords or true knots or from other factors such as anemia or haemorrhage (Morin and Weiss, 1992). These conditions all result in decreased oxygen content of the venous blood returning from the placenta and a hypoxaemic foetus. If this decrease is severe enough, the foetus eventually becomes acidotic.

Hypoxia causes a number of problems, including intrauterine growth retardation (IUGR), long term neurological problems (hypoxic ischaemic encephalopathy or HIE), intrapartum hypoxia and perinatal morbidity or mortality. The foetus adapts to decreased oxygen content

with a number of circulatory regulatory mechanisms in an attempt to sustain growth and development. Following a clear and early diagnosis of hypoxia, the clinician may employ a number of interventional procedures to reduce the risk of an unfavourable pregnancy outcome. Much of the current knowledge available is derived from studies in chronically prepared foetal sheep and the following sections will briefly review this literature. This review specifically focuses on the effects of hypoxia on relevant parameters of the foetal model. These are foetal heart rate, mean foetal arterial pressure, total combined ventricular cardiac output and blood flow distribution to foetal organs, the placental and the foetal periphery.

2.4.1 Acute maternal hypoxaemia

In the ewe, maternal hypoxaemia is generally produced by having it breathe hypoxic gas mixtures in order to reduce maternal arterial PO_2. This results in a corresponding reduction of foetal arterial PO_2. Sheldon et al. (1979), Peeters et al. (1979), Cohn et al. (1974), Gunnarsson et al. (1998), Reuss and Rudolph (1980) and Block et al. (1984) all investigated relatively short term effects of up to 4 hours of maternal hypoxaemia and they tend to concur on the major points. These are that during induced mild acute foetal hypoxia, cardiac output is maintained and circulating arterial blood is redistributed to the heart, brain and adrenals at the expense of the peripheral organs, whilst umbilical and placental blood flow remains constant. Venous return is redistributed by a preferential streaming of umbilical venous blood through the ductus venosus and the foramen ovale to the upper body. Mean arterial pressure is increased and heart rate is decreased. Thus stroke volume also increases to compensate for a decreased heart rate in order to maintain a constant cardiac output (Cohn et al. 1980). During severe acute foetal hypoxia, accompanied by acidosis, a similar redistribution takes place but total cardiac output falls and umbilical and placental flow is increased.

2.4.2 Chronic maternal hypoxemia

During prolonged hypoxia, the foetal heart is required to maintain its output to sustain an adequate supply of oxygen to the tissues, whilst potentially being affected detrimentally by the hypoxia. The foetal heart has been shown to be operating near the plateau of its function curve (Gilbert 1982) and it appears to have little reserve for increasing its output. Thus it is important to find out if the observed redistribution in cardiac output with acute hypoxemia may be sustained during long term hypoxemia. Chronic maternal hypoxemia may be induced by reduction of inspired maternal oxygen for prolonged periods. Krasney et al. (1984), Alonso et al. (1989), Kamitomo et al. (1993, 1994), Kitanka et al. (1989) and Jacobs et al. (1988) experimentally investigated chronic maternal hypoxemia lasting between 4 and 105 days. There

appears to be a degree of variation amongst the results concerning chronic maternal hypoxaemia. This variation is best explained by both the severity and duration of the hypoxia. In dealing with possible growth retardation, those researchers that observed significant reductions in growth generally allowed the hypoxaemia to continue for extended periods, or at very low levels of arterial tension during late gestation. According to Kitanaka et al. (1989), hypoxaemia must be maintained longer than 20-30 days during the last trimester, or be rather severe, if it is to produce growth retardation. Studies conducted at altitude throughout the entire gestation have reported lowered newborn weights and increased mortality (Mazess 1965; McCullough et al. 1977). Thus chronic maternal hypoxaemia may loosely be divided into mild and severe categories. In the mild category, the only changes are a redistribution of blood flow to the head and heart and away from the body, as well as an increase in haematocrit. In the severe category, a reduction in total cardiac output, in addition to a redistribution of the cardiac output away from the central body to the head and heart takes place. Growth reduction will be present, and in those growth retarded foetuses, arterial blood pressure is reduced and heart rate increased above control conditions.

2.4.3 Umbilical cord occlusion

According to a review conducted by Sherer and Manning (1999) on umbilical cord compression, it is considered to be the most common identifiable single factor associated with stillbirth and is present in approximately 15 % of cases. Clapp et al. (1988) showed a strong relationship between intermittent partial occlusion of the umbilical cord and subsequent neurodevelopmental handicap. Itskovitz et al. (1987) suggest that umbilical cord compression is one of the most common causes of foetal and subsequent neonatal distress. Clinically, there are various kinds of cord compression that may occur. These are entanglement of the umbilical cord around the foetal neck, known as a nuchal cord, true knots of the umbilical cord, foetal grasping which may occur intermittently, foetal sucking of the cord, stretching, compression, alterations in temperature if it prolapses, haematoma and rarely umbilical artery aneurysms (Sherer and Manning 1999). Experimental work has been conducted on foetal sheep which reduces umbilical and placental blood flow by umbilical cord restriction in order to assess its effects on the foetal circulation. The cord may be partially occluded by placement of a balloon catheter to restrict flow at a particular site along the umbilical arteries or by compression of the arteries along their entire length. Pharmacological vasoconstriction may also be performed. Itskovitz et al. (1983, 1987), Ball et al. (1994), Richardson et al. (1996), Giussani et al. (1997) and Adamson et al. (1989) all studied the dynamics of cardiovascular responses to partial umbilical arterial occulsion in foetal lambs under a variety of conditions. Their studies indicate that there are differences in the response to umbilical cord restriction that depend on both the extent and duration of the restriction, as well as whether there was pre-exposure to the restriction. A detailed description

of each scenario would require separate investigation, however the common trend in acute severe umbilical cord occlusion appears to be a drop in combined ventricular output and umbilical flow, a decrease in heart rate and an increase in mean arterial pressure. Blood flow is redistributed in a manner that is different to that seen in maternal hypoxaemia, with an increased proportion of the flow going to the brain and heart, as well as to the carcass, kidneys and gastrointestinal tract.

2.4.4 Reduction in uterine blood flow

Uterine blood flow may be reduced during pregnancy for prolonged periods of time under a variety of clinical conditions such as hypertension, severe diabetes mellitus and some cases of intrauterine growth retardation (Bocking et al. 1988). Furthermore, repeated reductions in uterine blood flow occur quite frequently during the second stage of labour and expose the foetus to various degrees of distress (Jensen and Berger 1991) . Experiments on sheep which reduce uterine blood flow may be conducted using a variety of methods, including compression of the maternal aorta, maternal internal iliac artery, uterine arteries or the uterine veins or by embolisation of the uterine vascular bed (Jensen et al. 1999). Bocking et al. (1988), Block et al. (1990a) and Jensen et al. (1987, 1991) experimentally reduced uterine blood flow by a variety of methods and observed the associated foetal cardiovascular responses.

The effect of uterine blood flow restriction appears to be dependent on both the degree and duration of the restriction. Similar patterns to those seen in induced maternal hypoxaemia occur, with a redistribution of blood flow occurring, favouring the head, heart and adrenals at the expense of the rest of the body. Generally, heart rate, mean arterial pressure and total cardiac output remain unchanged provided there is no associated acidemia in addition to the hypoxia.

2.4.5 Changes in foetal blood volume

A reduction in foetal blood volume will lead to a reduction in foetal oxygen delivery. This is known as anaemic hypoxaemia and is most often caused by foetal haemorrhage, which is usually the result of vasa previa or cord rupture during labour in the case of a velamentous insertion into the placenta (MacDonald, 1995).

Gilbert (1980) and Toubas et al. (1981) examined the cardiovascular responses to changes in foetal blood volume in chronically instrumented sheep. They found that an acute decrease in blood volume decreased combined ventricular output, mean pressure and heart rate. The fraction of blood distributed to all the peripheral organs remained roughly the same. However, the actual volume of blood distributed to most of the organs decreased.

2.4.6 Placental embolisation

The term *placental insufficiency* has been used to describe those foetuses where oxygen depravation occurs as a consequence of problems with the placenta itself. Histological characteristics used to define placental insufficiency have been the syncytial knot count, placental infarction, cytotrophoblast hypertrophy, deficiency of vasculoendothelial membranes, fibrinoid necrosis of villi, basement membrane thickening, stromal fibrosis and oedema, apparent placental hypovascularity and villous maturation (Giles et al. 1985). Placental insufficiency is frequently observed in growth retarded foetuses. However, it is uncertain whether the placental lesion is primary or if it is a result of other foetal or maternal complications. Embolisation of the foetal placental vascular bed may simulate the effects of acutely reduced placental function and associated hypoxia. Trudinger et al. (1987), Adamson et al. (1989) and Block et al. (1989, 1990b) embolised the placental vascular bed in foetal lambs and observed subsequent changes in cardiovascular parameters.

As with other types of induced hypoxia, the degree of embolisation appears to determine the nature of the associated changes. It appears that placental embolisation results in subsequent growth retardation and reduced umbilical flow. However, a redistribution of flow to the vital areas as seen in maternal hypoxaemia does not always appear to take place in acute embolisation as observed by Block et al. (1990b). Block and co-workers also stated in this particular study that total cardiac output and blood pressure remained constant whilst placental flow was markedly reduced. This study fails to explain that if total cardiac output does not decrease, and mean arterial pressure does not increase, how the balance between reduced placental flow and total flow is maintained. This can only be answered by noting that the results are reported as statistical averages and may not hold true on each individual foetus. No long term embolisation studies have been conducted.

2.5 Placental response to IUGR

Foetal growth restriction may occur as a result of intrinsic foetal abnormalities or it may follow substrate deprivation. Thus it is debateable whether a diseased placenta is the cause of intrauterine growth retardation or whether IUGR subsequently leads to a maldeveloped placenta. Chronic maternal hypoxemia, long term reductions of uterine flow and placental embolisation all result in a maldeveloped placenta. A number of placental changes have been documented in association with IUGR babies and these morphological characteristics are briefly reviewed.

Giles et al. (1985) originally proposed that placental disease resulting in absent end diastolic flow velocity waveforms in the umbilical artery (AEDFV), was due to a selective obliteration

of arterioles in the 20-90μm diameter range. An alternative theory was proposed by Macara et al. (1995) and Krebs et al. (1996), who suggested that a symmetrical reduction in vascular development of the placental villous tree was responsible, as opposed to an obliterative process. Further findings from Hitschold et al. (1993) and Jackson et al. (1995) have suggested that the entire villous tree may be hypovascularised, rather than just a selection of small stem vessels. Nordenvall et al. (1991) showed that intra-uterine growth retarded foetuses with AEDFV frequently have abnormal arrangements of the chorionic plate vessels. Jackson et al. (1995) showed that IUGR is associated with reduced large vessel wall thickness and that the volume and surface areas of intermediate and terminal villi are diminished. These latter studies suggest that a global reduction in vascularity and an irregular vessel distribution, as opposed to luminal obliteration are responsible for AEDFV.

2.6 Regulation of the foetal circulation

The above sections have outlined changes which occur as a result of foetal adaptation to imposed hypoxic stress. The mechanisms for accomplishing these changes are tissue dependent and can be neural, hormonal or a form of local control which depends upon arterial blood gas tensions or the concentration of metabolites. Their effectiveness is determined by the particular tissues to which blood is supplied. In general, hypoxia tends to increase blood pressure, decrease heart rate and combined ventricular output and redistribute the total cardiac output in a manner which is dependent upon the nature of the induced hypoxia. It is essential to understand how the redistribution of cardiac output is mediated in order to effectively model these changes. From the model point of view, it is necessary to know which parameters to change in the representations of the vascular beds. In particular, a detailed understanding of associated changes in the placenta is essential for accurate modelling. Morin and Weiss (1992), Anderson (1992), Iwamoto (1992) and Adamson et al. (1989) provide detailed investigations into various aspects of neural or hormonal regulation of the foetal circulation. This section will summarise the findings that will have particular relevance on the foetal model. The focus will be on the foetus during the 3rd trimester.

2.6.1 Endocrine regulation of umbilical, placental and organ blood flow

The placental vascular bed and umbilical artery are considered to be under passive control as no autonomic innervation has been found in the umbilical vessels or the placental microcirculation. Placental vascular resistance changes in response to a number of exogenous hormones and this has been investigated in chronically catheterised foetal sheep. Unfortunately, the observed

effects in a particular regulatory system under observation may be minimised due to compensatory changes in the response of other regulatory systems. Thus the true physiological role of an individual system can be masked in an experimental investigation as it is difficult to control the numerous other variables. Given this limitation, the following section describes the effects of three hormones, which have been studied in detail and are shown to be highly significant in the regulation of the foetal circulatory system.

Angiotensin II.

Increases in the renin-angiotensin system, which result in the release of angiotensin II, are stimulated by haemorrhage, furosemide administration, hypotension, bilateral carotid occlusion, parturition, β-adrenergic stimulation and hypoxaemia. The effect of angiotensin II is to vasoconstrict the umbilical arteries, as well as the gastrointestinal, renal and thyroid vascular beds, but not the placental vascular bed (Iwamoto and Rudolph, 1981). Blood flow to the myocardium and pulmonary circulation is increased. Infusion of angiotensin II increases mean arterial pressure and total cardiac output but has no significant effect on heart rate. Inhibition of angiotensin II alters the foetal response to haemorrhage, however, available evidence does not indicate a role for angiotensin II in foetal responses to acute hypoxaemia. Under normal circumstances, umbilical vascular conductivity is not restrained by circulating angiotensin II.

Norepinephrine

Norepinephrine release is stimulated in most forms of experimentally induced chronic stress that result in hypoxaemia and acidemia. Norepinephrine infusion tends to increase arterial blood pressure, venous blood pressure, blood flow to the heart lungs and umbilical-placental circulation and decreases blood flow to the peripheral and gastrointestinal circulations. The effects of norepinephrine on heart rate vary and are dependent upon the rate of administration. Adamson et al. (1992) showed that norepinephrine increases placental vascular resistance but does not alter umbilical flow or umbilical artery resistance. This was probably due to the associated mean arterial pressure increase. Norepinephrine does not appear to be used under normal conditions for the restraint of foetal placental blood flow.

Vasopressin

Plasma vasopressin concentrations in the foetus may be increased by increases in plasma osmolality, isovolemic hypotension, parturition, haemorrhage and acute hypoxaemia. When vasopressin is infused intravenously, the foetus responds with hypertension and bradycardia in a

dose-dependent manner. Blood flow to the gastrointestinal tract and peripheral circulations are decreased and the proportion of flow to the umbilical-placental, cerebral and coronary circulations are increased. Vasopressin increases foetal placental vascular resistance. Vasopressin appears not to play an important role in circulatory regulation under basal conditions. Thus vasopressin appears to play a similar role to norepinephrine in hypoxic stress and indeed it is suggested that vasopressin and the sympathoadrenal system work in conjunction to regulate arterial pressure and other haemodynamic responses during acute hypoxaemic and haemorrhagic stress in the foetus.

Other hormones such as prostaglandins, atrial natriuretic peptide (ANP), the endogenous opiods and adrenocortical hormones all have a role in the foetal response to hypoxic stresses. These hormones either effect pressure, heart rate or the resistance of the vascular beds, but no studies have been performed to show at which level of the vascular arterial beds they exhibit greater effects. In general the foetal circulation responds to a decreased blood oxygen content with a competition between the local and the systemic control of blood flow. Local control of the circulation results in increased blood flow and maintenance of oxygen consumption throughout the hypoxic period and would thus target areas such as the brain and heart. Systemic control, mediated by humoral and reflex mechanisms, tends to increase resistance and thus maintain a constant blood flow in leu of increased pressure or decreased cardiac output. This would therefore be focused on organs such as the digestive tract, kidney and carcass. The foetus is limited in its ability to adapt to decreased oxygen levels and the essential organs may consume so much of the available oxygen that the amount left over for the nonessential organs is inadequate, resulting in metabolic acidosis and circulatory collapse. Should the levels of oxygen still remain inadequate for the essential organs, neurological damage or death may result. The important result of this section regarding the model is that blood flow redistribution is a result of increased or decreased resistance of the various important vascular beds, in combination with changes in mean arterial pressure. The umbilical circulation may be regulated at the levels of both the umbilical artery as well as the placental vascular bed.

2.7 Changes of blood viscosity and arterial elasticity in response to foetal distress

It has been shown that the foetal haematocrit increases in response to hypoxia. The blood viscosity is dependent upon the haematocrit and hence the viscosity increases too. In addition the arterial wall elasticity, wall thickness or the amount of surrounding tissue may undergo changes with hypoxia. It is necessary to examine the role of these variables in the various types

of hypoxic stresses, in order to accurately assess their impact on flow velocity waveforms. This can be achieved through the use of the foetal model.

Steel et al. (1989) demonstrated that there is a significant increase in plasma viscosity in patients with both pre-eclampsia and growth retardation when compared with control patients. Although those foetuses that were just IUGR or pre-eclamptic had higher viscosities than the controls, this increase was not significant.

Giles et al. (1986) showed elevated blood viscosities in those foetuses that had abnormal umbilical arterial Doppler S/D ratios when compared with those that had normal ratios. Abnormal Doppler ratios are frequently associated with hypoxia, suggesting that hypoxia increases blood viscosity.

Pawlicka et al. (1999) investigated morphological changes in the structure of the umbilical arterial wall in pregnancies complicated by Edema, proteinuria, hypertension (EPH) gestosis or preeclampsia. They found that EPH gestosis was associated with a significant reduction of elastin content in the umbilical cord arteries, as a result of a decrease in the elastin biosynthesis rate and accelerated degradation of elastin. Elastin is replaced by collagen and may thus decrease the hydration of the arterial wall, effectively reducing its elasticity and compliance. In fact umbilical arteries taken from newborns of mothers with EPH gestosis contained twice the amount of collagen in comparison to corresponding arteries taken from foetuses with healthy mothers. The changes in collagen composition were further accompanied by a premature reduction of Wharton's jelly.

Bruch et al. (1997) used computerised microscope morphometry to study cross sections of the umbilical arteries in patients with IUGR. They observed a significant reduction in wall thickness and amount of Wharton's jelly in the IUGR group when compared with the control group. Although the luminal area was slightly decreased, this reduction was not significant.

Labarrere et al. (1985) described three clinical cases characterised by a complete absence of Wharton's jelly around the umbilical cord arteries. All three instances were associated with prenatal death. Although a complete absence of Wharton's jelly is extremely rare and the deaths are more likely to be attributed to a lack of protective mechanisms rather than hypoxic stress, this report is included as an extreme example of observed reductions of jelly in association with hypoxic stresses.

2.8 Summary

It is essential to understand the anatomical and physiological functions in both the normal and compromised foetus in order to accurately model these functions. This chapter began with a

review of the anatomy and physiology of the healthy foetus and subsequently examined those changes that are known to occur in the compromised foetus. Clinical studies on human foetuses are limited by ethical constraints that confine the number of measurable variables as a result of non-invasive procedures. Thus, many of the reported results were obtained via animal experimentation. Unfortunately these are influenced by species characteristics and surgery or anesthesia which affects cardiovascular reflex responses. Furthermore, a particular interventional procedure may have a more holistic effect than affecting only those areas that are under investigation. Despite these considerations, the information in this chapter offers insight into those parameters that may change with foetal compromise, how they may change and which other parameters are influenced. This will enable realistic simulations with the foetal model and highlights relevant areas for further investigation with the model.

Chapter 3

Overview of the foetal model

3.1 Background to foetal models

The similarity between haemodynamic fluid equations and electrical circuit equations has lent itself to haemodynamic analyses being carried out in terms of electrical analogies, with voltage being equivalent to pressure and current to flow. Resistance and impedance have the same meaning in the haemodynamic analogy as they do in the electrical theory.

The earliest recorded mathematical description of the foetal circulation was by Veth et al. (1976, 1978), who constructed a model containing a nonpulsating heart, a systemic and umbilical circulation and several control mechanisms. The model represented the systemic circulation by a simple resistance and the placental vascular bed by a reservoir containing resistive and compliant arterial inflow and venous outflow components. Their study was restricted to the analysis of the response of the foetal circulation to temporary occlusion of the umbilical cord.

Huikeshoven et al. (1980) developed a model consisting of six peripheral blood compartments and a detailed description of the heart. Each compartment was modeled as a resistance and a compliance, where the values were selected based upon experimental data obtained from sheep experiments. The effects of increasing blood volume and umbilical cord clamping were studied using this model.

The above models operated on the basis of experimentally chosen values for resistive and compliant components. The first model which selected these values based upon equations considering arterial fluid and wall properties was that of Thompson and Stevens (1989) who used a linearised, lumped element electrical circuit equivalent consisting of a resistor and capacitor to model the umbilical arteries. The placental villous bed was modelled by a two-step parallel branching structure. A relatively simple input waveform was used at the entrance to the umbilical artery and the effect of placental disease (modelled as obliteration of a fraction of the

placental branches) on the pulsatility index was investigated. Essentially the same model was employed by Thompson and Trudinger (1990) to examine the effect of different physiological variables on the pulsatility index of the umbilical artery Doppler waveform. These physiological variables were foetal heart rate, foetal blood pressure and placental vascular disease.

A similar model consisting of simple lumped electrical analogies for the umbilical artery and placental villous bed was constructed by Guiot et al. (1992), but they represented the placental tree structure as a network of dichotomously branching vessels of progressively reduced cross-sectional area and length. The model was used to demonstrate the dependence of the mean values of blood flow and the pulsatility index on the cross sectional area ratio between vessels belonging to two successive generations. Todros et al. (1992) applied the same model to investigate the effect various degrees of obliteration of the villous vascular tree on the pulsatility index.

The first model of the complete foetal circulation, and not just the umbilico-placental circulation, and using anatomical and physiological values rather than estimated lumped constants was proposed by Guettouche et al. (1992). This model was based upon a non-linear numerical solution for mass and momentum conservation equations for one-dimensional flow. The vascular system was represented by 16 anatomical segments terminated in specified peripheral resistances. The input blood velocity waveforms were obtained from Doppler measurements at the ascending aorta and pulmonary trunk inlet segments. Geometrical tapering of the arteries were considered. The model was validated with comparisons to ultrasound measurements but no investigative analyses were reported.

Hill et al. (1995) developed an electrical analog model of the umbilical artery and placenta based on haemodynamic measurements in foetal sheep. Their model differed from earlier lumped component models by representing the umbilical artery as a transmission line and the placenta by a resistive load. Transmission line models offer the advantage of being able to model flow and pressure continuously along the entire length of the artery. Measured waveforms from foetal sheep were used as the model input and in order that the model fit the measured data, the somewhat unrealistic step of including a resistive load halfway along the artery was included. Essentially this was done in order to account for the distributed nature of the placental load. The model was used to predict input impedance and flow waveforms under baseline conditions, following placental embolization and during angiotensin II infusion.

Surat and Adamson (1996) used the same model modified by adding a bifurcation in the umbilical artery. Once again, this representation is clearly anatomically incorrect. The effect of variations in placental resistance, wall thickness, elastic modulus and radius on pulsatility index and diastolic-to-systolic blood velocity were studied.

Pennati et al. (1997) created a full foetal circulatory system model. Their model consisted of two major parts, the heart and the foetal vascular circulation, which was divided into 19 compliant vascular compartments. The heart was modelled using electrical analogies and consisted of three components to describe both ventricular and atrial contractility. The vascular circulation was implemented using a time domain, numerical formulation based on mass and momentum conservation laws. Values of resistance, compliance and inertances were calculated based on physiological and anatomical parameters derived from the literature on foetal sheep or from ultrasound imaging of human foetuses. The model was validated by comparing several index values of simulated velocity curves to those of experimental Doppler measurements, as well as by comparing regional blood flow distribution with those obtained from the literature. No further investigative tasks were performed.

A further model of the entire foetal circulatory system was developed by Menigault et al. (1998). This model represents the arterial tree by non-linear, one-dimensional Navier-Stokes based flow equations and the peripheral circulation by a simple Windkessel model. The solution was obtained using the method of characteristics, which is a numerical, time domain method. Arterial parameters were obtained from anatomical and physiological data from the literature and geometric tapering was taken into account. The foetal heart was modeled on a ventricular pressure and volume relationship, using cardiac elastance values measured on dogs. The model was validated under physiological conditions by comparing predicted and measured haemodynamic indices, as well as by computing the distribution of blood flows and comparing them with values reported in the literature. The effect of placental disease on blood flow distribution was investigated through increasing the value of placental resistance. Unfortunately many of the values used in the model were obtained from measurements on foetal sheep and it is known that mean pressure, cardiac output and the percentage distribution of the total cardiac output to foetal organs differs between human foetuses and foetal sheep.

Kleiner-Assaf et al. (1999) chose a more complex linear two-dimensional model of viscous flow in a thin-walled elastic tube, that was proposed by Atabek and Lew (1966), to represent the umbilical artery. An assumed pressure gradient imposed between the ends of the umbilical artery was used to investigate the dependency of Doppler indices on many anatomic, geometric and physical variables. Whilst an investigation of this nature is clearly of great importance, their study failed in two important regards : a non-frequency dependent expression for the wave speed in the artery was used, and they failed to take into account the reflected waveform which occurs at the umbilico-placental interface. By considering only a forward propagating waveform, their results cannot be indicative of downstream resistance.

All of the models presented above are only valid at a particular gestational age, however anatomical and physiological variables change throughout gestation. Pennati and Fumero (2000)

adapted their earlier model to account for foetal body size increases using allometric scaling techniques. Capper and Myers (2000) independently presented a similar model that allowed investigation of the effect of foetal growth on the FVW's.

Many foetal circulatory models have been presented, however they all fall short of adequately accomplishing the complete list of criteria described in chapter 1. Shortcomings of these models are :

- None have accounted for curvature.
- Those that consider tapering are only one-dimensional models and do not consider both elastic taper and geometric taper together.
- None have adequately investigated the effects of surrounding tissues and possible anisotropy.
- Many of the models use anatomical and physiological parameters obtained from measurements on foetal sheep and although this provides a degree of insight, it may not always be possible to extend these results to human foetuses.
- No model that provided a picture of the complete foetal circulation presented any detailed investigative analyses.
- The representations of the peripheral vasculatures, especially that of the placenta were frequently inadequate to account for the interdependency on mean arterial pressure, cardiac output distributed to that region, input resistance, input impedance and overall tree morphology. The most detailed representation of the placenta was that by Guiot et al. (1992), however emmendations are suggested to their useful work.
- One model which considered foetal growth does not take into consideration asymmetric growth rates of the various foetal organs.
- No model was found which conducted simulations on each of the possible determinants of the Doppler indices outlined in chapter 1.

3.2 Functional simplifications of the foetal circulation and model description

A diagram of the foetal heart is show in figure (2.2). The foetal heart is responsible for pumping blood around the foetal arterial system and may be modeled as a single flow source. The ductus arteriosus and the aortic arch have similar dimensions and therefore the two ventricles could be assumed to have equal output volumes and mean pressures (Dawes, 1968; DeMuylder

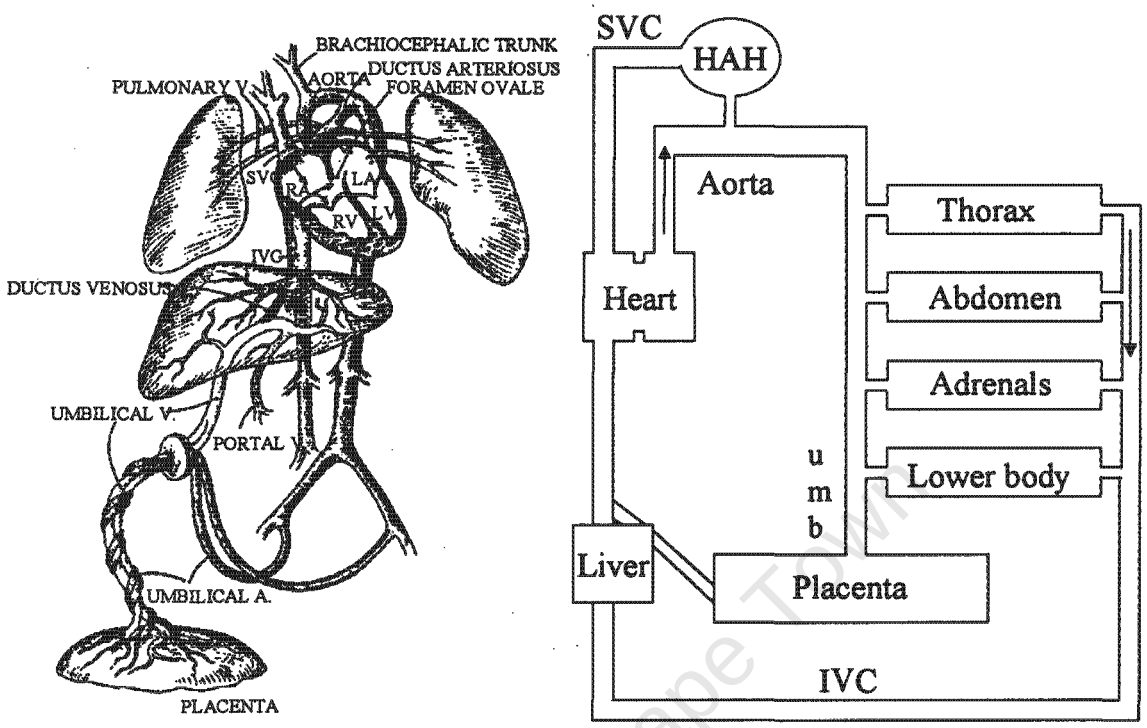

Figure 3.1: Schematic simplification of the foetal arterial system.

et al., 1984). Thus the ascending aorta and the ductus arteriosus are combined into a single, functionally equivalent vessel with an area equal to the sum of the areas of these two vessels.

The foetal vasculature may be simplified into a number of functional compartments, consisting of several vessels branching off the aorta and may be considered to be the concatenation of a number of arterial segments of different dimensions and physiological properties. (See figure (3.1)) The descending aorta is subdivided into 2 sections, respectively representing the thoracic aorta and the abdominal aorta. The aorta subsequently feeds into the iliac arteries which in turn lead to the umbilical arteries, terminating in the placenta. The vessels supplying blood to the cerebral and myocardial tissue are grouped into a single branch off the thoracic aorta, labelled HAH (Head and Heart). Vessels supplying blood to the upper body and thorax, abdomen and adrenals are simplified using three staggered branches off the thoracic and abdominal (descending) aorta. The external iliac, superior gluteal and ischiadic arteries are grouped together into a single vessel supplying the lower body. These lumped vasculatures may frequently be referred to as the terminal or peripheral arterial beds. A functional diagram of the arterial model is depicted in figure (3.2), with appropriate labels for each unit which will be referred to throughout the thesis.

The model begins by assuming that the heart ejects a continuous stream of flow pulses, with

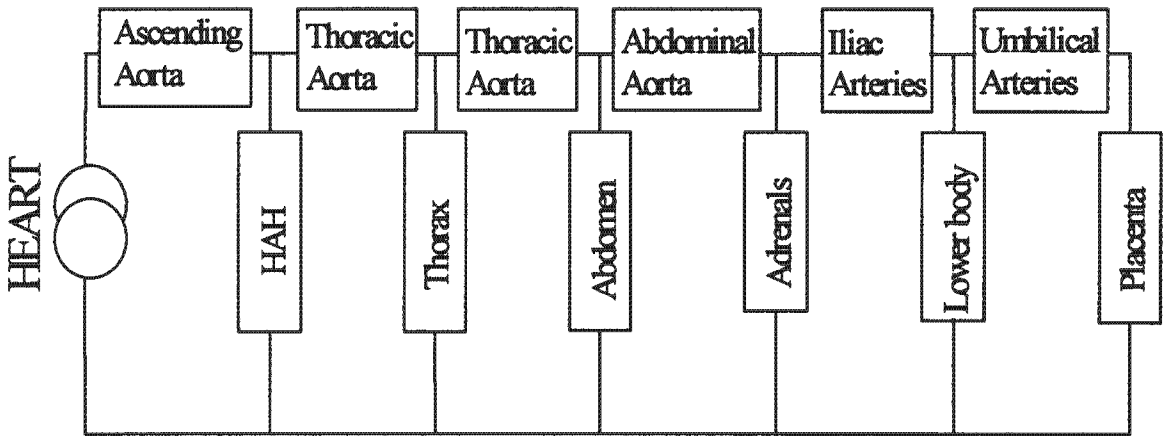

Figure 3.2: Functional diagram of the foetal model. Each horizontal block represents a major artery in the model and each vertical block a peripheral vascular bed. The heart is the model flow source.

each pulse equal to the stroke volume of the foetal heart, into the foetal aorta. Each time the heart beats, a single flow pulse is assumed to be delivered and the shape of that flow pulse during the cardiac cycle is a known function. Each of these time domain flow pulses is Fourier transformed in order to represent them in the frequency domain. The model is assumed to be linear and thus each significant harmonic of the Fourier representation is propagated through the model, one at a time, and pressures, impedances and flows are calculated at various positions in the arterial system. The frequency domain representations of the pressures and flows are then inverse Fourier transformed in order to obtain their time-domain equivalents. A conceptual diagram of the model procedure is depicted in figure (3.3).

Each of the main arteries in the model are modeled as a fundamental arterial segment, using frequency dependent equations that calculate flow for an imposed pressure gradient along the arterial segment. These equations are modified to include tapering in the aorta and peripheral vascular beds and coiling in the umbilical arteries. The peripheral beds and the placenta are modelled as a branching network of compliant vessels using fractal relationships as outlined in chapter 7.

3.3 Blood flow distribution

The model assumes that the percentage of the total combined cardiac output to each peripheral arterial bed is a known quantity. This is then used to determine the impedances of these peripheral beds as detailed in chapter 7 and thus it is important to obtain values from the

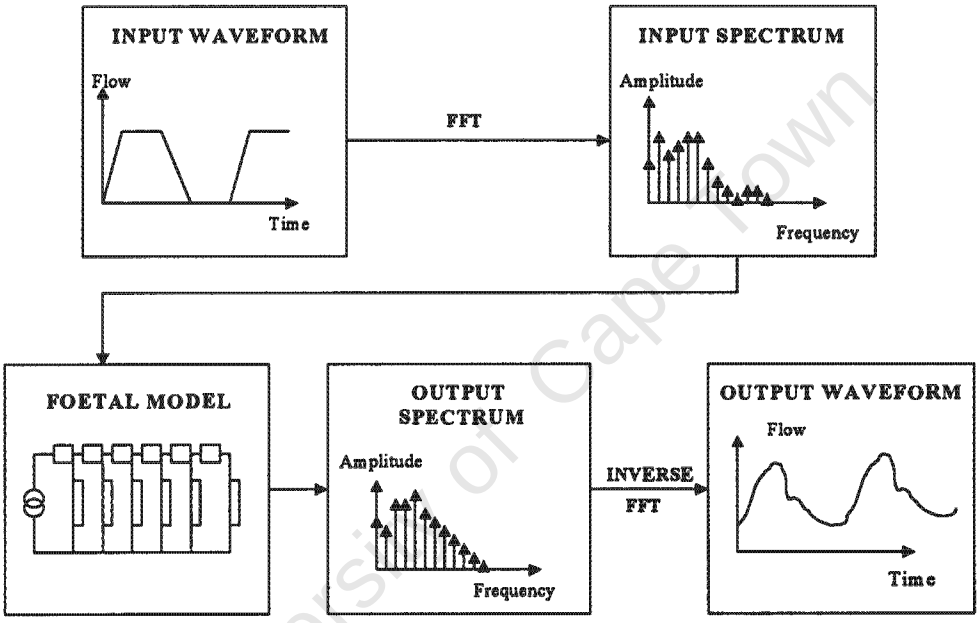

Figure 3.3: Conceptual diagram of the model procedure. The heart generates a time domain flow waveform which is Fourier transformed. Each harmonic of the input spectrum is propagated through the foetal model to generate an output at that harmonic. The output flow, pressure or impedance spectra may be acquired at any point in the foetal model and inverse Fourier transformed to obtain their time domain equivalents.

literature for the blood flow distributions. For the foetal lamb, this has been well documented using experimental investigations (Rudolph, 1985). However, the distribution in human foetuses differs considerably from foetal sheep and thus available data from animal experimentation is not directly applicable to the model. A number of authors have obtained flow measurements in the human foetus using ultrasound and these measurements have been used as the basis of the values selected in the model.

The human foetal cardiac output has been estimated to lie between 450 and 560 ml/min/kg (Reed et al. 1986, 1987; Rudolph, 1985; St. John Sutton et al. 1992; Rudolph and Heymann, 1974; Guettouche et al. 1992) . Furthermore, the cardiac output per unit of foetal body mass is known to remain constant from 18 weeks until term in a human foetus (St. John Sutton et al, 1992). Using an average of these for a foetus at a gestational age of 28 weeks, the cardiac output is assumed to be 500 ml/min/kg.

Placental blood flow in human foetuses has been estimated to fall within the range of 106-120 ml/min/kg of foetal mass (Eik Nes et al, 1982; Gill et al, 1981; Van Lierde et al, 1984; Erskine and Ritchie, 1985; Guettouche et al., 1992). A placental flow of 120ml/min/kg is assumed and is approximately 25% of the chosen cardiac output.

St John Sutton et al.(1992) measured the brachiocephalic flow to be about 40% of the cardiac output. This is the flow to the upper body and to the head and heart units in the model and values of 27% for the head and heart and 15% for the thorax have been selected. This totals to 42%, leaving 58% of the cardiac output for the mid thoracic descending aorta. This is approximately 290 ml/min/kg, which compares favourably with values between 213 and 273 ml/min/kg, reported by Marsal et al. (1987) and Guettouche et al. (1992). Rudolph et al. (1971) using microspheres in previable human foetuses measured flow in the inferior vena cava to be 64-75% of cardiac output. These values also compare satisfactorily well with the values selected in the model.

Guettouche et al. (1992) measured flow to the lower limbs and kidneys to be 8% and 25% respectively. These estimates have been used in model which assumes the flow to the abdomen to be 7.7% with 0.3% going to the adrenals. The data for the percentage blood flow distributions is summarised in table (3.1).

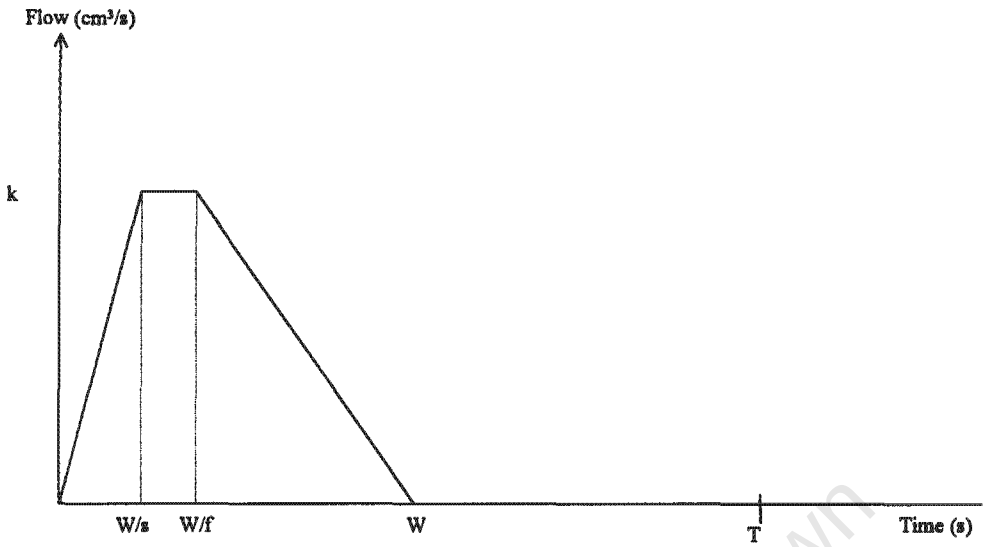

Figure 3.4: Representation of the flow pulse ejected into the equivalent vessel used for the ascending aorta and pulmonary trunk. The period of the pulse is T seconds and the portion of this that is non-zero is W seconds. The fraction that is the rise time is W/s seconds and the steady period lasts until W/f seconds. The amplitude is denoted by k.

Peripheral compartment	% Cardiac output
Head and Heart	27
Thorax	15
Abdomen	7.7
Adrenals	0.3
Lower body	25
Placenta	25

Table 3.1: Data of model reference values of the percentage of total cardiac output distributed to each of the labelled peripheral vascular compartments. These percenatge distributions are for a healthy foetus and remain constant from 28 weeks until term.

3.4 The foetal heart

The model assumes that the time domain description of the flow ejected into the aorta (input flow pulse) is known. This is calculated as follows :

A flow profile with known ventricular ejection times, systolic rise times and diastolic times is assumed and the chosen form of the pulse is depicted in figure (3.4). The aortic pulse (flow ejected by combined ventricular output), has a waveform period given by $T = \frac{60}{HR}$. W denotes the duration of the systolic pulse, W/s the rise time, the steady period lasts until W/f and the flow during the diastolic portion of the cardiac cycle is assumed to be zero. The peak systolic flow is denoted by k.

The mean of this waveform multiplied by the period must be equal to the stroke volume $= \frac{\text{total cardiac output } (CO)}{\text{heart rate } (HR)}$. Thus k may be solved for by integrating to obtain the average area under the waveform as follows :

$$\frac{CO}{HR} = \frac{1}{T}\int_0^T \left(\frac{W}{2s}k + \left(\frac{W}{f} - \frac{W}{s}\right)k + \frac{1}{2}\left(W - \frac{W}{f}\right)k\right)dt = \frac{kW}{2}\frac{s+sf-f}{sf} \tag{3.1}$$

i.e.

$$k = \frac{CO}{HR}\frac{1}{W}\frac{2sf}{s+sf-f} \tag{3.2}$$

The dependency of human ventricular ejection times on heart rate has been demonstrated by various authors (Wolfson et al. 1977; Goodlin et al. 1972; Wladimiroff et al. 1979; Sahn et al. 1980). Based upon an average of these measurements, the ejection time is chosen to be 180 ms at a heart rate of 140 bpm. Thus for these values, $T = 0.43$s, $W = 0.18$ s, $s = 4$ and $f = 2$. Minor perturbations around these nominal values demonstrated no addition of harmonics of significant amplitudes or any signifcant changes to existing harmonics and thus these values were held constant for all subsequent analyses.

This flow pulse is Fourier transformed into the frequency domain to serve as the model input. The frequency resolution is equal to $1/(4T)$ and in order to obtain an acceptable resolution, four consecutive heart cycles are analysed. At a heart rate of 140 b.p.m, this results in a frequency resolution of $\Delta f = 0.58$ Hz.

Chapter 4

Fundamental arterial model

4.1 Background

The determination of flow in an artery from a known applied pressure gradient, has been a much researched subject for over three centuries. As early as 1628, William Harvey (1628) observed that despite the pulsatile action of the heart, blood flow is relatively steady in the peripheral arteries. In 1733, Stephen Hales (1733) noted the similarity between this idea and that of a fire hose and pipe organs, which provides a steady flow through an outlet with intermittent pumping through an inlet. The German, Otto Frank (1899) put this idea into a mathematical formulation and pioneered the theory known as the "Windkessel" theory (chamber theory), in order to derive flow information from pressure data. This theory conceived the arteries as a system of interconnected tubes with fluid storage capacity. Fluid is pumped in at one end to represent ventricular ejection and outflow at the other end, representing peripheral resistance, is held approximately constant.

Unfortunately, the Windkessel model fails to realistically represent measured flow data. It ignores time differences and assumes that pressure generated by the heart travels instantaneously through the Windkessel, whereas it is known that a small, yet finite time is required for the propagation of pressure pulses. Furthermore it incorrectly assumes a transient nature of the pressure pulse signal. Despite the conceptual inaccuracies of the Windkessel model, the idea was increasingly popular and a large number of modified versions were developed to attempt to account for these discrepancies. Conceptual models of this type are referred to as "lumped parameter models", where distributed properties of the arteries are lumped together into a number of single parameters with specific physical meanings. These are commonly represented in terms of electric circuit analogies, where the original Windkessel model is known as the RC-model or 2-element model, with R the total resistance and C the total compliance of the large

arteries.

More complicated 3 and 4 element configurations have been developed in an attempt to refine the pressure-flow relationship and an overview of the more common models may be found in Toy et al. (1985). The disadvantage of these types of models are that in order to obtain realistic data, the number of elements must increase, which in turn lessens the interpretation of the physical meaning of each individual parameter. In general, it appears that Windkessel models have reached the stage where their complexity exceeds their utility and alternative theories have become far more attractive (Milnor, 1989) .

An alternative approach to analysing blood flow was originally proposed by Euler in 1755, and is based upon the application of the laws of classical mechanics to the artery. In 1914, Witzig (1914) published an analysis of wave propagation in distensible tubes and it was this approach that foretold the direction which subsequent work would follow. He considered a thin-walled tube and a simplified, linearised Navier-Stokes formulation to develop his results. Subsequently Morgan and Kiely (1954) and Womersley (1955a and b; 1957a and b) developed essentially similar models which became the foundation for modern blood flow analysis.

These analyses consider a formulation of the Navier-Stokes equations for the fluid motion and a further formulation of equations governing the arterial wall mechanics and interaction with the fluid. A large variety of assumptions on the nature of the flow conditions, fluid properties and types of vessel walls, as well as on the solution to the equations, are considered. A brief discussion of assumptions that may be made pertaining to the development of a foetal flow model will be discussed below.

It is convenient to assume that blood is a Newtonian fluid. This implies that the coefficient of viscosity is constant at all rates of shear. However, it is known that at low shear rates, the apparent viscosity of blood increases markedly. Furthermore, blood viscosity is dependent, to a small degree, on arterial diameter and for vessels of small radius (< 1mm), the apparent viscosity at higher shear rates is less than it would be in larger vessels. Taylor (1959) theoretically demonstrated that using a constant, asymptotic value of viscosity, a maximum of a 2% error is incurred in the Womersley calculations of flow from pressure gradient in large arteries. Several mathematical descriptions of non-Newtonian behaviour of blood have been put forward (Taylor 1959; Gerrard and Taylor, 1977; Nakamura and Sawada, 1990; Mazumdar et al. 1991). However, due to the complexity of these models and the low percentage error in using a constant viscosity model, blood has been modelled as a Newtonian fluid. Furthermore, due to the increasingly non-Newtonian behaviour in vessels of small radii, an effort has been made to limit the model to those vessels of larger radius, as will be explained in chapter 7.

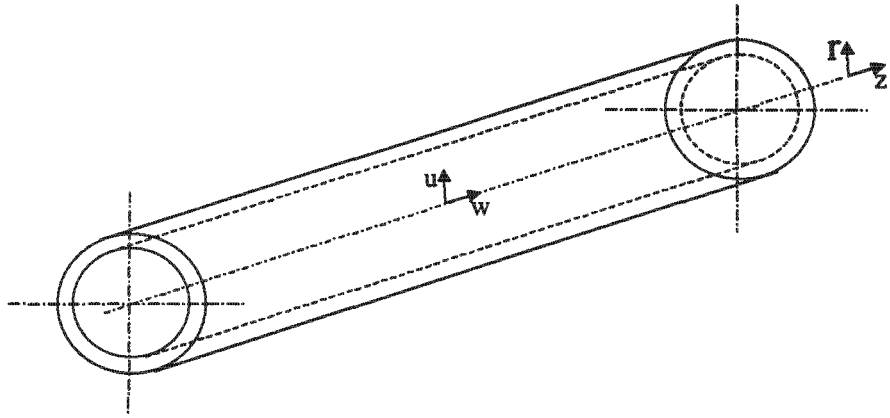

Figure 4.1: Flow through an elastic, symmetrical artery. Geometry and notations.

It is further assumed that the blood flow in the foetal circulation exhibits no turbulence and is considered as laminar flow. Turbulent flow has been show to occur in the larger blood vessels of the adult circulation but very little elsewhere and given that the diameter of the foetal vessels are significantly smaller, this appears to be a valid assumption. The analyses considered here attempt to describe fully established, axially symmetric flow and do not focus on entrance effects. With the exception of the coiling of the umbilical artery, which will be dealt with in chapter 5, the arteries are assumed to be sufficiently long and straight, in which case tangential velocities are absent. In general the artery is considered as a hollow cylindrical tube with a spherical-cross section as depicted in figure (4.1). The above assumptions conveniently allow the equations of fluid motion to be expressed by force equations expressing the conservation of momentum and the continuity equation expressing the conservation of mass. This results in the Navier-Stokes (equations 4.1 and 4.2) and continuity equations (equations 4.3) and in a cylindrical co-ordinate system these are the basis for the development of most of the models to be discussed, and are thus presented here for convenience :

$$\frac{\partial w}{\partial t} + u\frac{\partial w}{\partial r} + w\frac{\partial w}{\partial z} = -\frac{1}{\rho}\frac{\partial p}{\partial z} + \nu\left(\frac{\partial^2 w}{\partial r^2} + \frac{1}{r}\frac{\partial w}{\partial r} + \frac{\partial^2 w}{\partial z^2}\right) \tag{4.1}$$

$$\frac{\partial u}{\partial t} + u\frac{\partial u}{\partial r} + w\frac{\partial u}{\partial z} = -\frac{1}{\rho}\frac{\partial p}{\partial r} + \nu\left(\frac{\partial^2 u}{\partial r^2} + \frac{1}{r}\frac{\partial u}{\partial r} - \frac{u}{r^2} + \frac{\partial^2 u}{\partial z^2}\right) \tag{4.2}$$

$$\frac{\partial u}{\partial r} + \frac{u}{r} = -\frac{\partial w}{\partial z} \tag{4.3}$$

where r and z are the radial and axial coordinates, t is time, u and w are the radial and axial velocity components, p is the pressure, ρ the density of the fluid and ν the kinematic viscosity of the fluid. Equations (4.1) and (4.2) contain non-linear convective acceleration terms which

result from the radial motion of a fluid particle causing a change in the longitudinal acceleration and from the convergence of tapering walls. Non-linearities are particularly difficult to deal with and two principal approaches are employed when dealing with them. The first approach limits the solution to *one-dimensional flow* and considers the average velocity as opposed to the distribution of velocities across the vessel wall. The one-dimensional equations may be obtained by integrating the Navier-Stokes and continuity equations which results in the following two equations :

$$\frac{\partial v}{\partial t} + v\frac{\partial v}{\partial z} = -\frac{1}{\rho}\frac{\partial p}{\partial z} + f \tag{4.4}$$

$$\frac{\partial (Av)}{\partial z} + \frac{\partial A}{\partial t} = 0 \tag{4.5}$$

where v is the averaged axial velocity, A is the cross-sectional area of the tube and f represents the resultant of all longitudinal body and dissipative forces to be considered, such as wall friction, gravitation and centrifugal forces. These equations have been solved successfully using a numerical technique known as the method of characteristics and the results have been presented in a number of publications. (Lambert, 1958; Evans, 1962; Streeter et al. 1963; Wiggert and Keitzer, 1964; Taylor, 1965). Primary disadvantages of this method are the limitation to one-dimensional flow; the cumbersome time domain procedure which is required to solve the equations and that the values of f must be empirically formulated and are thus prone to error. Thus it would be preferable to obtain a complete solution to the original two-dimensional equations. This has been successfully solved by Ling and Atabek (1972), Ling et al. (1973), Belardinelli and Cavalcanti (1992) and Wang and Tarbell (1992, 1995). A solution to the non-linear equations is not possible by Fourier analysis as the harmonics interact with one another and the principle of superposition ceases to remain valid. When comparing the non-steady harmonics, Ling (1973) found that a solution to the linearised Navier-Stokes equations (obtained by neglecting the non-linear terms) differed only slightly from the non-linear solution. However, the same comparison for the steady flow term showed that the linear solutions seriously overestimated this. Wang and Tarbell (1995) confirmed that the non-linear interactions with the mean component generate a steady streaming flow which changes the shape of the mean velocity profile. The magnitude of this effect was shown to be dependent on the steady-streaming Reynolds number, R_s, defined as the ratio of the magnitudes of the steady convective effects to the steady viscous effects. $R_s = \epsilon^2\alpha^2$, where ϵ is the diameter variation and is $(a_{\max} - a_0)/a_0$, a_0 is the undisturbed radius of the artery and $a_{\max}$ is the largest radius due to expansion from the pressure pulse, $\alpha = a_0(\omega/\nu)^{1/2}$ (this is often referred to as the Womersley parameter in honour of his pioneering contributions) and ω is the angular frequency. For small values of R_s the effect of the non-linear terms may be neglected, with no significant loss in accuracy. The largest value of α in the foetal circulation is located in the full term aorta and is approximately

$(0.23)(2\pi 140/60/0.056)^{1/2} = 3.72$ and at a maximum $\epsilon \simeq 0.05$, which makes $R_s = 0.03$ and thus the non-linearities have very little effect on the mean velocity and a linearised solution is sufficient to describe the flow. A further effect of non-linearities is on pulse propagation in tapered arteries. Ling et al. (1972, 1973) used a numerical, non-linear solution to the Navier-Stokes equations for blood flow velocities in tapered elastic arteries of circular cross-section. They demonstrated that the effect of the convective acceleration terms on the pulse propagation cannot be ignored. Ye et al. (1993) used a simplified linearised solution for blood flow velocities and subsequently modified the solution to account for tapering by the addition of two time-varying terms to their equation of resistance per unit length. However, use of this solution is limited as it is assumed that the pulse wave velocity is constant for the tapered segment. Einav et al. (1988) proposed a tapered transmission line model to analyse impedance and local reflection factors. The model consists of cascaded segments each with a constant phase velocity. Chang et al. (1994, 1995) and Fogliardi et al. (1997) looked at exponential and geometrically tapered T-tube models to investigate the aortic input impedance under various complex loads but neither provide a clear and uncomplicated way of calculating velocities along the tapered arterial segment. In this thesis, a method based on non-uniform transmission line theory, is proposed in order to determine the flow velocity in a tapered artery at any point along the artery. A linearised solution of the two-dimensional Navier-Stokes flow equations is obtained and modified to result in a final closed form expression which may easily be incorporated into existing transmission line models. This approach avoids the complexity of solving the non-linear equations, with no loss in the accuracy of the solution. This will be dealt with in chapter 5. Having reduced the flow equations to their linearised counterparts by dropping the non-linear terms, in order to formulate a solution, it is common to consider each harmonic of the Fourier representation of the input pressure waveform separately. The solution to the total flow waveform may then be constructed by the inverse Fourier transform of the superposition of the solutions to each individual harmonic. Assuming the form of the pressure pulse is a travelling wave in the z direction with complex wave velocity c and angular frequency ω_n, then the Fourier series representation of the pressure waveform is :

$$P(\omega, z, t) = \sum_{n=0}^{k} A_n e^{i\omega_n(t-z/c)} \tag{4.6}$$

The angular frequency ω_n is given by $n\omega_1$, where $\omega_1 = 2\pi \mathrm{FHR}/60$, and FHR is the foetal heart rate in beats per minute and A_n is the amplitude of each harmonic of the Fourier decomposition of the time domain pressure pulse. The form of the solution for the steady (A_0) and unsteady $\left(A_n e^{i\omega_n(t-z/c)}\right)$ components differ and these are discussed separately, beginning with an examination of the unsteady components.

4.2 Unsteady flow solution

The equations for the fluid motion must be solved along with equations governing the arterial wall motion and its interaction with the fluid. A proper description of the behaviour of the vessel wall requires the examination of many assumptions. These concern the elasticity or viscoelasticity of the wall, the wall thickness, wall compressibility, wall isotropy and wall loading or constraint. The most widely cited work on the linearised pressure-flow relationship in an artery was performed by Womersley in a series of papers (1955a, 1955b, 1957a, 1957b). The first paper dealt with flow in a rigid cylindrical tube. In turn, the papers then dealt with the introduction of an elastic vessel wall, external loading and constraint and lastly both a viscous and elastic wall. In order to simplify his solution, Womersley restricted the arterial wall to be an isotropic material and limited the wall thickness to radius ratio (h/a_0) to be $<<1$. Two further linearised equations governing the motion of the vessel wall were introduced based upon classical mechanical considerations and a solution was formulated by equating the fluid and wall motion at the fluid-wall interface resulting in a system of 4 homogenous linear algebraic equations in 5 unknowns. This system of equations was simplified by a further approximation which required $\omega a_0/c << 1$, which is a valid enough assumption in most arteries. The 5th unknown, the wave speed, was determined by the condition that for the system of equations to have a solution, the determinant of the coefficient matrix must be equal to zero. This results in what is termed a *frequency equation* as it is responsible for the determination of the wave speed. These frequency equations occur in many forms of the solutions for the linearised two-dimensional system of pressure-flow equations. Knowledge of the complex wave speed allows for determination of the remaining coefficients and thus the full solution is developed. Use of the term 'complex-wave velocity' may be misleading and for clarification purposes, it may be represented by

$$\frac{1}{c} = \frac{b - ia}{\omega} \tag{4.7}$$

where a is the *attenuation constant* and b the *phase constant*. The speed with which the pressure pulse travels will be given by ω/b (Milnor, 1989). Womersley's final solution will be presented here. It has been chosen as one of the basic arterial models to be used in this model as it provides a good starting point for discussion of more elaborate models. The unsteady solution

for the axial velocity is

$$w_n(r,z,t) = \frac{A_n}{\rho c}\left(1 + m\frac{J_0\left(\alpha_0 \frac{r}{a_0}\right)}{J_0(\alpha_0)}\right) e^{i\omega_n(t-z/c)} \tag{4.8}$$

where $m = \frac{2+x(2\sigma-1)}{x(F_{10}-2\sigma)}$, $\alpha_0^2 = i^3\alpha^2$, $x = \frac{Eh}{(1-\sigma^2)a_0\rho c^2}$, $F_{10} = \frac{2J_1(\alpha_0)}{\alpha_0 J_0(\alpha_0)}$, ρ is the density, σ is Poisson's ratio, E is Young's modulus, $J_0(x)$ and $J_1(x)$ are Bessel functions of the first kind of order 0

and 1 respectively and of argument x, and c is the solution to the frequency equation :

$$4(1-F_{10})\left(\frac{c_0}{c}\right)^4+\left(\frac{2}{1-\sigma^2}\right)\times\left(-k(1-F_{10})+F_{10}\left(2\sigma-\frac{1}{2}\right)-2\right)\times\left(\frac{c_0}{c}\right)^2+F_{10}+2k=0 \tag{4.9}$$

where $c_0^2=\left(\frac{Eh}{2a_0\rho}\right)$ and h is the wall thickness, $k=\frac{\rho_t h}{\rho a_0}$ and ρ_t is the wall density. The effect of the surrounding tissues is incorporated into this solution by the inclusion of an elastic constraint in the longitudinal equation of motion of the wall. Womersley found that the only adjustment in this case to his solution was to use k' instead of k, where

$$k'=\frac{\rho_t h}{\rho a_0}\left(1-\frac{M^2}{\omega^2}\right) \tag{4.10}$$

in which M is the natural frequency of the constraint. Viscoelastic behaviour of the blood vessel wall was introduced by substituting the Young's modulus of elasticity by a complex viscoelastic modulus defined as $E_c=E(1+i\omega\Delta E)$, where $\omega\Delta E=\tan\phi$ and ϕ is the angle between pressure and radial distension for a sinusoidal input. Taylor (1966) demonstrated the importance of including visco-elasticity into the arterial walls and offered an empirical relation to represent the viscoelasticity :

$$E=|E|\,e^{i\phi_0\left(1-e^{-\omega}\right)} \tag{4.11}$$

where $|E|$ is the static Young's modulus and according to Taylor, ϕ_0 generally varies between 0 and 30. Peterson et al. (1960) , Patel et al. (1969), Bergel (1961) , Gow and Taylor (1968) and Pearson et al. (1994) measured h/a_0 in various arteries and found that the ratio lay between 0.1 and 0.15. Hill et al. (1995) measured h/a_0 in the umbilical artery in foetal sheep and found it to be 0.34, while Bruch et al. (1997) used sonography to measure the h/a_0 ratio in the umbilical artery of human foetuses and recorded this as 0.3. Given these values, it is clear that Womersley's restriction on wall-thickness is not applicable to all the arteries that will be considered. A thin wall assumption incorrectly predicts the wave velocity in a vessel. Bergel (1961) derived an alternative expression for the wave velocity in a thick walled tube, and this is given by :

$$c_0^2=\frac{E\left(a_{outer}^2-a_{inner}^2\right)}{3\rho a_{outer}^2} \tag{4.12}$$

where a_{outer} and a_{inner} are the outer and inner radii of the arterial wall. Inclusion of this correction for c_0 in Womersley's equations, reduces the error when applying them to thick-walled tubes. An *isotropic* elastic material is one where the elastic properties are independent of the direction in which force is applied. However, measurements made by Patel et al. (1969) indicate that this relationship does not hold with arteries and thus they are to be considered as

an *anisotropic* or *orthotropic* material. Patel et al. (1969) demonstrated that the error incurred on pressure-flow and wave velocity relationships through an assumption of isotropy was small. However, anisotropy does become important when considering shear stresses. Patel's study took place on the aorta of a dog and it is possible that the effects of isotropy on human foetal vessels may be more relevant. Womersley's model assumed the vessel wall to be isotropic and thus cannot be used to study the effect of isotropy. A convenient way to determine the relevancy of a particular parameter is to examine the flow behaviour under certain assumptions and then to compare this behaviour with the changes that occur as a result of relaxing or dropping those assumptions. One of the criteria for which no experimental or theoretical studies have been performed on human foetal vessels is that concerning the isotropic nature of the vessel. Three papers deal with anisotropic thin walled vessels and thus could serve as a useful comparison with Womersley's model to determine the effect of anisotropy. The first is a paper by Atabek (1968) who extended the results of the work by Atabek and Lew (1966) to include orthotropic and tethering effects. Atabek's work is essentially similar to Womersley's but differs in the choice of the form of longitudinal tethering (tube is constrained by an additional mass, dashpot and spring), as well as the fact that the artery is considered to be initially stressed. Dropping the initial stresses and assuming isotropy, allows his solution to reduce to the exact same one as Womersley's. The other two papers dealing with anisotropy are by Schwerdt and Constantinesco (1975) and by Tsangaris and Drikakis (1989), and these two are essentially similar. They assume prestressed arteries but do not include tethering and the form of their equations and their solution for the arterial wall differ quite considerably and thus do not make for an easy comparison with Womersley's solution. Mirsky (1968) developed a solution for a longitudinally tethered, orthotropic, thick walled vessel. Equations allowing a numerical evaluation of the wave velocity were presented, however no solution was offered for determining the flow from a measured pressure gradient and thus we cannot make use of Mirsky's solution. In comparing the results of calculated wave velocity, Atabek (1968) reported that the largest difference between his and Mirsky's solution was less than 3%. A further difficulty with Womersley's solution concerns the representation of the external constraint by an additional constant, M. This represents the combined influence of longitudinal tethering and loading by the surrounding tissues and unfortunately no clear guidelines are available to determine a realistic value. Atabek's model offers an alternative and more detailed representation of the tethering effects and also takes into consideration prestressed arteries. For these reasons and that of anisotropy, Atabek's solution has been chosen to assess these effects on foetal FVW indices and the solution is presented here as follows : His solution for the axial velocity is of the same form as equation (4.8) and is :

$$w_n(r,z,t) = \frac{A_n}{\rho c}\left(1 + m\frac{J_0\left(\alpha_0 \frac{r}{a_0}\right)}{J_0(\alpha_0)}\right) e^{i\omega_n(t-z/c)} \tag{4.13}$$

but where the definition for m differs and is defined as

$$m = \frac{\left[2\gamma_2\sigma_\theta - (1-\tau_\theta)\right] c_0^2/c^2 + 1 - \gamma_2\sigma_\theta^2}{\left[(1-\tau_\theta)\, F_{10} - 2\gamma_2\sigma_\theta\right] c_0^2/c^2} \tag{4.14}$$

and where the complex wave-speed is determined by the frequency equation

$$\frac{4\,(1-F_{10})}{\left(1-\gamma_2\sigma_\theta^2\right)^2}\left[\gamma_1\,(1-\tau_\theta) - \gamma_2\sigma_\theta\,(\gamma_1\sigma_\theta + \tau_t - \tau_\theta)\right]\frac{c_0^4}{c^4} +$$

$$\frac{2}{1-\gamma_2\sigma_\theta^2}\left[-k\,(1-F_{10})\,(1-\tau_\theta) + F_{10}\left((\gamma_1+\gamma_2)\,\sigma_\theta + \tau_t - \frac{1}{2}\tau_\theta - \frac{1}{2}\right) - 2\gamma_1\right]\frac{c_0^2}{c^2} +$$

$$F_{10} + 2k = 0 \tag{4.15}$$

and where $\tau_\theta = T_{\theta_0}/\left[E_\theta h/\left(1-\gamma_2\sigma_\theta\right)\right]$, $\tau_t = T_{t_0}/\left[E_\theta h/\left(1-\gamma_2\sigma_\theta^2\right)\right]$, $F_{10} = \frac{2J_1(\alpha_0)}{\alpha_0 J_0(\alpha_0)}$, $c_0 = \left(\frac{E_\theta h}{2a_0\rho}\right)^{1/2}$, $k = M - i\frac{C}{\alpha^2} - \frac{K}{\alpha^4}$, E_θ and E_t are Young's moduli in the circumferential and longitudinal directions respectively, σ_θ and σ_t are the corresponding Poisson's ratios, $\gamma_1 = E_t/E_\theta$, $\gamma_2 = \sigma_t/\sigma_\theta$, T_{t_0} and $T_{\theta_0} = p_0 a_0$ are initial stresses in the longitudinal and circumferential directions and p_0 is the initial circumferential pressure. The total tethering is represented by k with $M = M_0/a_0\rho$, $M_0 = \rho_0 h + M_a$, $C = C_l a_0/\mu$, $K = K_l a_0^3\rho/\mu^2$. K_l, C_l and M_a represent respectively (per unit area) the spring coefficient, frictional coefficient of dashpot, and additional mass of the mechanical model of longitudinal tethering. Although Atabek did not consider the viscoelasticity of the arterial wall, this may easily be included by the introduction of a complex Young's modulus. Unfortunately both Womersley's and Atabek's models are limited by the requirement of the so-called thin-walls ($h/a_0 << 1$). Even with the correction for this offered by equation (4.12), accuracy may still be limited and thus it becomes necessary to investigate thick-walled models so that the importance of relaxing or including this requirement may be assessed. Thick walled models have been proposed by Whirlow and Roleau (1965), Jager et al. (1965), Klip et al. (1967), Mirsky (1968), Cox (1968) and Dinnar (1975, 1981) . The general effect of a thicker wall is to increase the value of the complex wave speed. These models essentially proceed in the same manner as Atabek's and Womersley's models and often include a more complicated frequency equation in more than 4 dimensions, resulting in computational difficulties in evaluating the wave speed. Many of these authors do not present equations for the determination of flow from the pressure gradient and their work is limited to the calculation of the wave velocity. Dinnar (1975) further extended this type of solution by considering a model for the flow consisting of three distinct regions as shown in Figure (4.2) : Region I - the fluid, Region II - the visco-elastic tube and Region III - the surrounding visco-elastic tissues. This necessitated the solution of the complete elastic equation for the tube, solved simultaneously with the elastic equation for tissue motion, with matched boundary conditions at both fluid-wall and wall-tissue interfaces. The additional boundary condition was a radiation condition of waves in the out-going direction only and diminishing stresses. His model is attractive to use as it

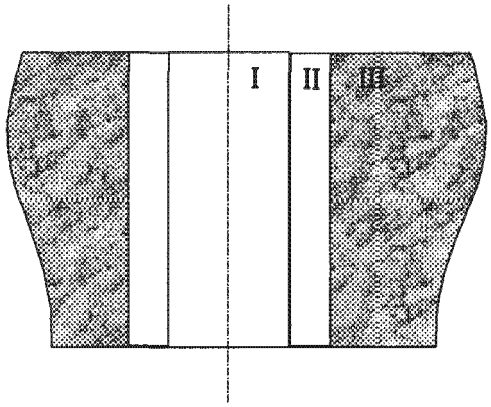

Figure 4.2: The three regions used in the formulations of Dinnar's model. Region I is the fluid, region II is the viscoelastic tube and region III is the surrounding tissues.

allows for a variable wall thickness and includes the most realistic model of the tissue constraint considered thus far. The form of his solution is once again similar to that of Womersley's and Atabek's and due to these conditions has been chosen to be used as a third fundamental arterial model for the foetal model. It is presented here as follows :

The axial flow is once again the same as equation (4.8) and is given as

$$w_n(r,z,t) = \frac{A_n}{\rho c}\left(1 + m\frac{J_0\left(\alpha_0 \frac{r}{a_0}\right)}{J_0(\alpha_0)}\right) e^{i\omega_n(t-z/c)} \tag{4.16}$$

where m is now a function given by

$$m = \frac{1}{F_{10} - 2\nu}\left(\frac{2}{x} + 2\nu - 1\right) \tag{4.17}$$

and x is given by the solution to

$$\left(1-\nu^2\right)x = G \pm \sqrt{G^2 - H'\left(1-\nu^2\right)} \tag{4.18}$$

with $G = \frac{\frac{5}{4}-\nu}{1-F_{10}} + k' + \nu - \frac{1}{4}$, $H' = \frac{1+2k'}{1-F_{10}} - 1$ and $k' = \frac{h\rho_w}{\rho}\left(1 - \frac{k}{\rho h^2}\right)$.
The complex wave-speed is determined from

$$c = c_0\left(3X\frac{1-S}{2S}\right)^{1/2} \tag{4.19}$$

and X is the solution to :

$$\left(\frac{ZS^2}{N} - 1\right)\left(T + f(X) + f(X-1)\right) - R\left(f(X) - f\left(X - \frac{1}{g}\right)\right) = \frac{iR}{g} - \frac{ZS^2}{N}\frac{2\ln S}{\pi} \tag{4.20}$$

The following non-dimensional groups were used : $Z = \frac{g-1}{g+1}$, $S = \frac{a_1}{a_0}$, $T = 0.36746 + i + \frac{1}{\pi}\ln\left(\frac{\alpha\mu\omega}{4\mu_w S^2}\right)$, $N = 1 - \frac{1-F_{10}}{F_{10}}\left(\left(1 - ZS^2\right) + X\left(1 + ZS^2\right)\right)$, $R = \frac{1}{S^2} - 1$, $f(x) = \frac{1}{\pi}x\ln x$, and g is the ratio of the complex visco-elastic Young's modulus for the tissue to that of the vessel wall, a_1 is the outer radius of the wall, μ_w is the wall viscosity, ρ_w the wall density and ρ is the fluid density.

No exact solution exists for the equation for the wave-velocity and thus solution by a numerical, iterative scheme is required. A non-linear least squares implementation of the Levenberg-Marquardt algorithm is well suited to a non-linear problem of this nature and requires minimal computational effort (More, 1977). As this is an iterative routine, an initial estimate is required and the most suitable approximate starting guess is the wave speed determined using Womersley's solution in equation (4.9)

A comparison of the assumptions used by various authors when modelling blood flows indicates that no single author has managed to include a complete, general solution, that considers all possible assumptions. Thus, three different solution formulations have been identified as appropriate tools for the basic arterial building block of the foetal model. Each solution has the same fundamental equation for the flow, requiring that only the values of m and c change when interchanging between methods. (See equations (4.8), (4.13) and (4.16)). The sensitivity of Doppler indices to wall thickness, wall isotropy and tethering may be investigated using these three models. The final selection of which model to use was based upon a sensitivity analysis of the various parameters.

It is informative to examine the volumetric flow rate and this may easily be obtained by integrating the equation for the flow across the vessel cross section. This yields :

$$Q_n(z,t) = \int_0^{a_0} 2\pi w_n r dr = \pi a_0^2 \frac{A_n}{\rho c}\left(1 + mF_{10}\right) e^{i\omega_n(t - z/c)} \tag{4.21}$$

where Q_n is the instantaneous unsteady volumetric flow rate at harmonic n.

4.3 Steady flow solution

The solution for the steady flow component is less cumbersome than that for the oscillatory or unsteady flow components. Solving the Navier-Stokes equations for a constant pressure gradient and assuming a Newtonian fluid, rigid walls and no-slip at the walls, results in the well known Poiseuille's equation :

$$w_0(r,z,t) = \frac{A_0\left(a_0^2 - r^2\right)}{4\mu} \tag{4.22}$$

where A_0 is the zeroth frequency or constant pressure gradient given by $\frac{\Delta P}{L}$ or $\frac{P(0)-P(L)}{L}$ where L is the length of the artery under consideration, $P(L)$ is the distal pressure and $P(0)$ the proximal pressure. In order to obtain the volumetric flow rate, equation (4.22) may be integrated across the tube cross-section in order to obtain :

$$Q_0 = \int_0^{a_0} 2\pi w_0 r dr = \frac{\pi a_0^4 A_0}{8\mu} \tag{4.23}$$

The steady flow is maintained by a pressure gradient between the proximal and distal ends of an artery. Thus the pressure in the artery is nonuniform and higher at the proximal end than at the distal end. Given that blood vessels are distensible, the high pressure end will distend more than the low pressure end, resulting in a non-uniform diameter, where the degree of nonuniformity or tapering will depend on the flow rate (Fung, 1997). The mathematical development of this idea requires a consideration of the elastic properties of the arterial wall and the formulation given by Kleiner-Assaf et al. (1999) is useful to describe the steady flow in an elastic vessel. Here the arterial wall was assumed to be an isotropic, visco-elastic and thick-walled material and the radius variation as a function of distance along the artery was shown to be :

$$a(z) = \frac{\frac{a_0\sigma}{E}P(z) - a_0}{\frac{a_0}{Eh}\left(1-\frac{\sigma}{2}\right)P(z) - 1} \tag{4.24}$$

Chapter 5 deals with the necessary adjustments to account for this geometric nonuniformity in an artery.

4.4 Forward and reflected waves

The solutions for Womersley's, Atabek's and Dinnar's model are based on the linearised flow equations and the following manipulation of these equations yields further information regarding the nature of these solutions. Discarding the non-linear terms and re-writing equation (4.2) yields:

$$\begin{aligned}
\frac{\partial u}{\partial t} &= -\frac{1}{\rho}\frac{\partial p}{\partial r} + \nu\left(\frac{\partial^2 u}{\partial r^2} + \frac{1}{r}\frac{\partial u}{\partial r} - \frac{u}{r^2} + \frac{\partial^2 u}{\partial z^2}\right) \\
&= -\frac{1}{\rho}\frac{\partial p}{\partial r} + \nu\frac{\partial}{\partial r}\left(\frac{\partial u}{\partial r} + \frac{u}{r}\right) + \nu\frac{\partial^2 u}{\partial z^2} \\
&= -\frac{1}{\rho}\frac{\partial p}{\partial r} + \nu\frac{\partial}{\partial r}\left(-\frac{\partial w}{\partial z}\right) + \nu\frac{\partial^2 u}{\partial z^2} \\
&= -\frac{1}{\rho}\frac{\partial p}{\partial r} - \nu\left(\frac{\partial^2 w}{\partial r \partial z} - \frac{\partial^2 u}{\partial z^2}\right)
\end{aligned} \tag{4.25}$$

Now taking time derivatives of either side of the equation of continuity, equation (4.3) yields:

$$\begin{aligned}\frac{\partial}{\partial t}\left(\frac{\partial u}{\partial r}+\frac{u}{r}\right) &= \frac{\partial^2 u}{\partial t \partial r}+\frac{1}{r}\frac{\partial u}{\partial t} \\ &= -\frac{1}{\rho}\frac{\partial^2 p}{\partial r^2}-\nu\left(\frac{\partial^3 w}{\partial r^2 \partial z}-\frac{\partial^3 u}{\partial z^2 \partial r}\right)+\frac{1}{r}\left(-\frac{1}{\rho}\frac{\partial p}{\partial r}-\nu\left(\frac{\partial^2 w}{\partial r \partial z}-\frac{\partial^2 u}{\partial z^2}\right)\right) \\ &= -\frac{1}{\rho}\left(\frac{\partial^2 p}{\partial r^2}+\frac{1}{r}\frac{\partial p}{\partial r}\right)-\nu\frac{\partial w}{\partial z}\left(\frac{\partial^2 w}{\partial r^2}+\frac{1}{r}\frac{\partial w}{\partial r}\right)+\nu\frac{\partial^2}{\partial z^2}\left(\frac{\partial u}{\partial r}+\frac{u}{r}\right) \qquad (4.26)\end{aligned}$$

and

$$\begin{aligned}\frac{\partial}{\partial t}\left(-\frac{\partial w}{\partial z}\right) &= -\frac{\partial}{\partial z}\left(\frac{\partial w}{\partial t}\right) \\ &= \frac{1}{\rho}\frac{\partial^2 p}{\partial z^2}-\nu\left(\frac{\partial^2}{\partial r^2}+\frac{1}{r}\frac{\partial}{\partial r}+\frac{\partial^2}{\partial z^2}\right)\frac{\partial w}{\partial z} \qquad (4.27)\end{aligned}$$

equating and simplifying left and right hand sides :

$$\begin{aligned}-\frac{1}{\rho}\left(\frac{\partial^2 p}{\partial r^2}+\frac{1}{r}\frac{\partial p}{\partial r}\right)-\nu\frac{\partial w}{\partial z}\left(\frac{\partial^2 w}{\partial r^2}+\frac{1}{r}\frac{\partial w}{\partial r}\right)+\nu\frac{\partial^2}{\partial z^2}\left(\frac{\partial u}{\partial r}+\frac{u}{r}\right) = \\ \frac{1}{\rho}\frac{\partial^2 p}{\partial z^2}-\nu\left(\frac{\partial^2}{\partial r^2}+\frac{1}{r}\frac{\partial}{\partial r}+\frac{\partial^2}{\partial z^2}\right)\frac{\partial w}{\partial z} \qquad (4.28)\end{aligned}$$

implies

$$\frac{\partial^2 p}{\partial z^2}+\frac{\partial^2 p}{\partial r^2}+\frac{1}{r}\frac{\partial p}{\partial r}=\mu\frac{\partial^2}{\partial z^2}\left(\frac{\partial u}{\partial r}+\frac{u}{r}+\frac{\partial w}{\partial z}\right)=0 \qquad (4.29)$$

as the right hand side is the equation of continuity which is equal to zero.

Equation (4.29) may be solved using a separation of variables technique as follows :
Let

$$p(t,r,z)=p_t(t)\,p_r(r)\,p_z(z) \qquad (4.30)$$

then :

$$-\frac{1}{p_z}\frac{\partial^2 p_z}{\partial z^2}=\frac{1}{p_r}\left(\frac{\partial^2 p_r}{\partial r^2}+\frac{1}{r}\frac{\partial p_r}{\partial r}\right) \qquad (4.31)$$

Since the left hand side is a function of z and the right hand side is a function of r only and they are equal, they must therefore be equal to a constant, k^2 :
i.e.

$$\frac{\partial^2 p_z}{\partial z^2}+k^2 p_z=0 \qquad (4.32)$$

and solving this yields :

$$p_z(z) = A_1 e^{ikz} + A_2 e^{-ikz} \tag{4.33}$$

In other words this demonstrates that the pressure pulse propagating along the z axis is the sum of a wave travelling in the forward direction and one in the reverse direction. The form of solution presented for Womersley, Atabek and Dinnar is for an infinitely long tube with no reflections. As show in equation (4.33), reflected waves will be present for finite arteries with some termination. Transmission line theory is well developed and suited to handle reflected wave phenomena propagating along a medium and thus a transmission line analogy of the equations which have been developed thus far will now be formulated. It should be noted that the reflected waves are only present for the unsteady or oscillatory flow harmonics and that the steady flow component has no reflections.

4.5 Transmission line formulations

The steady flow term contains no reflections and thus a transmission line formulation needs only to focus on the development of the unsteady flow components. This development is for a uniform transmission line and modifications for subsequent nonuniformities are considered in chapters 6 and 7.

4.5.1 Unsteady flow

The solution for the flow is now built into a transmission line equivalent analogy for a single terminated arterial segment of length l. Proceeding with definitions for the longitudinal and transverse impedance (Milnor, 1989) evaluated in terms of the pressure and flow from equations (4.6) and (4.8).

The longitudinal impedance for each harmonic is defined as

$$Z_L = \frac{-dP/dz}{Q} = \frac{i\omega_n \rho}{\pi a_0^2 (1 + mF_{10})} \tag{4.34}$$

The transverse or wall impedance is defined as

$$Z_W = \frac{P}{-dQ/dz} = \frac{\rho c^2}{i\omega_n (1 + mF_{10}) \pi a_0^2} \tag{4.35}$$

The characteristic impedance is easily defined in terms of these impedances as

$$Z_0 = \sqrt{Z_L Z_W} = \frac{\rho c}{(1 + mF_{10}) \pi a_0^2} \tag{4.36}$$

and the propagation constant is given by

$$\gamma = \sqrt{\frac{Z_L}{Z_W}} = \frac{i\omega_n}{c} = a + ib \tag{4.37}$$

Following the transmission line derivations in Chipman (1968), the $e^{i\omega t}$ is discarded from the expressions for pressure and flow and only phasors are considered. Taking into account the reflected waveforms, the form for the pressure at any point along the arterial segment may be obtained from equation (4.33) and written as :

$$P = P_f e^{-\gamma z} + P_r e^{\gamma z} \tag{4.38}$$

and the expression for total volumetric flow including reflections is

$$\begin{aligned} Q &= \frac{1}{Z_0}\left(P_f e^{-\gamma z} + P_r e^{\gamma z}\right) \\ &= Q_f e^{-\gamma z} - Q_r e^{\gamma z} \end{aligned} \tag{4.39}$$

This gives the corresponding relations :

$$Q_f = \frac{P_f}{Z_0} \tag{4.40}$$

and

$$Q_r = \frac{P_r}{Z_0} \tag{4.41}$$

Thus it may be seen that the characteristic impedance, Z_0, is the input impedance of the artery if no reflections are present. Assuming that an arterial segment terminates in an impedance given by Z_t, then a terminal reflection coefficient may be defined as

$$\Gamma_t = \frac{Z_t - Z_0}{Z_t + Z_0} \tag{4.42}$$

Similarly the input impedance of the arterial segment will then be given by

$$Z_{in} = Z_0 \frac{(Z_t + Z_0)\, e^{\gamma l} + (Z_t - Z_0)\, e^{-\gamma l}}{(Z_t + Z_0)\, e^{\gamma l} - (Z_t - Z_0)\, e^{-\gamma l}} \tag{4.43}$$

4.6 Summary

The model divides the foetal arterial system into a number of functional compartments, each composed of a set of fundamental building blocks designed to accurately calculate the resultant flow in response to an imposed pressure gradient. Many previous studies have developed in varying detail the relationship between pressure and flow in a cylindrical tube subject to a variety of simplifying assumptions. The selection of a particular solution for the basic arterial segment

is of fundamental importance as this forms the foundation for the subsequent development of the foetal model. Therefore a careful examination of the assumptions specifically relevant to the unique haemodynamics. of the foetal system were considered in order that the most appropriate model be selected. Three models that were expressed in the same basic format were elected as they satisfied most of the necessary conditions. These solutions were described after the primary authors who developed them and they are Womersley's, Atabek's and Dinnar's models.

Defining characteristics of these models are that they are all linearised solutions to the two-dimensional, Navier-Stokes equations. They all assume that the blood flow is axisymmetric, pulsatile and laminar, and that the blood is an incompressible Newtonian fluid. The assumptions pertaining to the arterial wall differ slightly between the three models. Womersley's model assumes a thin-walled, isotropic, visco-elastic model with no initial stresses, where the effect of the surrounding tissues and longitudinal tethering is simply modelled as an additional elastic constraint. Atabek's model uses the same basic model as Womersley, but is adapted to include arterial anisotropy and initial stresses. In addition the tethering and influence of surrounding tissue are modelled in a more detailed manner by a uniformly distributed additional mass, dash-pot and spring. Dinnar's model differs in that a more comprehensive model of the surrounding visco-elastic tissues was formulated and that the model considered the arterial wall as a thick-walled model. This model assumed an isotropic wall with no initial stresses. Womersley's and Atabek's model were subsequently adapted to relax the thin-walled constraint. All three models assume sufficiently long and straight arteries, so that no entrance effects or non-linear components due to nonuniform geometries are obtained. The motivation for the selection of three basic arterial models was to compare the effects of different models of isotropy, longitudinal tethering and the influence of surrounding tissues on the foetal arterial system. All three models calculate flow in the frequency domain by Fourier decomposition of the time domain driving pressure gradient into frequency dependent oscillatory components superimposed on a steady flow component. In addition, all three models utilise the same form for the steady flow component, which is essentially Poiseuille's equation. These equations will all require further adaptations to take into account the effects of arterial non-uniformities and this is dealt with in chapters 6 and 7.

A simple manipulation of the linearised Navier-Stokes equations demonstrated that the solutions to the equations must consist of both forward travelling and reverse travelling components. This occurrence in arteries is a well known phenomenon, however the particular form of manipulation of the Navier-Stokes equations that lead to this result is, as far as has been assessed by the author, an original method of demonstrating this result. This brief section was included for both the sake of completeness and to present a new means of illustrating reflection phenomena

resulting from the original equations.

In order to concatenate the basic arterial segments into a comprehensive arterial model, the pressure and flow relations were converted into electrical transmission line analogies. This type of analogy is frequently utilised in haemodynamic modelling applications and is particularly advantageous to model the forward and reflected wave phenomenon that are encountered at arterial junctions and impedance mismatches. Furthermore, transmission line models easily facilitate development in the frequency domain.

Chapter 5

Arterial tapering

5.1 Introduction

Blood vessels in the arterial system often have variable cross sectional areas along their lengths due to geometrical tapering. In addition there is also an elastic taper where the lumen radii and wall thickness become progressively smaller and arterial elastic modulus increases towards the periphery. Further taper may also be generated due to elastic deformation of the vessel wall in response to a nonuniform pressure gradient. Tapering is known to result in a progressive increase in both arterial impedance and pulse wave velocity along the artery. For the purposes of the model developed in this thesis, it is necessary to evaluate and incorporate the effect that tapering has on the actual FVW's as measured by Doppler ultrasound.

A number of authors have investigated flow in tapered arteries and this was discussed in Chapter 4. Most of these works focused on tapered models to analyse impedance and local reflection factors. However, no one has as yet provided a clear and uncomplicated way of calculating velocities along the tapered arterial segment. Furthermore, the solutions that do exist for analysing impedance and local reflections often make use of cascaded or segmented models. These increase the error and the computational time and both elastic and geometric tapering are never considered together.

It is known that the foetal aorta exhibits both a radial and elastic taper along its length and thus it is necessary for the proposed foetal model to account for variations in velocity and impedance caused by this taper. Neglecting this will result in lower velocities and impedances than are actually present. Furthermore, the effect of taper on Doppler indices of FVW's may be investigated. It is unknown whether the umbilical artery exhibits any form of tapering (geometric or elastic) and future clinical measurements may indeed demonstrate the existence of such tapering, in which case an analytical model that easily accounts for tapering would be

a useful tool.

The development of a theoretical tool that accounts for the inclusion of arterial tapering in blood flow velocity determinations has widespread use beyond the foetal model. In general, Doppler ultrasound is frequently used to produce time varying waveforms for subsequent clinical diagnosis of arterial pathologies (Griffin et al. 1983; Macpherson et al. 1984; Sherriff et al. 1982). Computational models of these arterial systems offer a useful tool to theoretically investigate such pathologies. These models provide an aid for further interpretation of clinical Doppler measurements and may offer insight and understanding into causal mechanisms. Thus it is necessary to produce models with greater accuracy. As the degree of tapering may alter the blood flow velocity, it is necessary to be able to account for this variation in a theoretical model.

Furthermore, the accurate determination of blood flow velocity is advantageous in order to gain a greater insight into shear stresses along the arterial wall, as these stresses play an important role in degenerative arterial diseases (Caro et al 1971; Fry et al 1968). Many proposed systemic circulatory models are based upon electrical transmission line analogies. (Westerhof et al, 1969; Avolio 1980; McIlroy et al 1986; Mo et al 1988; Hill et al 1995) . Thus a transmission line representation of a solution that accounts for the effects of tapering offers a convenient and useful tool for refining these models in order to improve their accuracy.

In this thesis a method which is based on non-uniform transmission line theory has been developed to determine the flow velocity in a tapered artery at any point along the artery. A linearised solution of the two-dimensional Navier-Stokes flow equations is represented in the form of transmission line equations and then the final result is presented in a closed form expression which may easily be incorporated into existing transmission line models. Exact analytical expressions for the input impedance, reflection coefficients and flow velocities are presented.

5.2 Theoretical formulation

The transmission line equations presented in chapter 4 provide a convenient starting point for the development of a tapered transmission line solution. Once again, it is possible to write separate solutions for the oscillatory and constant flow components obtained by Fourier analysis.

5.3 Oscillatory flow

A short arterial segment of length L, terminated by a complex impedance Z_t, with a total source pressure and flow given by P_s and Q_s respectively, is depicted in figure (5.1). The

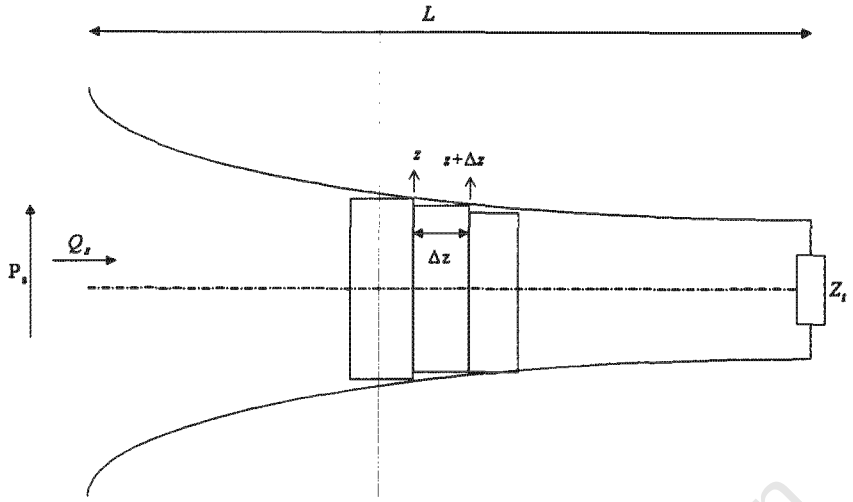

Figure 5.1: Arterial segment of length L, terminating in a load impedance, Z_t. The source pressure and flow are denoted by P_s and Q_s respectively. The artery is approximated by a series of small constant segments of length Δz.

arterial segment is assumed to have both radial and elastic taper. If both the radius and the Young's modulus taper, then equations (4.36) and (4.37) may be used to determine the characteristic impedance and the propagation constant at the beginning and termination of the arterial segment. Assuming that the characteristic impedance at the beginning of the arterial segment is Z_s and that it is Z_f at the termination, an exponential may be fitted to this, so that the characteristic impedance is now a function of the length variable :

$$Z_0(z) = Z_s e^{hz} \tag{5.1}$$

where $h = \frac{1}{L}\ln\frac{Z_f}{Z_s}$ is a complex number representing the characteristic impedance tapering constant. Similarly, if the propagation constants at the beginning and termination of the segment are γ_s and γ_f respectively, then again fitting an exponential yields a solution for the propagation constant as a continuous function of the distance variable and is

$$\gamma(z) = \gamma_s e^{-qz} \tag{5.2}$$

where $q = -\frac{1}{L}\ln\frac{\gamma_f}{\gamma_s}$is a complex number representing the propagation constant tapering constant. It should be noted that $|Z_0(z)|$ will increase moving towards the termination of the arterial segment and that $|\gamma(z)|$ will decrease and hence the use of the positive and negative exponential forms respectively. No direct measurements of the nature of arterial taper in the human foetal system have been performed. However there is no reason to beleive that this system would behave differently from the adult circulation and thus exponential tapering has been assumed

Derivation of input impedance Riccati equation

To proceed, the non-linear differential equation for input impedance along a tapered artery is derived. This derivation is essentially the same as that found in Collin (1966). Collin assumed a line with no attenuation. i.e. if the propagation constant $\gamma = \alpha + i\beta$, where α is the attenuation constant and β the phase constant, then Collin's solution was derived for $\gamma = i\beta$. Here the same steps are followed, except γ is used instead of just $i\beta$.

Assume the characteristic impedance at the inlet of an arterial segment of length L is Z_0. The tapered segment terminates at distance, L, with a load Z_t. Let Z_{in} be the input impedance at z and $Z_{in} + dZ_{in}$ be the input impedance at $z + dz$. Then

$$Z_{in} = Z_0 \frac{Z_{in} + dZ_{in} + Z \tanh \gamma dz}{Z_0 + (Z_{in} + dZ_{in}) \tanh \gamma dz} \tag{5.3}$$

Assuming γdz to be small, $\tanh \gamma dz$ may be approximated by γdz and then by neglecting products of differential terms and some manipulation :

$$\begin{aligned} Z_{in} &\simeq Z_0 \frac{Z_{in} + dZ_{in} + Z_0 \gamma dz}{Z_0 + (Z_{in} + dZ_{in})\, \gamma dz} \\ &\simeq (Z_{in} + dZ_{in} + Z_0 \gamma dz) \left(1 - \frac{Z_{in}}{Z_0} \gamma dz\right) \\ &\simeq Z_{in} - \frac{Z_{in}^2}{Z_0} \gamma dz + dZ_{in} + Z_0 \gamma dz \end{aligned} \tag{5.4}$$

i.e.

$$\frac{dZ_{in}(z)}{dz} = \gamma(z) \frac{Z_{in}^2(z)}{Z_0(z)} - Z_0(z)\, \gamma(z) \tag{5.5}$$

This is the non-linear differential Riccati equation for the input impedance as a function of the distance variable. Previously, the only solutions to this equation, for all values of z, that have been derived are for a constant propagation constant and assume that the reflection coefficient, $|\Gamma(z)|^2 << 1$. These two assumptions are not always valid and a general solution for exponential tapering is presented in the following section.

Solution procedure

The following transformation allows the differential equation to be linearised :

$$Z_{in} = -\frac{Z_0}{\gamma} \left(\frac{1}{u} \frac{du}{dz}\right) \tag{5.6}$$

Substituting this transformation into equation (5.5) and then using the product and chain rules and noting that Z_0 and γ are both functions of z gives :

$$\frac{d^2u}{dz^2} + \frac{1}{Z_0}\frac{dZ_0}{dz}\frac{du}{dz} - \frac{1}{\gamma}\frac{d\gamma}{dz}\frac{du}{dz} - \gamma^2 u = 0 \tag{5.7}$$

and using the expressions for Z_0 and γ gives :

$$\frac{1}{Z_0}\frac{dZ_0}{dz} = h \tag{5.8}$$

and

$$\frac{1}{\gamma}\frac{d\gamma}{dz} = -q \tag{5.9}$$

therefore equation (5.5) now becomes a linear 2nd order differential equation and substituting in the expression for $\gamma(z)$, this is :

$$\frac{d^2u}{dz^2} + (h+q)\frac{du}{dz} - \gamma_s^2 e^{-2qz}u = 0 \tag{5.10}$$

Once again it is necessary to make a transformation in order to solve this as γ is still a function of z.

Let $y = e^z$ and then using this transformation the differential equation now becomes :

$$e^{2z}\frac{d^2u}{dy^2} + e^z\frac{du}{dy} + e^z(h+q)\frac{du}{dy} - \gamma_s^2 y^{-2q}u = 0 \tag{5.11}$$

or

$$y^2\frac{d^2u}{dy^2} + (h+q+1)\,y\frac{du}{dy} = \gamma_s^2 y^{-2q}u \tag{5.12}$$

This equation requires a further transformation :

Let $\alpha = -(h+q)$ and $x = y^\alpha$ which then results in a new differential equation :

$$x^{2/\alpha}\left(x^{1-2/\alpha}(\alpha-1)\,\alpha\frac{du}{dx} + \left(x^{1-1/\alpha}\alpha\right)^2\frac{d^2u}{dx^2}\right) + (h+q+1)\,x^{1/\alpha}x^{1-1/\alpha}\alpha\frac{du}{dx} = \gamma_s^2 x^{-\frac{2q}{\alpha}}u \tag{5.13}$$

or

$$x(\alpha-1)\,\alpha\frac{du}{dx} + x^2\alpha^2\frac{d^2u}{dx^2} + (h+q+1)\,x\alpha\frac{du}{dx} = \gamma_s^2 x^{-\frac{2q}{\alpha}}u \tag{5.14}$$

Since $\alpha = -(h+q)$, then $\alpha - 1 = -(h+q+1)$ and so the equation reduces to :

$$\frac{d^2u}{dx^2} = \frac{\gamma_s^2}{(h+q)^2}x^{-2\frac{h}{h+q}}u \tag{5.15}$$

This is the Emden-Fowler equation, where a solution may be found in Polyanin and Zaitsev (1995) and this is :

$$u(x) = \sqrt{x}\left(C_1 I_{\frac{h+q}{2q}}\left(\frac{\gamma_s}{q}x^{\frac{q}{h+q}}\right) + C_2 K_{\frac{h+q}{2q}}\left(\frac{\gamma_s}{q}x^{\frac{q}{h+q}}\right)\right) \tag{5.16}$$

where C_1 and C_2 are arbitrary constants and $I_{\frac{h+q}{2q}}\left(\frac{\gamma_s}{q}x^{\frac{q}{h+q}}\right)$ and $K_{\frac{h+q}{2q}}\left(\frac{\gamma_s}{q}x^{\frac{q}{h+q}}\right)$ are modified Bessel functions of order $\frac{h+q}{2q}$ and argument $\frac{\gamma_s}{q}x^{\frac{q}{h+q}}$ of the 1st and second kinds respectively. As both h and q are complex variables, special attention to the evaluation of the modified Bessel functions for complex order and argument are required. Appendix C describes an efficient algorithm used to evaluate these functions.

Given that x was defined as $y^{\alpha} = y^{-h-q} = y^{-(h+q)}$, substituting this back into the solution yields :

$$u(y) = \sqrt{y^{-(h+q)}}\left(C_1 I_{\frac{h+q}{2q}}\left(\frac{\gamma_s}{q}y^{-q}\right) + C_2 K_{\frac{h+q}{2q}}\left(\frac{\gamma_s}{q}y^{-q}\right)\right) \tag{5.17}$$

and y was defined as e^z so substituting this back into the solutions yields :

$$u(z) = \sqrt{e^{-z(h+q)}}\left(C_1 I_{\frac{h+q}{2q}}\left(\frac{\gamma_s}{q}e^{-qz}\right) + C_2 K_{\frac{h+q}{2q}}\left(\frac{\gamma_s}{q}e^{-qz}\right)\right) \tag{5.18}$$

Lastly this must be converted back from $u(z)$ to $Z_{in}(z)$ and using the substitution from equation (5.6), this simplifies to :

$$Z_{in}(z) = \frac{Z_s}{\gamma_s}e^{(h+q)z}\frac{\left(\begin{array}{l} C_1\left(I_{\frac{1}{2}\frac{h+q}{q}}\left(\frac{\gamma_s}{q}e^{-qz}\right)h + I_{\frac{1}{2}\frac{h+q}{q}}\left(\frac{\gamma_s}{q}e^{-qz}\right)q + I_{\frac{1}{2}\frac{h+3q}{q}}\left(\frac{\gamma_s}{q}e^{-qz}\right)\gamma_s e^{-qz}\right) + \\ C_2\left(K_{\frac{1}{2}\frac{h+q}{q}}\left(\frac{\gamma_s}{q}e^{-qz}\right)h + K_{\frac{1}{2}\frac{h+q}{q}}\left(\frac{\gamma_s}{q}e^{-qz}\right)q - K_{\frac{1}{2}\frac{h+3q}{q}}\left(\frac{\gamma_s}{q}e^{-qz}\right)\gamma_s e^{-qz}\right) \end{array}\right)}{C_1 I_{\frac{h+q}{2q}}\left(\frac{\gamma_s}{q}e^{-qz}\right) + C_2 K_{\frac{h+q}{2q}}\left(\frac{\gamma_s}{q}e^{-qz}\right)} \tag{5.19}$$

At $z = L$, the termination, $Z_{in}(L) = Z_t$

This may be used to solve for C_1 in terms of C_2 so :

$$Z_t = \frac{Z_s}{\gamma_s}e^{(h+q)L}\frac{\left(\begin{array}{l} C_1\left(I_{\frac{1}{2}\frac{h+q}{q}}\left(\frac{\gamma_s}{q}e^{-qL}\right)h + I_{\frac{1}{2}\frac{h+q}{q}}\left(\frac{\gamma_s}{q}e^{-qL}\right)q + I_{\frac{1}{2}\frac{h+3q}{q}}\left(\frac{\gamma_s}{q}e^{-qL}\right)\gamma_s e^{-qL}\right) + \\ C_2\left(K_{\frac{1}{2}\frac{h+q}{q}}\left(\frac{\gamma_s}{q}e^{-qL}\right)h + K_{\frac{1}{2}\frac{h+q}{q}}\left(\frac{\gamma_s}{q}e^{-qL}\right)q - K_{\frac{1}{2}\frac{h+3q}{q}}\left(\frac{\gamma_s}{q}e^{-qL}\right)\gamma_s e^{-qL}\right) \end{array}\right)}{C_1 I_{\frac{h+q}{2q}}\left(\frac{\gamma_s}{q}e^{-qL}\right) + C_2 K_{\frac{h+q}{2q}}\left(\frac{\gamma_s}{q}e^{-qL}\right)} \tag{5.20}$$

and thus $C_1 = \xi C_2$, where

$$\xi = -\frac{\left(-Z_t\gamma_s + Z_s e^{L(h+q)}(h+q)\right) K_{\frac{1}{2}\frac{h+q}{q}}\left(\frac{\gamma_s}{q}e^{-qL}\right) - Z_s K_{\frac{1}{2}\frac{h+3q}{q}}\left(\frac{\gamma_s}{q}e^{-qL}\right)\gamma_s e^{Lh}}{\left(-Z_t\gamma_s + Z_s e^{L(h+q)}(h+q)\right) I_{\frac{1}{2}\frac{h+q}{q}}\left(\frac{\gamma_s}{q}e^{-qL}\right) + Z_s I_{\frac{1}{2}\frac{h+3q}{q}}\left(\frac{\gamma_s}{q}e^{-qL}\right)\gamma_s e^{Lh}} \tag{5.21}$$

Substituting this relation back into equation (5.19) and simplifying gives

$$Z_{in}(z) = \frac{Z_s}{\gamma_s}e^{(h+q)z}\left(h+q+\gamma_s e^{-qz}\frac{\xi I_{\frac{1}{2}\frac{h+3q}{q}}(\beta) - K_{\frac{1}{2}\frac{h+3q}{q}}(\beta)}{\xi I_{\frac{h+q}{2q}}(\beta) + K_{\frac{h+q}{2q}}(\beta)}\right) \tag{5.22}$$

where $\beta = \frac{\gamma_s}{q}e^{-qz}$.

The input impedance of the arterial segment is given by $Z_{in}(0)$ and is

$$Z_{in}(0) = \frac{Z_s}{\gamma_s}\left(h+q+\gamma_s\frac{\xi I_{\frac{1}{2}\frac{h+3q}{q}}\left(\frac{\gamma_s}{q}\right) - K_{\frac{1}{2}\frac{h+3q}{q}}\left(\frac{\gamma_s}{q}\right)}{\xi I_{\frac{h+q}{2q}}\left(\frac{\gamma_s}{q}\right) + K_{\frac{h+q}{2q}}\left(\frac{\gamma_s}{q}\right)}\right) \tag{5.23a}$$

Mathematical verification of solution

The solution may be verified by substituting equation (5.22) back into the equation (5.5) and equating left and right hand sides. This procedure requires calculation of the derivatives of the bessel functions and these are obtained using the following relations for derivatives (McLachlan, 1934)

$$I'_x(z) = \frac{1}{z}\left[xI_x(z) + zI_{x+1}(z)\right] \tag{5.24}$$

$$K'_x(z) = \frac{1}{z}\left[xK_x(z) - zK_{x+1}(z)\right] \tag{5.25}$$

This results in expressions for $I_{x+1}(z)$ and $K_{x+1}(z)$, which may further be simplified using the following recursive relations for bessel functions (Watson, 1948):

$$I_{x-1}(z) - I_{x+1}(z) = \frac{2x}{z}I_x(z) \tag{5.26}$$

$$K_{x-1}(z) - K_{x+1}(z) = -\frac{2x}{z}K_x(z) \tag{5.27}$$

This results in the following relations which are required for verification of the solution.

$$I_{\frac{1}{2}\frac{h+5q}{q}}\left(\frac{\gamma_s}{q}e^{-qz}\right) = I_{\frac{1}{2}\frac{h+q}{q}}\left(\frac{\gamma_s}{q}e^{-qz}\right) - \frac{h+3q}{\gamma_s}e^{qz}I_{\frac{1}{2}\frac{h+3q}{q}}\left(\frac{\gamma_s}{q}e^{-qz}\right) \tag{5.28}$$

$$K_{\frac{1}{2}\frac{h+5q}{q}}\left(\frac{\gamma_s}{q}e^{-qz}\right) = K_{\frac{1}{2}\frac{h+q}{q}}\left(\frac{\gamma_s}{q}e^{-qz}\right) + \frac{h+3q}{\gamma_s}e^{qz}K_{\frac{1}{2}\frac{h+3q}{q}}\left(\frac{\gamma_s}{q}e^{-qz}\right) \tag{5.29}$$

Performing this substitution and simplifying using the above relations verifies that equation (5.22) is indeed an exact solution.

Determination of the flow in a tapered arterial segment

A reflection coefficient that varies as a function of the distance variable may be calculated using

$$\Gamma(z) = \frac{Z_{in}(z) - Z_0(z)}{Z_{in}(z) + Z_0(z)} \tag{5.30}$$

Once the reflection coefficient as a function of the distance variable is known, it is necessary to calculate the forward and reverse flows in the arterial segment. In order to determine the flows, the artery is divided into a series of infinitesimal segments of length Δz as displayed in figure (5.1). The properties of the tube are assumed constant for these short segments.

The total flow at the source of the first segment is

$$Q_s = Q_f(z) - Q_r(z) \tag{5.31}$$

where Q_f and Q_r are forward and reverse flows respectively. The reflection coefficient at the input of this segment is assumed known and is $\Gamma(z)$. From this Q_f and Q_r may be calculated according to

$$Q_f(z) = \frac{Q_s}{1 - \Gamma(z)} \tag{5.32}$$

and

$$Q_r(z) = Q_f(z)\Gamma(z) = Q_s\frac{\Gamma(z)}{1 - \Gamma(z)} \tag{5.33}$$

At the end of this segment, $z + \Delta z$, the forward flow is $Q_f(z + \Delta z) = Q_f(z)e^{-\gamma\Delta z}$ and the reverse flow is $Q_r(z + \Delta z) = Q_r(z)e^{\gamma\Delta z}$. The total flow is now

$$Q(z + \Delta z) = Q_f(z)e^{-\gamma\Delta z} - Q_r(z)e^{\gamma\Delta z} = \frac{Q_s}{1 - \Gamma(z)}\left(e^{-\gamma\Delta z} - \Gamma(z)e^{\gamma\Delta z}\right) \tag{5.34}$$

Following this reasoning, the forward and reflected flows at the end of the next segment are

$$\begin{aligned} Q(z + 2\Delta z) = {} & \frac{Q_s(z)}{1 - \Gamma(z)}\left(e^{-\gamma\Delta z} - \Gamma(z)e^{\gamma\Delta z}\right)\frac{1}{1 - \Gamma(z + \Delta z)}e^{-\gamma(z+\Delta z)\Delta z} - \\ & \frac{Q_s}{1 - \Gamma(z)}\left(e^{-\gamma\Delta z} - \Gamma(z)e^{\gamma\Delta z}\right)\frac{\Gamma(z + \Delta z)}{1 - \Gamma(z + \Delta z)}e^{\gamma(z+\Delta z)\Delta z} = \\ & \frac{Q_s}{1 - \Gamma(z)}\left(e^{-\gamma\Delta z} - \Gamma(z)e^{\gamma\Delta z}\right)\frac{1}{1 - \Gamma(z + \Delta z)}\left(e^{-\gamma(z+\Delta z)\Delta z} - \Gamma(z + \Delta z)e^{\gamma(z+\Delta z)\Delta z}\right) \end{aligned} \tag{5.35}$$

This may be generalised along the entire length of the artery so that the flow at a distance, L, will be given by $z + n\Delta z$ and will be

$$Q(z + n\Delta z) = Q(L) = Q_s\prod_{k=0}^{n}\frac{1}{1 - \Gamma(z + k\Delta z)}\left(e^{-\gamma(z+k\Delta z)\Delta z} - \Gamma(z + k\Delta z)e^{\gamma(z+k\Delta z)\Delta z}\right) \tag{5.36}$$

In the limit as $\Delta z \to 0$, the product $\to 1$ and thus exists. Therefore the product may be written in the form :

$$\prod_{k=0}^{n} f(z) = \prod_{k=0}^{n} (1 + g(z)) \tag{5.37}$$

i.e.

$$Q(L) = Q_s \prod_{k=0}^{n} \left(1 + \frac{1 - \Gamma(z+k\Delta z) - e^{-\gamma\Delta z} + \Gamma(z+k\Delta z)\, e^{\gamma\Delta z}}{\Gamma(z+k\Delta z) - 1}\right) \tag{5.38}$$

Taking logs yields :

$$\begin{aligned} \ln Q(L) &= \ln Q_s + \sum_{k=0}^{n} \ln\left(1 + \frac{1 - \Gamma(z+k\Delta z) - e^{-\gamma(z+k\Delta z)\Delta z} + \Gamma(z+k\Delta z)\, e^{\gamma(z+k\Delta z)\Delta z}}{\Gamma(z+k\Delta z) - 1}\right) \\ &\simeq \ln Q_s + \sum_{k=0}^{n} \left(\frac{-1 + \Gamma(z+k\Delta z) + e^{-\gamma(z+k\Delta z)\Delta z} - \Gamma(z+k\Delta z)\, e^{\gamma(z+k\Delta z)\Delta z}}{1 - \Gamma(z+k\Delta z)}\right) \end{aligned} \tag{5.39}$$

since the power series expansion of $\ln(1+x) \simeq x + O(x^2)$

Expanding $e^{\gamma(z+k\Delta z)\Delta z} \simeq 1 + \gamma(z+k\Delta z)\,\Delta z + O(\Delta z^2)$ and $e^{-\gamma(z+k\Delta z)\Delta z} \simeq 1 - \gamma(z+k\Delta z)\,\Delta z + O(\Delta z^2)$ gives :

$$\ln Q(L) = \ln Q_s - \sum_{k=0}^{n} \frac{1 + \Gamma(z+k\Delta z)}{1 - \Gamma(z+k\Delta z)} \gamma(z+k\Delta z)\,\Delta z \tag{5.40}$$

In the limit as the number of segments tends to ∞ and the length of each segment tends to 0, this becomes a Riemann integral and it is possible to integrate to obtain the flow - i.e.

$$\lim_{\substack{n\to\infty \\ \Delta z \to 0}} \sum_{k=0}^{n} \frac{1 + \Gamma(z+k\Delta z)}{1 - \Gamma(z+k\Delta z)} \gamma(z+k\Delta z)\,\Delta z = \int_0^L \frac{1 + \Gamma(z)}{1 - \Gamma(z)} \gamma(z)\, dz \tag{5.41}$$

Thus

$$\ln Q(L) = \ln Q_s - \int_0^L \frac{1 + \Gamma(z)}{1 - \Gamma(z)} \gamma(z)\, dz \tag{5.42}$$

Using equation (5.30),

$$\frac{1 + \Gamma(z)}{1 - \Gamma(z)} \gamma(z) = \frac{\gamma_s}{Z_s} e^{-z(h+q)} Z_{in}(z) \tag{5.43}$$

So that the integral becomes

$$\int_0^L \frac{\xi(h+q)\, I_{\frac{1}{2}\frac{h+q}{q}}(\beta) + \xi I_{\frac{1}{2}\frac{h+3q}{q}}(\beta)\, \gamma_s e^{-qz} + (h+q)\, K_{\frac{1}{2}\frac{h+q}{q}}(\beta) - K_{\frac{1}{2}\frac{h+3q}{q}}(\beta)\, \gamma_s e^{-qz}}{\xi I_{\frac{h+q}{2q}}(\beta) + K_{\frac{h+q}{2q}}(\beta)} dz \tag{5.44}$$

Let

$$f(z) = \xi I_{\frac{1}{2}\frac{h+q}{q}}\left(\frac{\gamma_s}{q}e^{-qz}\right) + K_{\frac{1}{2}\frac{h+q}{q}}\left(\frac{\gamma_s}{q}e^{-qz}\right) \tag{5.45}$$

then the integral may be expressed as

$$\int_0^L \frac{1}{2}(h+q)\,dz - \int_0^L \frac{f'(z)}{f(z)}dz = \frac{L}{2}(h+q) - \ln\frac{f(L)}{f(0)} \tag{5.46}$$

where

$$f'(z) = -\xi I_{\frac{1}{2}\frac{h+3q}{q}}(\beta)\,q\beta - \frac{1}{2}\xi(h+q)\,I_{\frac{1}{2}\frac{h+q}{q}}(\beta) + K_{\frac{1}{2}\frac{h+3q}{q}}(\beta)\,q\beta - \frac{1}{2}(h+q)\,K_{\frac{1}{2}\frac{h+q}{q}}(\beta) \tag{5.47}$$

and thus the flow at a distance L along the artery is given by the exact solution :

$$\begin{aligned} Q(L) &= \exp\left(\ln Q_s + \frac{L}{2}(h+q) - \ln\frac{f(L)}{f(0)}\right) \\ &= Q_s\frac{f(0)}{f(L)}e^{\frac{L}{2}(h+q)} \end{aligned} \tag{5.48}$$

5.3.1 Constant flow

The steady component of flow has no travelling waves and therefore is only subject to radial taper. The solution for the constant or steady flow component was Pousille's solution and is :

$$Q = \frac{A_0\pi a^4}{8\mu} \tag{5.49}$$

where A_0 is the pressure differential and μ is the viscosity. However, the radius a is now a function of the distance variable z. The computation procedure of the transmission line model is discussed in chapter 9, where it is demonstrated that the steady flow in a particular artery is dependent upon the sum of the resistance of that artery and its terminal resistance, as well as the pressure at the proximal end of the artery. Thus, it is sufficient to obtain an expression for the adjusted resistance of the artery, as this will entail subsequent computation of the flow in the artery. The development of this solution proceeds in the same manner as for the unsteady flow solution and considers a segment of artery of length Δz. For this arterial segment, the input pressure is known and is $P(z)$, the terminal impedance is $Z_{in}(z+\Delta z)$ because the terminal impedance of this segment is the input impedance of the next segment. The resistance of the segment is given by

$$R = \frac{8\mu\Delta z}{\pi a(z)^4} \tag{5.50}$$

and thus the input resistance, R_{in}, is

$$R_{in}(z) = R_{in}(z+\Delta z) + \frac{8\mu\Delta z}{\pi a(z)^4} \tag{5.51}$$

Generalising this to n segments yields :

$$R_{in}(z) = R_{in}(z + n\Delta z) + \frac{8\mu}{\pi}\sum_{k=0}^{n}\left(\frac{1}{a(z+k\Delta z)^4}\right)\Delta z \tag{5.52}$$

and in the limit this becomes an integral and is given by

$$R_{in}(z) = R_t + \frac{8\mu}{\pi}\int_0^L \frac{1}{a(z)^4}dz \tag{5.53}$$

where R_t is the terminal resistance.

For an assumed exponential variation, $a(z) = a_{0s}e^{-pz}$, where $p = -\frac{1}{L}\ln\frac{a_{0f}}{a_{0s}}$ and is a geometric constant representing the degree of radial taper, and a_{0s} and a_{0f} are the radii at the proximal and terminal ends of the arterial segment, then

$$R_{in}(z) = R_t + \frac{8\mu}{\pi}\int_0^L \frac{1}{(a_{0s}e^{-pz})^4}dz = R_t + 2\frac{\mu}{\pi}\frac{e^{4Lp}-1}{pa_{0s}^4} \tag{5.54}$$

At this stage it is necessary to distinguish between the taper which results in an elastic tube as the consequence of an applied nonuniform pressure gradient and that which is an intrinsic anatomical property of the vessel itself. The former kind of taper was discussed in section 4.3 and this results in an additional radial taper over and above the intrinsic radial taper. However from a mathematical viewpoint, they both result in a variation of the radius with the distance variable, given by $a(z)$, and therefore measurement of the radius at the proximal and distal ends of an artery is sufficient information to determine the resistance due to radial tapering. Thus it is assumed that both types of taper are accounted for together in the resultant expression for $a(z)$.

5.4 Summary

The foetal aorta and many of the smaller arteries comprising the peripheral vasculature exhibit varying degrees of geometric and elastic taper along their lengths. These non-uniformities introduce non-linear effects which alter the complex wave velocities, impedance, reflection coefficients and flow velocity waveforms as measured by Doppler ultrasound. In order to incorporate the full effects of tapering on all of these parameters for a transmission line model, it becomes necessary to adapt the original transmission line equations. An exact solution to the previously unsolved non-linear Ricatti equation for the impedance at any point along exponentially tapering geometric and elastic arteries was obtained by a process of original substitutions which facilitated the solution procedure. This solution was further utilised to develop an exact expression for the actual flow velocities at any point along the artery. This expression was obtained by what

is submitted to be an innovative procedure which decomposed a tapered arterial segment into infinitesimal segments of constant properties. The transmission line relations of flow in these segments were subsequently combined into a single integral expression for the entire segment. The exact solution to this integral was consequently evaluated. These solutions were presented in a form compatible with the original transmission line equivalents of the three basic models, thus allowing the effects of arterial tapering to be accurately studied. The scope of these solutions clearly extends beyond the arena of foetal modelling and they may be utilised in any transmission line haemodynamic models that seek to account for arterial tapering. In Chapter 10 a further validation of this theory is produced by comparing the results with those obtained by cascading a number of short segments of transmission line together. The effect of taper on Doppler indices is studied in chapter 11.

Chapter 6

Umbilical artery coiling

6.1 Introduction

Within the umbilical cord, the two umbilical arteries spiral around the umbilical vein along the cords long axis. This helix is well established by the 9th week of gestation and the number of spirals is believed to remain constant throughout the duration of the pregnancy (Degani et al, 1995). The advancement of ultrasound techniques have made it possible to perform cord measurements antenatally. This has allowed a number of researchers to investigate umbilical arterial coiling. The cause of the coiling is poorly understood and is thought to be either due to the passive rotation of the foetus, unequal vascular growth rates, non uniform uterine mechanics, umbilical wall vascular mechanics or foetal movement.

An increased incidence of adverse foetal outcome has been reported in neonates with both hypercoiled or hypocoiled umbilical vessels (Sherer and Anyaegbunam, 1997). Rana et al. (1995) showed that hypocoiled cords are associated with foetal heart rate disturbances and interventional delivery, whilst hypercoiling is well correlated with maternal cocaine use and premature delivery. Strong et al. (1994) proposed the umbilical coiling index (UCI), which is the number of vascular coils per centimeter. Degani et al. (1995) demonstrated a correlation between postpartum assigned UCI values and those obtained sonographically in utero. They also reported no significant correlations between the sonographic UCI and umbilical artery Doppler indices. However, UCI is well correlated with time-averaged velocity and flow in the umbilical vein. Atalla et al. (1998) showed that umbilical venous pH and PCO_2 and umbilical artery pH are related to the UCI, although foetal heart rate decelerations, colour of amniotic fluid, and placental weight are not related to the UCI.

Ercal et al. (1996) demonstrated that when comparing a hypocoiled group with a normocoiled group of foetuses, statistically significant higher incidences of meconium staining, inter-

ventional delivery, apgar scores, fetal blood pH and intrapartum foetal heart rate disturbances occurred. Dado et al. (1997) investigated the association between umbilical cord coiling and perinatal morbidity by applying external compression, twisting and longitudinal compression to cord segments. They concluded that the correlation between poor perinatal outcome and coiling should not be attributed solely to differences in mechanical properties of the cords. Nishio et al. (1999) investigated the effect of coiling in growth-restricted foetuses on haemodynamic blood flow indices in the umbilical artery, vein, abdominal aorta and inferior vena cava. They reported a decrease in resistance index in the umbilical artery in hypercoiled cases, and concluded that the foetal blood flow disturbance due to a hypercoiled umbilical cord may indeed be a cause of growth restriction.

The contradictory findings of Degani et al. (1995) and Nishio et al. (1999) suggest that further investigation is necessary to ascertain the relationship between the coiling index and Doppler indices. A mathematical investigation of the effect of coiling on the haemodynamics. of umbilical arterial flow is useful to understand how coiling effects the flow and flow indices. This chapter develops a theoretical model so that coiling effects may easily be incorporated into a transmission line representation of an arterial segment.

6.2 Background to flow in curved tubes

Blood flowing through a region of curvature in an artery will be affected by centrifugal forces which tend to set up secondary flows in that artery. The nature of these secondary flows have been examined in considerable detail in many past papers. However, very little attention has been directed towards addressing the effects of curvature on the axial flow velocity waveforms (FVW's), which are frequently measured using Doppler ultrasound. It is of significant value to be able to quantify the expected degree of variation of the Doppler waveform with corresponding variations in the curvature. The focus of many papers dealing with the effects of curvature has been motivated by the effect it has on wall shear stresses in relation to atherosclerotic disease and the examination of time varying volumetric axial flow velocity waveforms have largely been neglected.

The earliest studies were conducted by Dean (Dean, 1927; 1928) , who analysed steady laminar flow in a rigid curved pipe by the perturbation method. This was limited to small values of the Dean number, $D_n = (a/R)^{1/2}\,\mathrm{Re}$, where a is the radius of the pipe cross section, R the radius of curvature of the pipe axis and Re is the Reynolds number. Many further theoretical, numerical and experimental studies on this work have been conducted and have extended the range of solution to small, intermediate and large Dean numbers (Topakoglu,

1967; Sankaraiah and Rao, 1973; Li, 1976; Van Dyke, 1978; Barua, 1963; Ito, 1969; Truesdell and Adler, 1970; Austin and Seader, 1973; Tarbell and Samuels, 1973; Manlapaz and Churchill, 1980).

The problem of unsteady flow is more complicated and the simplification of pure oscillatory flow has been considered in many of these studies. This work was initiated by Lyne (1970) who used boundary-layer approximations to solve linearised Navier-Stokes equations for large values of the frequency parameter $\alpha = a(\omega/\nu)^{1/2}$ and both very large and very small values of the parameter $K^2/(Ra\omega^4)$. Here K is proportional to the pressure gradient amplitude, ω is the radial frequency, and ν the kinematic viscosity. This work showed the existence of a four-vortex secondary flow system which could be divided into two regions : a core region in which the flow is essentially inviscid and a boundary region in which viscous effects dominate. The net effect was to shift the maximum axial velocity towards the inner wall of the curvature. Lyne's studies were again for a rigid walled tube.

Zalosh and Nelson (1973) carried out an analysis using finite Hankel transforms and a perturbation solution to linearise the Navier-Stokes equations and confirmed Lyne's results. Mullin and Greated (1980) carried out an essentially parallel analysis using the same solution procedure. Difficulties in these solutions were encountered at high frequencies, due to the lack of convergence of the Inverse Hankel transform and Zapryanov and Matakiev (1980) obtained a closed-form analytic solution for all values of α. Bertelsen and Thorsen (1982) experimentally verified Lyne's findings. Numerical solutions to purely oscillatory flow have been derived by Sudo, Sumida and Yamane (1992).

Oscillatory flow with a mean was investigated by Smith (1975) who again used boundary-layer approximations to derive several different flow attributes ranging between the limiting cases of steady flow in curved tubes to purely oscillatory flow in straight tubes. Simon, Chang and Chow (1977) investigated this using similar perturbation techniques and finite Hankel transforms. Numerical investigations have been conducted by Rabadi, Simon and Chow (1980) and Hamakiotes and Berger (1988, 1990). Chang and Tarbell (1985) provided a complete numerical solution of pulsatile flow but once again their result was for a rigid tube.

The only non-experimental analysis of pulsatile flow in a curved, elastic walled tube was done by Chandran et al. (1974, 1979) , where a thin-walled model was applied to linearised Navier-Stokes equations and a numerical solution used to solve the ensuing equations.

None of the above studies have explicitly demonstrated the effect of the curvature on the axial flow velocity waveform in a curved elastic tube. In this thesis a simple analytical solution is provided for this problem. This solution has widespread use beyond that of investigating the

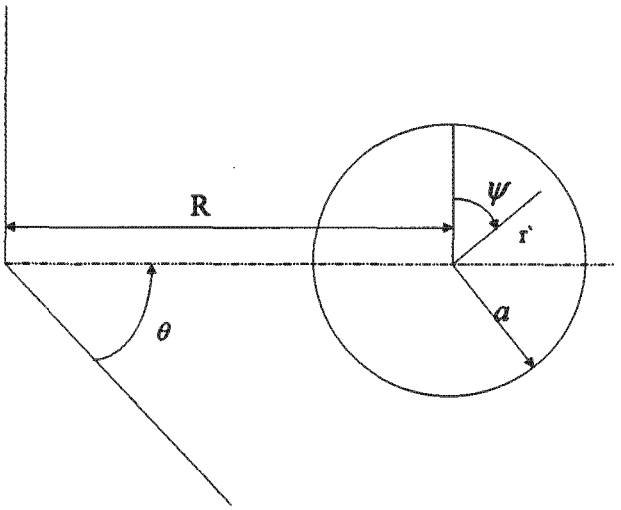

Figure 6.1: Torroidal co-ordinate system.

umbilical artery and may be applied to investigate relationships between variations in curvature with corresponding variations in axial flow velocity as measured by Doppler ultrasound.

6.3 Theoretical analysis

6.3.1 Background

For a given radius of curvature, R, the toriodal coordinate system (r', θ, ψ), shown in Figure (6.1), is used to define the governing differential equations for fully developed, time-dependent flow of a Newtonian fluid in a curved elastic tube. Here a is the radius of the tube. The arterial wall is assumed to be made of a homogenous isotropic material with a constant modulus of elasticity. The continuity and Navier-Stokes equations as well as the equations for the motion of the fluid wall were presented by Chandran (1974) for this case. These equations are given in Appendix A. Chandran simplified these equations by performing an order of magnitude study on the fluid equations, where terms of $O(a/l)$ and $O(w/c)$ were neglected when compared to the leading term. Here l is the wavelength, c the wave velocity of the pulse and w is the axial velocity of the fluid. This led to a set of quasi-linearised equations for the flow which are also presented in Appendix A.

6.3.2 Solution

The solution proceeds from here by considering only those tubes where $R >> a$ and then by non-dimensionalising the system of equations according to the following relationships :

$$\begin{aligned} r &= r'/a \\ U &= u\nu/a \\ V &= v\nu/a \\ W &= w\nu/a \\ P &= P'\rho(\nu/a)^2 \\ t &= t/\omega \end{aligned} \tag{6.1}$$

where ν is the kinematic viscosity.

This results in the following (now non-dimensional) set of relations for the fluid motion:

Continuity equation :

$$\frac{\partial u}{\partial r} + \frac{u}{r} + \frac{1}{r}\frac{\partial v}{\partial \psi} + \lambda u \sin\psi + \lambda v \cos\psi + a\frac{\partial w}{\partial \theta} = 0 \tag{6.2}$$

Momentum equations :

$$\begin{aligned} \alpha^2\frac{\partial u}{\partial t} - \lambda w^2 \sin\psi = &-\frac{\partial P}{\partial r} + a\frac{\partial^2 u}{\partial r^2} + \frac{a}{r}\frac{\partial u}{\partial r} + \frac{1}{r^2}\frac{\partial^2 u}{\partial \psi^2} - \frac{\lambda}{r}v\cos\psi - \lambda^2 2\sin\psi\frac{\partial w}{\partial \theta} + \\ &\lambda\sin\psi\frac{\partial u}{\partial r} + \frac{\lambda}{r}\cos\psi\frac{\partial u}{\partial \psi} - \frac{u}{r^2} - \frac{2}{r^2}\frac{\partial v}{\partial \psi} \end{aligned} \tag{6.3}$$

$$\begin{aligned} \alpha^2\frac{\partial v}{\partial t} - \lambda w^2 \cos\psi = &-\frac{1}{r}\frac{\partial P}{\partial \psi} + \frac{\partial^2 v}{\partial r^2} + \frac{1}{r}\frac{\partial v}{\partial r} + \frac{2}{r^2}\frac{\partial^2 u}{\partial \psi^2} + \frac{\lambda}{r}u\cos\psi + \\ &\lambda\sin\psi a\frac{\partial v}{\partial r} + \frac{\lambda}{r}\cos\psi\frac{\partial v}{\partial \psi} + \frac{1}{r^2}\frac{\partial^2 \nu}{\partial \psi^2} - \frac{v}{r^2} \end{aligned} \tag{6.4}$$

$$\alpha^2\frac{\partial w}{\partial t} = -\frac{1}{\rho}\frac{\partial P}{\partial \theta} + \frac{\partial^2 w}{\partial r^2} + \frac{1}{r}\frac{\partial w}{\partial r} + \frac{1}{r^2}\frac{\partial^2 w}{\partial \psi^2} + \lambda a\sin\psi\frac{\partial w}{\partial r} + \frac{\lambda}{r}\cos\psi\frac{\partial w}{\partial \psi} \tag{6.5}$$

where it is assumed that $R + ar\sin\psi \simeq R$ as $R >> a$, $\lambda = a/R$ and $\alpha = \sqrt{\omega a^2/\nu}$.

A perturbation solution is used to further linearise the equations. As λ was assumed to be small, the dependent variables u, v and w for the flow and η, ξ and ζ for the tube motion, are

expanded in a power series in λ :

$$\begin{aligned} u &= u_0 + \lambda u_1 + \lambda^2 u_2 + ... \\ v &= v_0 + \lambda v_1 + \lambda^2 v_2 + ... \\ w &= w_0 + \lambda w_1 + \lambda^2 w_2 + ... \\ \eta &= \eta_0 + \lambda \eta_1 + \lambda^2 \eta_2 + ... \\ \xi &= \xi_0 + \lambda \xi_1 + \lambda^2 \xi_2 + ... \\ \zeta &= \zeta_0 + \lambda \zeta_1 + \lambda^2 \zeta_2 + ... \end{aligned} \tag{6.6}$$

A similar procedure is performed for the equations for the tube motion.

These expansions are substituted into the flow and tube equations and terms of $O(0)$ and $O(1)$ equated. The ensuing equations for u_0, v_0 and w_0, as well as η_0, ξ_0 and ζ_0 are the same as the linearised two-dimensional straight tube equations and the solution to these is presented by Womersley (1957a). As the $O(0)$ equations are linear, solutions for a constant or steady component and for oscillatory or unsteady components using Fourier analysis may be written. The form of the pressure pulse is a travelling wave with velocity c and for each harmonic, n, is given by equation (4.6), where in this case, $z = R\theta$. The steady component solution is simply Poiseuille's solution and is

$$w_0(r, \theta, \psi, t) = A_0 \frac{a^2 - r^2}{4\mu} \tag{6.7}$$

Writing the solution for the volumetric flow gives

$$Q_0(t) = \frac{A_0 \pi a^4}{8\mu} \tag{6.8}$$

The unsteady solution for the axial velocity is Womersley's solution, presented in equation (4.8) and in dimensionalised notation is

$$w_0(r', \theta, \psi, t) = \frac{A_n}{\rho c} \left(1 + m \frac{J_0\left(\alpha_0 \frac{r'}{a}\right)}{J_0(\alpha_0)} \right) e^{i\omega_n (t - z/c)} \tag{6.9}$$

and the unsteady volumetric flow is

$$Q_0(t) = \pi a^2 \frac{A_n}{\rho c} (1 + m F_{10}) e^{i\omega_n (t - z/c)} \tag{6.10}$$

As the form of equation (6.10) is identical for each of Womersley's, Atabek's or Dinnar's models, the subsequent derivations are applicable to any of these models. Obtaining the solution to the zeroth order set of equations, allows the first order set of equations to be solved. The perturbation solution indicates that the effect of curvature on the axial velocity is thus an additive component and the governing equation is obtained by equating terms of λ :

$$\alpha^2 \frac{\partial w_1}{\partial t} = \frac{\partial^2 w_1}{\partial r^2} + \frac{1}{r} \frac{\partial w_1}{\partial r} + \frac{1}{r^2} \frac{\partial^2 w_1}{\partial \psi^2} + a \sin\psi \frac{\partial w_0}{\partial r} + \frac{1}{r} \cos\psi \frac{\partial w_0}{\partial \psi} \tag{6.11}$$

From the above equation, it may be seen that the additive axial flow contribution w_1 is only dependent on the primary axial flow w_0 and not on the radial and tangential components. The equations for these are :

$$\alpha^2\frac{\partial u_1}{\partial t} - w_0^2\sin\psi = \frac{\partial^2 u_1}{\partial r^2} + \frac{1}{r}\frac{\partial u_1}{\partial r} + \frac{1}{r^2}\frac{\partial^2 u_1}{\partial \psi^2} - \frac{1}{r}v_0\cos\psi + \sin\psi\frac{\partial u_0}{\partial r} + \frac{1}{r}\cos\psi\frac{\partial u_0}{\partial \psi} - \frac{u_1}{r^2} - \frac{2}{r^2}\frac{\partial v_1}{\partial \psi} \tag{6.12}$$

and

$$\alpha^2\frac{\partial v_1}{\partial t} - w_0^2\cos\psi = \frac{\partial^2 v_1}{\partial r^2} + \frac{1}{r}\frac{\partial v_1}{\partial r} + \frac{2}{r^2}\frac{\partial^2 u_1}{\partial \psi^2} + \frac{1}{r}u_0\cos\psi + \sin\psi a\frac{\partial v_0}{\partial r} + \frac{1}{r}\cos\psi\frac{\partial \nu_0}{\partial \psi} + \frac{1}{r^2}\frac{\partial^2 v_1}{\partial \psi^2} - \frac{v_1}{r^2} \tag{6.13}$$

The above equations indicate that for small a/R, first order effects of curvature on the axial flow velocity field (6.11) are only dependent upon the primary axial flow. However, the first order effects of curvature on the radial and tangential components are non-linear and dependent upon each other. Second order effects on the axial flow velocity are non-linear and dependent upon the behaviour of the secondary velocity components. Furthermore, solutions that fall out of the range of validity given by the perturbation limitations will be non-linear and the axial flow velocity will again be dependent on the secondary velocity components as shown by Lyne (1970) and Smith (1975). The solution here will be limited to first order effects of axial flow for small λ and this assumption will be shown to be valid for the umbilical artery.

As the governing equation for first order axial flow is linear (equation 6.11), once again it is possible to divide the solution up into constant and oscillatory components. The solution for the constant or steady flow has been solved by many researchers and the form of solution presented by Manlapaz and Churchill (1980) is used here. They investigated existing solutions for fully developed laminar flow in a coil of finite pitch and finite radius and calculated their own correlating equation as the best overall representation for the experimental data. This is

$$\frac{Q_c}{Q_s} = \left[\left(1 - \frac{0.18}{\left[1+\left(\frac{35}{D_n}\right)^2\right]^{1/2}}\right)^m + \left(1+\frac{\lambda}{3}\right)^2\frac{Dn}{88.33}\right]^{-1/2} \tag{6.14}$$

where $m = 2$ for $D_n < 20$, 1 for $20 < D_n < 40$ and 0 for $D_n > 40$. Q_c is the axial flow in a curved tube and Q_s is the corresponding flow in a straight tube.

To solve the unsteady or oscillatory flow components begin with the non-dimensionalised solution

$$w_0(r,\theta,\psi,t) = \frac{A_n\nu}{c\rho a}\left(1 + m\frac{J_0(\alpha_0 r)}{J_0(\alpha_0)}\right)e^{i\omega_n(t-z/c)} \tag{6.15}$$

As this is independent of ψ it is possible to rewrite the equation for w_1 as

$$\alpha^2 \frac{\partial w_1}{\partial t} = \frac{\partial^2 w_1}{\partial r^2} + \frac{1}{r}\frac{\partial w_1}{\partial r} + \frac{1}{r^2}\frac{\partial^2 w_1}{\partial \psi^2} + a \sin\psi \frac{\partial w_0}{\partial r} \tag{6.16}$$

A solution which satisfies this is assumed to be of the form

$$w_1(r,t,z,\psi) = F(r) \sin\psi e^{it} e^{-i\omega z/c} \tag{6.17}$$

Substituting (6.17) into (6.16) and differentiating the solution for w_0 with respect to r, yields an ordinary differential equation :

$$\frac{d^2F}{dr^2} + \frac{1}{r}\frac{dF}{dr} - \frac{F}{r^2} + i^3\alpha^2 F = \frac{Am\alpha_0\nu}{\rho c}\frac{J_1(\alpha_0 r)}{J_0(\alpha_0)} \tag{6.18}$$

This may be solved using the method of variation of parameters (Polyanin and Zaitsev, 1995), where the complementary solution (right hand side equal to zero) is

$$F(r) = C_1 J_1(\alpha_0 r) + C_2 Y_1(\alpha_0 r) \tag{6.19}$$

and the Wronskian of this is

$$J_1(\alpha_0 r)\frac{d}{dr}Y_1(\alpha_0 r) - Y_1(\alpha_0 r)\frac{d}{dr}J_1(\alpha_0 r) = \frac{2}{\pi r} \tag{6.20}$$

and thus the full particular solution is

$$F(r) = C_1 J_1(\alpha_0 r) + C_2 Y_1(\alpha_0 r) - \frac{A_n m\nu}{2\rho c J_0(\alpha_0)\alpha_0}(\alpha_0 r J_0(\alpha_0 r) - J_1(\alpha_0 r)) \tag{6.21}$$

The solution must be finite at $r = 0$, thus $C_2 = 0$ and the boundary condition $F(1) = 0$ is used as there is assumed to be negligible longitudinal wall movement. Inserting these boundary conditions and simplifying results in a final solution

$$w_1(r',t,z,\psi) = \frac{A_n m a}{2\rho c}\left(\frac{J_1\left(\alpha_0\frac{r'}{a}\right)}{J_1(\alpha_0)} - \frac{r J_0\left(\alpha_0\frac{r'}{a}\right)}{J_0(\alpha_0)}\right)\sin\psi e^{i\omega(t-z/c)} \tag{6.22}$$

This solution was verified by substituting equation (6.22) into equation (6.16) to ensure that the left and right hand sides equate.

The volumetric flow is obtained by integration :

$$Q_1(t) = 2\int_0^{\pi}\int_0^{a} r' \frac{A_n m a}{2\rho c}\left(-\frac{r J_0\left(\alpha_0\frac{r'}{a}\right)}{J_0(\alpha_0)} + \frac{J_1\left(\alpha_0\frac{r'}{a}\right)}{J_1(\alpha_0)}\right)\sin\psi e^{i\omega(t-z/c)} dr' d\psi \tag{6.23}$$

and thus the solution for volumetric flow is

$$\begin{aligned} Q_1(t) \;=\; & \frac{A_n m a^3}{\rho c \alpha_0} - \left[2a\frac{J_1(\alpha_0)}{J_0(\alpha_0)} + \pi\left(J_1(\alpha_0)\mathrm{H}_0(\alpha_0) - J_0(\alpha_0)\mathrm{H}_1(\alpha_0)\right)\times \right. \\ & \left.\left(\frac{1}{J_1(\alpha_0)} + \frac{a}{\alpha_0 J_0(\alpha_0)}\right)\right] e^{i\omega(t-z/c)} \end{aligned} \tag{6.24}$$

where $\mathrm{H}_0(\alpha_0)$ and $\mathrm{H}_1(\alpha_0)$ are the Struve functions shown in Appendix B.

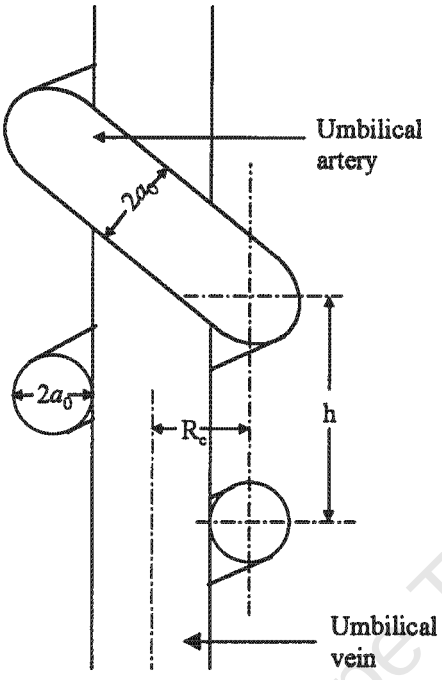

Figure 6.2: Geometrical variables for coiled umbilical artery around the umbilical vein. The radius of the umbilical artery is a_0, the radius of curvature, R_c and the pitch, h.

6.4 Adaption for umbilical artery transmission line model

6.4.1 Helical coils

The equations developed in the preceeding section are for a coiled artery. However, the umbilical artery is loosely coiled in a helical shape and therefore the effective radius of curvature, R, will be slightly larger for a helix and is calculated using the formulation of Truesdell and Adler (1970). They adjusted the radius of curvature in helical coils to account for the helical shape using the following formula :

$$R = R_c \left[1 + \left(\frac{h}{2\pi a_0}\right)^2\right] \tag{6.25}$$

where h is the pitch of the coil and R_c is the radius of curvature of a single segment. This is illustrated in figure (6.2). As the pitch is the inverse of the coiling index (no. of coils per cm), this equation allows for investigation of changes in coiling index on the FVW's.

6.4.2 Modification to transmission line parameters

Unsteady flow

It is necessary to recalculate the longitudinal and transverse impedances to provide correct representations of the characteristic impedance and propagation constant. This requires expressions for the pressure and total flow. The pressure remains unchanged and the form of the pressure pulse is $A_n e^{i\omega_n(t-z/c)}$, whilst the total flow is given by $Q = Q_0 + \lambda Q_1$.

Therefore the longitudinal impedance is

$$Z_L = \frac{-dP/dz}{Q} = \frac{i\omega_n \rho}{a_0^2}\left(1/\left[\pi\left(1+mF_{10}\right)+\frac{\lambda m a_0}{\alpha_0}\left[\begin{array}{c}-2a_0\frac{J_1(\alpha_0)}{J_0(\alpha_0)}+\pi\left(\frac{1}{J_1(\alpha_0)}+\frac{a_0}{\alpha_0 J_0(\alpha_0)}\right)\times\\ \left(J_1\left(\alpha_0\right)\mathrm{H}_0\left(\alpha_0\right)-J_0\left(\alpha_0\right)\mathrm{H}_1\left(\alpha_0\right)\right)\end{array}\right]\right]\right) \tag{6.26}$$

and the transverse or wall impedance is

$$Z_W = \frac{P}{-dQ/dz} = \frac{\rho c^2}{i\omega_n a_0^2}\left(1/\left[\pi\left(1+mF_{10}\right)+\frac{\lambda m a_0}{\alpha_0}\left[\begin{array}{c}-2a_0\frac{J_1(\alpha_0)}{J_0(\alpha_0)}+\pi\left(\frac{1}{J_1(\alpha_0)}+\frac{a_0}{\alpha_0 J_0(\alpha_0)}\right)\times\\ \left(J_1\left(\alpha_0\right)\mathrm{H}_0\left(\alpha_0\right)-J_0\left(\alpha_0\right)\mathrm{H}_1\left(\alpha_0\right)\right)\end{array}\right]\right]\right) \tag{6.27}$$

Here a_0 is used to replace a to describe the unstressed radius of the artery in order to be consistent with the earlier notation and development.

The expression for the characteristic impedance in a curved artery now becomes

$$Z_0 = \sqrt{Z_L Z_W} = \frac{\rho c}{a_0^2}\left(1/\left[\pi\left(1+mF_{10}\right)+\frac{\lambda m a_0}{\alpha_0}\left[\begin{array}{c}-2a_0\frac{J_1(\alpha_0)}{J_0(\alpha_0)}+\pi\left(\frac{1}{J_1(\alpha_0)}+\frac{a_0}{\alpha_0 J_0(\alpha_0)}\right)\times\\ \left(J_1\left(\alpha_0\right)\mathrm{H}_0\left(\alpha_0\right)-J_0\left(\alpha_0\right)\mathrm{H}_1\left(\alpha_0\right)\right)\end{array}\right]\right]\right) \tag{6.28}$$

and the propagation constant for a curved artery is

$$\gamma = \sqrt{\frac{Z_L}{Z_W}} = \frac{i\omega_n}{c} \tag{6.29}$$

and thus remains unchanged.

Steady flow

Figure (6.3) depicts a straight and curved arterial segment, each of length L and with the same applied pressure gradient across both segments held constant at ΔP. The resistance of the straight and curved segments are R_s and R_c respectively. The flow in the straight and curved arterial segments will be Q_s and Q_c respectively and the ratio of the flow in the curved to

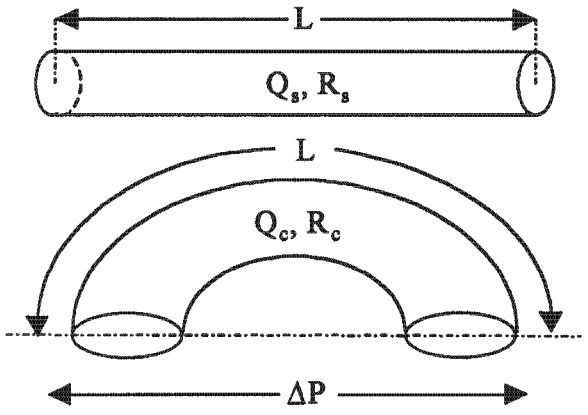

Figure 6.3: Straight and curved arterial segments, each of length L, with the same applied pressure gradient, ΔP between the ends of the arteries. The resultant flow and resistance is Q_s and R_s and Q_c and R_c for the straight and curved arteries respectively.

straight segment may be obtained as :

$$\frac{Q_c}{Q_s} = \frac{R_s}{R_c} = \left[\left(1 - \frac{0.18}{\left[1 + \left(\frac{35}{D_n} \right)^2 \right]^{1/2}} \right)^m + \left(1 + \frac{\lambda}{3} \right)^2 \frac{Dn}{88.33} \right]^{-1/2} = k_{cs} \tag{6.30}$$

from equation (6.14) and is abbreviated as k_{cs} to make the notation less cumbersome. This allows R_c to be solved to get

$$R_c = \frac{R_s}{k_{cs}} \tag{6.31}$$

Thus an expression for the equivalent resistance of a curved arterial segment is obtained. This will be incorporated into the full transmission line model in chapter 9.

6.5 Summary

In addition to arterial taper, a further and unique geometric nonuniformity encountered in the foetal arterial system is that of the coiled umbilical arteries, which spiral around the umbilical vein in a helical fashion. The degree of coiling may vary within a normal foetal population and furthermore hypocoiling or hypercoiling are associated with poor foetal outcome. Thus it is necessary to accurately account for any haemodynamic alterations to the flow velocity waveforms incurred by arterial curvature. No previous models completely account for the effects

of arterial curvature on longitudinal flow velocities or on the effects of curvature on the arterial impedance. A perturbation solution to the non-linear Navier-Stokes equations in a toroidal co-ordinate system for fluid flow in a hollow cylindrical tube with elastic walls was developed. A pertubation method was used to linearise the governing equations. This demonstrated that the effect of curvature on the unsteady components of the axial velocity is additive. The linearisation of these equations allowed a previously developed correlation equation to be used to calculate the effects of curvature on the steady flow components. This solution is compatible with the form of the three basic arterial models and allows the transmission line equations to be extended in a simple manner to include the effects of curvature on the impedance and flow velocities. Once again, these solutions are potentially useful for many haemodynamic modelling applications other than the foetal system. Myers and Capper (2001), present a general discussion of the impedance in curved arteries, however, as this detracts from the specific purpose of the curved model in this thesis such a discussion is not included herein.

It is of further interest to note that the propagation properties of the flow waveforms are unaffected by the curvature as the value of the wavespeed c is calculated from the frequency equation from the first order solution and is the same value used in the second order solution. Anisotropy, viscoelasticity and wall thickness primarily alter phase velocities and damping factors. Therefore due to this property and the form of the solution it is possible to interchange between Womersley's, Atabek's and Dinnar's solutions as presented in chapter 4.

Chapter 7

Peripheral arterial beds and placental model

7.1 Introduction

The foetal model requires a realistic, mathematical representation of the six compartmentalised vascular beds employed in the model. It is unnecessary to calculate the actual flow within the various branches of these regional vascular beds and an accurate representation of the input impedance of the entire bed is all that is required. Many earlier foetal models utilised simple lumped electrical analogies to represent the input impedance of the vascular bed. However the shape of the input impedance spectrum is dependent upon many distally generated reflections and the mutual interference of these reflections. Therefore, although it may be possible to accurately represent the peripheral input impedances with R,L,C circuits at a single frequency, the same circuit would not necessarily be valid at all frequencies. Thus a single lumped component with no reflections is inadequate to realistically represent the input impedance of a vascular network. Furthermore, it remains instructive to represent the placenta in as much detail as possible so that the effect of inter-placental morphological and physiological changes may be investigated on Doppler FVW's in the foetal arterial tree.

A number of treatments of vascular network models for various arterial tree systems have been proposed (Taylor, 1966; Wiener et al. 1966; Campbell et al. 1990; Bennett, 1994; Brown, 1996) . Taylor (1966) was the first to highlight the significance of asymmetry on the input impedance spectrum of a multi-level arterial tree, demonstrating that branch asymmetry increases the incidence of "destructive interferences", and results in progressive attenuation of primary spectral oscillations (Brown, 1996). The development of an accurate model of each

and every branch, as was done by Taylor (1966) and Brown (1996), is both tedious and computationally intensive. A simplifying approach would be to link the structure and function with a smaller number of parameters than the number of individual vessels comprising the tree. Fractal geometry offers an elegant tool for the accomplishment of this goal. The notion of a fractal implies that the properties of vessel elements are self-similar and that a structural pattern of branching is replicated throughout the vascular tree. It has been shown that pulmonary and coronary network systems are fractal in nature (Glenny and Robertson, 1990; Krenz et al. 1992; Dawson et al. 1999; Zamir, 1999) and more recently Bergman and Ullberg (1998) demonstrated fractal properties of the placental arterial tree. Taylor's model incorporated asymmetry through a random number generator used to produce a gamma distributed range of vessel lengths at each generation level. Random components in a model cannot allow the model to be identically reproduced on repeated simulations and thus renders such a model inapplicable for investigatory purposes. Brown (1996) analysed the input impedance of a set of compliant vascular branching tubes which were both asymmetrical and fractal in nature. However his model is computationally expensive owing to its asymmetric nature and the computational effort increases exponentially with each additional generation of branching. Todros et al. (1993) compared the symmetric branching model of Guiot et al. (1992) with a modified asymmetric version by introducing a randomly varying parameter at each branching point. Their results indicated that flow velocity waveforms obtained by the two models are very similar. For these reasons, a symmetrical model was selected to represent the peripheral arterial beds. Although not entirely accurate, this is still superior to a single lumped parameter model and allows for both a more realistic representation of the input impedance spectra and investigation within the placenta.

7.2 Fractal model of the vascular beds

Morphometric data from the intrapulmonary arteries of dog, human, and cat lungs indicate a linear relationship between the log of the vessel number, or length, in each level versus the log of the mean radius in each level. This suggests that a scale-independent self-similar or fractal structure may underlie the observed relationships (Gan and Yen, 1994; Horsfield, 1978; Huang et al. 1996; Jiang et al. 1994; Krenz et al. 1992) . According to Krenz et al. (1992) and Dawson et al. (1999), this data can be well approximated by the following formulas:

$$N_i = N_r r_i^{-b_1} \tag{7.1}$$

and

$$l_i = l_r r_i^{b_2} \tag{7.2}$$

where i denotes the level (order or generation) number measured from the largest vessel at the entrance of the arterial tree to the smallest vessel at the entrance of the capillary bed, N_i is the number of vessels in generation i, l_i is the average length in generation i, r_i is the average radius of generation i and N_r, l_r, b_1 and b_2 are parameters summarising the tree morphometry. Although no specific measurements of this nature have been performed on the other arterial beds, it is assumed that similar structural relationships apply.

Data from the cardiovascular systems of man and various animals indicate that the most common mode of branching is the dichotomous mode, whereby a parent vessel divides into only two daughter vessels (Zamir et al., 1979, Zamir and Brown, 1982; Zamir and Medeiros, 1982; Zamir et al., 1983). Although no specific study has been performed on placental villous vessels, there is no reason to indicate they would branch in a non-dichotomous manner and thus a dichotomous branching pattern has been assumed.

A symmetrical network of n generations of dichotomously branching vessels of progressively reduced radius and length was used to represent the vascular beds. A linear relationship was assumed between the radii at each level and that of the succeeding generation, represented by the constant k, where

$$k = r_i/r_{i+1} \tag{7.3}$$

and the subscript i denotes the vessel generation. Dawson et al. (1999) cite a number of references measuring morphometric data in the pulmonary arterial tree which indicates that $b_2 \simeq 1$. Again, it is assumed that the same value applies for the other arterial trees in the model. This implies that the length of a vessel segment is directly proportional to the radius of that segment and the ratio of length to radius is therefore denoted by

$$l_r = l/r \tag{7.4}$$

A further relationship between the radius of the parent and daughter vessels at a bifurcation was derived by Murray (1926). He proposed a cost function that was the sum of the friction power loss and the metabolic power dissipation which is proportional to total blood volume. Minimisation of the cost function led to an optimal condition for a vascular bifurcation commonly referred to as Murray's law. This states that the cube of the radius of the parent vessel must equal the sum of the cubes of the radii of the two daughter vessels. This rule may be generalised for symmetrical branching as

$$r_i^K = r_{i+1}^K + r_{i+1}^K = 2r_{i+1}^K \tag{7.5}$$

where K depends on the optimality criterion used to obtain the power-law relationship. The square law relation, $K = 2$, corresponds to a condition of zero expansion in cross-sectional area

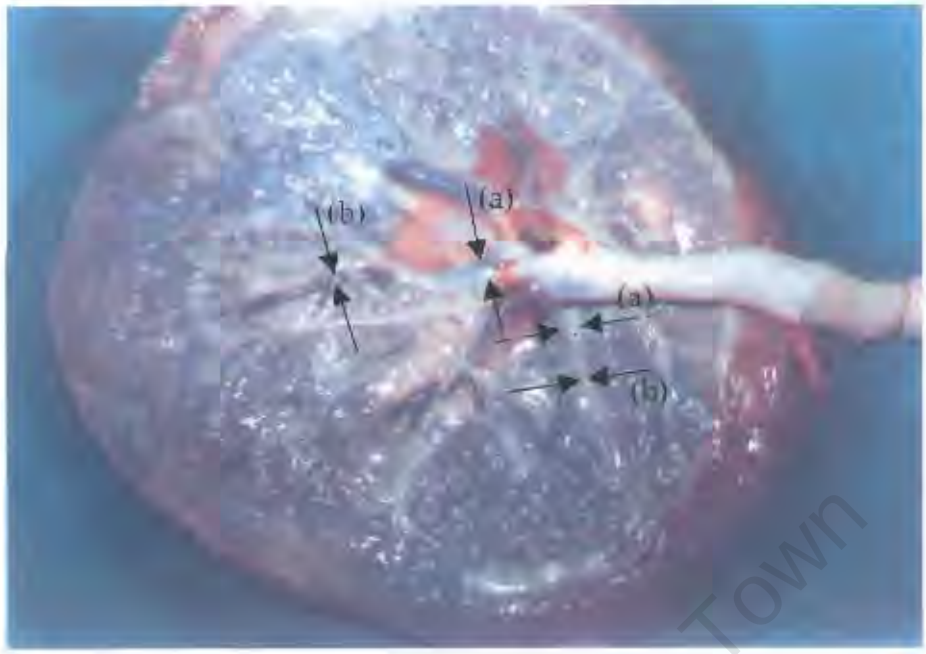

Figure 7.1: Photo of a healthy placenta. The arrows indicate examples of tapering present in the chorionic arteries. The arteries gradually taper from a larger radius (a), to a smaller radius (b).

available. Physiological data indicates that sometimes the square law holds and at other times the cube law holds (Zamir, 1999) , however placental branching has not yet been assessed in terms of Murray's law. Choosing a value of K allows k to be solved using

$$k = \frac{r_i}{r_{i+1}} = 2^{1/K} \tag{7.6}$$

The equations used to determine the input impedance of the peripheral vasculature are developed in the following sections for steady and unsteady flow.

Visual inspection of the larger chorionic arteries of the placental vascular bed indicate that they taper smoothly between one generation and the next. This is also depicted in a photo of a placenta as shown in figure (2.3). It is further known that wave speed increases from one generation to the following (Taylor, 1966) and it would therefore be plausible that an elastic taper also be present. No previous studies of tapered peripheral arterial models have been conducted and solutions for both non-tapered and exponentially tapered vascular trees will be presented in this thesis.

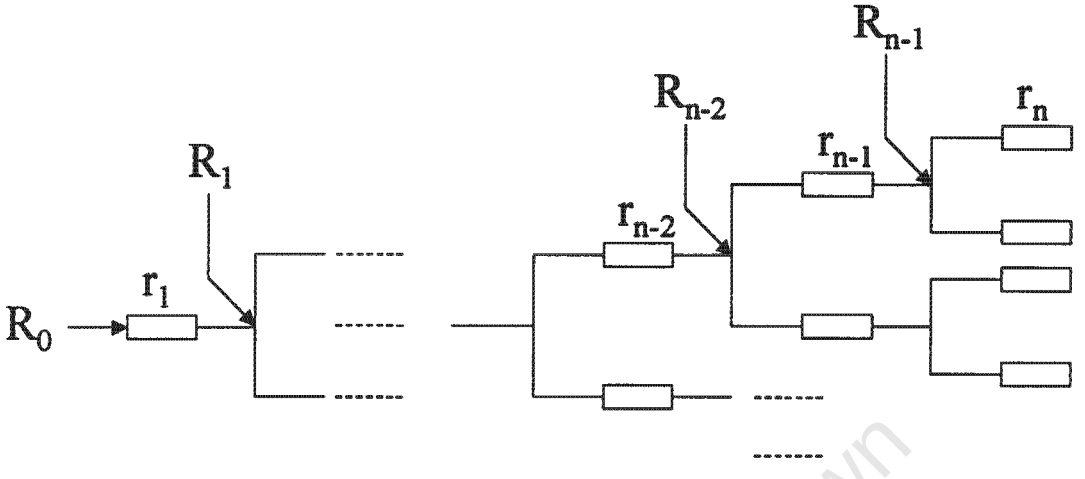

Figure 7.2: Schematic of symmetric arterial network. The total input resistance of the network is R_0. There are n levels of branching, with each level containing 2^{n-1} branches. The radius of each branch is denoted by the variable r, where the subscript indicates the level of branching. The input resistance of each pair of branches is dentoed by the variable R with appropriate subscripts.

7.2.1 Steady flow

From the model point of reference, both mean arterial pressure and the proportion of cardiac output distributed to each vascular bed are predetermined quantities. Thus the input resistance of each vascular bed may be computed according to $R_{in} = P_{mean}/fractionCO$. Specification of the relationship between input resistance and number of generations of branching allows the number of generations of a vascular bed to be calculated in order to achieve a desired input resistance. This relationship between input resistance and number of levels of branching for a given network morphology will now be developed.

No Tapering present

Figure (7.2) depicts the schematic layout used to derive the following equations. The network consists of n levels of branches, with the resistance to steady flow of each level described by a resistor with the radius subscript denoting the level of branching. The total input resistance is denoted by R_0. Poiseuille's law is used to represent the resistance of a single vessel segment in the arterial tree. For a given branch, the resistance is therefore

$$R = \frac{8\mu l}{\pi r^4} = \frac{8\mu l_r}{\pi r^3} \tag{7.7}$$

For a tree of n levels, the input resistance of one pair of the n^{th} branch will be :

$$R_{n-1} = \frac{1}{2}\frac{8\mu l_r}{\pi r_n^3} \tag{7.8}$$

The input resistance of one pair of the $(n-1)^{th}$ branch will be :

$$\begin{aligned} R_{n-2} &= \frac{1}{2}\left(R_{n-1} + \frac{8\mu l_r}{\pi k^3 r_n^3}\right) \\ &= \frac{1}{2}\left(\left(\frac{1}{2}\frac{8\mu l_r}{\pi r_n^3}\right) + \frac{8\mu l_r}{\pi k^3 r_n^3}\right) \end{aligned} \tag{7.9}$$

where the input resistance of the n^{th} branch is added as the terminal resistance of the $(n-1)^{th}$ branch . This relation may be generalised for n generations of branching to give :

$$R_0 = \frac{\beta}{r_n^3}\sum_{i=1}^{n}\frac{1}{2^i k^{3(n-i)}} \tag{7.10}$$

where $\beta = 8\mu l_r/\pi$.

This is a geometric series with sum :

$$\sum_{i=1}^{n}\frac{1}{2^i k^{3(n-i)}} = \frac{k^3\left(2^{-n} - k^{-3n}\right)}{k^3 - 2} \tag{7.11}$$

Thus

$$R_0 = 2\left(\frac{\beta}{r_0^3}k^{3n}\frac{k^3\left(2^{-n} - k^{-3n}\right)}{k^3 - 2}\right) \tag{7.12}$$

where the final result has been multiplied by 2 as the first branch of the tree is not in parallel.

Solving for the number of generations, n, yields :

$$n = \frac{\ln 2\beta\frac{k^3}{-2R_0 r_0^3 + R_0 r_0^3 k^3 + 2\beta k^3}}{\ln\frac{2}{k^3}} \tag{7.13}$$

An ideal vascular network model represents the arterial bed right through the arteriole and capillary levels, until the venous arterial tree is encountered. However, it is known that after a radius of about $20\mu m$, Poiseuille's law ceases to remain valid (Dinnar, 1981). The model presented above may be considered to represent the vascular bed prior to the microvessel level. Thus the last generation of branches (of radius r_n) may be seen as a lumped resistance representing the total input resistance of the remaining micro-vascular tree.

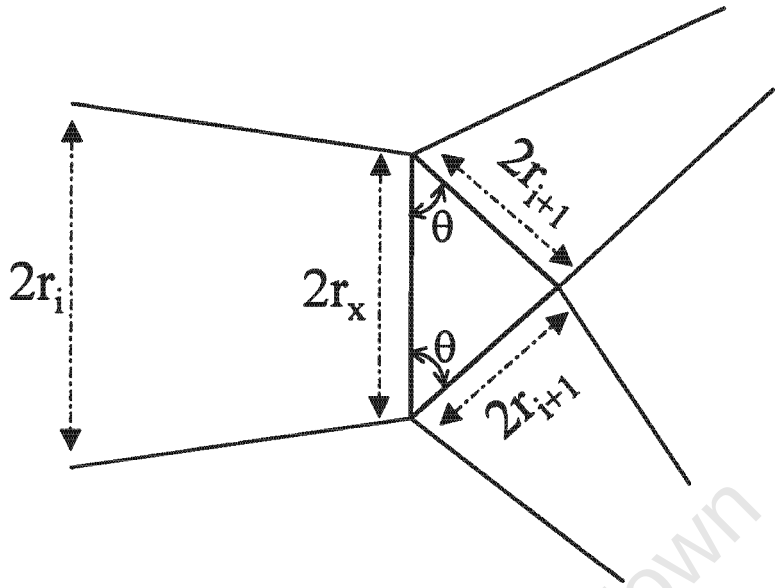

Figure 7.3: A cross section of the branching between a parent and daughter vessel within a tapered arterial netowrk. The parent vessel begins at a diameter of $2r_i$, and tapers down to a diameter of $2r_x$. Each daughter vessel begins at a diameter of $2r_{i+1}$. This forms a triangle where the tapering angle between parent and daughter vessels is denoted by θ.

Tapered version

Consider a diagram of the vessel cross-section. A vessel of diameter $2r_i$ feeds into two vessels, each of diameter $2r_{i+1}$. This forms a triangle, where the angle of the daughter vessels to the parent vessel is assumed to be θ and for symmetrical daughter vessels, they must branch at equal angles. The parent vessel tapers down to a diameter $2r_x$ and this can be calculated using the sine rule as follows :

$$r_x = \frac{\sin(180 - 2\theta)}{\sin\theta} r_{i+1} = 2\cos\theta r_{i+1} = x r_{i+1} \tag{7.14}$$

where $x = 2\cos\theta$.

For exponential radial taper, the series resistance of an arterial segment is obtained from equation (5.54) and is :

$$R = \frac{2\mu\left(e^{4Lp} - 1\right)}{\pi p r^4} = \frac{2\mu\left(e^{4rl_r p} - 1\right)}{\pi p r^4} \tag{7.15}$$

Therefore, assuming an exponential form of radial taper, $r(z) = r_i e^{-pz}$ and

$$p = -\frac{\ln\frac{x}{k}}{r_i l_r} \tag{7.16}$$

so that

$$R = \frac{4\mu l_r}{x^4 \pi r_i^3} \frac{x^4 - k^4}{\ln \frac{2}{k^2}} \tag{7.17}$$

and letting

$$\beta = \frac{4\mu l_r}{x^4 \pi} \frac{x^4 - k^4}{\ln \frac{2}{k^2}} \tag{7.18}$$

yields the same form of solution obtained for the non-tapered sections. Thus the only difference between the tapered and non-tapered solutions is the selection of the parameter β.

7.2.2 Unsteady flow

The solution for the steady flow resistance determines the number of generations of branching. Each branch is then modelled using either Dinnar's, Atabek's or Womersley's solution and the transmission line solution for input impedance is used to obtain the input impedance from each branch. Taylor (1966) and Brown (1996) assumed that the wavespeed increases moving further down the tree towards the microvessels. They modelled this increase using the empirical formula

$$c_i = c_0 \left(3 - 2e^{-5i/n}\right) \tag{7.19}$$

For the model presented in this thesis, this formula is also used. The Young's modulus is proportional to the square of the wavespeed and so the relation between Young's moduli at each generation is given by

$$E_i = E_0 \left(3 - 2e^{-5i/n}\right)^2 \tag{7.20}$$

A characteristic impedance and propagation constant is calculated for each branch and for the non-tapered arterial tree, the input impedance of each branch is determined according to

$$Z_{i-1} = \frac{1}{2}\left(Z_{0i-1} \frac{(Z_i + Z_{0i-1})\, e^{\gamma_{i-1} l} + (Z_i - Z_{0i-1})\, e^{-\gamma_{i-1} l}}{(Z_i + Z_{0i-1})\, e^{\gamma_{i-1} l} - (Z_i - Z_{0i-1})\, e^{-\gamma_{i-1} l}}\right) \tag{7.21}$$

This is the transmission line equation for input impedance, divided by two as each branch is in parallel and with the terminal impedance given by the input impedance of the next level. The n^{th} branch is modelled as a pure resistance calculated from the steady flow solution and is the terminal impedance for the $(n-1)^{th}$ branch. The final input impedance is multiplied by two as the first branch is not a parallel branch.

The same approach is used for the tapered solution, where an initial and final characteristic impedance and propagation constant is calculated for each branch, using the initial radius and

the radius specified from equation (7.14). The final Young's modulus is the initial Young's modulus of the next level of branching. These initial and final values are then used to fit exponentials for the characteristic and propagation constants and thus tapering constants, h and q are calculated for each branch. The input impedances of each branch are computed using equation (5.23a) and again the parallel combination of two level i branches serves as the terminal impedance of the level $i-1$ branch.

7.3 Summary

It is extremely tedious and complicated to accurately model each and every artery in the entire circulatory system and thus the smaller arterial networks and microvasculatures comprising the peripheral circulations were combined into meaningful compartments. It is unnecessary to determine actual flow velocities at various points within these arterial beds, however it is essential to accurately model the input impedance spectra thereof. Due to the interference of multiple reflections, it has been demonstrated that single lumped parameter models are inadequate to accurately model impedance spectra at every frequency under consideration. Furthermore, with specific reference to the placental arterial bed, it is beneficial to possess a degree of detail concerning the morphological arrangements of these arterial beds, as many structural changes are known to occur in association with foetal compromise. In addition, examination of actual arterial beds appear to indicate that the vessels within these beds taper from one generation to the next and a comparison of tapered versus non-tapered peripheral arterial network models requires further assessment. No previous works identified have described tapered arterial network models. A fractal model of these arterial trees was developed which assumed that many of the properties of the individual vessel elements were self-similar and therefore linked the structure and function of each vessel comprising the tree with a reduced set of parameters. Specification of these parameters determined the impedance spectra of the arterial networks. The model specifies the total input resistance of the peripheral arterial beds from the fraction of cardiac output supplying a particular bed and the mean arterial pressure. This specification allows the number of levels of branching to be determined for a given set of parameters governing the branching ratio (K), the branching angle for the tapered model (θ) and the length to radius ratio (l_r). Arterial wave velocities are assumed to increase with the level of branching and an empirical relationship was used to determine this increase. The results of this chapter present a new set of relations with which arterial trees may conveniently be modelled. These models may be used for further haemodynamic modelling applications beyond the scope of the foetal circulatory system.

Chapter 8

Gestational age dependency of the model

8.1 Introduction

During the course of gestation the growth of the human fetus proceeds at a greater relative rate than that of the adult. This growth rate is the summation of growth of the various organs and tissues that constitute the whole foetus. Additionally anatomical and functional modifications occur, which result in changes to fundamental cardiovascular quantities such as pressures and blood flows to the various vascular compartments. To further enhance the utility of a mathematical model of the foetal circulation, it is necessary to adapt the model to remain valid at any gestational age. The model presented thus far is designed using anatomical and physiological variables representing a 28 week old foetus. During the first trimester, many foetal organs are not wholly formed or functional, thereby increasing the complexity required in order to model the early stages of development. Furthermore, most reported cases of abnormal Doppler recordings occur in the third trimester of pregnancy and many studies only document the results in this period (Dornan and Beattie, 1992). Thus, in this thesis, foetal growth has only been modelled between 28 weeks of gestation and term.

Previous works have modelled foetal growth related vascular and cardiac parameters to anatomical dimensions of vessels using allometric equations. These in turn are dependent on total foetal body mass and gestational age (Pennati and Fumero, 2000; Capper and Myers, 2000). However, the placenta and various foetal organs do not grow at the same rate as the foetal mass and thus these models may be improved. A growth model that is based on scaling factors is developed and adapted to account for disproportionate growth rates of total foetal mass, placental mass and individual organ mass. Special consideration is given to the structure

Figure 8.1: Gestational age vs. total foetal mass using the regression model of Theron and Thompson (1985).

of the peripheral vascular arterial tree model developed in Chapter 7.

8.2 Regression equations for total foetal, placental and organ mass

Typical regression equations relating the total foetal mass with gestational age have been developed by Theron and Thompson (1995), Gallivan et al. (1993) and Wosilait et al. (1992). The equation selected for use with this model was that of Theron and Thompson and is:

$$M_{G_A} = -0.073G_A^3 + 9.95G_A^2 - 226G_A + 1443 \tag{8.1}$$

where M is the foetal mass in kg and G_A is the gestation age measured in weeks. Figure (8.1) depicts the mass versus gestational age from 28 weeks to 40 weeks.

Luecke at al. (1995) used allometric equations to describe the correlation of 16 individual foetal organ weights with that of the total foetal mass, using organ and tissue weights pooled from a number of sources. The equation relating the mass of each organ (M_0) to the total foetal mass (M_F) was given by :

$$M_O = aM_F^{b+c\ln M_F} \tag{8.2}$$

Organs and tissues were split into groups belonging to each vascular compartment of the foetal model and the values of a, b and c are shown for each organ and vascular compartment in

table (8.1). It is assumed that the head growth is governed by the rate of growth of the brain and that the lower limbs and upper body compartments respectively account for 50% and 40% of the total mass of the bone and skeletal muscle. Figure (8.2) shows the corresponding growth curves for each vascular compartment. Parameters for placental growth were not supplied by Lucke et al. and therefore equation (8.2) was fitting to the data presented by Dombrowski et al. (1994), who measured placental weight in 29 989 foetuses. The fit was performed by the non linear regression technique of minimising the sum squared error of the differences between the measured and fitted values, using the Gauss-Newton algorithm (Dennis, 1977). The resulting parameters for a, b and c are included in table (8.1). Figure (8.2) also depicts the placental growth versus gestational age. It should be noted that the portion of the total foetal mass consisting of fat, bone marrow and extracellular fluid is not included in each compartment as the distributions of these components to each compartment is unknown. However, it may be assumed that these quantities are equally distributed amongst all the compartments.

Vascular Compartment	a	b	c
Head and Heart			
- Brain	0.1871	0.9585	0
- Heart	0.01012	0.9489	0
Upper body and Thorax			
- Lung	0.09351	1.552	-0.05945
- 40% Skeletal muscle	0.02668	1.234	0
- 40% Bone	0.05169	0.9288	0
Abdomen			
- Kidney	0.004203	1.255	-0.02127
- Pancreas	0.1883	0.3854	0
- Spleen	0.0001302	1.204	0.02909
- Liver	0.06050	0.9737	0
Adrenals			
- Adrenal	0.007467	0.8902	0
Lower limbs			
- 50% Skeletal muscle	0.02668	1.234	0
- 50% Bone	0.05169	0.9288	0
Placenta			
- Placenta	0.8554	0.8536	0

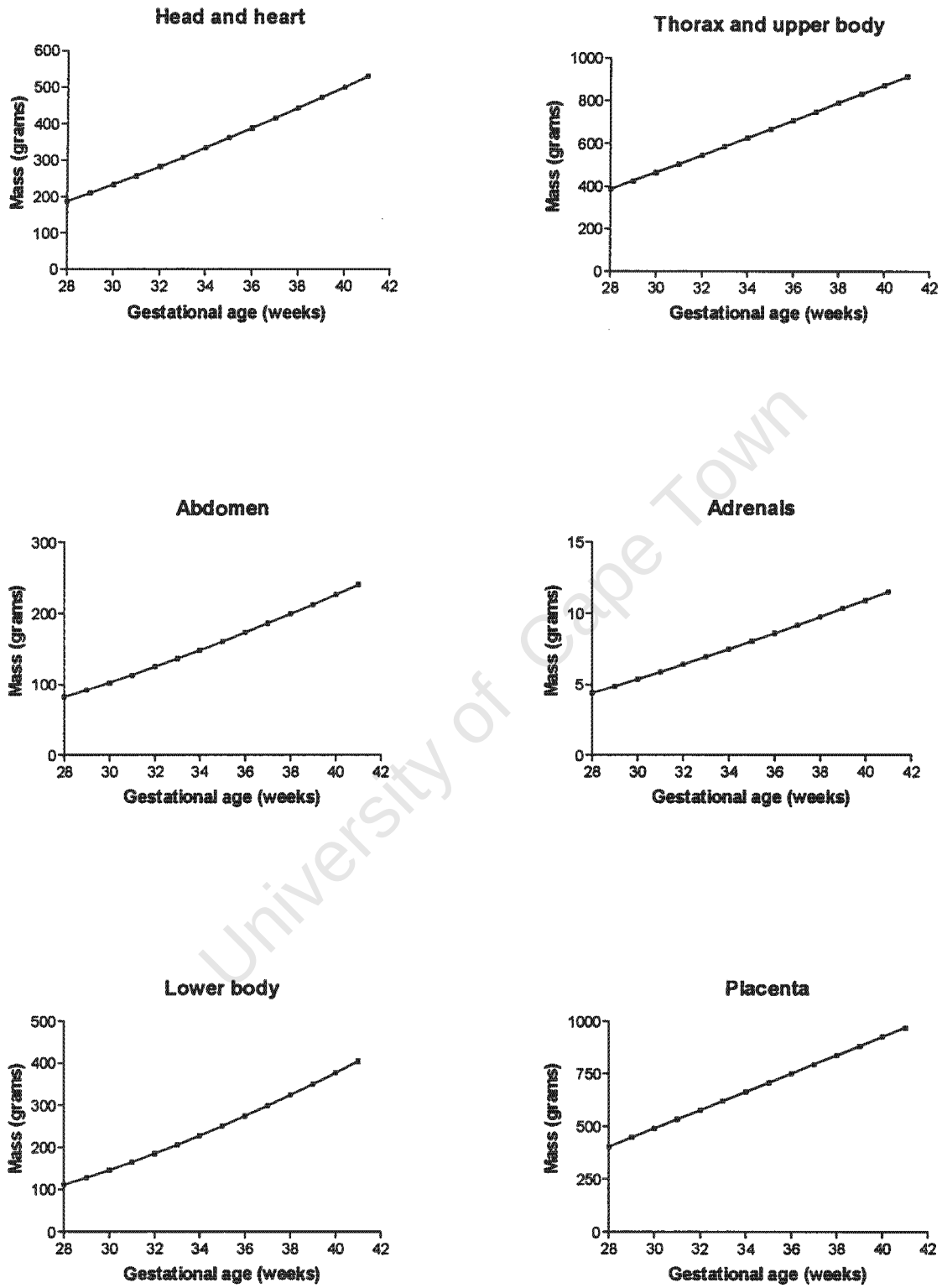

Figure 8.2: Gestational age versus foetal organ mass for the organs comprising each of the six vascular compartments used in the model to represent the peripheral circulation.

Table 8.1: Allometric parameters for foetal organs and tissues from Luecke et al. (1995). Foetal parameters are subdivided into the model vascular compartments that they belong to. Placental parameters were fitted to the data of Dombrowski et al. (1994) using a non-linear least squares regression technique.

8.3 Growth of cardiovascular parameters

The total cardiac output normalised to unit fetal body mass is reported to remain constant from 18 weeks to term in humans (St John Sutton et al. 1992). In this model, for a foetus of 28 weeks gestational age, it was assumed that the cardiac output is 500 ml/min/kg. The total cardiac output at each gestational age may be now determined as the mass at each gestational may now be calculated. Furthermore, the proportion of the combined cardiac output directed to the various peripheral vascular beds does not appear to vary with gestational age from the second trimester onwards (St John Sutton et al. 1992).

Mean foetal heart rate decreases only slightly over the course of gestation and Kenney et al. (1986) provide the following regression equation relating foetal heart rate and gestational age :

$$HR = -0.35G_A + 151 \tag{8.3}$$

There is no evidence of changes in blood pressure with advancing gestational age and the mean blood pressure is assumed to remain constant at 60 mmHg.

8.4 Growth of major foetal vessels

It is assumed that the linear dimensions of the major or central foetal vessels are roughly related to the cube root of the total body volume and therefore, assuming constant density, the total body mass. This cube root scaling factor has been shown to apply to the radii and lengths of most of the major foetal vessels (Pennati and Fumero, 2000). Let the reference mass at 28 weeks be denoted by M_{28}, then the values of a length or radius variable at a particular age may be scaled according to

$$r_{G_A} = r_{28}\left(\frac{M_{G_A}}{M_{28}}\right)^{1/3} \tag{8.4}$$

where r_{28} is the reference radius or length at 28 weeks. Table (8.2) shows a comparison of the estimated dimensions of selected arteries at gestational ages from 28-40 weeks, with corresponding clinical measurements. Holt et al. (1981) confirmed this relation by performing

measurements in plastic corrosion casts of several adult animals for body sizes ranging between a 10 g mouse and a 1000 kg cow. They demonstrated that the diameters and lengths of the aorta and its major branches could be described using scaling factors close to 1/3.

		DA		UAL		UAD		
GA (weeks)	Mass (kg)	Measured (mm)[1]	Predicted (mm)	Measured (mm)[2]	Predicted (mm)	Measured (mm)[3]	Smoothed (mm)[4]	Predicted (mm)
28	1.3	4.8	4.8	450	430	3.1	3.2	3.0
30	1.6	5.1	5.2	480	463	3.4	3.3	3.2
32	2.0	5.5	5.5	500	495	3.6	3.5	3.5
34	2.4	5.8	5.9	530	525	3.3	3.6	3.7
36	2.8	6.1	6.2	560	553	3.7	3.8	3.9
38	3.2	6.5	6.5	570	579	4.2	3.9	4.0
40	3.6	6.9	6.8	600	604	3.9	4.0	4.2

Table 8.2: The foetal mass as a function of GA has been used to predict the arterial dimensions in the model (see text). The predicted Descending Aorta (DA) diameter is compared with Chen[1] et al. (1988)'s regression of clinical measurements, ($DA = 3 \times 10^{-4} G_A^2 - 2.05 \times 10 G_A^4 + 0.26$). The predicted umbilical artery length and diameter are compared with clinical measurements by Naeye (1985)[2] and Sherer and Anyaegbunam (1997)[3] respectively. The umbilical artery diameter (UAD) has been regressed with GA for ease of comparison[4], using $UAD = -0.0003 G_A^2 + 0.094 G_A + 0.7714$.

8.5 Growth of peripheral vascular beds and placenta

As the foetus grows, its vascular beds grow in both size and mass, with the radii and lengths of individual vessels, in addition to the number of generations of vessels, increasing. The rate of growth of individual foetal organs differ from that of the total foetal mass. Therefore, if the vessels comprising a peripheral arterial tree were to grow at the same rate as the total foetal mass, the volume of each peripheral arterial tree would grow at a different rate to the organs that it supplies. Furthermore, the resistance of each arterial bed is inversely proportional to the blood flow supplying that bed, and this flow increases in direct proportion with the total foetal cardiac output and hence the total foetal mass. As the mean arterial pressure remains constant with growth, this implies that the resistances of the vascular beds decrease at the same rate as the rate of growth of the total foetal mass. If the dimensions of the arterial tree were to

grow at this rate, the number of generations of branching would remain constant as the foetus grew, and not increase as expected. Alternatively, if the arterial vessels were to grow in direct proportion with organ growth rate, then the arterial area would grow at a different rate to the area of the vessel which feeds the arterial tree (this is assumed to be a major vessel growing at the same rate as the total foetal mass). In this case, flow velocities would have to increase or decrease in a discontinuous manner as the foetus grew and this cannot happen. Thus the peripheral arterial tree vessel areas must grow at the same rate as the areas of the major feeding vessels. However, the arterial volume of the tree is required grow at the rate of the particular organ or organs represented by that tree. Furthermore, the resistance of the tree must still change in proportion with the total foetal mass. This may be achieved by assuming that the length of each vessel need not grow at the same rate as the radius. The growth rate for the length variable is calculated as follows :

8.5.1 Non-tapered arterial trees

The volume of an individual vessel of the arterial tree is given by $V = \pi r_i^2 l_i = \pi r_i^3 l_r$. For n levels of branching, the cumulative arterial volume at 28 weeks is then given by :

$$V_{a28} = N_p \sum_{i=1}^{n} 2^{i-1} \left(\pi \left(\frac{r_0}{k^{i-1}} \right)^3 l_r \right) = \pi r_0^3 l_r k^3 \frac{k^{-3n} 2^n - 1}{2 - k^3} \tag{8.5}$$

where N_p identical trees arise in parallel from the feeding artery. For the placenta, four arterial trees were assumed to leave the umbilical arteries and for the other peripheral beds, N_p is assumed to be one. It is therefore possible to solve for the number of generations as a function of the volume :

$$n_{28} = \frac{\ln \left(N_p \pi r_0^3 l_r \frac{k^3}{2V_{a28} - V_{a28} k^3 + N_p \pi r_0^3 l_r k^3} \right)}{\ln \left(\frac{k^3}{2} \right)} \tag{8.6}$$

Equation (7.13) related the number of vessels to the input resistance of the vascular bed, R_0. This offers a further means of determining the number of vessels at 28 weeks and is repeated here for convenience :

$$n_{28} = \frac{\ln \left(2 \left(8\mu l_r / \pi \right) \frac{k^3}{-2R_0 r_0^3 + R_0 r_0^3 k^3 + 2(8\mu l_r/\pi) k^3} \right)}{\ln \left(\frac{2}{k^3} \right)} \tag{8.7}$$

As the foetus ages, the mass and volume of the organs grow and it is assumed that the volume of the arteries grows at the same rate as the volume of the organs they supply. If the mass of an organ at 28 weeks is M_{o28}, and the mass at G weeks is M_{oG}, then assuming a constant density, the volume of the arteries at G weeks will be given by :

$$V_{aG} = V_{a28} \frac{M_{oG}}{M_{o28}} \tag{8.8}$$

Knowledge of the volume at G weeks, allows the number of vessels required to make up that volume to be computed. However, another expression for the number of vessels at a particular gestational age may be obtained from the equation relating resistance and number of vessels. Obviously the number of vessels obtained from both equations must be equal at all gestational ages. In order to satisfy this requirement, the length to radius ratio, l_r, cannot remain a constant at all gestational ages but must grow according to ml_r, where m is a scaling factor that changes for each gestational age. Replacing l_r with ml_r and equating the two expressions for the number of vessels, allows m to be solved for i.e.

$$n_G = -\frac{\ln\left(N_p\pi r_0^3 m l_r \frac{k^3}{2V_{aG}-V_{aG}k^3+N_p\pi r_0^3 m l_r k^3}\right)}{\ln\frac{2}{k^3}} = \frac{\ln\left(2\left(8\mu m l_r/\pi\right)\frac{k^3}{-2R_0r_0^3+R_0r_0^3k^3+2(8\mu m l_r/\pi)k^3}\right)}{\ln\frac{2}{k^3}} \tag{8.9}$$

and solving for m gives :

$$m = \left(k^3-2\right)V_{aG}R_0r_0^3\frac{\pi}{\left(N_p\pi^2r_0^6R_0-16V_{aG}\mu\right)l_rk^3} \tag{8.10}$$

Repeating this process for every gestational age, allows a curve to be fitted for each organs m as a function of gestational age.

8.5.2 Tapered arterial trees

The process is essentially the same with different formulas for the volume, number of vessels and m. The volume of a single tapered segment is given by :

$$V = \frac{1}{3}\pi\left(r_i^2+xr_{i+1}r_i+x^2r_{i+1}^2\right)l_rr_i \tag{8.11}$$

and the volume of the arteries comprising a peripheral vascular tree will be given by :

$$V_a = N_p\frac{1}{3}\pi\left(1+\frac{x}{k}+\frac{x^2}{k^2}\right)l_rr_0^3k^3\frac{k^{-3n}2^n-1}{2-k^3} \tag{8.12}$$

Solving for the number of vessels yields :

$$n = -\frac{\ln\left(N_p\pi r_0^3l_rk\frac{k^2+kx+x^2}{6V_a-3V_ak^3+N_p\pi r_0^3l_rk^3+N_p\pi l_rr_0^3k^2x+N_p\pi l_rr_0^3kx^2}\right)}{\ln\left(\frac{2}{k^3}\right)} \tag{8.13}$$

Substituting l_r for ml_r and equating this with equation (7.13), using the expression for β given by equation (7.18), yields a solution for m given by :

$$m = 3\left(-2+k^3\right)R_0r_0^3x^4\pi\left(\ln\frac{1}{2}k^2\right)\frac{V_{aG}}{\left(\begin{array}{c}24\mu k^6V_{aG}-24\mu k^2x^4V_{aG}+R_0r_0^6x^4\pi^2\left(\ln\frac{1}{2}k^2\right)N_pk^2+\\ R_0r_0^6x^5\pi^2\left(\ln\frac{1}{2}k^2\right)N_pk+R_0r_0^6x^6\pi^2\left(\ln\frac{1}{2}k^2\right)N_p\end{array}\right)l_rk} \tag{8.14}$$

8.6 Summary

It is necessary that the foetal model be able to compute arterial flow velocity waveforms at any gestational age from 28 weeks until term. This allows investigation into both the effects of growth on the Doppler indices and that of growth retardation. Previous growth models incorrectly assumed that the foetus and therefore the vessels within the foetus all grow at the same rate. However, it is known that the individual organs that comprise the foetus each grow at a different rate to each other and to that of the overall foetal mass. Therefore is was necessary to develop a model that accounts for disproportionate growth rates and such a model was presented in this chapter.

As the foetus grows, the number of vessels that comprise the various peripheral vasculatures will increase. Should the radii and length of these vessels remain unchanged, increasing the number of vessels would effectively increase the input resistances of the vascular beds . However, as the foetus grows, so too do the radii and lengths of these vessels increase, and should the number of vessels remain unchanged, this would reduce the input resistances of the vascular beds. Furthermore, mean arterial pressure remains constant and total combined ventricular cardiac output increases with advancing age. The relation between pressure, resistance and flow therefore indicates that peripheral input resistances must decrease with advancing age. Thus the following constraints govern a growth model : The peripheral input resistances must decrease; the number of vessels comprising a peripheral vascular bed must increase; the cross sectional areas of the vascular beds must increase at the same rate as the overall foetal mass; the volume of the vessels comprising a peripheral bed must increase at the same rate as the organs that the bed represents. In order to satisfy each of these constraints, it is necessary to grow the lengths of vessels of the vascular beds at different rates and equations were developed to calculate the rate of growth of the lengths for each vascular compartment. Growth curves for the lengths will be presented in chapter 10.

Chapter 9

Foetal model

9.1 Introduction

Each large artery in the foetal model is modeled using the frequency dependent fundamental arterial segment equations described in chapter 4. The aorta and iliacs are modified using the equations in chapter 5 to account for their tapered nature and the umbilical arteries are modified using the equations developed in chapter 6 to account for their coiled nature. The terminal arterial beds and placenta are each modeled as a branching network of compliant vessels and their representation was discussed in detail in chapter 7. Each of these building blocks are cascaded together to form the complete arterial system as depicted in figure (3.2) and the transmission line analogies presented in chapter 4 are used to compute the pressure, flow and impedances at any point. Model parameters for a 28 week old foetus may now be selected for each choice of fundamental arterial segment.

9.2 Representation of the foetal blood

The density of foetal blood in the model is assumed to be constant at $\rho = 1.06 g/cm^3$ (Guettouche et al. 1992; Thompson and Trudinger 1990; St John Sutton et al. 1992). The viscosity, μ, of blood is known to be dependent on both the hematocrit and the shear rate. Since the hematocrit of foetal blood is higher than that in an adult, so too is the viscosity. Bergqvisk and Zetterstrom (1974) measured the viscosity to be $\mu = 5.9$ cpoise at a shear rate of $230 s^{-1}$ and $\mu = 7.44$ cpoise at a shear rate of $46 s^{-1}$ in newborn babies, who have a hematocrit of 52%. Mackintosh and Walker (1973) found that the viscosity of foetal blood increased from $\mu = 5.5$ cpoise at a shear rate of $232 s^{-1}$ to $\mu = 33.7$ cpoise at a shear rate of $1.16\ s^{-1}$. For the shear rates applicable in the normal foetal circulation, a value of $\mu = 6.0$ cpoise was selected for use in this model.

9.3 Foetal vascular dimensions

Table (9.1) lists the vessel radii obtained from the literature as well as those used in this model to represent the fetus at 28 weeks gestational age. The radii of the aorta taper exponentially between successive values listed in the table. The lengths of the arteries at 28 weeks were estimated from the measurements performed by Guettouche (1992). The ascending aorta and pulmonary trunk were represented in the model by a single artery of length 2.6cm, with an area equal to the sum of the areas of these two vessels, and carrying the full output from the foetal heart. The length of the thoracic aorta was taken to be 5.2cm, the length of the abdominal aorta was taken to be 1.5cm, and the length of the iliac arteries, up to the umbilical bifurcation were taken to be 1.5cm. The length of the umbilical arteries were taken to be 43cm (Benirschke and Kaufmann 1990; Naeye 1985). The ratio of the wall thickness to the vessel radii was chosen to be 0.15 for all arteries except the umbilical artery, based on measurements by Peterson et al. (1960) in the adult aorta. A value of 0.3 was used for the umbilical artery, based on computerised microscope morphometric measurements of umbilical arteries performed by Bruch et al. (1997).

9.4 Tethering and external loading by the surrounding tissue

Each of the three basic models proposed utilise different forms of tethering or loading. Dinnar's model requires the selection of a constant, g, that represents the ratio of the complex visco-elastic Young's modulus for the surrounding tissue to that of the vessel wall. This ratio has both real and imaginary components and the real part is considered to represent the 'solid' part of the surrounding tissue, whilst the imaginary part represents the 'viscous' part. Dinnar (1975) suggests that the real part should be approximately 0.1, a figure that roughly corresponds to the fraction of white muscle fibres, which are the main factor for determining that coefficient. The imaginary part may lie between 0.001 and 0.1 (Dinnar, 1975). He also demonstrated that the real part was responsible for more significant changes in wave speed and damping than the imaginary part, thus indicating that some error is allowable in the selection of the imaginary part. Wharton's Jelly is regarded as a loose mucous connective tissue consisting of fibroblasts, collagen fibres and an amorphous ground substance composed mainly of hyaluronic acid. These components endow Wharton's jelly with a high degree of elasticity, which functions to protect the umbilical vessels from cord compression, torsion and bending (Takechi et al. 1993) . A value of $g = 0.1 + 0.01i$ was selected for all the arteries, except for the umbilical artery, where a value of $g = 0.2 + 0.01i$ was used. The larger real part was selected to account for the higher degree of elasticity of the Wharton's Jelly.

Arteries	Ascending aorta	Pulmonary trunk	Thoracic aorta	Abdominal aorta	Iliac arteries	Umbilical arteries
Measured	0.25[1]	0.285[1]	0.22[2] 0.23[3] 0.24[1,4,5] 0.25[6,7,8]	0.20[6] 0.21[1] 0.23[4]	0.14[1]	0.12[1] 0.15[9]
Model	0.38**		0.24*	0.21*	0.15*	0.15*

Table 9.1: The measured arterial radii (in cm) of the main vessels in the 28 week GA fetal circulation, as well as those used in this model (denoted by *). Note that the radii of the ascending aorta and pulmonary trunk were estimated from the measurements of Guettouche et al. (1992). These were then combined to form an equivalent vessel, with an area equal to the sum of the areas of these two vessels, and carrying the full output from the fetal heart (denoted by **). The aorta radii smoothly taper between successive values presented in the table. Sources: (1) Guettouche et al. 1992; (2) Struijk et al. 1992; (3) Lingman and Marsal, 1986; (4) Stale, 1991; (5) Chen et al. 1988; (6) Marsal et al. 1987; (7) Erskine and Ritchie, 1985; (8) Kenny et al. 1986; (9) Sherer and Anyaegbunam 1997.

Womersley's tethered model requires the selection of the natural frequency of the additional constraint, M. However, no guidelines are available for selection of this value. A value equal to the frequency of the first harmonic, (at a foetal heart rate of 140 b.p.m), of the flow and pressure waves was selected for all arteries except for the umbilical artery, where a value of twice this was chosen, in order to account for the additional elasticity of the Wharton's jelly.

Atabek's constrained model requires the selection of three parameters, M, C and K, representing the contributions of the inertial, viscous and elastic constraints to the total tethering respectively. Atabek (1968) cites Patel et al. (1966) who experimentally determined these dimensionless parameters to be $M = 0.70$, $C = 550$ and $K = 1.6 \times 10^6$. These values were selected for all arteries, except the umbilical arteries, where a value of $K = 3 \times 10^6$ was chosen to represent the increased elasticity.

9.5 Anisotropy

Atabek's model requires further parameters representing arterial orthotropy to be selected. Once again, Atabek (1968), followed the experimental results of Patel et al. (1966) and de-

termined these parameters to be $\gamma_1 = \gamma_2 = 0.63$. These values were selected for inclusion in Atabek's anisotropic model.

9.6 Selection of Young's moduli

The Young's moduli, E, of the arteries in this model have been estimated from measurements of wave velocity that have been published by various authors. The complex wave speed was represented as $\frac{1}{c} = \frac{b-ia}{\omega}$ in section 4.2, with the actual velocity of propagation or phase velocity given by $\frac{\omega}{b}$. Equations (4.9), (4.15) or (4.19) relate wave velocity to Young's modulus and the particular model choice for the fundamental arterial segment governs their selection. Thus E may be estimated using the measured velocity and the arterial dimensions. In the abdominal aorta, Struijk et al. (1992) measured a wave velocity of 320ms^{-1}. A lower velocity would be expected for the aorta closer to the heart, (McDonald, 1998), and in this model, a velocity of 200ms^{-1} for the ascending aorta has been used. This value was chosen so that the resulting wall compliance would give pressure amplitudes in this vessel which are within the normal physiological range for a human fetus. A wave velocity of 250ms^{-1}, was used for the thoracic aorta. Although the wave velocity in the umbilical arteries is not easily measured in humans, Adamson et al. (1992) measured wave velocities of about 623ms^{-1} in the umbilical arteries of foetal sheep, which should be close to the value in humans.

Artery	Wave speed (ms^{-1})	$\|E\|$ Dinnar (dynes/cm^2)	$\|E\|$ Womersley (dynes/cm^2)	$\|E\|$ Atabek (dynes/cm^2)
Ascending aorta	200	5×10^5	9×10^5	1×10^6
Thoracic aorta (segment1)	210	6×10^5	1×10^6	1.1×10^6
Thoracic aorta (segment 2)	250	8×10^5	1.25×10^6	1.35×10^6
Abdominal aorta	345	1.6×10^6	2.2×10^6	2.7×10^6
Iliac arteries	370	2×10^6	4.3×10^6	4.7×10^6
Umbilical arteries	645	6×10^6	8×10^6	7.4×10^6

Table 9.2: Static elastic modulus used for each main artery in the model. Moduli are given for each of Dinnar's, Womersley's and Atabek's models so that the desired wavespeeds are obtained for given arterial dimensions and properties. The elasticity is smoothly tapered in each artery, where the values indicated in the table are values for the proximal segments, which taper down to the next value in the table (i.e. distal elasticity = proximal elasticity of the next segment). It is assumed that the umbilical artery has no elastic tapering.

The viscoelastic behaviour of the blood vessel walls were approximated by substituting the Young's modulus of elasticity by a complex viscoelastic modulus defined according to Taylor (1966) as $E = |E| e^{i\phi_0(1-e^{-\omega})}$. Taylor stated that ϕ_0 generally varies between 0° and 20° and a value of 10° was selected for the model. Both the Young's modulus and wave speed are frequency dependent and the values quoted for wave velocities are assumed for the first or fundamental harmonic. A simple iterative procedure was used to determine the values of the Young's modulus for the desired wavespeeds and these are shown in table (9.2) for each artery and model type.

9.7 Umbilical coiling

The radius of curvature for the umbilical arterial coiling may be calculated from equation (6.25), where R_c is the radius of the umbilical artery plus the umbilical vein. The umbilical vein radius at 28 weeks is approximately 0.33 cm (Sherer and Anyaegbunam, 1997). The pitch, h, is measured as the inverse of the coiling index (no. of coils per cm) which ranges from 0.05 to 0.6, and is gestational age independent. Thus h ranges from 20 cm to 1.67 cm, with a mean coiling index of 0.25 i.e. $h = 4$ cm (Strong et al., 1994; Sherer and Anyaegbunam, 1997; Rana et al., 1995).

9.8 Peripheral vascular bed parameter values

There are relatively few guidelines concerning the selection of some of the arterial tree parameters, however it is possible to keep parameter choices within physiologically realistic boundaries. Measurements of the length to radius ratio, l_r, in the coronary arterial tree has demonstrated that it has an upper bound of around 35 and averages between 10 - 20 (Zamir, 1999). A value of $l_r = 20$ was assumed for all the arterial trees.

The power law or branching ratio parameter, K, may be related to the morphometric parameters in equation (7.1) and for dichomotous branching, $K = b_1$ (Bennett, 1996; Dawson, 1999). Measurements made in the pulmonary vascular bed of adult humans, indicate that b_1 lies between 2.4 and 2.71 (Horsfield, 1978; Huang et al. 1994). Furthermore, chapter 7 indicated that K generally lay somewhere between 2 and 3 and thus a value of 2.6 was chosen for all the foetal arterial beds and a slightly higher value of 2.8 was selected for the placental arterial tree.

For the tapered version of the arterial tree, a further constraint may be imposed on the branching angle, θ by examining the equation for the resistance of a single vessel within the tree (equation (7.17)). The resistance of a vessel must be a positive value and therefore $\frac{x^4-k^4}{x^4} > 0$.

Equation (7.14) indicated that $x = 2\cos\theta$ and given that θ must lie between 0° and 90°, and for values of K around 2.6-2.8, this inequality implies that $\theta > 50°$.

Vascular compartment	θ	Terminal radius (μm) (Tapered)	No. of levels of branching (Tapered)	Terminal radius (μm) (Non-tapered)	No. of levels of branching (Non-tapered)
Head and Heart	52°	69	32	110	31
Upper body and Thorax	51°	110	29	575	22
Abdomen	53°	323	24	211	26
Adrenals	65°	425	22	1	46
Lower limbs	50°	821	19	1651	8
Placenta	58°	898	21	9	41

Table 9.3: Values of tapered branching angle, no. of levels of branching of arterial tree and radius of terminal arterial tree branches for tapered and non-tapered arterial trees for each of the six vascular compartments employed in the foetal model. The terminal radius of the lower limbs for the tapered version is larger than desired but cannot be lowered as θ is at its minimum. The corresponding values for the non-tapered version result in terminal radii that are too low for the adrenals and the placenta and too high for the lower limbs.

The microcirculation is defined as the site where flow can no longer be approximated by laminar flow since the vessel radius is only slightly larger than the actual size of the red blood cells. Flow must therefore be considered as multiphase flow with the red blood cells flowing in a single file formation. The vessels in this definition are around 20μm in diameter (Dinnar, 1981). The peripheral vascular tree model presented in chapter 7, modelled a branching network up until just before the level of the microcirculation. The terminal branches of the network were considered to be a lumped resistance which represents the microcirculation. Thus θ was selected for each arterial tree so that the radius of the terminal branch was between 50μm and 200μm. The terminal branches of the placental arterial tree were selected to be slightly larger than the tertiary or terminal villi, which are around 600μm (Benirschke and Kaufmann, 1990). Table (9.3) depicts the values of θ used for each vascular compartment, along with the resulting terminal radii of the arterial networks for both the tapered and non-tapered networks. As θ approaches 50°, the number of branches that are required increase and the terminal branch radii decrease.

The initial Young's modulus and radius for the peripheral arterial trees were respectively assumed to be equal to the Young's modulus and radius of the feeding vessel that they branch from. The viscoelastic angle, ϕ, was assumed to be the same as for the larger vessels in the model and this was 10°.

9.9 Computational procedure

The characteristic impedance and propagation constants are calculated from equations (4.36) and (4.37) respectively, for each arterial segment at each harmonic. The computational procedure consists of a backward and a forward pass, for each frequency component analysed. The backward pass commences at the peripheral branches and proceeds systematically towards the input at the ascending aorta, calculating input impedances at every node as it advances, using equation (4.43) for a straight segment and equation (5.23a) for a tapered segment. The input impedance, Z_{in}, of a distal artery becomes the terminal impedance, Z_t, for the proximal artery connecting to it. Wherever a bifurcation exists, a parallel impedance is computed as :

$$\frac{1}{Z_{parallel}} = \frac{1}{Z_1} + \frac{1}{Z_2} \tag{9.1}$$

The total time domain input flow waveform from the heart is calculated according to the procedure outlined in section 3.4. This flow pulse is then Fourier transformed and each harmonic is individually propagated through the system. These components are decomposed into forward and reflected waveforms according to

$$Q_{in} = Q_f - Q_r = Q_f \left(1 - \Gamma_t e^{-2\gamma l}\right) \tag{9.2}$$

where Γ_t is determined from equation (4.42) using the input impedances which were calculated in the backward pass.

Having determined both the forward and reflected flow waveforms at the source end of the artery, these are then converted to pressure waveforms and referred to the load end as follows :

$$P_f(l) = Q_f(0)\, e^{-\gamma l} Z_0 \tag{9.3}$$

$$P_r(l) = Q_r(0)\, e^{\gamma l} Z_0 \tag{9.4}$$

The total pressure at the termination of arterial segment x is the same as the total pressure at the beginning of arterial segment $x + 1$ and thus the forward pass proceeds in this manner working towards the periphery and calculating pressure and flow at every point along the arterial tree.

In order to solve for the steady flow components, each arterial segment is considered as a real valued resistance. The values for the radii listed in table (9.1) take into account both the intrinsic geometrical taper and the taper that arises as a result of an applied pressure gradient. Equation (5.54) is used to obtain the input resistance of a tapered arterial segment. However, no intrinsic radial taper is present in the umbilical arteries and therefore it is necessary to calculate the degree of taper due to the pressure gradient. Beginning with an untapered umbilical artery, the model calculates the pressure at the proximal end of the artery to be 58.1 mmHg and the pressure at the distal end to be 44.4 mmHg. Substituting these values into equation (4.24), yields a proximal radius of 0.154 cm and a distal radius of 0.153 cm. These values are not considered to be sufficiently different from the untapered radius of 0.15 cm and thus the effect of this taper may be neglected in the umbilical arteries. The pressure gradient in the umbilical arteries will be the largest gradient due to the length of the arteries and therefore this taper will exert negligible effects on the arteries and the values specified in table (9.1) may be considered to be predominantly a result of intrinsic taper. The resistance and characteristic impedance of the umbilical artery is modified using equations (11.14) and (6.28) respectively to include the effects of coiling.

The steady input resistances of the periphery are determined by the ratio of mean arterial pressure to the fraction of cardiac output distributed to each vascular compartment. Peripheral resistances are added in series with arterial resistances and these are combined in parallel with subsequent branches. In this manner the total input resistance is computed proceeding towards the aortic input and this constitutes the backward pass. There are no reverse travelling waves.

The forward pass proceeds from the input to the aorta and calculates the pressure from the product of the known input flow and input resistance. The mean flow is constant for each arterial segment and the pressure at the distal end is given by the difference between the proximal pressure and the product of the flow and the arterial resistance. This distal pressure is then identical to the pressure at the proximal end of the subsequent artery and thus the forward pass proceeds in this manner.

The solutions for the forward and reverse components of flow and pressure at each harmonic and at every point along the arterial tree are stored and then the inverse Fourier transform is implemented to reconstruct the time domain waveforms.

9.9.1 Adaption for umbilical coiling

The steady component of flow in the coiled umbilical artery is determined by adjusting the steady flow resistance using equation (11.14). However, this equation is dependent upon the Dean number, which is in turn dependent upon the mean flow in the artery. In order to

circumvent this circular dependency, an initial estimate for the mean flow is assumed based upon the fraction of known cardiac output distributed to the umbilical artery and placenta. This estimate is used to determine the coiling resistance and hence a new value of the mean flow in the umbilical artery is calculated. This new value is compared with the original estimate and unless their percentage difference is less than a threshold accuracy of 0.01 %, the new value is used to recalculate the coiling resistance and hence a new mean flow. This procedure is repeated until the two values of mean flow converge as depicted in the flow chart in figure (9.1).

9.9.2 Adaption for tapering

The proximal and distal Young's moduli and radii of each tapered artery is specified in tables (9.2) and (9.1) respectively. The chosen fundamental model (Dinnar, Atabek or Womersley) is then used to calculate the transmission line parameters, Z_0 and γ at either end of each artery. Exponentials are then fitted to these parameters using equations (5.1) and (5.2) and subsequently the tapered expressions for input impedance and flow are employed for further calculations. Thus tapering is originally specified in terms of fundamental arterial properties (radius and elasticity) and not in terms of transmission line properties.

9.10 Simulink coding

A visual programming approach was used to code and simulate the foetal model. This was achieved by using Simulink for Matlab^{TM}, which is a graphical interface for the high level Matlab programming language that is often used to solve complex time domain control problems. However, by setting the start time equal to the stop time of the simulation, Simulink effectively functions as a graphical flow chart. This allows functional building blocks for arterial segments to be defined, where the relationships between the inputs and outputs of the blocks are determined by custom Matlab functions. These building blocks may subsequently be interconnected or cascaded to form the entire working model. Anatomical or physiological parameters are readily changed through use of a simple mouse driven interface. This novel use of Simulink for the synthesis of transmission line haemodynamic simulations was originally proposed by John (2000) and although the principle idea remains the same, the foetal model in this thesis uses an entirely different set of building blocks and functional relations that were developed from the start to incorporate the flow equations presented in this thesis. Details of each model building block and its code, as well as the complete model, may be located in Appendix D.

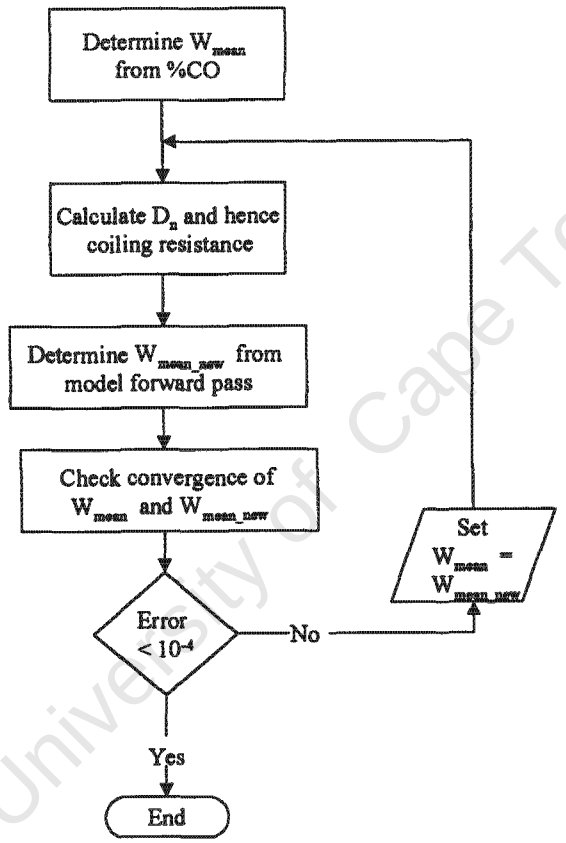

Figure 9.1: Flow chart for determination of W_{mean} (the mean axial flow) and coiling resistance in the umbilical artery.

9.11 Summary

This chapter detailed the selection of anatomical and physiological variables to model a healthy 28 week old foetus. This selection was largely based on measured values obtained from the literature and where necessary, estimations of parameters were based upon physiologically realistic constraints. The computational algorithm to calculate the flow velocities at any point along the model arterial tree was described. This was a further extension of standard transmission line theory and was adapted for coiling and tapering. The model was coded using the graphical interface of Simulink^{TM} and the algorithmic programming language of Matlab^{TM}.

Chapter 10

Model validation and simulations for a normal foetus

10.1 Model validation

The model of the normal physiological conditions of a 28 week gestational age foetus may be validated both qualitatively and quantitatively. Qualitative validation is performed by comparing the shapes of model generated waveforms with those obtained clinically at a number of sampling sites along the foetal arterial tree. As a fair degree of variation is to be expected, this method of validation sufficiently serves to assess whether any gross differences in shape are present. Indeed, qualitative descriptions of foetal flow velocity waveforms have previously been used as a diagnostic measure by dividing measured waveforms into one of four distinct blood flow classes based upon visual inspection (Malcus, 1991; Laurin et al. 1987). Quantitative validation, to a large degree, is performed by comparison of Doppler indices of model generated flow velocity waveforms with those obtained clinically. A variety of indices have been proposed for investigation of the foetal circulation and these will be discussed in further detail below. Further model validation may be accomplished by determining pressure waveforms and impedance spectra and comparing these with those obtained through clinical measurements. Unfortunately these measurements require invasive procedures which are unethical for human research. However, data of this nature has been attained for foetal sheep and although the degree of discrepancy with human data is unknown, comparison with the sheep data may still be of use in model validation.

Following physiological validation of the 28 week old foetus, it is necessary to verify the equations for growth. This may be achieved by comparing model generated indices at each

gestational age from 28-40 weeks with those obtained from sources in the literature. Validation of foetal pathology is a far more complex task owing to the large variety of pathological conditions and foetal responses. However, this may be performed on a simple level by ensuring that the model follows the same trends in disease as reported in the literature. This will be considered in the following chapter.

Validation of the tapering equations is easily performed by dividing each tapered arterial segment into a number of smaller subsegments of uniform radial and elastic properties. Ideally as the number of cascaded uniform subsegments approaches infinity, the flow velocities and impedance spectra should match those obtained via the exact solution for tapered arterial segments.

Measurements for model validation are performed at clinically relevant measurement sites. These are at the levels of the thoracic and abdominal aorta, the iliac arteries and both ends of the umbilical arteries. Many studies have investigated different measurement sites along the umbilical arteries. The majority of these indicate that a Doppler index gradient is present in the umbilical artery, with the higher indices being obtained at the foetal end of the artery (Forouzan et al. 1991; Vieyres et al. 1991; Abramowicz et al. 1989; Kay et al. 1989; Mehalek et al. 1989; Bruner et al. 1994). Furthermore, it has also been demonstrated that differences between indices at either end of the cord diminish with advancing gestational age and increase with foetal growth retardation and placental pathology (Sonesson et al. 1993; Skoll et al. 1997). This may serve as a further means of model validation. Although, this index gradient has been demonstrated to exist in a number of works, it must be noted that it exists in a statistical sense and that a few individual foetuses may not exhibit such a gradient. Indeed, a study by Ruissen et al. (1990) found no evidence of flow gradients and thus the model may be of use to determine those factors that contribute to the precise nature of umbilical arterial Doppler index gradients.

10.1.1 Doppler Indices

Ultrasound measurement of flow velocity waveforms is dependent upon the angle between the probe beam and the blood vessel. This angle is difficult to estimate and thus a requirement of any clinically useful Doppler index is to yield the same value regardless of the measurement angle. Several angle independent indices have been proposed to classify flow velocity waveforms and these may be described with reference to figure (10.1). These indices are listed in table (10.1).

In order to validate the model, it is necessary to obtain clinical data using these indices. However, only the Pulsatility Index, the Resistance Index and the A/B ratio have been examined

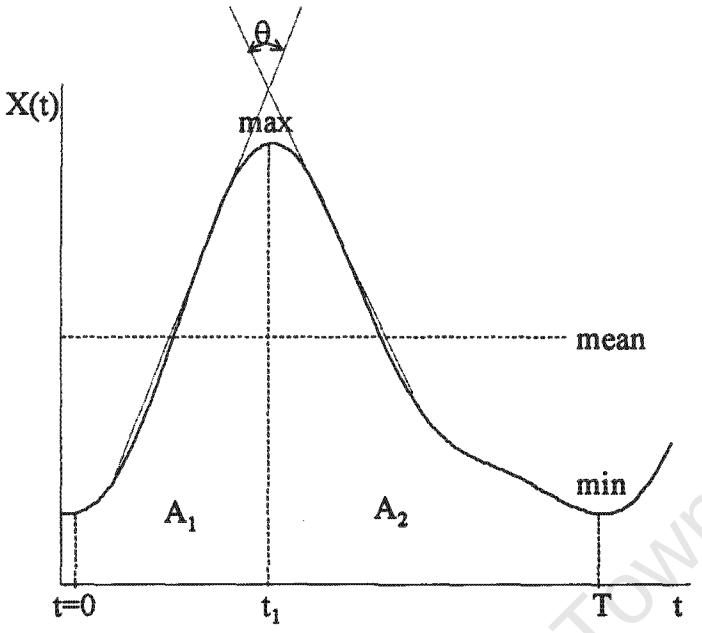

Figure 10.1: Derivation of indices used to characterise the Doppler flow velocity waveforms. The blood flow waveform X(t) is first normalised to make all the indices angle independent. Table 10.1 contains a description of the indices used.

in any significant detail in the literature and reference values for many of the other indices are unobtainable. Furthermore, many of these indices are highly correlated with one another and in clinical settings it is unlikely that one index offers any clear advantage over the others (McParland and Pearce, 1988) . Additionally, the A/B ratio and the Resistance Index are related by $A/B = 1/(1-\mathrm{RI})$ and thus all further validations and analyses in this thesis only consider the Pulsatility Index and the Resistance Index.

Index	Description	Reference
Pulsatility Index (PI)	$\frac{\max - \min}{\text{mean}}$	Gosling and King, 1975
Resistance Index (RI)	$\frac{\max - \min}{\max}$	Pourcelot, 1974
A/B ratio (AB)	$\frac{\max}{\min}$	Stuart et al. 1980
Constant flow ratio[1] (AA)	$\frac{\min \times T}{A}$	Thompson et al. 1985
Normalization factor (N)	$\frac{t_1}{T - t_1}$	Thompson et al. 1985
Relative flow index (R_0)	$\frac{A_1}{A_2}$	Thompson et al. 1985
Relative flow rate index (R)	$\frac{A_1/t_1}{A_2/(T-t_1)}$	Thompson et al. 1985
Systolic decay time index[2] (D)	$\frac{t_r/t_1}{t_d/(T-t_1)}$	Thompson et al. 1985
Height width index (HWI)	$\frac{\max - \min}{\text{mean}} \times \frac{T}{t_1}$	Johnston et al. 1983
Path length index[3](PLI)	$\sum_{i=0}^{N-1} \left[\begin{array}{c} (f_{i+1} - f_i)^2 \overline{f}^2 - \\ (t_{i+1} - t_i)^2 / T \end{array} \right]^{1/2}$	Johnston et al. 1983
Laplace transform indices[4]	Third order frequency domain fit : $H(s) = 1/\left(s^2 + 2\delta\omega_0 s + \omega_0^2\right)(s + \gamma)$	Skidmore and Woodcock, (1979, 1980,1980a,1980b)
Pulse related index (PRI)	$\frac{\max - \min}{T}$	Beksac et al. 1995
Area ratio of wave (ARW)	$\frac{A(T-t_1)}{\max - \min}$	Beksac et al. 1995
Coincident slope angle (ACS)	θ	Beksac et al. 1995
High resistance state index[5] (HRSI)	See [5] in caption	Szentkuti et al. 1995

Table 10.1: Doppler indices evaluated on normalised flow velocity waveforms, along with their sources. Notes : (1) $A = A_1 + A_2$. (2) t_r is the rise time from 0.75max to max and t_d is the decay time from max to 0.75max. (3) The time axis is divided into N segments where the maximum instantaneous frequency at time t_i is f_i. $\overline{f}$ is the mean frequency. (4) The Laplace transform technique originally proposed by Skidmore and Woodcock (1979, 1980a,b) suggests that the parameter δ is related to proximal conditions, ω_0 is related to arterial elasticity and γ is related to the distal impedance of the measurement location. This technique has subsequently been evaluated on umbilical arterial measurements by Stone et al. (1990) and Brackley et al. (1998a,b). (5) The HRSI was proposed to characterise further changes in AEDF foetuses and is evaluated by first generating a new curve called the resistance profile area : RPA(t) = [max$-X(t)$]/max. The HRSI ratio is given by RPA that falls within the 95th percentile RI and RI=1 (AEDF) is expressed as a percentage of the rectangle representing abnormal Doppler resistance.

10.2 Qualitative validation

Figures (10.2), (10.3), (10.4), (10.5) and (10.6) depict model generated flow velocity waveforms placed alongside actual measured normal Doppler waveforms. The source of the Doppler waveform was either obtained from published literature or from measurements conducted at Groote Schuur Hospital in Cape Town, South Africa. Waveforms are displayed for the descending thoracic aorta, abdominal aorta, external iliac artery, foetal and placental insertions of the umbilical artery. The mean values of the model generated waveforms are indicated by the horizontal line through the waveforms. This makes it easy to see that the mean value decreases as the measurement location moves towards the placenta. It should be noted that a number of sources of variation exist within a measured population. Variation of waveforms may be attributed to differences in anatomical and physiological variables, as well as due to measurement location, differences in measurement sensors and filters and foetal breathing, heart rate and movements. Given that exact values for each variation source are not available, comparisons of waveform shape should not be expected to be identical. A further beat to beat variation is often encountered between successive waveforms and thus averages are frequently utilised. However, as may be seen from the figures, the general trend and shape of the graphs appear to match. These features are a steep rise time, positive end diastolic flow and an abrupt change in the decay slope at about 3/4 of the waveform period. As the measurement location proceeds towards the placenta, the end diastolic flows increase, the mean flows decrease and the change in decay slope becomes less abrupt. It should further be noted that the model generates the volume flow rate waveform, Q, whilst the Doppler frequency shift is proportional to velocity. When the velocity profile is close to parabolic, it is reasonable to assume proportionality between the Q waveform, the maximum velocity waveform and the mean velocity waveform. This is certainly the case for the smaller arteries (the umbilical and even the aorta in young foetuses). Kleiner-Assaf et al. (1999) confirmed this by demonstrating, using their model, that the exact radial site of measurement did not significantly affect the subsequently derived Doppler indices. It is possible in the aorta of older foetuses that this is not the case and this shortcoming of the model validation is noted.

10.3 Quantitative validation

Both the pulsatility index and the resistance index of each of the computer simulated waveforms were compared with those reported in the literature, obtained from a number of sources. A

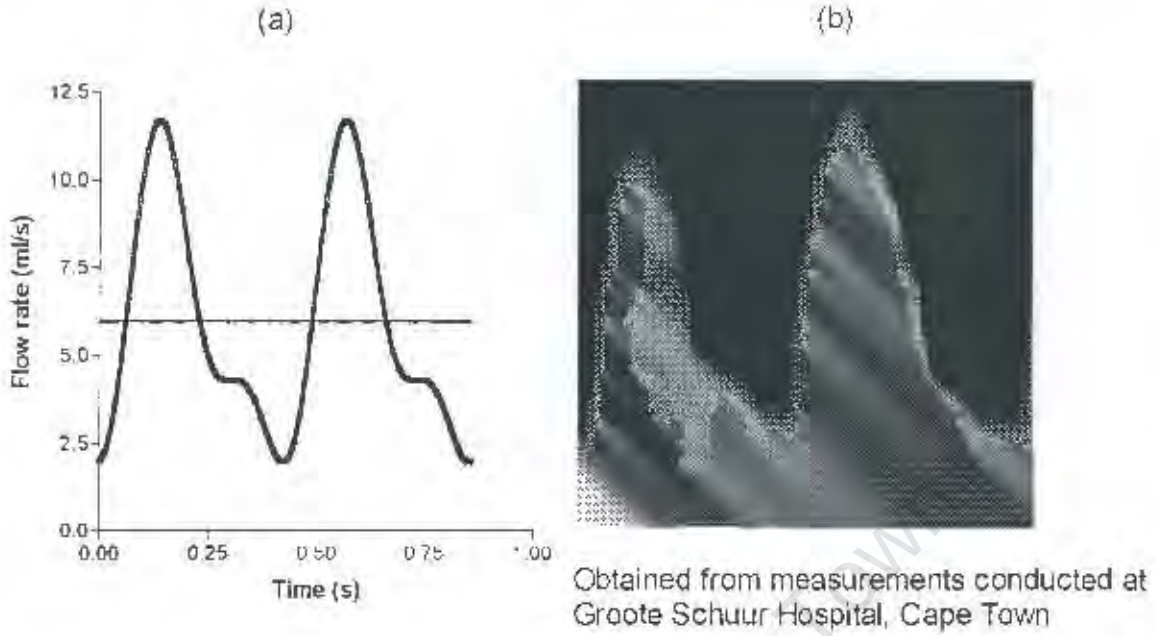

Figure 10.2: Flow velocity waveforms from the foetal thoracic aorta at 28 weeks. (a) Model generated waveform. The mean value is indicated by the horizontal line through the waveform (b) Clinically measured waveform.

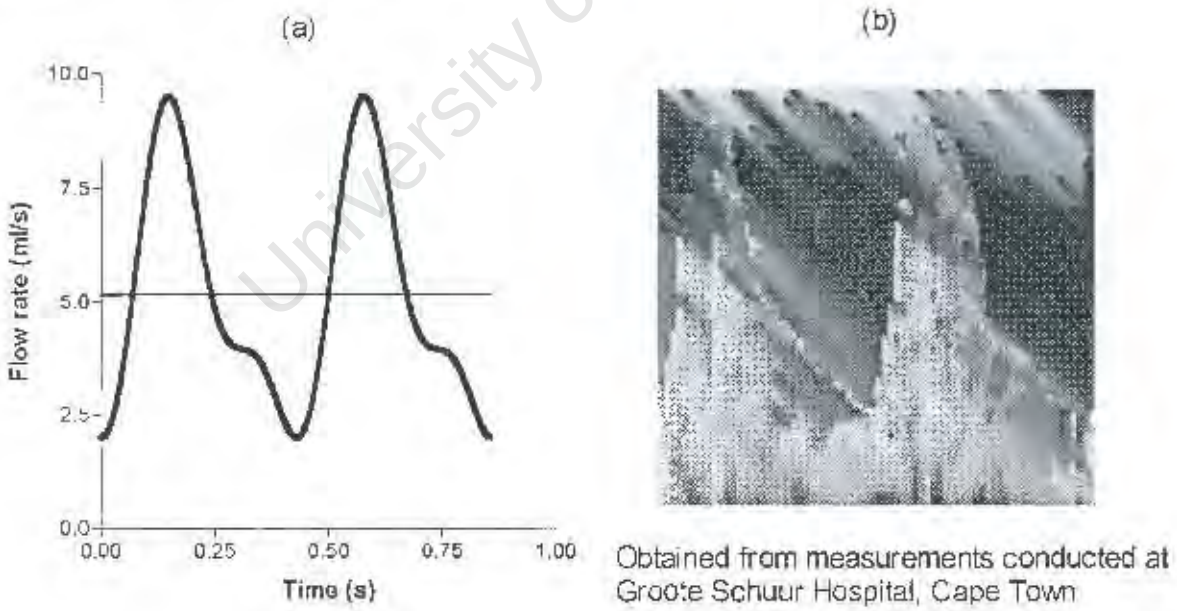

Figure 10.3: Flow velocity waveforms from the foetal abdominal aorta at 28 weeks. (a) Model generated waveform. The mean value is indicated by the horizontal line through the waveform (b) Clinically measured waveform.

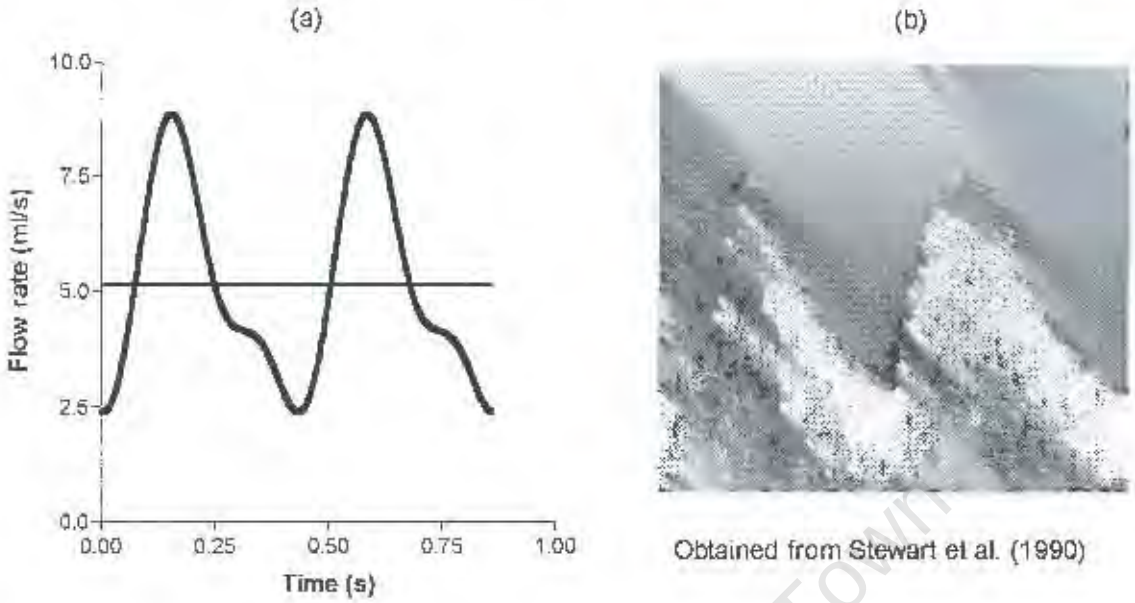

Figure 10.4: Flow velocity waveforms from the foetal external iliac artery at 28 weeks. (a) Model generated waveform. The mean value is indicated by the horizontal line through the waveform (b) Clinically measured waveform.

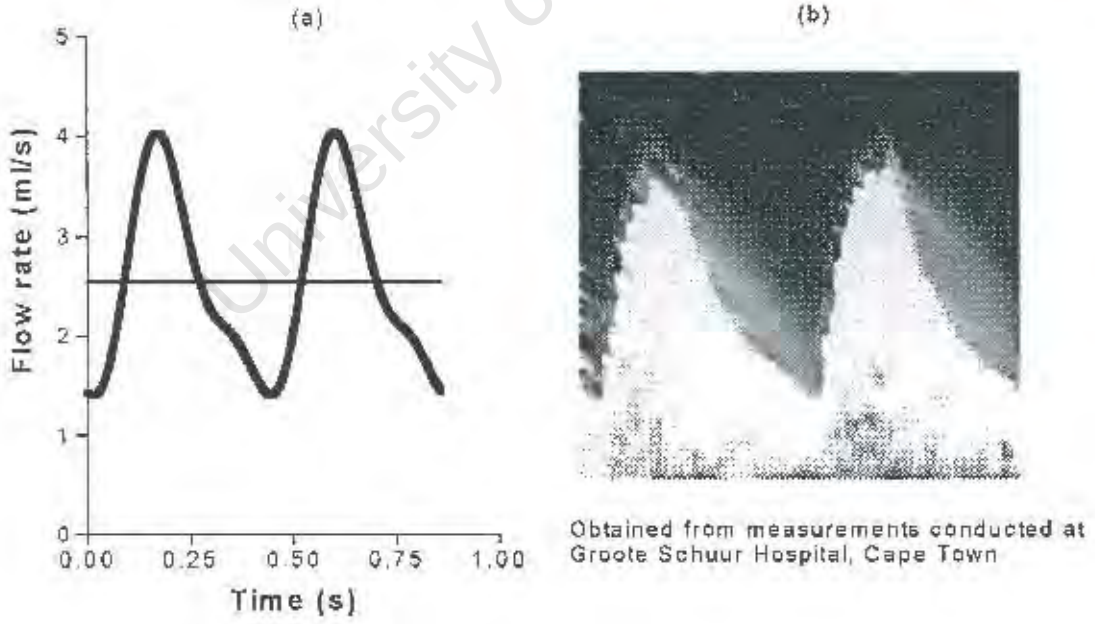

Figure 10.5: Flow velocity waveforms from the foetal end of the umbilical artery at 28 weeks. (a) Model generated waveform. The mean value is indicated by the horizontal line through the waveform (b) Clinically measured waveform.

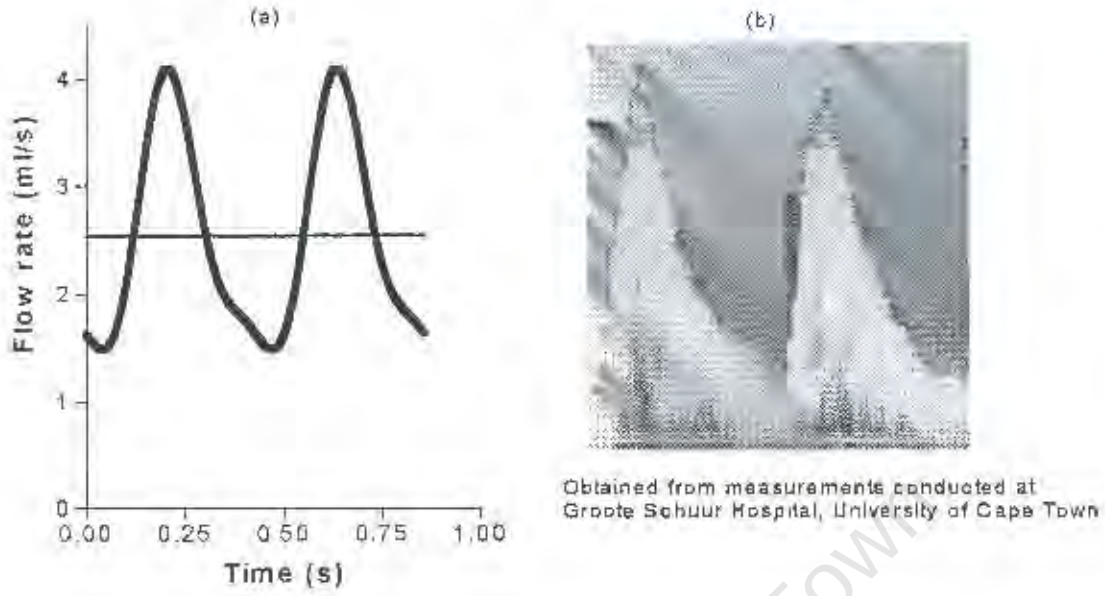

Figure 10.6: Flow velocity waveforms from the placental end of the umbilical artery at 28 weeks. (a) Model generated waveform. The mean value is indicated by the horizontal line through the waveform (b) Clinically measured waveform.

further degree of accuracy is obtained by using both these indices for comparison. Tables (10.2) and (10.3) present the results for Dinnar's, Womersley's and Atabek's models with tapered arterial trees with the pulsatility and resistance indices respectively, obtained from the literature.

The data in the tables indicates that all three models approximate the resistance and pulsatility indices with a great deal of accuracy. The maximum errors, as compared with the mean from clinical measurements, for Dinnar's model are 13.8% for the pulsatility index (in the thoracic aorta) and 1.5% for the resistance index (at the foetal end of the umbilical artery). Womersley's model offers a maximum error of 7.98% for the pulsatility index (in the thoracic aorta) and 7.2% for the resistance index (in the thoracic aorta). For Atabek's model, the maximum errors are 3.7% for the pulsatility index (in the thoracic aorta) and 7.2% for the resistance index (in the thoracic aorta). Total average errors may be obtained by addition of the errors at each measurement location divided by the number of measurement locations. The total average errors for Dinnar's model are 9.7% for the pulsatility index and 0.69% for the resistance index. For Womersley's model, the total average errors are 6.3% for the pulsatility index and 5.7% for the resistance index and for Atabek's model, the errors are 6.8% for the pulsatility index and 4.2% for the resistance index.

Artery	Reference PI	Model PI (Dinnar)	Model PI (Womersley)	Model PI (Atabek)
Thoracic Aorta	1.15-2.05[1], 1.83[2], 1.87[3], 2[4], 1.8[5], 2.16[6] **[1.88]**	1.62	1.73	1.81
Abdominal Aorta	1.58[3], 1.7[5] **[1.64]**	1.45	1.53	1.55
Iliac	1.25[9],1.27[10] **[1.26]**	1.25	1.31	1.3
Umbilical - foetal end	1.6[7], 1.03[3], 0.91-1.42[8],1.1[10] **[1.22]**	1.09	1.11	1.08
Umbilical - placental end	1.1[7], 0.68-1.48[8] **[1.09]**	1.00	1.09	1.02

Table 10.2: Values of pulsatility indices (PI) obtained from literature and the model predictions. Mean values are indicated in bold font. Sources :(1) Groenenberg et al., 1989; (2) Griffin et al., 1984; (3) van Vugt et al., 1987; (4) Tonge et al., 1986; (5) Lingman and Marsal, 1986; (6) Bilardo et al., 1988; (7) Mehalek et al., 1989; (8) Sonesson et al., 1993; (9) Stewart et al., 1990; (10) Mari, 1991.

Artery	Reference RI	Model RI (Dinnar)	Model RI (Womersley)	Model RI (Atabek)
Thoracic Aorta	0.82[1], 0.83[2], 0.84[3] **[0.83]**	0.83	0.89	0.89
Abdominal Aorta	0.78[2] **[0.78]**	0.79	0.83	0.83
Iliac	-	0.73	0.77	0.76
Umbilical - foetal end	0.71[4], 0.65[2], 0.61-0.78[5], 0.68[6] **[0.68]**	0.67	0.70	0.68
Umbilical - placental end	0.67[4], 0.49-0.77[5] **[0.63]**	0.63	0.67	0.65

Table 10.3: Values of resistance indices (RI) obtained from literature and the model predictions. Mean values are indicated in bold font. Sources :(1) Griffin et al., 1984; (2) van Vugt et al., 1987; (3) Jouppila and Kirkinen, 1986; (4) Mehalek et al., 1989; (5) Sonesson et al., 1993; (6) Kurmanavicius et al., 1997

Thus for the pulsatility index, Womersely's model offers the best results and for the resistance index, the optimum model is Dinnar's model. Overall, Dinnar's model provides the best

performance, however it must be noted that all three models provide acceptable results and error levels.

10.4 Anisotropy

Artery	γ				
	0.49	0.63	0.75	0.9	1
Thoracic Aorta	1.82	1.81	1.81	1.80	1.79
Abdominal Aorta	1.56	1.55	1.55	1.54	1.53
Iliac	1.31	1.3	1.29	1.29	1.28
Umbilical - foetal end	1.04	1.08	1.08	1.07	1.07
Umbilical - placental end	1.02	1.02	1.03	1.03	1.03

Table 10.4: Values of Pulsatility indices obtained in the various arteries using Atabek's model for varying degrees of anisotropy. The parameters $\gamma_1 = \gamma_2$ are varied from 0.49 to a value of 1 representing complete isotropy. It may clearly be seen that anisotropy has a neglibaly small effect on the Pulsatility index.

Artery	γ				
	0.49	0.63	0.75	0.9	1
Thoracic Aorta	0.89	0.89	0.89	0.89	0.89
Abdominal Aorta	0.83	0.83	0.83	0.83	0.82
Iliac	0.76	0.76	0.75	0.75	0.75
Umbilical - foetal end	0.68	0.68	0.68	0.68	0.67
Umbilical - placental end	0.65	0.65	0.65	0.65	0.65

Table 10.5: Values of Resistance indices obtained in the various arteries using Atabek's model for varying degrees of anisotropy. The parameters $\gamma_1 = \gamma_2$ are varied from 0.49 to a value of 1 representing complete isotropy. It may clearly be seen that anisotropy has a negligably small effect on the Resistance index.

Atabek's model provides an easy way of determining the effects of varying degrees of arterial anisotropy on the Doppler flow waveform indices. This model specifies two parameters, γ_1 and γ_2 which determine the ratios of the longitudinal to circumferential Young's moduli and

Poisson's ratios respectively. Following the convention of Atabek (1968) who stated that no experimental information was available for the parameter γ_2, it is assumed for these simulations that $\gamma = \gamma_1 = \gamma_2$ and that based on Atabek's simulations, this varies between 0.49 and 1. Tables (10.4) and (10.5) list the changes in pulsatility and resistance indices respectively for a range of anisotropic ratios.

From these results, it may be seen that anisotropy appears to have very little effect on the value of the Doppler indices with no greater than a 2% difference. Although, actual values of possible anisotropy in the foetal arterial system have not been measured, these simulations demonstrate that anisotropy may be neglected and an isotropic model may be assumed.

From this point on, it is no longer necessary to determine results using all three models, and Dinnar's model has been chosen for all further simulations. Dinnar's model was deemed the most appropriate due to it having the lowest overall total average error, as well as it being the only thick walled model and also for the way that the wall tethering and surrounding tissues are taken into consideration.

Artery	1	2	5	10	15	20	50	Exact solution
Thoracic Aorta	1.35	1.39	1.54	1.60	1.62	1.62	1.62	1.62
Abdominal Aorta	1.18	1.19	1.33	1.38	1.40	1.42	1.45	1.45
Iliac	0.98	1.01	1.14	1.20	1.25	1.25	1.25	1.25
Umbilical - foetal end	0.85	0.88	0.98	1.04	1.09	1.10	1.09	1.09
Umbilical - placental end	0.78	0.81	0.89	0.95	0.99	1.00	1.00	1.00

Table 10.6: Pulsatility indices at the model measurement locations for cascaded arterial segments and for the exact tapered solution. Each tapered artery is divided into a number of blocks as shown in the table. Each block has uniform non-tapered properties. The cascaded solution converges to the exact solution after about 20-50 blocks have been used.

10.5 Tapering

The tapering equations may be validated by replacing each tapered arterial segment with a number of smaller arterial segments, each containing uniform elastic and geometric properties as depicted in figure (10.7). This may conveniently be performed using the simulink interface by replacing each tapered arterial building block with a large number of uniform or non-tapered arterial building blocks. As the number of these cascaded uniform segments increase, the

results should be expected to converge to those of the tapered solution. These results are performed using Dinnar's solution. Tables (10.6) and (10.7) display the values of the pulsatility and resistance indices in each artery for 1, 2, 5, 10, 15, 20 and 50 non-tapered arterial segments per tapered artery. An identical number of divisions per artery is used to simplify this approach, although it is expected that the longer an artery, the more divisions it would require. A further validation of the tapering equations may be obtained by comparing input impedances. The input impedance at the entrance to the thoracic aorta incorporates the results of the input impedances at all the downstream arteries and is used as a site of comparison. Figures (10.8 a and b) display the magnitude and phase plots of the impedance spectra versus an increasing number of cascaded uniform arterial segments.

Artery	1	2	5	10	15	20	50	Exact solution
Thoracic Aorta	0.72	0.75	0.80	0.82	0.83	0.83	0.83	0.83
Abdominal Aorta	0.65	0.69	0.74	0.77	0.79	0.79	0.79	0.79
Iliac	0.60	0.63	0.68	0.71	0.72	0.73	0.73	0.73
Umbilical - foetal end	0.57	0.58	0.63	0.65	0.66	0.67	0.67	0.67
Umbilical - placental end	0.53	0.54	0.58	0.60	0.62	0.62	0.63	0.63

Table 10.7: Resistance indices at the model measurement locations for cascaded arterial segments and for the exact tapered solution. Each tapered artery is divided into a number of blocks as shown in the table. Each block has uniform non-tapered properties. The cascaded solution converges to the exact solution after about 20-50 blocks have been used.

These simulations demonstrate the validity of the exact tapering equations, with the solution converging to within 2% accuracy using approximately 15 cascaded sections per arterial segment and becoming exact with 50 segments. The total average error incurred by neglecting tapering altogether is 20.2% for the pulsatility index and 15.9% for the resistance index. In this situation the values at the proximal end of the artery were used for the entire arterial segment. These errors are large enough to merit the use of an exact tapered solution. It should be noted that 15 cascaded sections per arterial segment, totals 45 segments for the entire descending aorta.

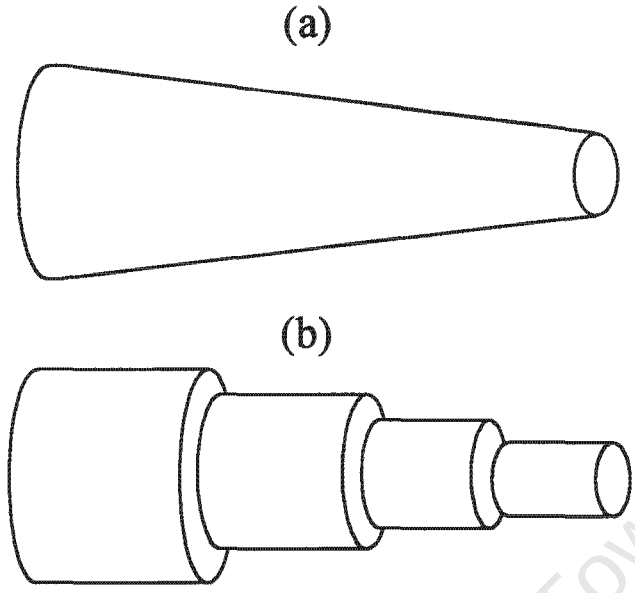

Figure 10.7: A single tapered arterial segment is depicted in (a) and an approximation to this segment consisting of a number of smaller segments, each with uniform geometric and elastic properties is depicted in (b).

10.5.1 Tapered peripheral arterial trees

Artery	PI Tapered	PI Non-tapered	RI Tapered	RI Non-Tapered
Thoracic Aorta	1.62	1.96	0.83	0.88
Abdominal Aorta	1.45	0.48	0.79	0.37
Iliac	1.25	0.35	0.73	0.29
Umbilical - foetal end	1.09	0.24	0.67	0.21
Umbilical - placental end	1.00	0.13	0.63	0.12

Table 10.8: Values of Pulsatility and Resistance indices obtained in the various arteries using Dinnar's model for both tapered and non-tapered peripheral vascular compartment models. Compared with the results of the tapered model, which has been shown to closely match clinical data, the non-tapered model significantly underestimates the value of flow indices, with increasing error, as the measurement location moves towards the placenta.

The number of levels of branching and the radii of the terminal branches in the arterial tree models were presented in table (9.3) for tapered and non-tapered peripheral arterial networks. These values indicate that the tapered peripheral tree model exhibits more realistic values for

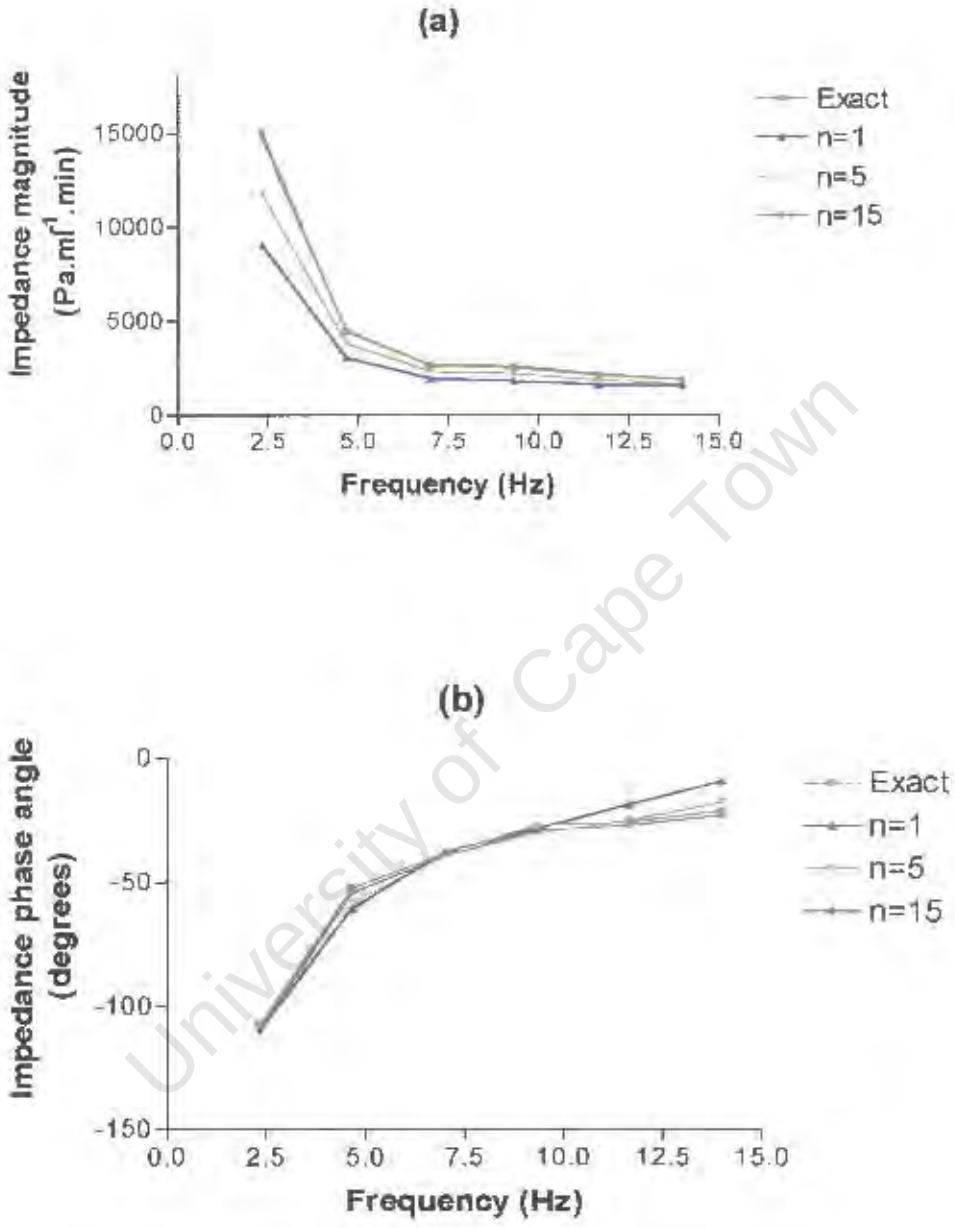

Figure 10.8: Thoracic input impedance magnitude (a) and phase (b) plots using the exact solution for tapering as well as 1, 5 and 15 cascaded uniform segments per tapered artery.

the terminal radii. Based on these results, the tapered peripheral arterial tree model has been used for the simulations up until this point. However it is instructive to further test the validity of the tapered versus the non-tapered peripheral tree model via a comparison of the predicted pulsatility and resistance indices of the non-tapered version of the vascular compartments and these are presented in table (10.8). These results have only been presented for Dinnar's model and the results of the other two models follow similar trends. From these results it may be seen that with the exception of the thoracic aorta, the non-tapered version introduces significant errors for the indices in each artery, with a maximum error of 81% for the resistance index and 87% for the pulsatility index, obtained at the placental end of the umbilical arteries. These results further signify the need to use the tapered peripheral network model.

10.6 Impedance Spectra

Adamson et al. (1992) measured impedance magnitude and phase at the entrance to the umbilical cord in several sheep foetuses under control conditions. These data were obtained from their research laboratories and used as a comparison for model generated impedance spectra. Several important physiological differences exist between the human and sheep umbilical circulations that may result in distinctions between the two data sets. The most consequential difference is the proportion of cardiac output that is distributed to the umbilical cord and placenta. This is significantly higher in foetal sheep and around the order of 40% (compared with only 25% in humans). Further differences are the existence of the common umbilical artery in the sheep, which is a short, nonvasoactive, thin walled segment of artery (Hill et al. 1995) and that the viscosity of foetal blood is lower in the sheep and of the order of magnitude of 2.4 cP (compared with 6cP in humans). Mean arterial pressure in foetal sheep is approximately 40 mmHg, which is a lower value than in human foetuses (60 mmHg). Thus given these differences, it is unlikely that the human and sheep impedance spectra should match, however it is reasonable to expect that similar trends may occur and as impedance spectra in human foetuses have never been measured, it is instructive to generate this data using the model. Figure (10.9) compares model generated impedance magnitude and phase data with averaged data from seven control sheep. Both the model generated magnitude and phase data are surprisingly similar to those obtained via measurements, following the same directional trends, if not in the same proportions.

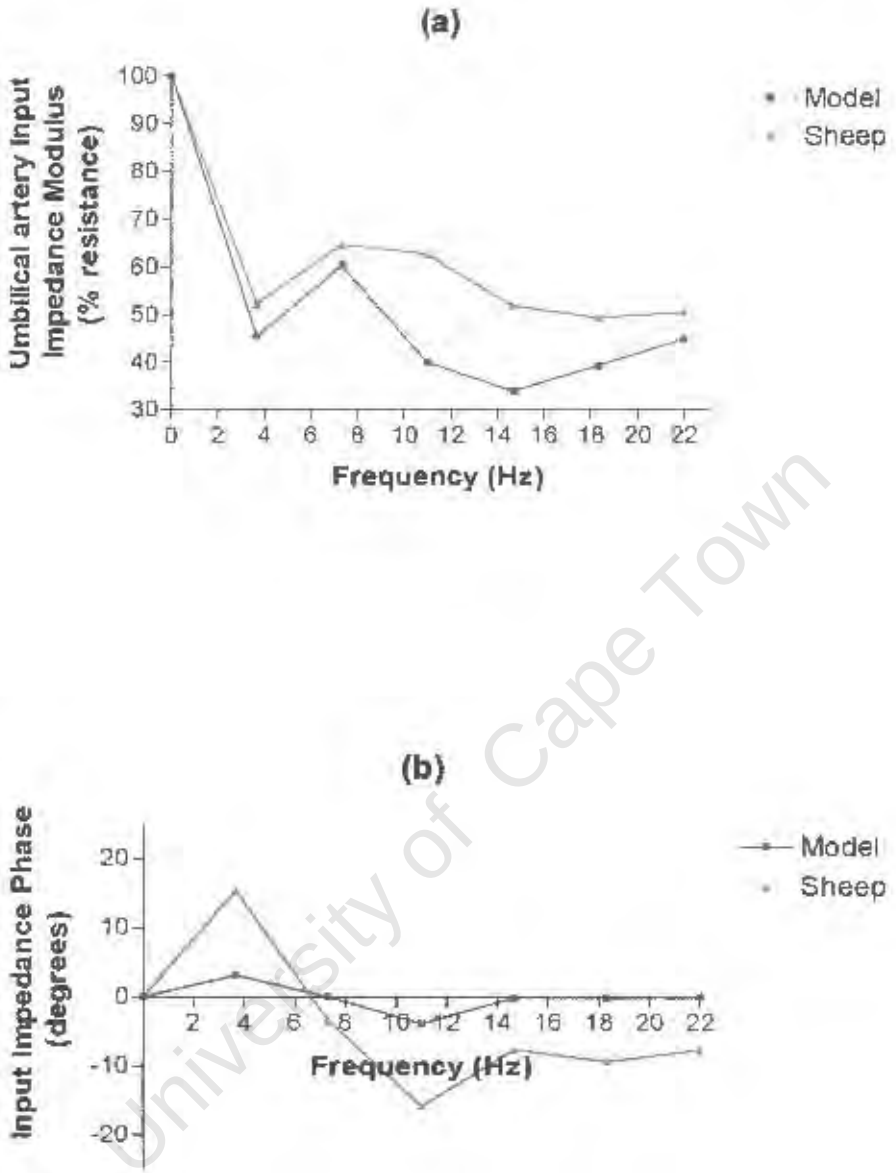

Figure 10.9: Graphs of umbilical impedance modulus (a) and phase (b), at the entrance to the umbilical arteries, versus frequency. Impedance modulus is presented as a percentage of mean resistance to steady flow. The line labelled 'sheep' represents measured impedance spectra of foetal sheep under control conditions and averaged over seven foetuses. These data were obtained from Adamson et al. (1992). The line labelled 'model' represents the model generated impedances.

10.7 Validation of foetal growth model

Chapter 8 described how the length and therefore the ratio of radius to length parameter, l_r, was required to grow at a different rate to that of the radius, which grows at the same rate as the total foetal mass. This requirement allows the combined mass of each peripheral arterial tree to grow at an equivalent rate to the organs that it represents. The assumed value of l_r at 28 weeks was 20 and this will therefore decrease until term. Figure (10.10) is a plot of the length to radius ratio versus gestational age in each of the six vascular compartments, modelled for the tapered peripheral tree.

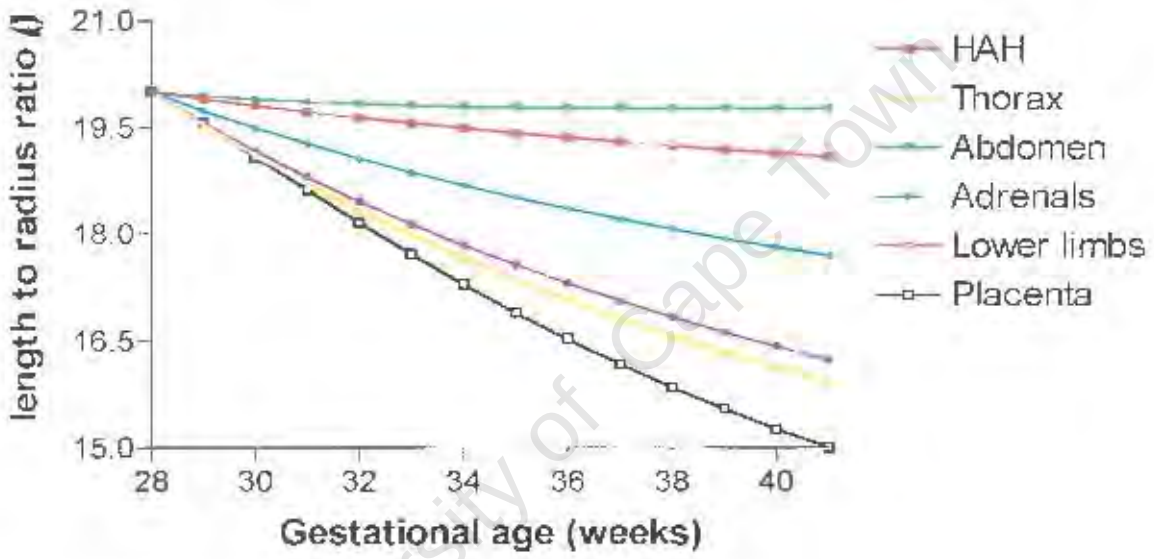

Figure 10.10: Length to radius ratio, l_r versus gestational age for each of the six tapered peripheral vascular trees. The initial value at 28 weeks is 20 and this decreases at a different rate with gestation for each vascular compartment.

An important point to note is that l_r does not decrease below a value of 15 and a minimum of 10 was noted in vascular trees by Zamir (1999). Thus the growth model of the peripheral compartments remains within physiological boundaries.

10.7.1 Doppler indices and foetal growth

A number of authors have published tables of reference ranges or regression equations for common Doppler indices in various arteries for healthy appropriate for gestational age foetuses. These may serve as a convenient means of comparison or verification of the foetal growth model.

Figures (10.11) depict graphs of model generated pulsatility and resistance indices versus gestational age in the thoracic and abdominal aorta's. Griffin et al. (1984), Groenenberg et al. (1989) , van Vugt et al. (1987), Tonge et al. (1986), Jouppila and Kirkinen (1986) and Lingman and Marsal (1986) all report that on average both the pulsatility and resistance indices in the thoracic and abdominal aortas remain relatively constant during the third trimester. From the graphs it may be seen that the model generated curves appear to remain relatively constant, although there is a slight tendency to decrease with advancing gestation.

Relatively few Doppler examinations have been performed on the iliac arteries. However, Stewart et al. (1990) do provide regression equations for the pulsatility index in the external iliac arteries. Figure (10.12) depicts the model generated resistance and pulsatility indices for the iliac artery, along with the regression values provided by Stewart et al. The trend is for the indices to decrease with advancing gestation and the model generated curves clearly do so, although not at quite the same rate as the regression curve.

The largest collection of reference values of Doppler indices for clinical interpretation is undoubtedly for the umbilical artery. However, the majority of these publications are performed using continuous wave Doppler equipment and thus the actual site of measurement location is unknown. As mentioned previously, it is now well established that an index gradient exists between the ends of the umbilical artery. Figures (10.13 a and b) respectively display model generated resistance and pulsatility indices versus gestational age for the proximal (foetal) and distal (placental) ends of the umbilical artery. It may be seen that both indices and the difference of indices between either end of the artery decrease with advancing gestation. Superimposed on these figures are clinical reference values obtained from various sources as indicated on the figures. The model generated values lie somewhere in-between the clinical reference ranges and thus the model correctly predicts the trends and range of values of the indices with gestational age.

Sonesson et al. (1993) measured the differences in Doppler indices obtained between recording sites of the placental and foetal ends of the umbilical artery and established regression equations for these differences with gestational age. Figures (10.14 a and b) display the model generated differences of resistance and pulsatility index, along with Sonneson et al.'s regression curves. It may be seen that the model closely predicts the trend of diminishing differences and offers a close approximation to the actual values of the differences

10.8 Summary

An attempt to validate the model under normal physiological conditions by both quantitative and qualitative methods was conducted. Current non-invasive measurement procedures in

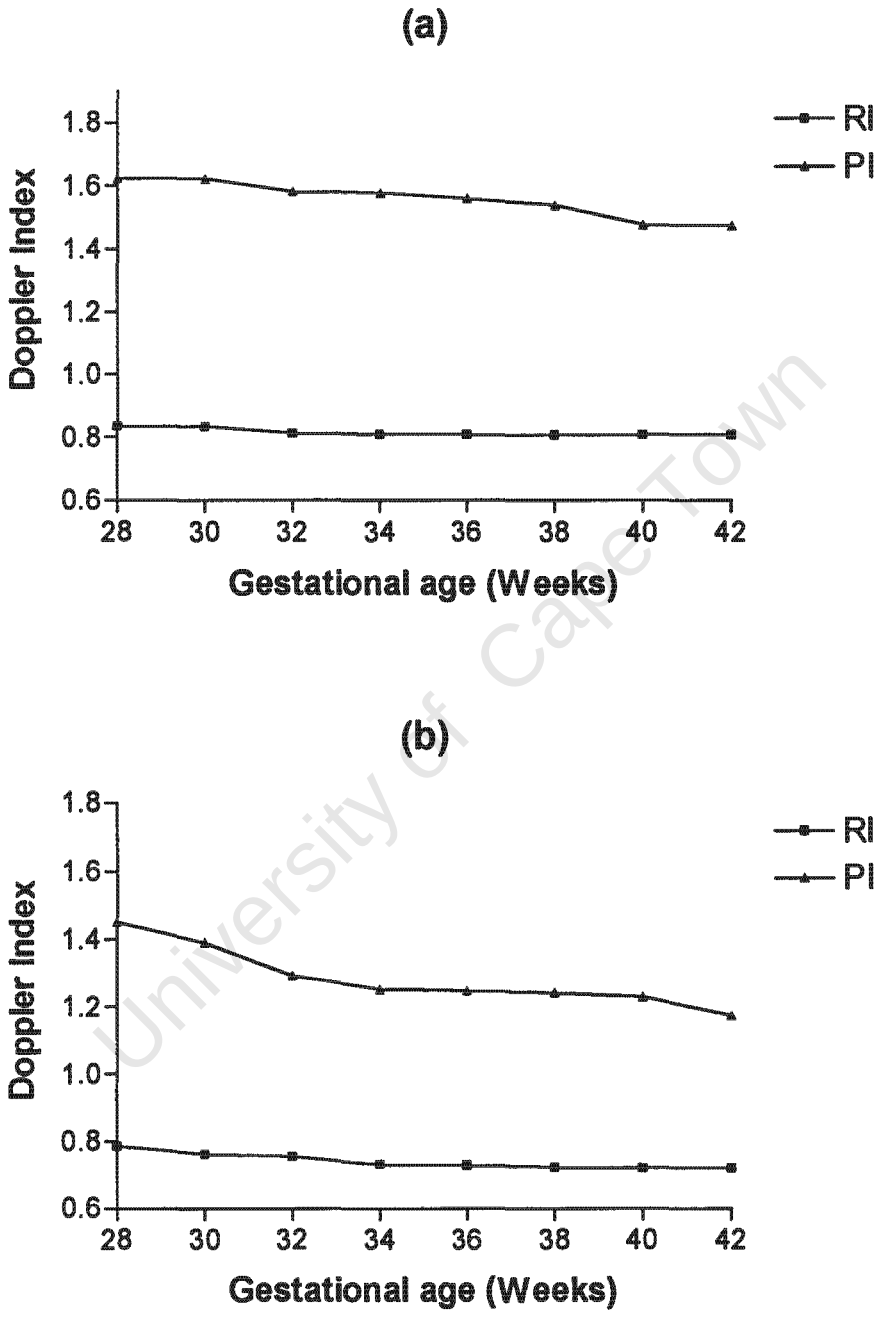

Figure 10.11: Model generated resistance and pulsatility indices versus gestational age in the thoracic aorta (a) and the abdominal aorta (b)

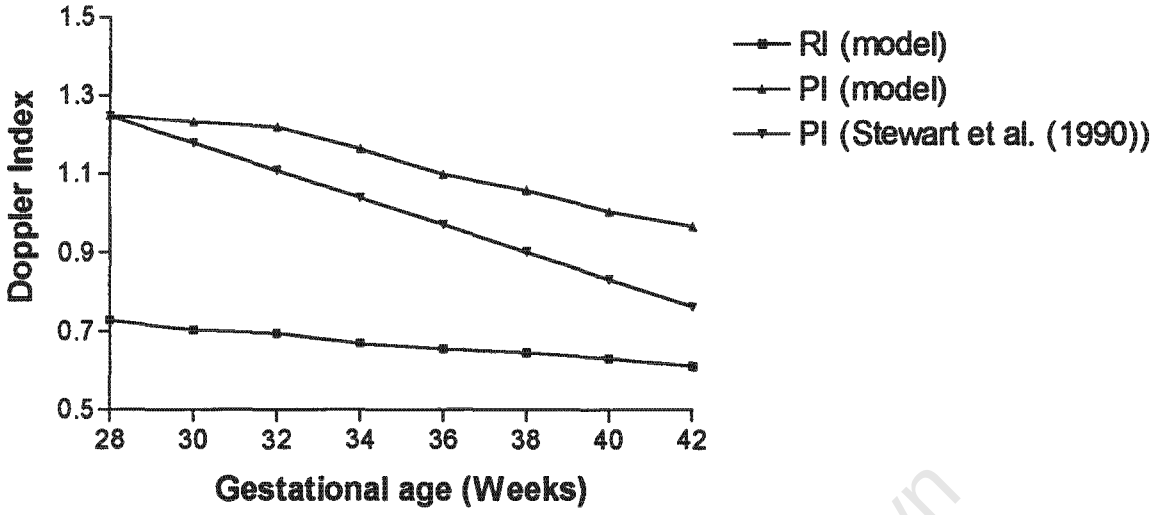

Figure 10.12: Model generated resistance and pulsatility indices versus gestational age in the iliac artery. Included in the figure is the regression equation for the pulsatility index provided by Stewart et al. (1990)

the human foetus are unable to obtain pressure and impedance measurements, and thus most validation methods must focus on the flow waveforms. Clinically, these are obtained through the use of Doppler ultrasound. Unfortunately, the angle between the beam probe and the vessel wall are unknown and thus angle independent measures must be used to quantify these measurements. The quantitative validation demonstrated that the model produces results that correlate well with averages of clinical measures. Accurate results are obtained at all the model measurement locations and at all gestational ages from 28 weeks until term. A comparison of the different model building blocks indicated that Dinnar's, Atabek's and Womersley's models all produce similar results. Dinnar's model was selected for all subsequent simulations as it incorporates the most detail, while simultaneously producing the lowest overall error. The only potential shortcoming of this model was its failure to incorporate the effects of anisotropy, however a comparison of different anisotropic parameters using Atabek's model showed that this may be effectively neglected. Simulations for both tapered and non-tapered peripheral networks indicated that the tapered networks produced results that were considerably more accurate than those produced by the non-tapered networks. Thus all subsequent simulations use the tapered model for the peripheral vascular beds. Having successfuly validated the model under normal physiological conditions, and having selected the most appropriate models for further use, it is now feasible to continue to determine the effects of changing various parameters (to simulate pathological conditions and reactions to these conditions) on the Doppler indices.

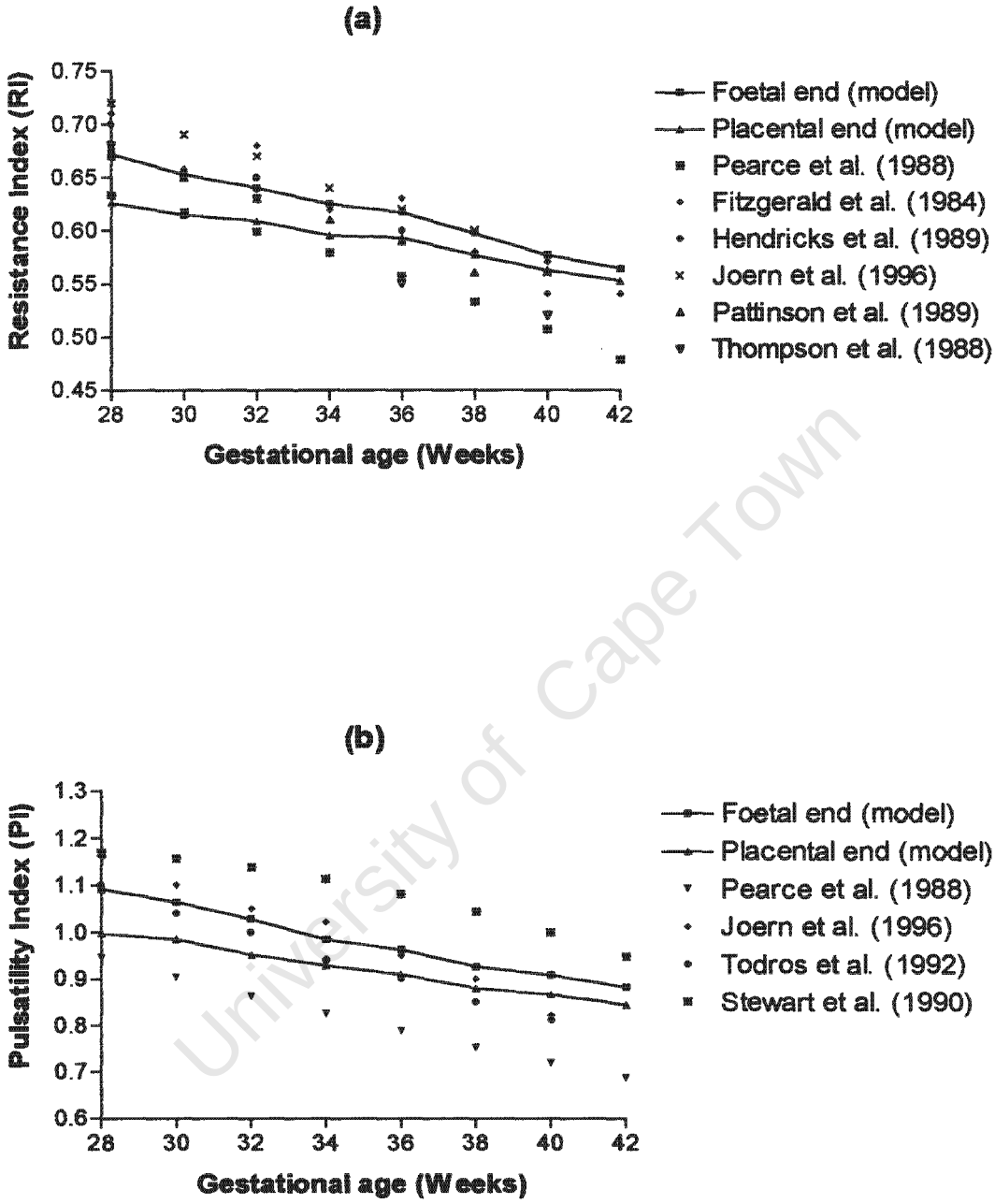

Figure 10.13: Model generated resistance and pulsatility indices versus gestational age for the foetal and placental ends of the umbilical arteries. Included in the figures are reference values obtained from the sources indicated in the legends.

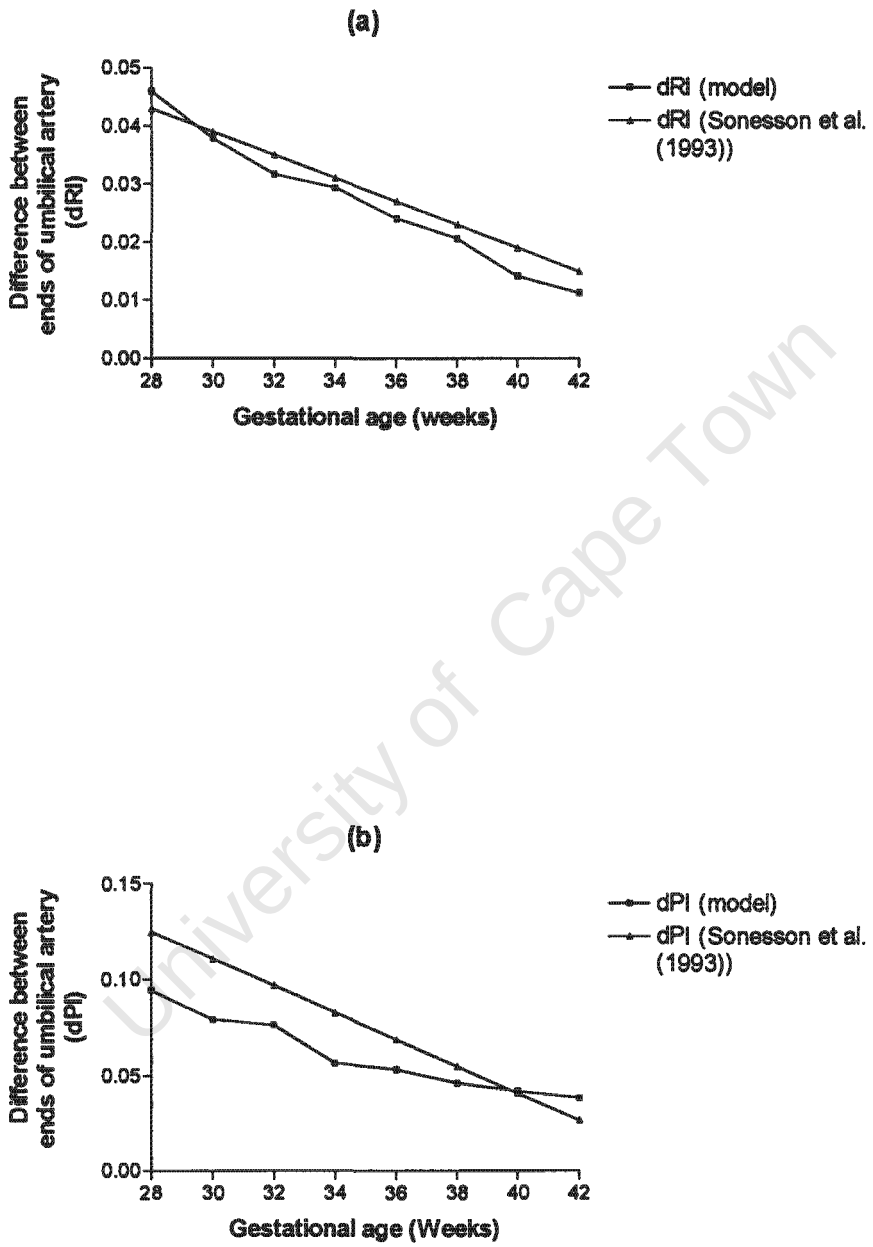

Figure 10.14: RI (a) and PI (b) differences between the foetal and placental ends of the umbilical artery, along with regression equations for the differences obtained from Sonesson et al. (1990)

Chapter 11

Determinants of Doppler indices

11.1 Introduction

The foetal circulation is composed of a large number of vessels, each of which needs to be represented by a set of parameters in the foetal model. Each of these parameters may vary within a statistically normal range amongst the population of healthy foetuses. In addition, they may also vary as a result of foetal pathology or distress, clinical intervention or activated foetal compensatory mechanisms in response to induced changes. These changes may loosely be divided into *acute* and *chronic* categories. Acute categories refer to those changes that occur in a relatively short time frame and are often due to clinical intervention or are a response to the sudden onset of distress. Chronic categories refer to changes that take place over a longer time interval. These include changes that occur due to the natural response mechanisms in response to a slowly developing pathology, as well as those due to normal physiological variations. Common causes of both acute and chronic alterations were discussed in chapter 2.

Many of these changes result in alterations of the resistances of the terminal vascular beds, due to 'brain sparing' redistribution processes. These alterations tend to cause the total blood flow supplying the peripheral beds to change as the foetus attempts to maintain the supply of nutrients to the essential organs. Compensatory mechanisms at the foetuses disposal include modification of the mean arterial pressure and the total cardiac output, redistribution of the cardiac output or to alteration of the morphology of the vascular networks. Morphological alterations may either occur through changes to the number of levels of branching or by dilation or constriction of the radii of the individual vessels comprising the network. Many characteristics of the morphology of the vascular networks are fixed at a particular stage of growth and parameters such as the length or branching angles cannot suddenly undergo changes. Thus in modelling an acute change, the only manner by which the vascular network resistances may be

modified would be through corresponding changes in the vessel radii. However, when modelling a chronic change that occurs over a longer time period, the peripheral network may be considered to have begun growing in a different manner from the time of onset of the pathology. This would subsequently result in different values of network parameters from those of a healthy foetus at the same gestational age. To illustrate this principle, consider an elevated mean arterial pressure as a result of a hypoxic insult. It is necessary that the mean pressure be equal to the flow in a vascular bed multiplied by the resistance of that vascular bed. However the pressure has now increased and from a modelling point of view this must be compensated for either by maintaining constant flow and increasing the peripheral resistances, or maintaining constant resistances and increasing the flow or by some combination of the two. In the acute situation, for constant flow, the increase in peripheral resistance may be modelled by constricting the radii of the peripheral trees, whilst keeping the number of levels of branching, lengths of the vessels and branching ratios and angles constant. However, should this elevated pressure arise over an extended period of time due to a slowly developing chronic change, then assuming constant flow, the increased peripheral resistance may be modelled by a decrease in the network radii due to decreased growth capacity.

Many vascular parameters change simultaneously in response to foetal substrate deprivation. However, it is instructive to keep all but one parameter fixed at a nominal or reference value and vary each parameter one at a time over a physiologically relevant range, in order to directly assess the effects of each individual variable on the Doppler indices. The sensitivity of the Doppler indices to changing vascular parameters may therefore be explored. Unfortunately, the foetus may respond to induced changes in a number of ways as discussed and it is not possible to simulate each and every possible scenario. The purpose of this chapter is to identify the most important determinants of the Doppler indices and to obtain further insights into some experiments that have previously been conducted. Therefore, in this chapter, results are displayed for a reduced set of simulations for each significant variable for situations of acute and chronic (includes normal population variance) alterations at 28 weeks gestation. These simulations should not be considered to accurately reproduce every change that occurs in response to an induced change but rather illustrate this models power and ability to isolate one variable at a time and investigate the sensitivity of the Doppler indices to changes in that variable.

In a further attempt to reduce the volume of graphs displayed in this thesis, a number of space saving procedures have been adopted. The first was to note that with the exception of heart rate simulations, identical trends were observed for both the pulsatility and resistance indices and therefore no additional benefit is obtained by displaying graphs of both indices for each simulation. This correlation has been shown to exist in a number of clinical or experimental studies (Thompson et al. 1986, 1988; Mulders et al. 1987; Pearce et al. 1988; Adamson et al.

Artery	Display Colour
Thoracic aorta	
Abdominal aorta	
Iliac artery	
Umbilical artery – Foetal end	
Umbilical artery – Placental end	

Figure 11.1: Key indicating the colour representations of arteries to be used for all subsequent simulations.

1990). It should be noted that possible differences observed in these studies for at risk foetuses may be attributed to the associated heart rate changes that occur in a compromised foetus. Thus the resistance index was chosen as the index to be displayed for all subsequent simulations. It was felt that this index offered the advantage of clear interpretation for situations of both absent end diastolic flow (RI = 1) and reverse diastolic flow (RI > 1). Furthermore, Thompson et al. (1988) demonstrated that the pulsatility index may not be normally distributed, whereas the resistance index is.

Results for the pulsatility index are however included for simulations involving changing heart rate. This is because the two indices reacted differently, and thus could be explored using published regression curves for both indices. The second observation was that with the exception of umbilical coiling simulations, the trends of all the simulations were independent of gestational age between 28 and 39 weeks. This is not to say that differences were not noted, but it was felt that these differences were small and do not detract from the general trends. Thus all results are displayed for 28 week old foetuses only and may be generalised to subsequent gestational ages. Umbilical coiling is dealt with in a separate manner.

The final convention adopted in order to reduce space is to adopt an identical colour coding for all subsequent diagrams. The simulations display results in each of the model arteries and these are coded as indicated in figure (11.1). When the trends in all arteries are relatively similar, subsequent discussion focuses on quantifying the percentage changes in only the umbilical arteries as these are the most commonly used for diagnostic evaluations.

11.2 Modelling acute and chronic changes in peripheral resistances

11.2.1 Acute changes

Acute changes to the peripheral resistance require that all network parameters, except for the vessel radii, remain constant at their nominal values. Thus the resistance is altered by assuming that the radii change by a parameter, ϵ, so that the new radius and the old radius are related by

$$r_{new} = \epsilon r_{old} \tag{11.1}$$

From a modelling perspective, the pressure and fraction of cardiac output distributed to a vascular bed, and thus the resistance of that vascular bed, are known quantities and thus it is possible to solve for ϵ to obtain this desired resistance. Equation (7.12) relates the resistance of the vascular bed to the parameters characterising the morphology of the arterial network. Rewriting this in terms of r_{old} gives :

$$R_0 = 2\left(\frac{\beta}{r_{0old}^3} k^{3n} \frac{k^3\left(2^{-n} - k^{-3n}\right)}{k^3 - 2}\right) \tag{11.2}$$

where for tapered networks,

$$\beta = \frac{4\mu l_{rold}}{x^4\pi} \frac{x^4 - k^4}{\ln \frac{2}{k^2}} \tag{11.3}$$

Here $l_{rold} = l/r_{old}$ and keeping the length l unchanged, this may be rewritten as $l_{rnew} = l\epsilon/r_{old} = l_r/\epsilon$. Thus β may be replaced with β/ϵ and r_{0old} with ϵr_{0old} yielding a new expression for the resistance in terms of the new radius. i.e.

$$R_0 = 2\left(\frac{\beta}{\epsilon^4 r_{0new}^3} k^{3n} \frac{k^3\left(2^{-n} - k^{-3n}\right)}{k^3 - 2}\right) \tag{11.4}$$

which may be solved for ϵ to obtain

$$\epsilon = \left(2\beta k^{3n+3} \frac{2^{-n} - k^{-3n}}{r_{0new}^3 R_0\left(k^3 - 2\right)}\right)^{1/4} \tag{11.5}$$

where $\epsilon > 1$ implies dilation and $\epsilon < 1$ implies constriction.

11.2.2 Chronic changes

Chronic changes to the peripheral resistance are the result of modified growth and therefore results in a different number of levels of branching than would be expected had the foetus grown

normally. The morphological parameters r_0, K, θ, n and the input resistance R_0, are all related by equation (7.12). The simulations are conducted by allowing the peripheral networks to grow to a different level of branching (n_{new}), which would be a fraction of the level obtained during normal growth (n_{old}). i.e. $n_{new} = \delta n_{old}$ with $0 < \delta < 1$ for reduced growth. Reduced growth may be accomplished by either reducing the branching ratio, K or by increasing the branching angle θ. Thus by specifying δ, it is possible to solve for K or θ. Keeping K fixed, θ may be determined according to

$$\theta = \arccos\left(\frac{1}{2}\left(\frac{k^4 A}{R_0 + A}\right)^{1/4}\right) \tag{11.6}$$

where

$$A = 8\mu l_r k^3 \frac{k^{3n_{new}} 2^{-n_{new}} - 1}{r_0^3 \left(k^3 - 2\right) \pi \ln \frac{1}{2} k^2} \tag{11.7}$$

Specifying δ and fixing θ allows K to be determined. However no exact solution for this exists and thus the solution for K must be obtained using iterative techniques. Newton's method (Dennis, 1977) is an efficient algorithm with which equation (7.12) may be solved to obtain K.

11.3 Placental insufficiency

Placental insufficiency occurring either as a primary placental problem, or as a secondary consequence of other foetal or maternal complications, may be simulated using the foetal model. The net effect of placental insufficiency is that, compared with a healthy, normally grown placenta, a reduced amount of flow is directed towards the placenta. This may be the result of a reduced percentage of the total cardiac output distributed to the placenta, with the difference redistributed to the remaining foetal organs, or a drop in the total cardiac output, or a combination of the two. Experimentally induced placental embolisation with microspheres results in the occlusion of a number of the smaller vessels of the placenta. This effectively increases the asymmetry of the vascular network. However, a more simple approach was employed in order to model this process. Here, it was assumed that embolisation was equivalent to reducing the vessel radii, sometimes to the point of total constriction. Thus, to model embolisation in which placental flow is rapidly reduced (acute changes), the branching ratio, branching angle and number of levels of branching of the placenta remain unchanged and only the placental vessel radii are reduced. Assuming for now that the pressure and total cardiac output remain constant, the peripheral resistances of the other organs must decrease so that they obtain a greater portion of the cardiac output and this is accomplished by dilation of the arteries comprising the other peripheral

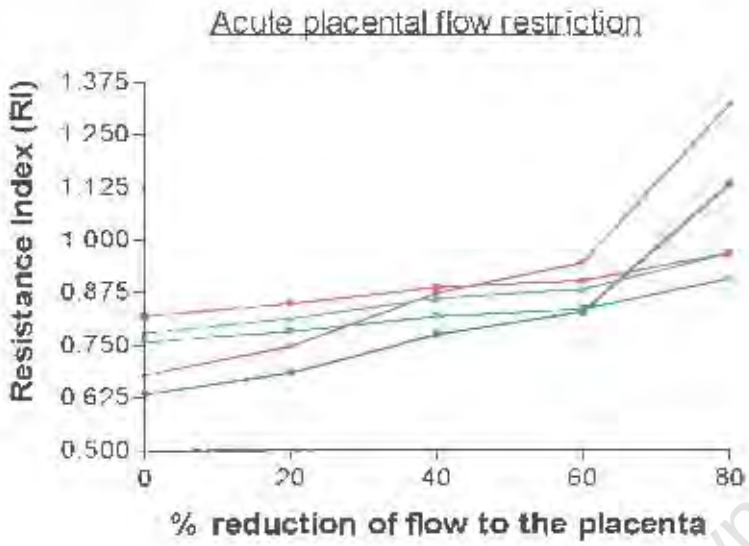

Figure 11.2: The resistance index in each of the model arteries versus percentage reduction of flow to the placenta. Placental flow is reduced by constricting the placental arteries to achieve the desired level of flow, whilst keeping the remaining tree morphology constant at reference values. Flow to the remaining vascular beds is increased as described in the text, with cardiac output and pressure remaining constant.

trees. Should the pressure or total cardiac output also change, the same response occurs but to a lesser degree. Chronic placental insufficiency may be simulated by assuming that placental development, and placental resistance, is altered over a longer period of time. Physiologically, it is reasonable to assume that a case of chronic insufficiency would result in fewer rather than a greater number of levels of branches and thus either K is reduced or θ increased to simulate this effect. The decrease in blood flow to the placenta must be redistributed to the remaining organs and this is assumed to be done in such a manner that every one percent decrease in placental flow is redistributed as a 0.6 percent increase to the head and heart, 0.025 percent increase to the adrenals and 0.125 percent increase to each of the remaining three vascular compartments. These figures have been chosen to replicate the type of redistribution observed from experiments on foetal sheep as indicated in chapter 2.

Simulations were performed in steps of 20% reductions of flow to the placenta due to both acute and chronic restrictions. In the cases of acute restrictions, the arterial radii were reduced while in the cases of chronic restrictions, either the branching angles (θ) were increased, or the branching ratios (K) were decreased. These simulations were performed for values of $\delta = 0.8, 0.6, 0.4$ and 0.2. Figure (11.2) depicts the results of the acute embolisation process for the

resistance index. Figures (11.3 a-d) and (11.4 a-d) are the results of the simulations for chronic placental insufficiency for changing θ and K respectively for the specified range of δ. The maximum overall value of θ was 75.6° and the minium overall value of K was 2.08, and these values were obtained for $\delta = 0.2$ (80% reduction of flow to the placenta). These values are still within the defined physiological constraints outlined in chapter 9, with θ confined to lie between 50° and 90° and K to be between 2 and 3. Chapter 7 explained that a power law value of K which approaches 2 indicates zero expansion in total arterial cross-sectional area and thus it is interesting to note that in a compromised placenta, K approaches this value. This suggests that the growth of the placenta is restricted by not allowing any significant expansion between one level of branching and the next.

Examination of the actual values of placental resistance demonstrate that a 20% reduction in flow to the placenta corresponds to an increase in placental resistance by a factor of 1.32, a 40% flow reduction corresponds to an increase by a factor of 1.85, a 60% flow reduction corresponds to an increase by a factor of 2.92 and an 80% reduction in flow corresponds to an increase in resistance by a factor of 6.12.

Visual inspection of figures (11.2), (11.3) and (11.4) indicate that there is very little difference. Therefore, no matter what the mechanism of placental blood flow restriction, the effects on the shapes of the flow waveforms are similar and also follow the same trends. Chronic placental insufficiency simulated by increasing the branching angle, appears to increase the resistance index at a greater rate than that achieved by reducing K or by acute embolisation. However this difference is slight. Increasing placental resistance results in an increase in the Doppler indices in all the arteries, with those in the umbilical artery increasing at a significantly greater rate than those in the upstream arteries. Absent end diastolic flow is reached just after a 60% reduction in flow, roughly corresponding to a three-fold increase in placental resistance. This same finding was reported by Sural and Adamson (1996) with their model of the vasculature of foetal sheep. Adamson et al. (1990) who did experiments on foetal sheep, found that placental resistance was required to increase by a factor of 6 to produce zero diastolic flow. This discrepancy may be attributed to differences between sheep and human foetuses, as well as due to the effects of associated changes that occurred in the sheep experiments.

Histologically, abnormal umbilical arterial Doppler flow indices are associated with a reduction in the number of small muscular arteries per unit area in the placenta to between 20% and 60% of control (Braccero et al. 1989; Giles et al. 1985; McCowan et al. 1987). However this reduction is not always observed (Jackson et al. 1995). The model simulations produce similar results in that by reducing the number of levels of branching to between 20% and 80% of control values, abnormal resistance index values are obtained. It must be noted that this reduction in the number of levels is accompanied by an effective reduction in the overall vessel radii, either

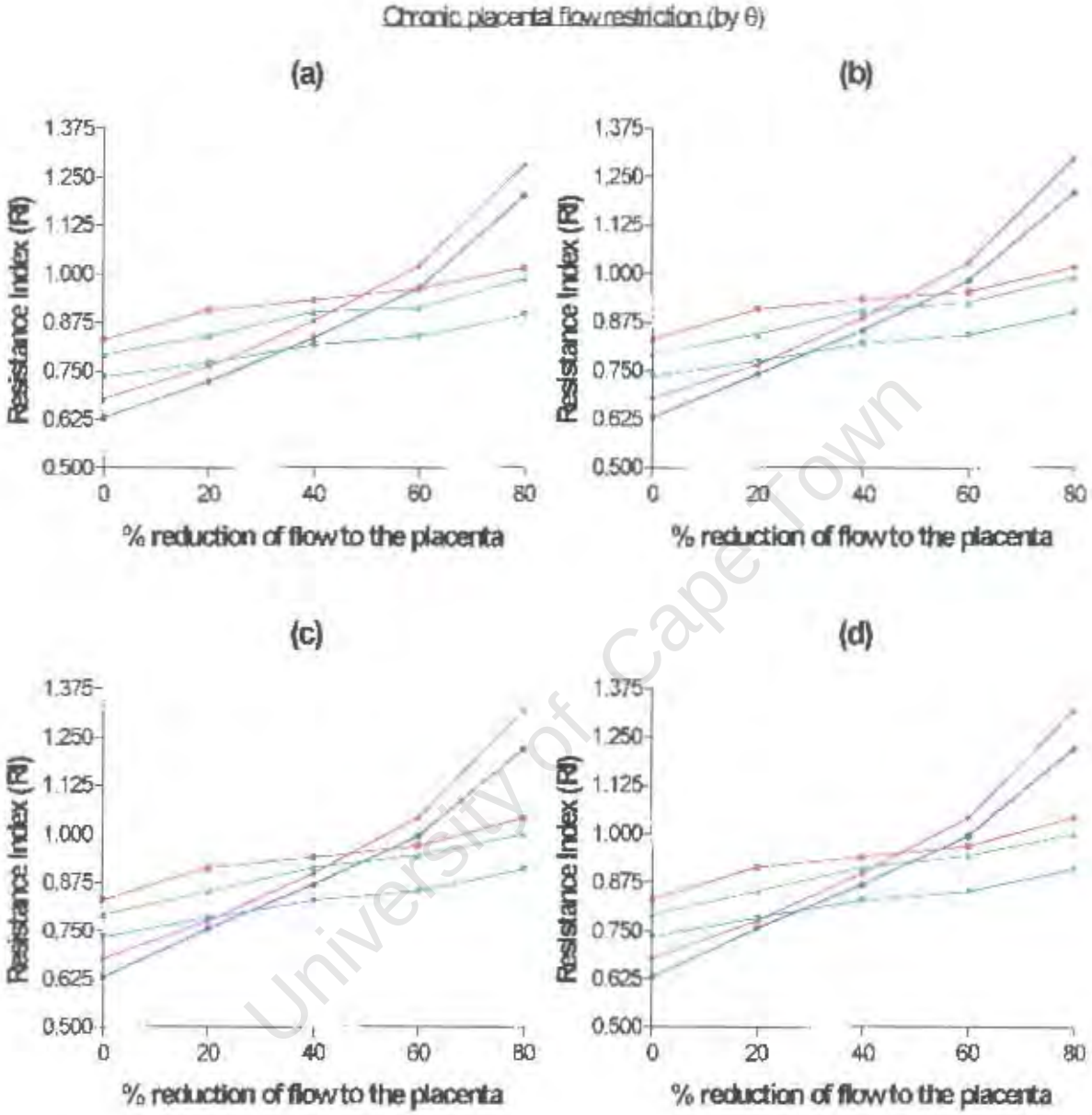

Figure 11.3: Simulations of chronic placental insufficiency for steps of 20% reduction of placental flow versus resistance index in each of the model arteries. The number of levels of branching of the placental villous tree is reduced by multiplying by factors of (a) 0.8, (b) 0.6, (c) 0.4 and (d) 0.2. This reduction in the number of levels is simulated by increasing the branching angle, θ, which is assumed to take place as a result of maldeveloped growth. This results in an elevated placental resistance and hence in reduced placental flow.

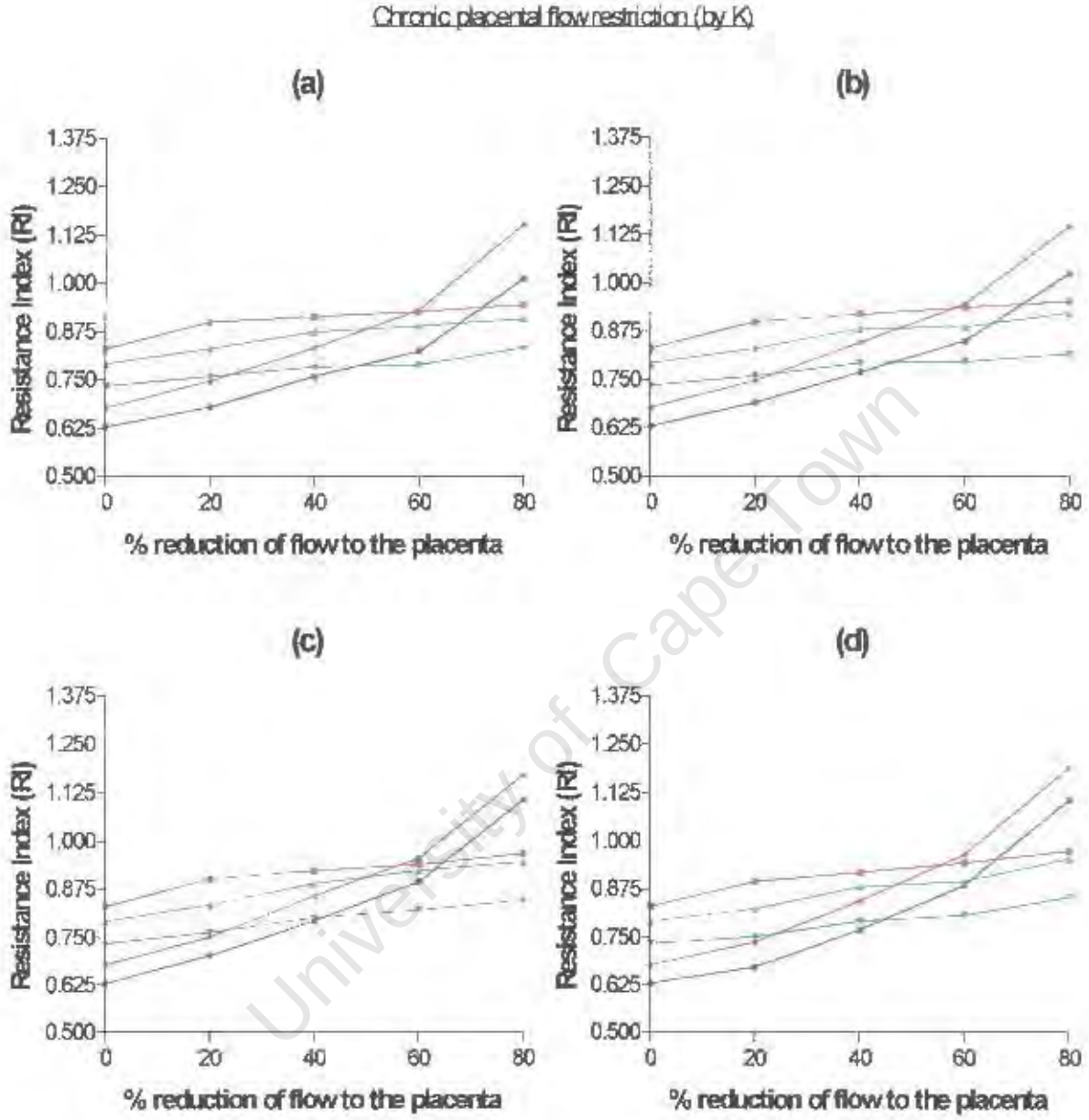

Figure 11.4: Simulations of chronic placental insufficiency for steps of 20% reduction of placental flow versus resistance index in each of the model arteries. The number of levels of branching of the placental villous tree is reduced by multiplying by factors of (a) 0.8, (b) 0.6, (c) 0.4 and (d) 0.2. This reduction in the number of levels is simulated by decreasing the power ratio, K, which is assumed to take place as a result of maldeveloped growth. This results in an elevated placental resistance and hence in reduced placental flow.

by altering the branching angle and hence the degree of taper or by altering the branching ratio, thereby progressively reducing the vessel radii with increasing branching level. If the vessel radii were to remain constant and the number of levels reduced, the placental resistance would decrease. However, as the resistance of a single vessel is inversely proportional to the fourth power of its radius, the reduction in radius dominates over the reduction in vessel number and it is this that is responsible for the elevated resistances. Thus a reduction in the number of vessels need not always be necessary to produce elevated placental resistances, as observed by Jackson et al. (1995).

The results further indicate that as the degree of placental insufficiency rises, the difference in resistance index, obtained from measurements at either end of the umbilical arteries, increases. This concurs with the findings of Skoll et al. (1997) who reported that when compared with normal foetuses, IUGR foetuses have significantly greater differences in the values of RI, PI and S/D ratios from the opposite ends of the cord.

In their modelling work on foetal sheep, Surat and Adamson (1996) demonstrated that the umbilical flow waveforms respond in a different manner to umbilical vessel changes when there is an elevated placental resistance to when placental resistance is normal. Thus it appears that the placental resistance may affect the sensitivities of Doppler indices to changes in various other vascular variables. It was therefore decided that each subsequent simulation should be conducted for situations of a normally developed placenta and a maldeveloped placenta (increased placental resistance). The results of figures (11.3) and (11.4) indicate that similar Doppler indices are obtained regardless of the manner with which placental resistance is elevated. Thus subsequent simulations for an underdeveloped placenta consider the placenta to be chronically altered due to changes in branching angles with $\delta = 0.6$. This choice over changes in K is arbitrary and does not effect the results in any significant manner. Simulations were conducted for a 50% reduction of flow through the umbilical arteries to the placenta, corresponding to a 228% increase in placental resistance, resulting in umbilical arterial flow that is just short of absent end diastolic flow.

11.4 Heart rate

There has been some controversy in the literature concerning foetal cardiovascular physiology about the effect of heart rate on the cardiac output. Rudolph and Heymann (1974) reported that cardiac output was proportional to heart rate, whilst later reports indicate that the Frank-

Starling mechanism dominates and that heart rate has very little effect on cardiac output (Kirkpatrick et al. 1976; Anderson et al. 1986; Kenney et al. 1987) . A review by St. John Sutton et al. (1992) indicates strong evidence for the Frank-Starling mechanism being active in a similar manner to that of adults and this was the approach adopted to model changes in heart rate. Thus all parameters (including cardiac output) except for the heart rate were held constant, while the heart rate was varied between 60 and 220 b.p.m. Figures (11.5 a and b) are the model generated changes in PI and RI in each artery versus heart rate, with a normal placental resistance.

It may be seen from these figures that the indices decrease with increasing heart rate, with the PI decreasing at a greater rate than the RI. For a 267% increase in heart rate (from 60 b.p.m to 220 b.p.m), the PI and the RI in the umbilical arteries decrease by 76% and 56% respectively. It is possible that this trend contributes towards the decrease in indices with advancing gestation, as it is known that the heart rate increases as the foetus ages. Furthermore, changes in heart rate may be in response to foetal distress or may merely be indicative of variations within the foetal population. Indeed a number of authors have reported regression equations for umbilical arterial indices versus foetal heart rate and they all concur that an increasing heart rate corresponds to decreasing Doppler indices (Yarlagadda et al. 1989; van den Wijngaard et al. 1988; Brar et al. 1989; Mires et al. 1987). Most of these results are only reported at a particular gestational age with Yarlagadda and co-workers being the only authors who gave regression equations for heart rate at each gestational age. Figures (11.6 a and b) reproduce the model generated umbilical arterial curves versus heart rate along with the regression equation results of Yarlagadda et al. (1989). As may be seen from the figures, the foetal model approximates observed changes in Doppler indices with heart rate very well.

Chapter two demonstrated that the most common response of the foetal heart rate to induced hypoxia is a decrease in the heart rate. In situations of placental impairment, a diminished heart rate is likely to be encountered and it is necessary to characterise changes in Doppler indices with heart rate in these situations. Figures (11.7 a and b) are the model generated changes in PI and RI in each artery versus heart rate for foetus with chronic placental impairment.

It is interesting to note that in the case of impaired placental development, heart rate has a lesser effect on the resistance index than during normal placental function. For the same 267% increase in heart rate, the pulsatility index and the resistance index in the umbilical arteries now decrease by 77% and 44% respectively, compared with 76% and 56% for a normal placenta.

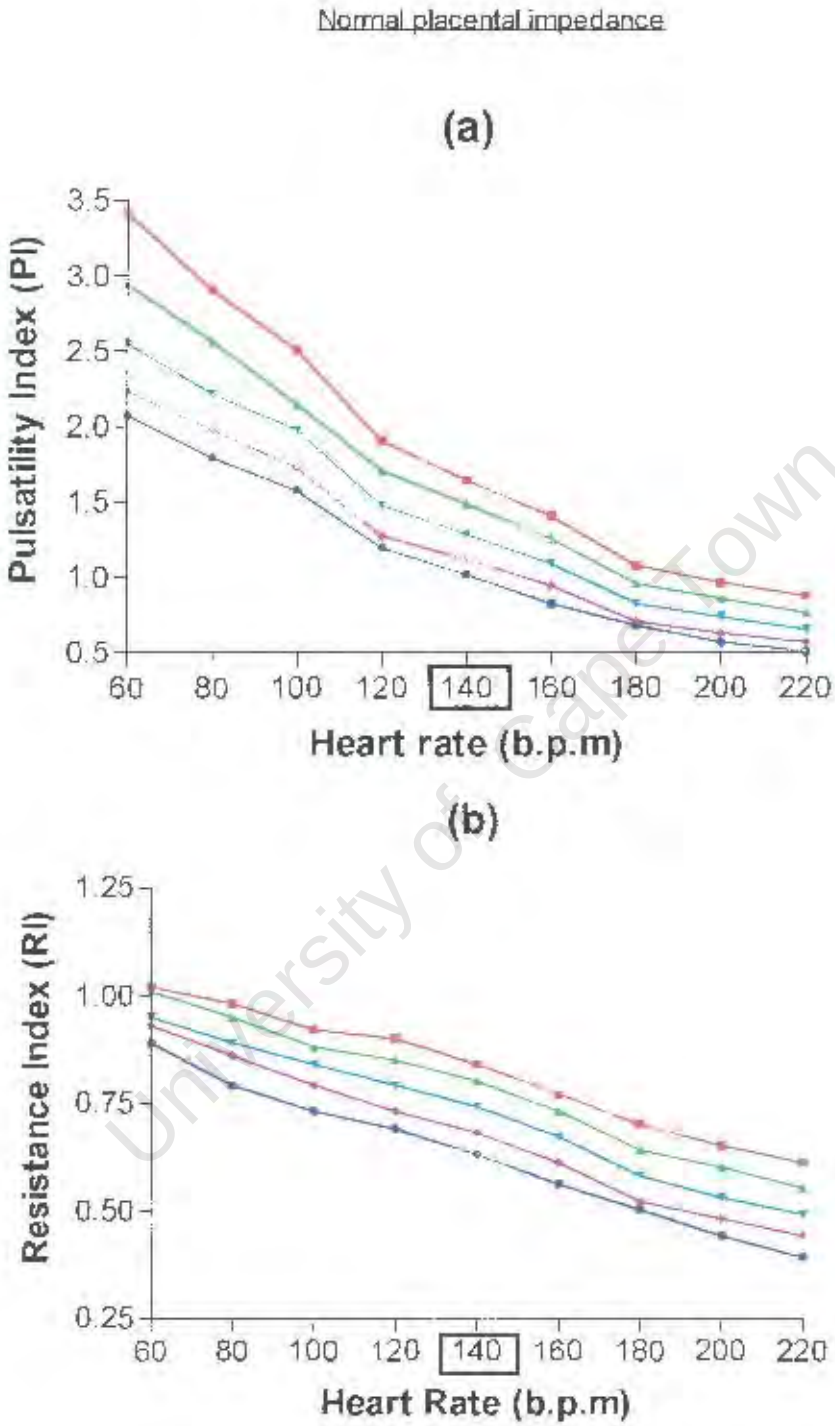

Figure 11.5: Changes in model generated PI (a) and RI (b) at each of the model arterial sampling sites versus heart rate. Simulations are for an normally developed placenta. The reference heart rate is indicated by the boxed value.

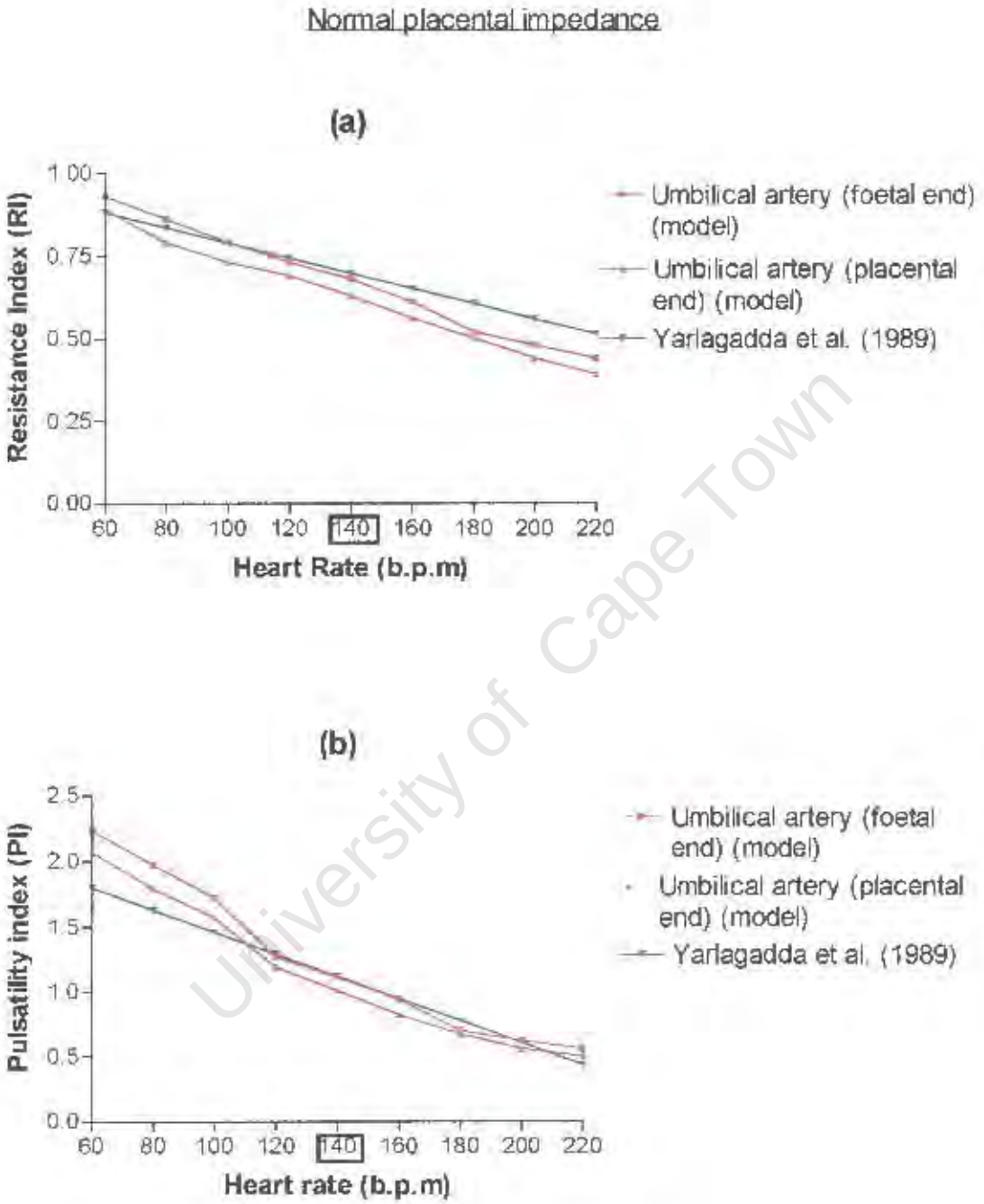

Figure 11.6: Changes in model generated RI (a) and PI (b) at either end of the umbilical arteries versus heart rate. The results of the regression equations of Yarlgadda et al. (1989) are superimposed. Results are for a healthy placenta. The reference heart rate is indicated by the boxed value.

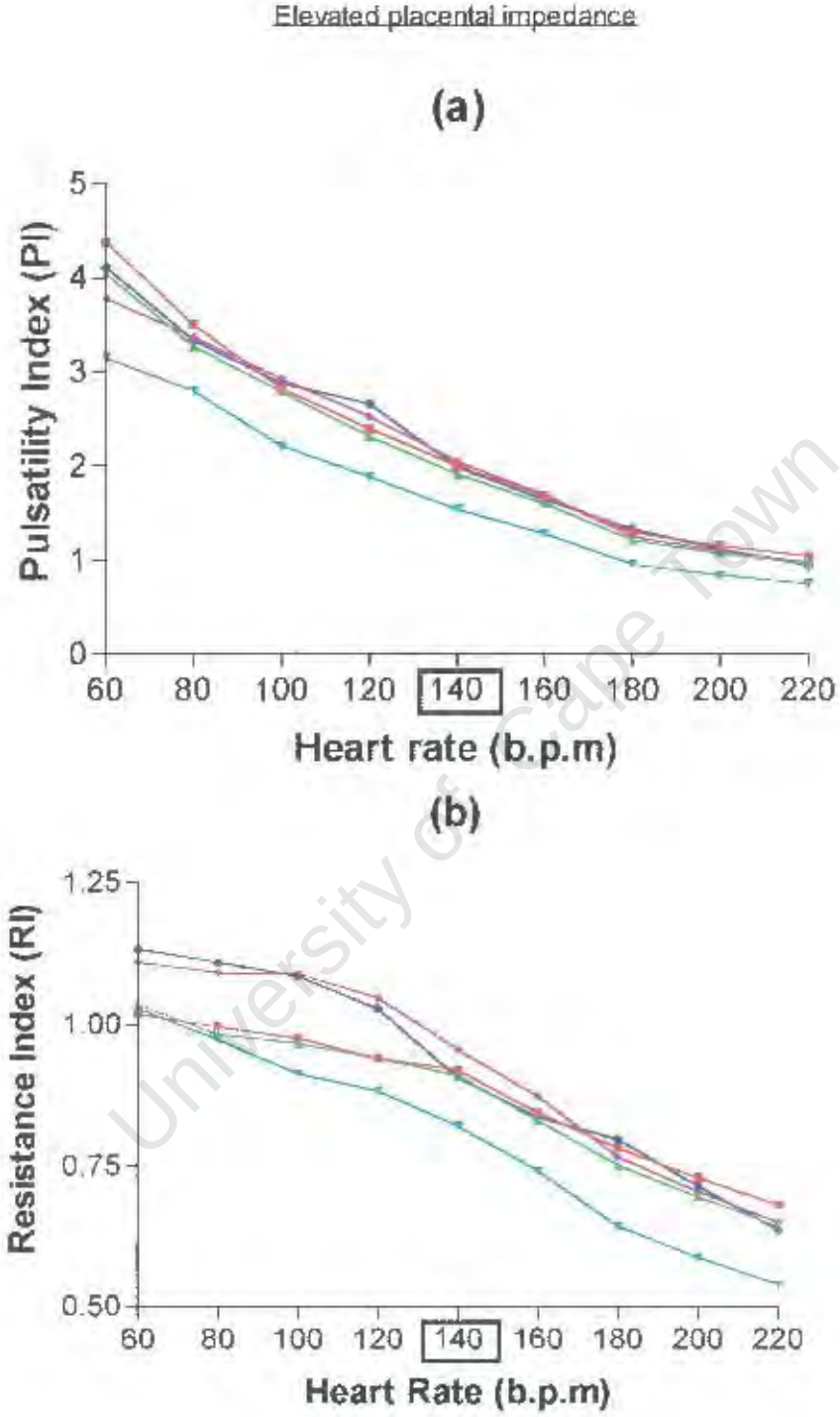

Figure 11.7: Changes in model generated PI (a) and RI (b) at each of the model arterial sampling sites versus heart rate. Simulations are for an abnormally developed placenta, resulting in elevated placental resistance. The reference heart rate is indicated by the boxed value.

11.5 Cardiac output

The foetus may adjust the total combined ventricular output in response to a variety of stresses. Usually the cardiac output is constant but under certain conditions may decrease. Gilbert (1980) performed experimental work on foetal sheep and concluded that the foetal heart operates near the upper limit of its Starling function curve and as a result has a very limited cardiac reserve. Thus it was decided to simulate changes in cardiac output between 250ml/min/kg and 550ml/min/kg, (from about half of normal to only slightly higher than the nominal cardiac output). Furthermore, changes in cardiac output may result from acute or chronic stresses. The change in cardiac output may either be balanced by a change in pressure whilst retaining vascular resistance constant, a change in vascular resistance whilst maintaining constant pressure or a combination thereof. Should the vascular resistances and impedances remain unchanged, the shape of the flow waveforms would not be altered and the only effect would be to proportionally scale the flow waveform. As the indices are independent of scaling, they would remain unchanged. Thus, only the extreme of constant pressure and maximally altered vascular resistances are investigated. Acute changes are modelled by keeping the morphology of the peripheral vascular trees consistent with the reference values at 28 weeks and then vasoconstricting the tree vessel radii in order to elevate the peripheral resistance and vasodilating them in order to decrease the peripheral resistance. Chronic changes in cardiac output imply that the foetus has grown over time in such a manner that a new tree morphology results which determines the peripheral resistances. These changes are modelled by regrowing the vascular beds to either increase or decrease their peripheral resistances. Figures (11.8 a and b) are the simulated results in each artery for the resistance indices, plotted against a changing cardiac output for acute and chronic changes respectively, for a healthy placenta. Figures (11.9 a and b) are the corresponding acute and chronic changes in cardiac output for a maldeveloped, high resistance placenta.

From these figures, it may be seen that for a normal placental resistance, in the acute scenario the net effect of a decreasing cardiac output is to increase the RI's at a similar rate in all but the thoracic artery, which remains relatively unchanged. When placental resistance is elevated, these trends remain comparatively unchanged, with the RI in the thoracic aorta beginning to decline with decreasing cardiac output and the index measured at the placental end of the umbilical artery increasing at a greater rate than that obtained at the foetal end, thereby decreasing the RI differences between the opposing ends of the cord with decreasing cardiac output. For an acute change in cardiac output from 500ml/min/kg to half this value, the resistance index at the placental end of the umbilical artery increases by 9.7% for a healthy placenta and by 13.5% for a situation of elevated placental resistance.

The net effect of a chronic decrease in cardiac output is for the indices to generally remain constant, with a slight increase in index obtained in the umbilical arteries and a decrease in

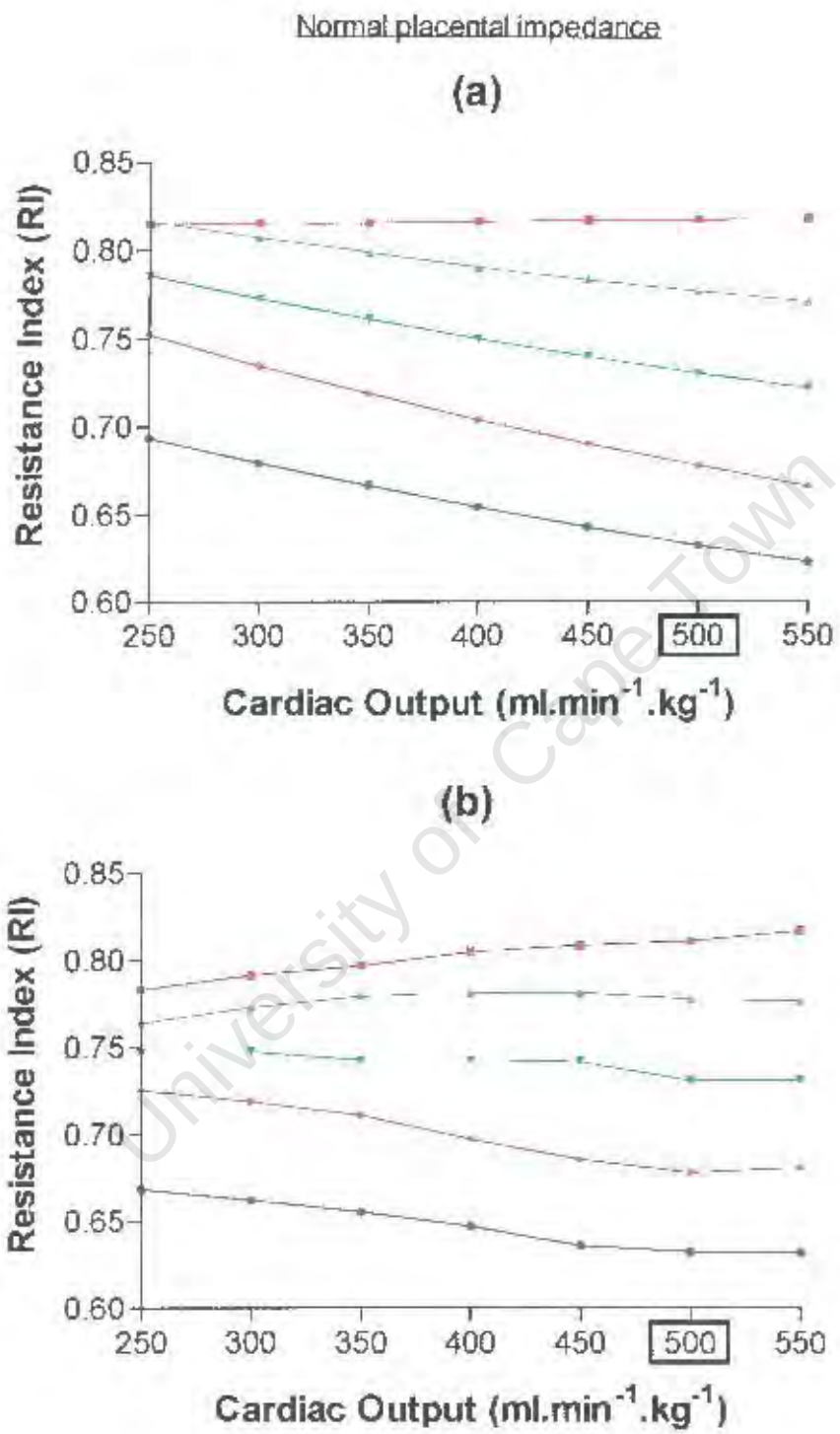

Figure 11.8: Changes in RI for each of the model arteries versus changing cardiac output in response to (a) acute stress and (b) chronic stress, for a normal placenta. Reference values of cardiac output are indicated by the boxed values.

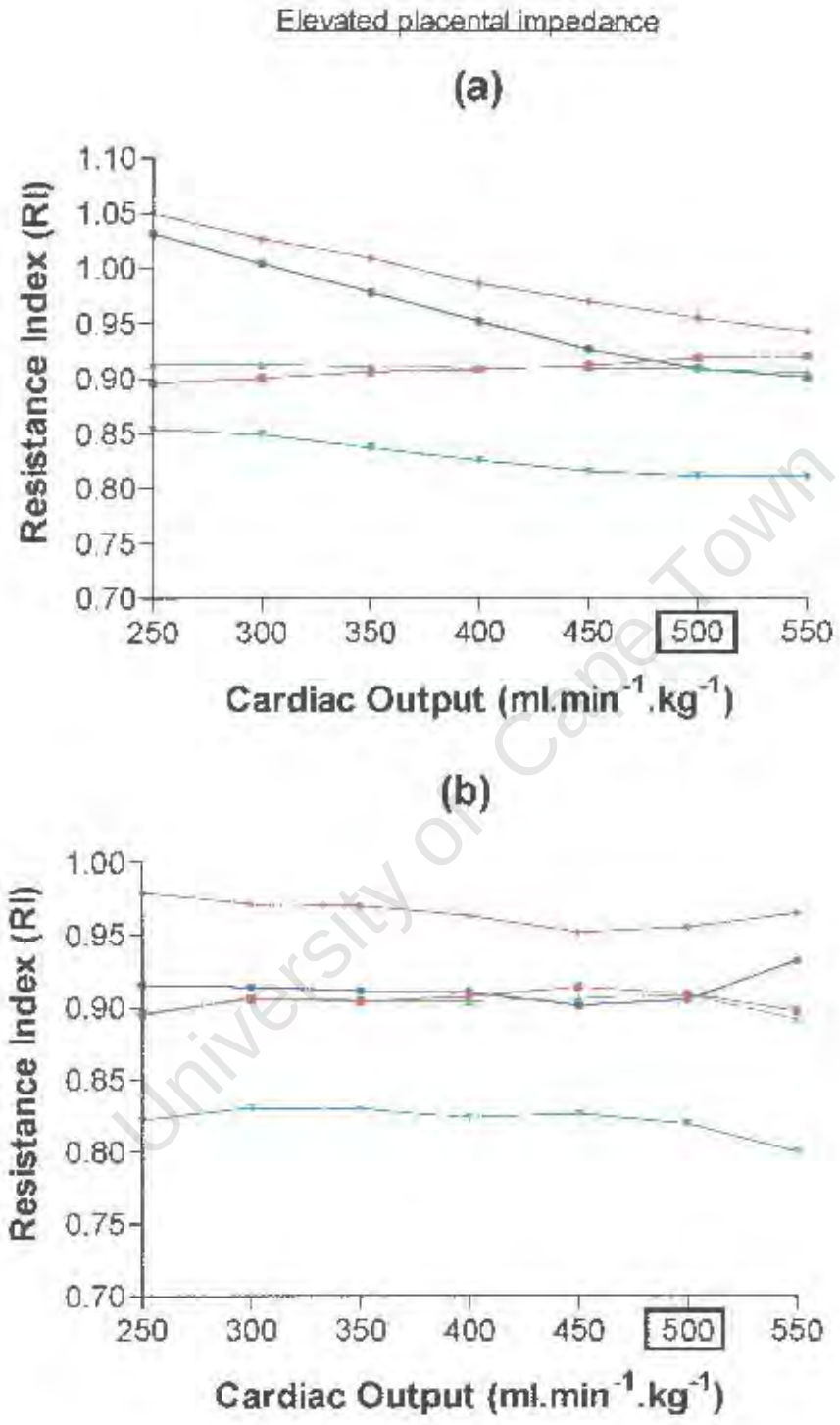

Figure 11.9: Changes in RI for each of the model arteries versus changing cardiac output in response to (a) acute stress and (b) chronic stress, for an impaired placenta. Reference values of cardiac output are indicated by the boxed values.

those obtained in the remaining arteries. This trend is even more gradual for the situation of elevated placental resistance. Increasing the cardiac output above the nominal value appears to reverse the trend by slightly increasing the RI's in all the arteries for the situation of a healthy placenta and for an impaired placenta, the indices in the umbilical arteries increase, whilst those in the remaining arteries decrease. The percentage increase in index at the placental end of the umbilical artery for a decrease in cardiac output to 250ml/min/kg is 5.7% for a healthy placenta and 1.1% for an impaired placenta.

11.6 Blood pressure

One of the mechanisms with which a foetus may respond to imposed stresses is to alter its mean arterial pressure. Chapter 2 described in detail various experimental situations whereby the pressure was altered. With the exception of a decreased blood pressure in response to a decreased blood volume, almost always, the response to both acute and chronic stresses was to increase the peripheral resistances, which, assuming a constant cardiac output, increases the mean pressure. Should the vascular resistances remain unaltered and the cardiac output change to compensate for altered pressure, the net effect would be to scale the FVW's and the indices would once again remain unchanged. Therefore only the extreme situation of constant cardiac output and changing peripheral resistances is considered. Once again, these changes in blood pressure may be acute or chronic. Acute changes are modelled by modifying the radii of the peripheral vascular networks, whilst keeping the remaining network morphology constant at its reference values. Chronic changes are modelled by allowing the number of levels of branching to grow to generate the new resistances. Simulations were conducted for both acute and chronic blood pressure changes between 50 and 80 mm.Hg, in steps of 5mm.Hg. Figures (11.10 a and b) are the simulated results in each artery for the RI's, plotted against the changing mean arterial pressure for acute and chronic changes respectively, for a healthy placenta. Figures (11.11 a and b) are for acute and chronic changes respectively for a maldeveloped placenta.

As may be seen from the figures, a changing mean arterial pressure generally has very little effect on the resultant Doppler indices, which remain relatively constant.

11.7 Blood flow redistribution

The foetus is able to compensate for imposed stresses to a limited degree by redistributing blood so that essential organs obtain a greater fraction of cardiac output at the expense of other organs less essential for sustaining life and growth. These redistributions may be the result of acute or chronic distress. As discussed in chapter 2, in the acute scenario, (such as

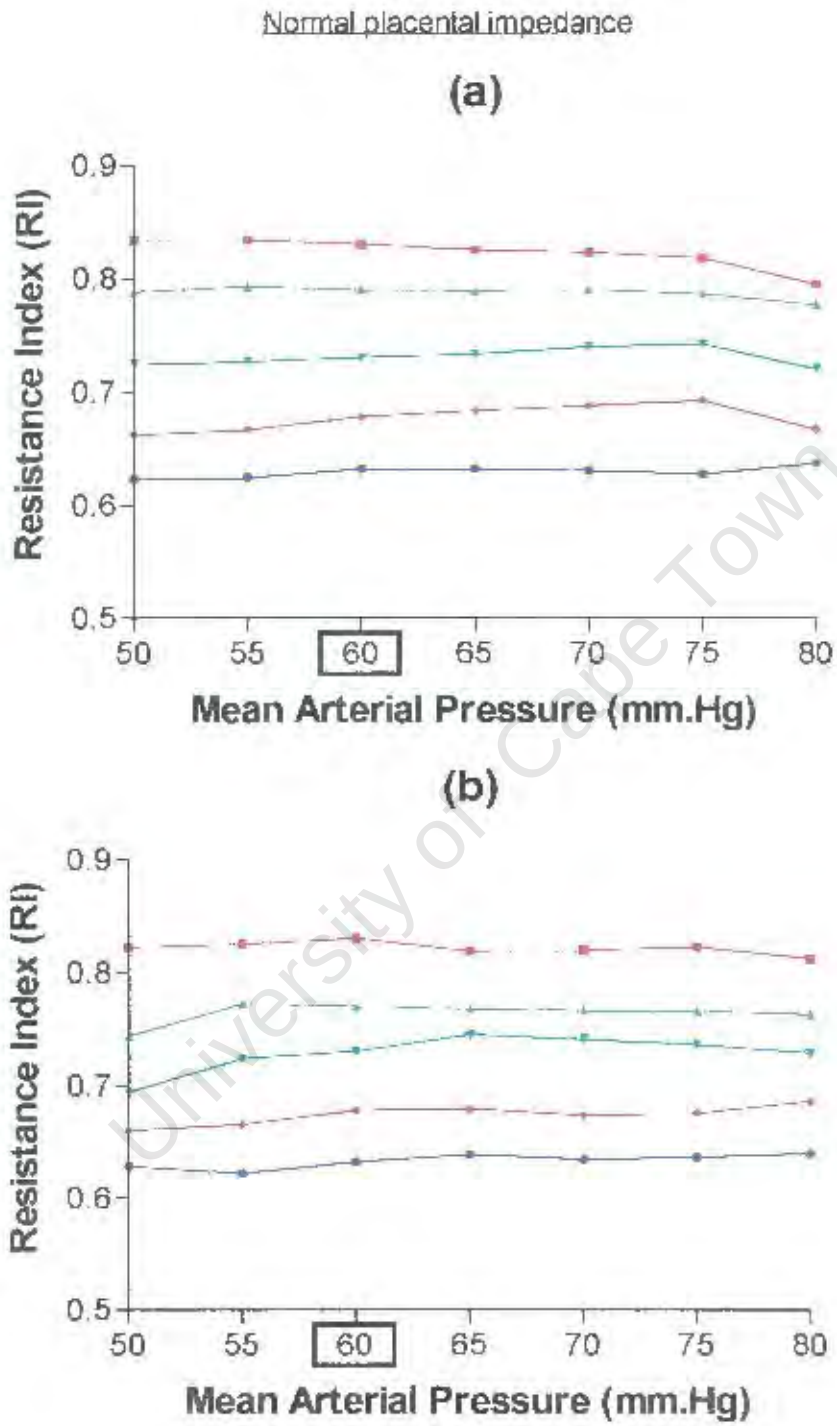

Figure 11.10: Changes in RI for each of the model arteries versus (a) acute and (b) chronic changes in mean arterial pressure for a healthy placenta. Reference values for the mean pressure are indicated by the boxed values.

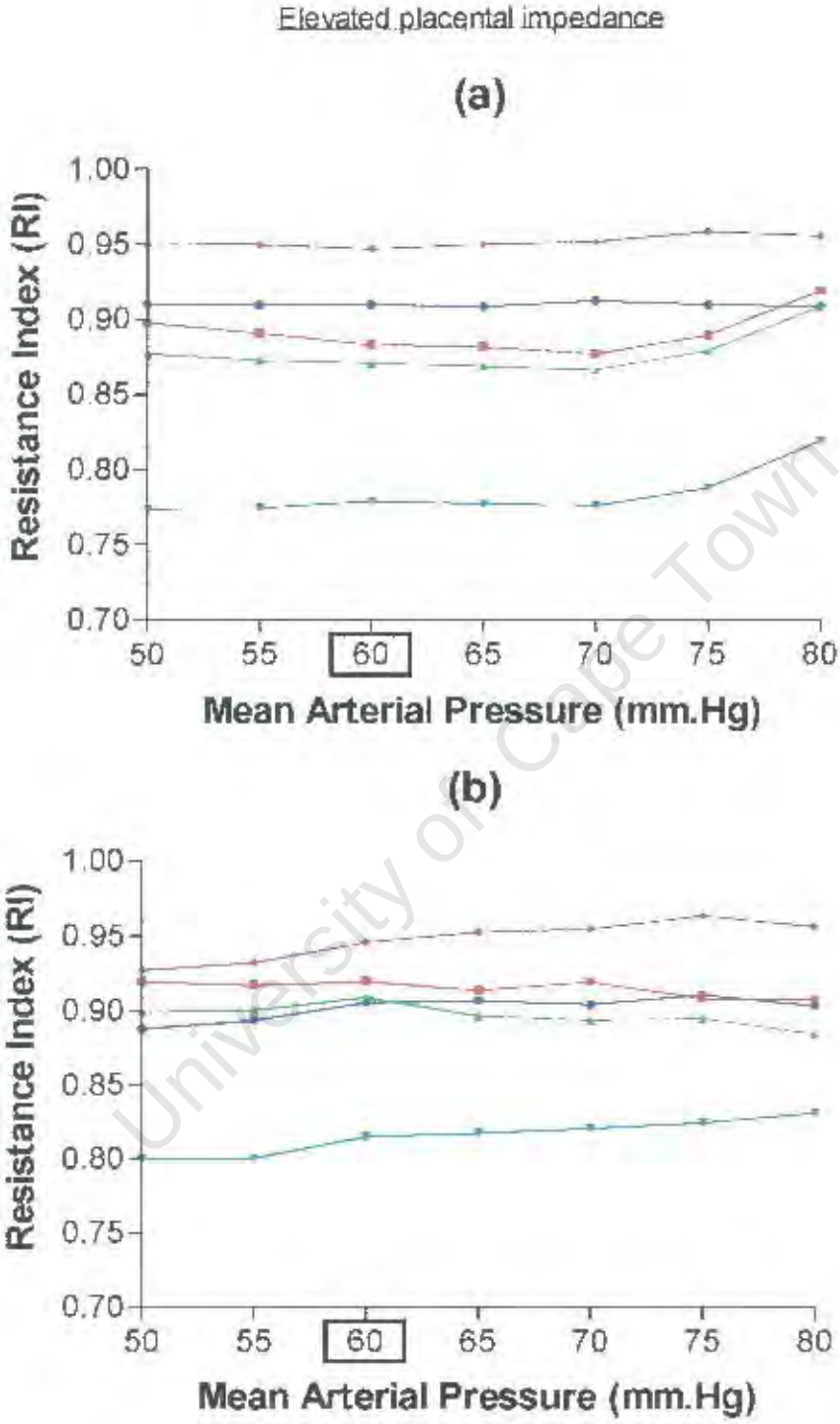

Figure 11.11: Changes in RI for each of the model arteries versus (a) acute and (b) chronic changes in mean arterial pressure for an underdeveloped placenta. Reference values for the mean pressure are indicated by the boxed values.

during acute maternal hypoxaemia), the fraction of cardiac output distributed to the placenta appears to remain constant, flows to the head, heart and adrenals increase, and flows to the lower limbs and abdomen decrease. In the more chronic responses, the proportion of cardiac output to the placenta begins to decline as more blood is diverted to the brain and myocardium. Placental changes have been dealt with in section (11.3) and this section will only consider redistribution responses to acute hypoxic stresses. Pressures and cardiac output are considered to remain constant in order to simulate the most extreme effect of altered vascular resistances. The resistance of those vascular beds that obtain a greater proportion of cardiac output must decrease, whilst the resistance of the peripheral beds that obtain less cardiac output increase. As these changes in resistance occur in a relatively short time interval, once again they are modelled by keeping the arterial tree morphology consistent with nominal or reference values, whilst dilating or constricting the tree vessel radii to accommodate alterations in resistance. The precise fractions of redistribution are unknown and some variance between individual foetuses would certainly be expected. However, it is known that particular vascular beds obtain greater fractions of cardiac output at the expense of others. Thus there is value in modelling varying degrees of redistribution in order to assess their effect. This may be simulated by the scenarios outlined in table (11.1). For a maldeveloped placenta, it was assumed that the redistribution pattern developed in section (11.3) occurs in addition to (over and above) the distribution scenarios in table (11.1).

Vascular bed	Redistribution Scenario Number.						
	1	2	3	4	5	6	7
Head and Heart	27	30	33	36	39	41	43
Upper body and Thorax	15	14	13	12	11	10	9
Abdomen	7.7	7.7	6.7	6.7	5.7	5.7	5.7
Adrenals	0.3	0.4	0.5	0.6	0.7	0.8	0.9
Lower Limbs	25	22.9	21.7	19.7	18.6	17.5	16.4
Placenta	25	25	25	25	25	25	25

Table 11.1: Values of percentage cardiac output distributed to each peripheral vascular bed for model simulations of acute redistribution. Simulations are labelled by a number between 1 and 7.

Figures (11.12 a and b) are graphs of the RI in the various model arteries versus a redistribution pattern as described by the number in table (11.1), for the situations of a normally and maldeveloped placenta respectively.

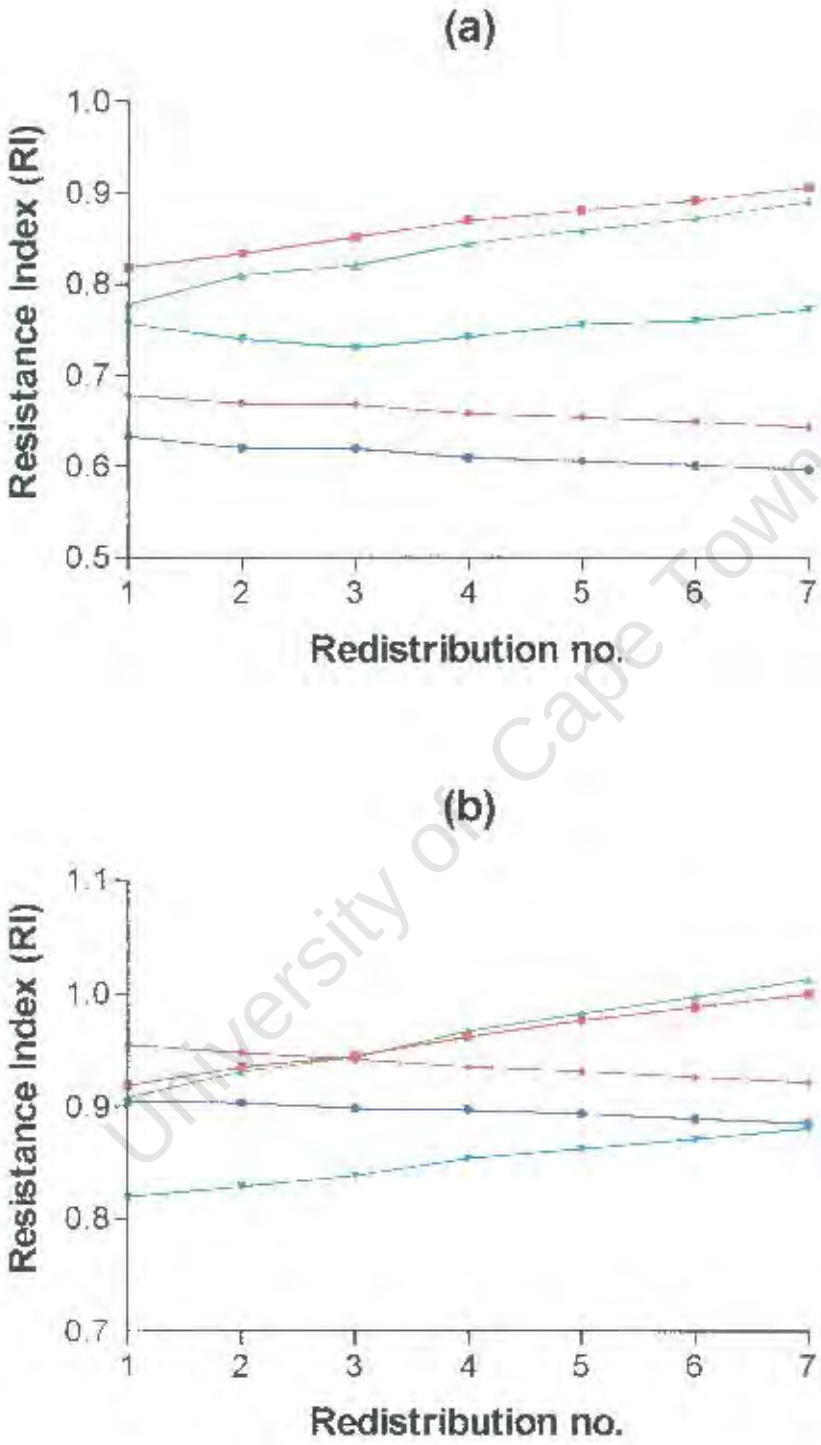

Figure 11.12: Changes in RI for each of the model arteries versus a redistribution of cardiac output according to table (11.1) for the cases of (a) a normal placenta and (b) an underdeveloped placenta.

Figures (11.12 a and b) clearly indicate that the effect of acute blood flow redistribution on the RI is the same whether a normal or increased placental resistance is present. The net effect is to increase the indices in the thoracic, abdominal and iliac arteries and to decrease them at both ends of the umbilical arteries, as further redistribution occurs (increasing distribution number). These increases or decreases are relatively small, with a maximum increase of 10.6 % in the thoracic artery and a maximum decrease of 5.8% at the placental end of the umbilical artery in normal and maldeveloped placentas.

11.8 Umbilical arterial wall morphology

In chapter 2 it was suggested that certain morphological changes in the structure of the umbilical arterial wall occurs in pregnancies complicated by oedema, proteinuria, hypertension gestosis or preeclampsia. These changes result in a reduction in the wall elasticity or compliance. Clinical studies also show a premature reduction of Wharton's jelly in association with foetal growth retardation. A reduction of umbilical arterial wall elasticity may be modelled by increasing the Young's modulus in the umbilical artery, which effectively increases the wave speed in the artery. Reduction of Wharton's jelly may be modelled by reducing the real part of g in Dinnar's model, which once again effectively increases the wave speed in the artery. Dinnar (1975) demonstrated that changes to the real part of g had a far greater effect than changes to the imaginary part, which represents the viscous effect of the surrounding tissue, and thus no changes to the imaginary part were simulated. In addition, Bruch et al. (1997) reported a significant reduction in medial wall thickness of the umbilical vessels in growth retarded foetuses. A reduction in wall thickness will reduce the wave speed in the umbilical artery. Lastly, due to limited information available on the visco-elasticity of the umbilical artery (Hill et al. 1995), it is necessary to account for some degree of expected variance in this variable. This may be modelled by varying ϕ_0 in the viscoelastic model between 0° and 30°. Decreasing the visco-elastic parameter marginally decreases the wave speed, although this decrease is insignificant. This section simulates changes in the umbilical arterial wall parameters of Young's modulus, surrounding tissue content, wall thickness and visco-elasticity. These changes may be the result of normal statistical variance or due to the pathologies discussed above. Figures (11.13 a - d) are the simulated results in each artery for RI's, plotted against a changing static Young's modulus, wall thickness, surrounding tissue (g) and viscoelastic angle (ϕ_0) respectively, for a normal placenta. Figures (11.14 a - d) are the corresponding cases for an underdeveloped or high resistance placenta.

An interesting observation that appears to be common for all simulations with changing umbilical arterial wall parameters is that the RI's measured at opposite ends of the umbilical artery tend to move in opposite directions as the various wall properties change. This therefore

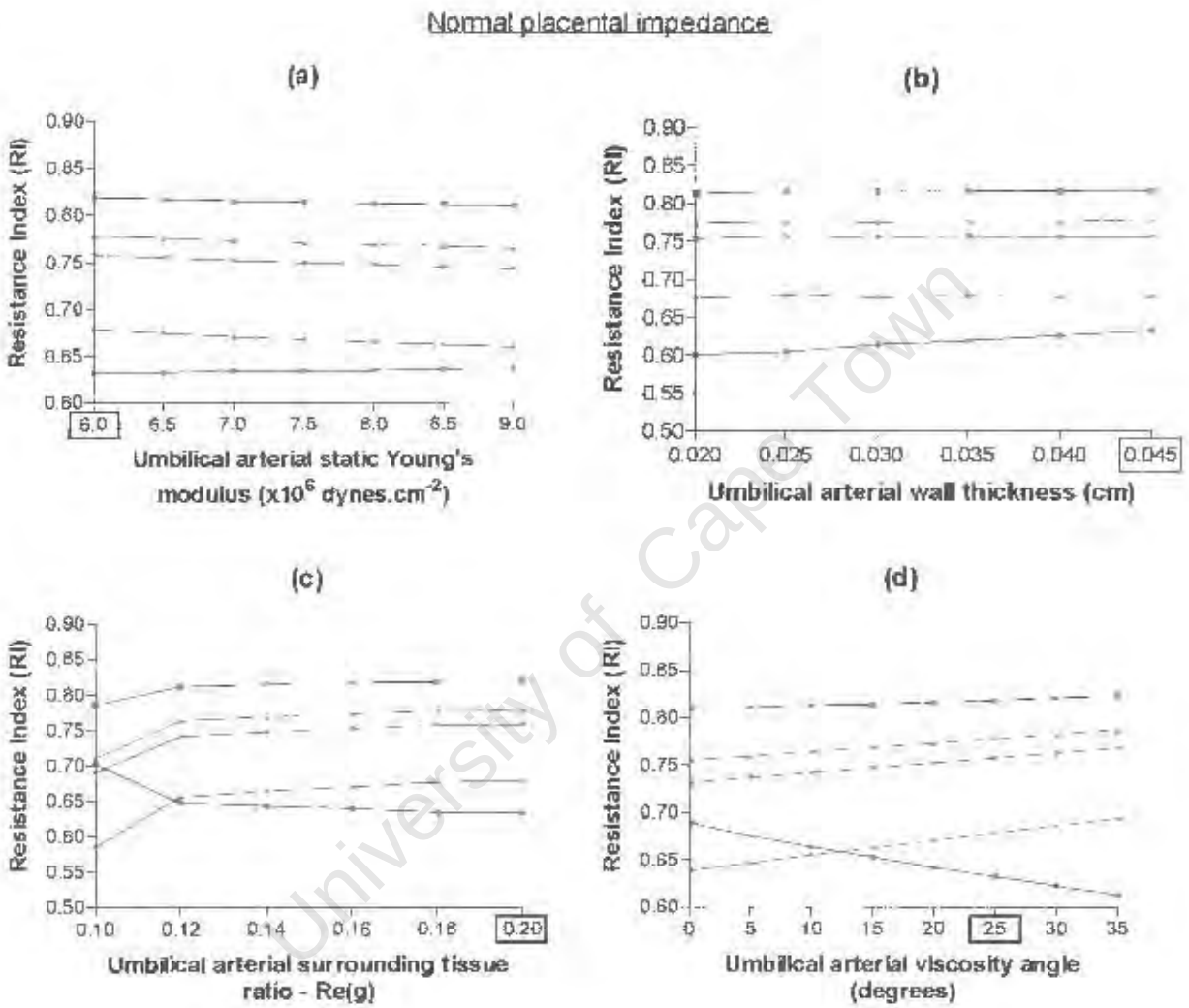

Figure 11.13: Model simulations of changes in RI brought about by changes in umbilical arterial wall parameters of (a) Young's modulus, (b) wall thickness, (c) Dinnar's model parameter representing the effect of the surrounding tissue, g, and (d) the viscosity angle ϕ. These simulations are for a healthy placenta. Reference values for the variables are indicated by the boxed values.

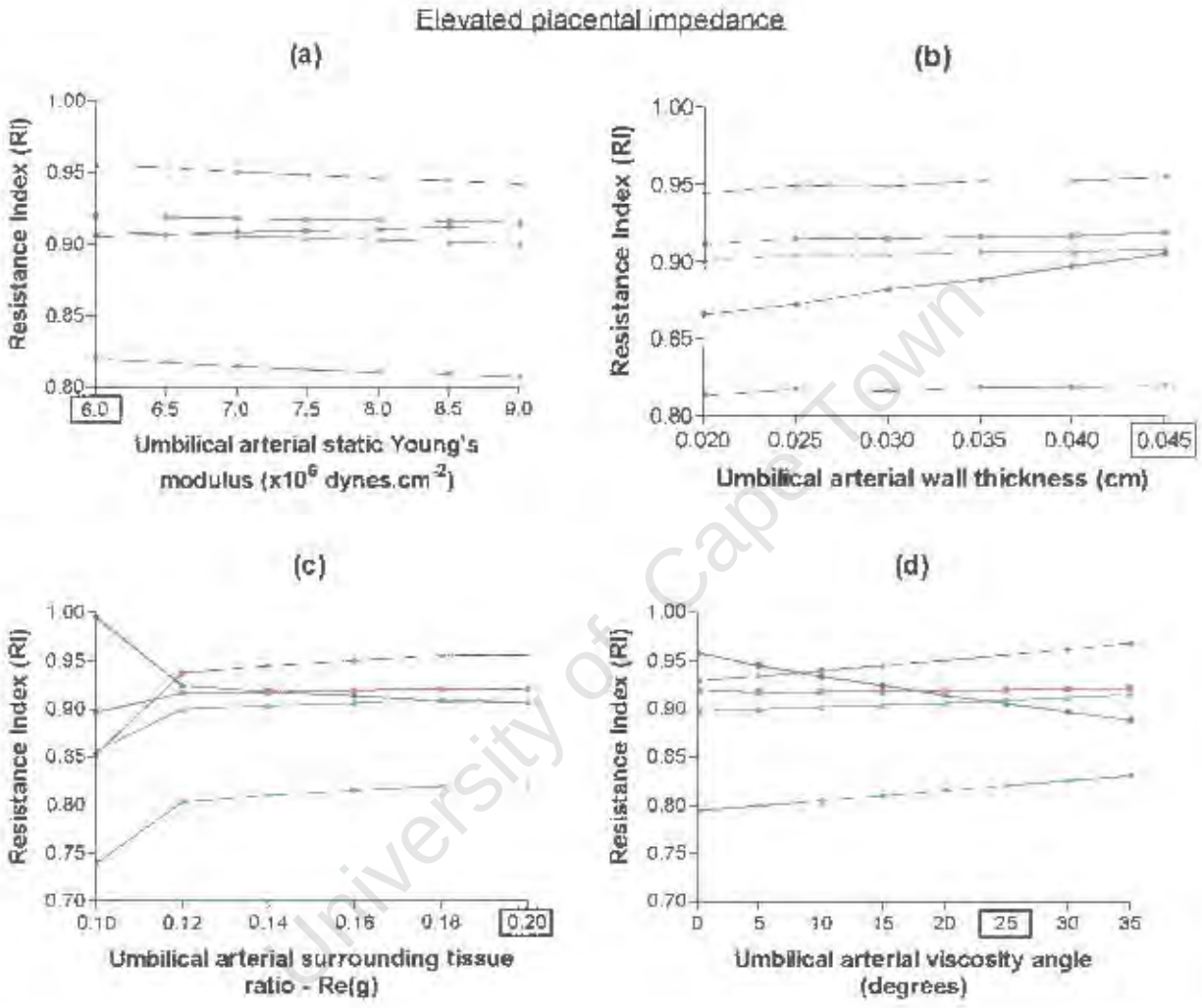

Figure 11.14: Model simulations of changes in RI brought about by changes in umbilical arterial wall parameters of (a) Young's modulus, (b) wall thickness, (c) Dinnar's model parameter representing the effect of the surrounding tissue, g, and (d) the viscosity angle ϕ. These simulations are for a maldeveloped placenta. Reference values for the variables are indicated by the boxed values.

either diminishes or increases their difference and may result in the placental end recording a higher index value than the foetal end. The trends of the indices measured in the thoracic, abdominal and iliac arteries were essentially the same to that of the umbilical artery measured at the foetal end and thus this discussion will only focus on the ends of the umbilical artery.

Increasing the static Young's modulus tended to decrease the resistance index at the foetal end of the umbilical artery and increase it at the placental end. These changes were slight and a maximum decrease in RI of 2.8% for a healthy placenta and 1.4% for a maldeveloped placenta were recorded at the foetal end of the umbilical artery. Increases of 0.65% and 0.81% respectively were found for the resistance index at the placenta end of the umbilical artery for the cases of a normal and of a maldeveloped placenta. These results essentially indicate that increases in the static Young's modulus over this range have very little affect on the actual Doppler indices recorded in the various arteries. Surat and Adamson (1996) and Kleiner-Assaf et al. (1999) reported similar findings of only slight decreases in resistance index in the umbilical artery for increasing Young's moduli. However they did not perform simulations at both ends of the arteries.

Decreasing arterial wall thickness tended to decrease the measured RI's at the placental end of the umbilical artery, whilst the RI measured at the foetal end remained relatively constant for both healthy and high resistance placentas. For the healthy placenta a maximum decrease of 5% at the placental end was recorded, with the index at the foetal end of the artery decreasing by a corresponding amount of 0.4%. In the situation of elevated placental resistance, the index measured at the placental end decreased by 0.81%, whilst the index measured at the foetal end decreased by 1.4%. Thus it may be said that changing the umbilical arterial wall thickness has a negligible effect on the measured Doppler indices. Once again, in their models, Surat and Adamson (1996) and Kleiner-Assaf et al. (1999) showed very slight changes in indices for decreasing wall thicknesses.

Decreasing the quantity of Wharton's jelly was simulated by decreasing the real part of g, which had the effect of increasing the resistance index measured at the placental end of the umbilical artery, whilst decreasing the index measure at the opposite end of the artery. When decreased by 80% of its original value, the indices rapidly changed their slopes and began to increase and decrease at a greater rate, causing the placental end to record a higher value of resistance index than at the foetal end. The maximum increases in RI were 11.1% for a healthy placenta and 9.9% when placental resistance was elevated. The maximum decreases in resistance index for the normal and abnormal placentas were 13.6% and 10.8% respectively. Thus although the magnitude of the changes due to a decreased Wharton's jelly content are relatively low, their effect is quite pronounced when examining differences between indices at either end of the umbilical arteries.

The effect of decreasing the viscosity angle is qualitatively similar to that of decreasing the real part of g, in that the resistance index measured at the foetal end decreases, whilst the index measured at the placental end increases. The indices reach the same value and then cross-over between 10° and 15° for a healthy placenta and when placental resistance is elevated, this cross over point is reached between 5° and 10°. The maximum increases in resistance index were 11.0% for a healthy placenta and 7.3% when placental resistance was elevated. The maximum decreases in resistance index for the normal and abnormal placentas were 8.6% and 4.2% respectively. Thus the effects of viscosity on the Doppler indices are reduced when placental resistance is elevated due to a maldeveloped placenta. Once again, the overall effect of a changing umbilical arterial viscosity on the resistance index is relatively low, however it has an important impact on differences between indices obtained from the two ends of the umbilical artery.

11.9 Umbilical radius

Chapter 2 outlined common causes of changes to the umbilical radius which may be simulated in three different manners. The first simulation (scenario 1) considers the changes attributed to individual variance amongst the foetal population and thus the percentage blood flow distribution to the peripheral organs remains the same as the reference values. Decreasing the umbilical radius will tend to decrease the flow to the placenta and in order to maintain the same fraction of cardiac output distributed to the placenta, the placental resistance must decrease. This decrease is achieved by a different rate of growth of the placenta, resulting in a decreased placental resistance. The reverse holds true for an increase in umbilical radius. The second scenario also assumes that the foetus responds to the umbilical radial changes by maintaining reference blood flow distribution. In this scenario, this is achieved by respectively vasoconstricting or dilating the radii of the placenta. In scenario 3, the flow to the placenta is allowed to decrease due to the constricted umbilical radius and this decrease in flow is redistributed to all the remaining organs, with a greater proportion to the head and heart, as demonstrated by Itskovitz et al. (1987). The precise proportion of redistribution is unknown and for simplicity it is assumed that for every one percent decrease in umbilical flow, 0.6% of this flow is redistributed to the head and heart, 0.025% to the adrenals and 0.125% to each of the remaining three other vascular compartments (as before). The increase in flow to the peripheral organs is achieved by a dilation of the radii of their arterial networks. This scenario only considers a decrease in umbilical radius. Figures (11.15 a - c) and figures (11.16 a - c) display the simulated results of changes to RI's in each artery for given changes in umbilical arterial radius for healthy and diseased placentas respectively. Graphs labelled (a) are for scenario 1, graphs labelled (b) are for scenario 2 and graphs labelled (c) are for scenario 3.

Adamson et al. (1990) infused Angiotensin II into the circulatory system of foetal sheep. This caused the highly vasoactive umbilical artery to vasoconstrict, whilst the placental vessels remained unchanged, thereby elevating the umbilico-placental resistance. The foetus responded to this vasoconstriction by increasing its mean arterial pressure, whilst heart rate remained constant. Adamson and co-workers did not report what happened to the overall cardiac output but Iwamoto and Rudolph (1981) found that angiotensin II infusion into the circulatory system of foetal sheep significantly increased the cardiac output. Thus an increase in pressure and total cardiac output, along with some blood flow redistribution is the most probable response to an infusion of Angiotensin II. This may be mathematically represented in the model by assuming that the resistance of the umbilical artery is increased by some factor k, causing the total flow to the umbilical arteries and the placenta to decrease by a corresponding factor y, with the mean arterial pressure being elevated by a factor z. If the flow to the umbilical arteries and the placenta is denoted by Q_{u+p} and the resistance of the placenta plus the umbilical arteries denoted by $R_u + R_p$ and the mean arterial pressure by P_A, then

$$R_u + R_p = P_A/Q_{u+p} \tag{11.8}$$

increasing the umbilical resistance results in the following expression

$$kR_u + R_p = zP_A/yQ_{u+p} \tag{11.9}$$

This increase in arterial pressure will also increase the flow to the other peripheral vascular beds. Additionally, the decrease in flow to the placenta and umbilical arteries must be redistributed to the other vascular beds and therefore the flow increase due to the pressure increase and the redistribution must be equivalent. This assumes that no morphological changes occur to the vascular tree networks and that each vascular bed increases its flow by the same proportion. Denoting the sum of the flow to each of the other vascular beds by $\sum_{VB} Q_{VB}$, and the total cardiac output by CO, the following relation must hold:

$$\sum_{VB} Q_{VB} + Q_{u+p} = CO \tag{11.10}$$

Decreasing the flow to the placenta and umbilical arteries by a factor y will result in the flow to the remaining vascular beds increasing by a factor x, where

$$x = \frac{CO - yQ_{u+p}}{\sum_{VB} Q_{VB}} \tag{11.11}$$

The flow to the remaining vascular beds also increases due to the increase in mean arterial pressure and this increase must also be equal to x. I.e. $x = z$. Substituting equation (11.9) for z, allows y to be solved for :

$$y = \frac{CO}{\left(\left(\sum_{VB} Q_{VB}\right)\left(kR_u + R_p\right) + P_A\right)} \frac{P_A^2}{Q_{u+p}} \tag{11.12}$$

Dividing the numerator and denominator through by the cardiac output, allows this equation to be represented in the form of the fractional cardiac output supplied to each bed. i.e.

$$y = \frac{R_u + R_p}{\left(\left(\sum_{VH} Q_{VB}/CO\right)\left(kR_u + kR_p\right) + P_A\right)} \tag{11.13}$$

where $\sum_{VB} Q_{VB}/CO = 0.75$ for a healthy 28 week old foetus.

Thus by specifying the factor by which the umbilical arterial resistance is elevated, (k), it is possible to determine how much the mean arterial pressure must be elevated by in response, (z), and the proportion the flow must be increased by to the remaining vascular beds,(x) ,to compensate for the decrease in flow to the umbilical arteries and placenta. This simulation assumes that the increase in flow is equally distributed to all the foetal peripheral beds, however Iwamoto and Rudolph (1981) found that angiotensin II infusion markedly increased blood flow to the myocardium and pulmonary circulation. Therefore, the model simulation may be adjusted by distributing an additional quarter of the increase in flow to the head and heart and decreasing the flow to the remaining vascular beds by one quarter. The radii of the vascular networks would contract and dilate respectively only to accommodate that extra increase and decrease over and above the increase by the factor z. This simulation is intended to reproduce the experiments conducted by Adamson et al. (1990), however it must be pointed out that not all the foetal responses to angiotensin II infusion have been accurately measured and therefore further changes over and above those included in this simulation may very well take place. The changes in RI with umbilical radius for this simulation are depicted in figure (11.17 a), whilst the corresponding increase in mean pressure (z) is depicted in figure (11.17 b) and the factor by which the flow to the peripheral organs increases is depicted in figure (11.17 c).

The results of the first two scenarios, (altering the number of placental vessels or the radii of the individual placental vessels), are relatively similar for both normal and high resistance placentas. These simulations indicate that when the umbilical arterial radius is decreased, and the placenta compensates so that the proportion of flow to the umbilical artery and placenta remains unchanged, the resistance index in all the arteries is dramatically reduced, with a greater rate of reduction in the umbilical arteries than in the other arteries. These simulations are most appropriate for simulating statistical variance amongst the foetal population, in which case it is unlikely that the radius would decrease to as low as the values simulated. Decreasing the umbilical radius from 0.17cm to 0.07cm causes RI decreases in the placental end of the umbilical

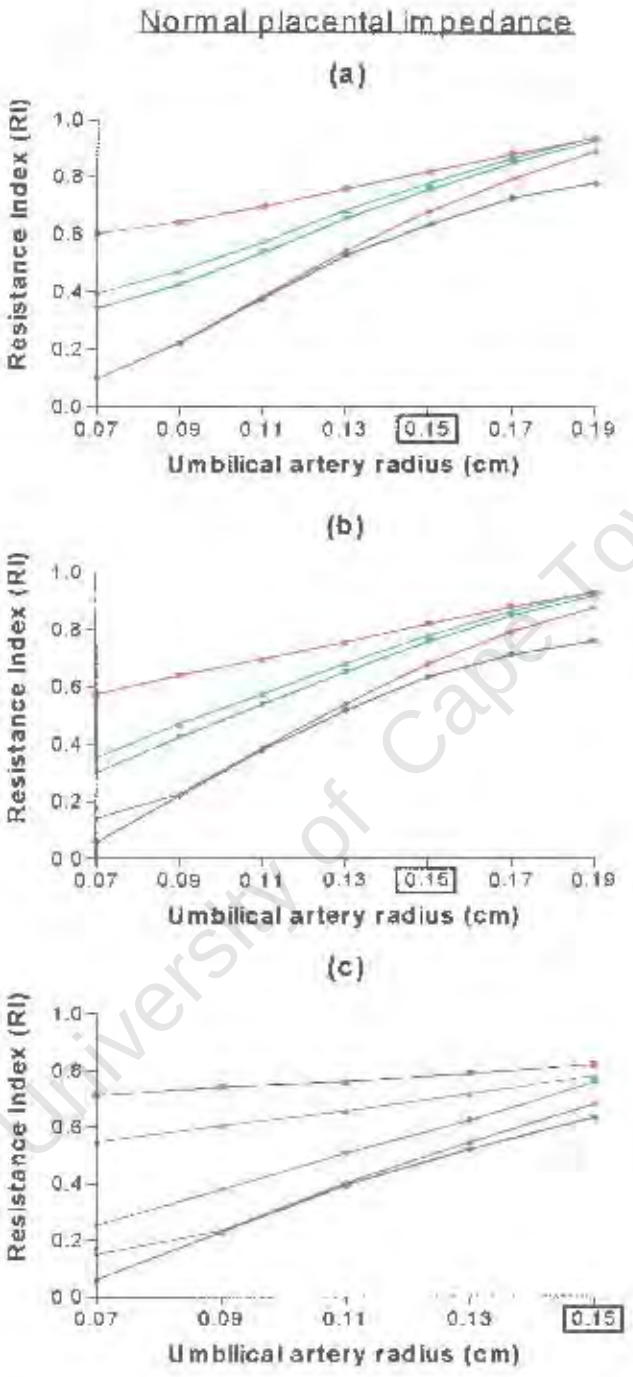

Figure 11.15: Simulated changes in RI in each of the model arteries for changes in umbilical arterial radius; (a) is scenario 1; (b) is scenario 2; (c) is scenario 3. (See text for explanations). These simulations are for a healthy placenta and reference values for the umbilical radii are indicated by the boxed values.

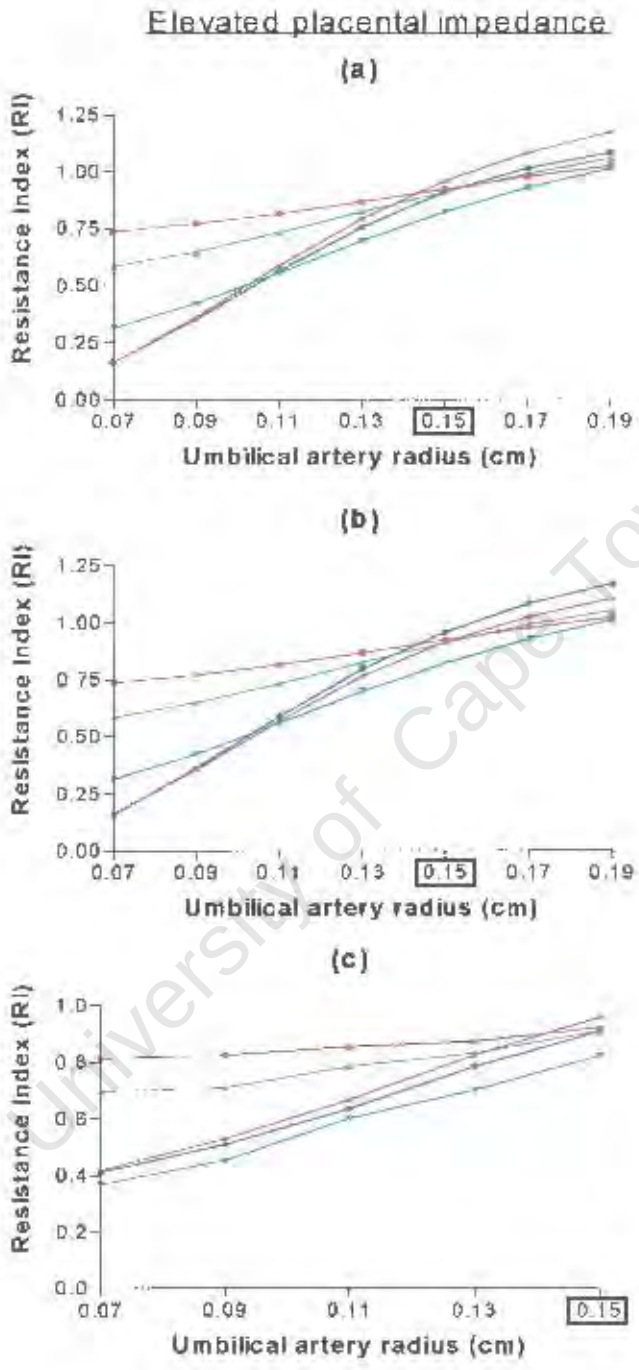

Figure 11.16: Simulated changes in resistance index in each of the model arteries for changes in umbilical arterial radius; (a) is for scenario 1; (b) is for scenario 2; (c) is for scenario 3. (See text for explanations). These simulations are for a chronically maldeveloped placenta and reference values for the umbilical radii are indicated by the boxed values.

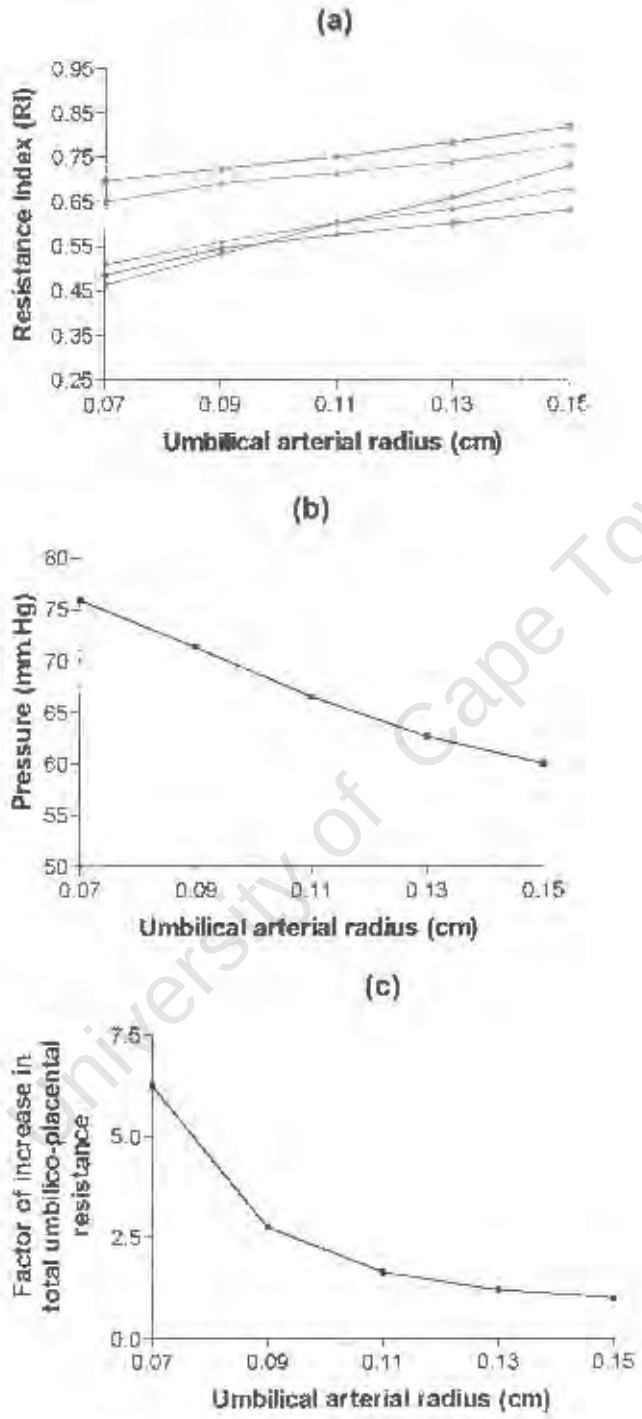

Figure 11.17: Simulation of angiotensin II infusion into the umbilical artery. (a) depicts the change in RI, (b) is change in pressure and (c) the factor by which the total umbilico-placental resistance increases. Reference values of the umbilical radii are indicated by the boxed values.

artery of 84.7% and 82.2% for a normal and maldeveloped placenta respectively. Corresponding decreases in the thoracic artery are 26.7% and 20.1% for normal and maldeveloped placentas respectively.

When the flow to the placenta is allowed to decrease due to the decreasing umbilical radius, and assuming constant pressure, heart rate and cardiac output, and that the decrease in flow to the placenta is redistributed to the remaining foetal vasculature, the RI's in all arteries still decrease. However this decrease is at less of a steep rate. Here, decreasing the umbilical radius from 0.17cm to 0.07cm causes a decrease in the placental end of the umbilical artery of 78.1% and 54.9% for a normal and maldeveloped placenta respectively. Corresponding decreases in the thoracic artery are 13.0% and 11.6% for normal and maldeveloped placentas respectively. Thus it is clear that when placental resistance is elevated, the decrease in RI due to decreasing the umbilical arterial radius is reduced.

In the experiments of Adamson et al. (1990), the umbilical arterial resistance was increased by a factor of 13, increasing overall umbilico-placental resistance by a factor of six fold. An increase in umbilical resistance by a factor of 13 roughly corresponds to decreasing the umbilical radius from 0.15cm to 0.08cm. In the simulation designed to reproduce their results, decreasing the umbilical radius from 0.15cm to 0.08 cm produced decreases in RI of 17.7% and 13.2% at the placental end of the umbilical artery and in the thoracic aorta respectively. Thus it is clear that in this situation, the decrease in indices are far less significant than for the other simulations. Adamson et al. (1990) reported no correlation of the resistance index measured in the common umbilical artery with increasing umbilical arterial resistance due to angiotensin II infusion. The results of the simulations in this thesis show that there is a correlation and that the resistance index would be expected to decrease slightly. However, this decrease may not be clinically significant. In their experiments, Adamson and co-workers reported that no significant change in heart rate was noted, although the heart rate did fall slightly. The model simulations kept heart rate constant at its nominal value and decreasing the heart rate would be expected to elevate the indices. Further discrepancies in the results may be attributed to haemodynamic and anatomical differences in the sheep and human foetal parameters, especially the actual values of arterial radii, as well as the fact that the mean arterial pressure in the model simulations did not rise quite as high as that in the experimental work. The pressure in the model increased by a factor of 21.7%, whilst that in the animal experiments increased by 61.5%.

A further observation that is common to all the experiments is that as the umbilical arterial radius decreases, the differences in indices between opposite ends of the umbilical artery decrease. This is due to the fact that the wave speed in the artery will increase with decreasing radius, and

therefore there will be less change in phase and attenuation of the velocity waveform between either end of the umbilical arteries. This decrease of difference in indices between opposite ends of the cord was also pointed out by Adamson (1999), regarding the experimental work performed with angiotensin II.

11.10 Blood viscosity

As described in chapter 2, there is a direct relationship between hypoxia and an elevated blood viscosity. Elevations in blood viscosity occur due to an increase in the haematocrit as a result of hypoxia and this cannot occur in a short time interval. An increase in blood viscosity will result in elevated arterial resistances, assuming that arterial morphology, pressure and cardiac output remain constant. Should this increase be chronic or as a result of statistical variance, and should pressure and cardiac output remain unchanged, the foetus must regrow the peripheral vascular beds so that the resistances of these beds remain unchanged. Interventional studies have been performed by Morrow et al. (1990), who infused packed cells into foetal sheep that resulted in an increased blood viscosity. Although this type of situation will not be encountered unless through interventional procedures, it must be simulated as an acute change in peripheral resistance. Morrow et al. (1990) reported that no significant change in blood pressure, cardiac output or heart rate occurred with the exchange transfusion. Therefore these parameters were kept constant for the simulation. As the morphology of the peripheral networks cannot change in this acute simulation, the radii of the resistance vessels of the vascular networks must dilate to counteract the increased resistance due to the added viscosity. Furthermore, the resistance of the umbilical artery also increases due to an increasing viscosity and therefore the placenta must further compensate with radial dilation to maintain constant flow. Kitanka et al. (1989) subjected pregnant ewes to hypoxia for 28 days by decreasing their inspired oxygen and compared the results with a control population. They found that foetal erythrocyte volume and whole blood volume increased during the course of the hypoxaemia, with the erythrocyte volume more than doubling. Thus using this as a rough physiological guideline, viscosity increases were simulated between the reference value of 0.06 dynes.s.cm^{-2} and double this value in steps of 0.02 dynes.s.cm $^{-2}$. Figures (11.18 a and b) are the simulated results in each artery for the RI's, plotted against blood viscosity for acute and chronic changes in viscosity respectively, for a normally developed placenta, whilst figures (11.19 a and b) are for a maldeveloped placenta.

These results indicate that in the acute scenario, for a normal placenta, the Doppler indices are relatively unchanged for increasing blood viscosity, with a slight tendency to decrease. A maximum of an 11.6% decrease occurs at the placental end of the umbilical artery. This type of simulation, confirms the findings of Morrow et al. (1990) who experimentally doubled the viscosity of blood in healthy foetal sheep and observed no significant change in the umbilical

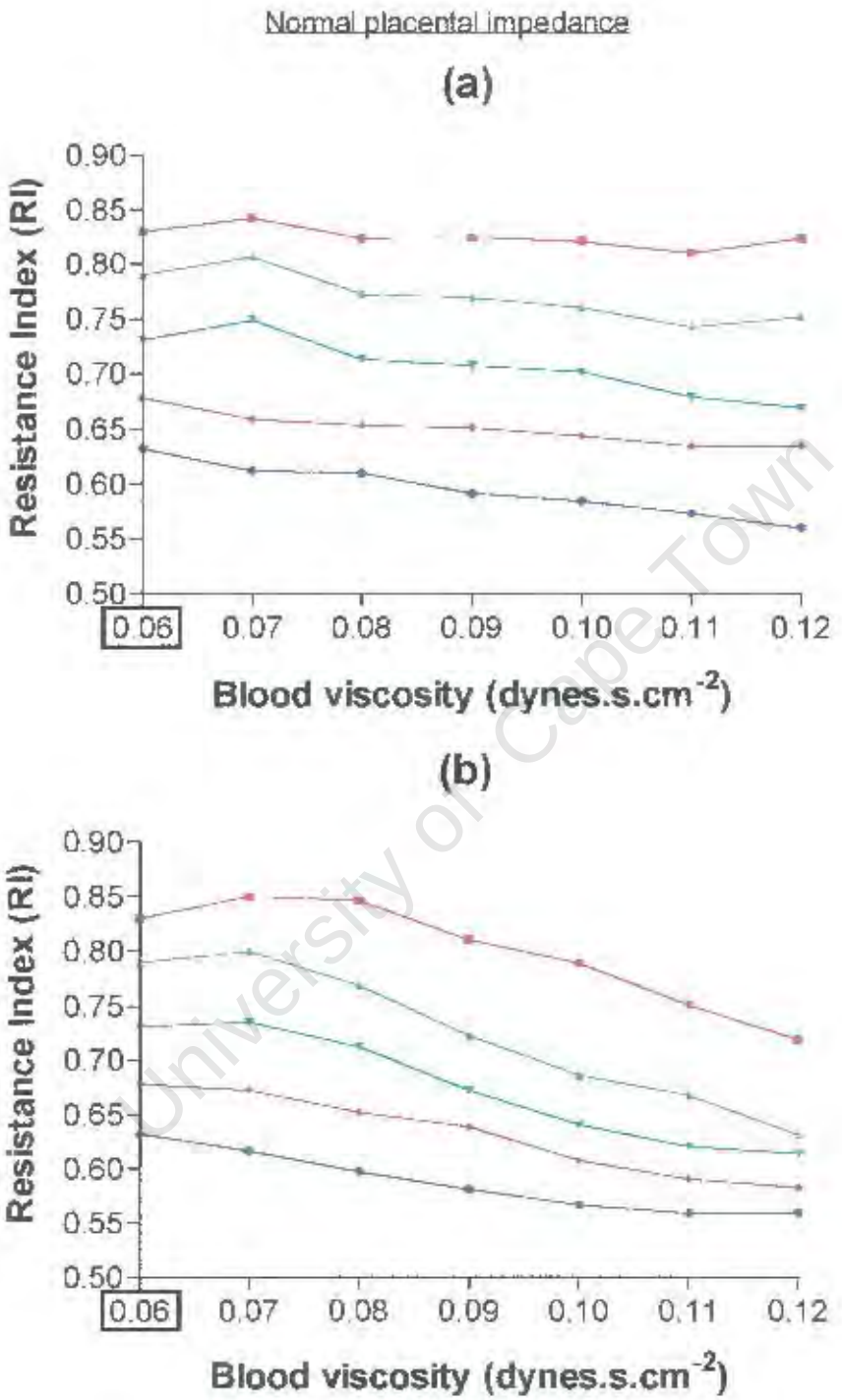

Figure 11.18: Simulated results in each artery of changes in RI for a given increase in foetal blood viscosity, for (a) acute and (b) chronic increases in viscosity. Results are for a normal placenta. Reference values for blood viscosity are indicated by the boxed values.

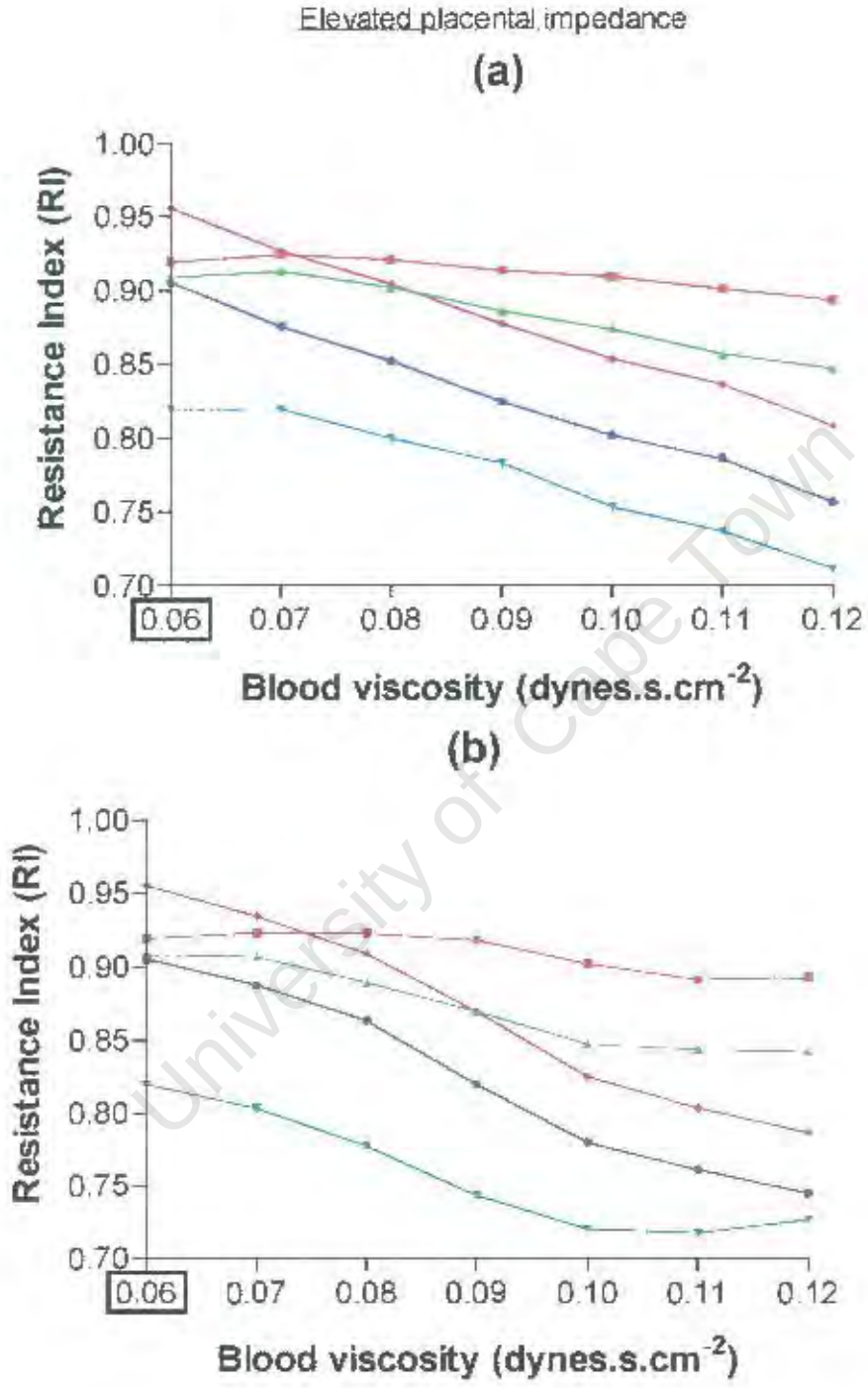

Figure 11.19: Simulated results in each artery of changes in RI for a given increase in foetal blood viscosity, for (a) acute and (b) chronic increases in viscosity. Results are for a maldeveloped placenta. Reference values for blood viscosity are indicated by the boxed values.

artery waveform one hour later. However, an acute change in blood viscosity in a situation of elevated placental resistance due to a maldeveloped placenta, tended to decrease the umbilical arterial waveform indices at a greater rate. Here, a maximum decrease of 17% occurred, whilst the indices in the thoracic and abdominal aortas decreased at a far slower rate, with a maximum decrease of 2.8% in the thoracic aorta. The results in response to a chronic increase in blood viscosity are quantitatively fairly similar, with the placental end of the umbilical artery decreasing by 13% for a healthy placenta and by 21.6% for a maldeveloped placenta.

11.11 Placental villous vessel wall properties

A number of researchers have examined morphological changes which occur within the placenta of growth restricted foetuses. A number of these works indicate that in addition to diameter changes of the placental vessels and the number of vessels present, further structural changes to the individual vessel wall properties are also present. It appears that a slight reduction in the wall thickness of the placental villous vessels occurs in growth-restricted foetuses (Jackson et al. 1995; Mitra et al. 1997). Macara et al. (1996) found that the placental vessels of IUGR foetuses were associated with increased fractions of collagen and laminin, suggesting that the Young's modulus may be increased. No studies concerning changes in the viscoelasticity have been conducted, however the findings of Macara et al. (1996) indicate that the arterial wall morphology is altered and therefore it is entirely possible that the viscoelasticity of the placental vessels is similarly altered. Furthermore, some extent of variance of these wall properties may be assumed to be present amongst the healthy foetal population and therefore it is of clear benefit to assess the sensitivity of the Doppler indices to this variability. Simulations were conducted for both healthy, fully developed placentae and underdeveloped placentae, with varying static Young's modulus, wall thickness and viscoelastic angle. Figures (11.20 a - c) indicate the results of these simulations on the RI in the various arteries of a healthy placenta, whilst figures (11.21 a - c) are for a maldeveloped placenta. As the Young's modulus of the placental vessels increases with increasing levels of branching, the simulations are conducted by specifying the initial value of Young's modulus for the first level of branching. Although the radii of each vessel decreases as the depth of branching increases, the ratio of wall thickness to radius remains constant and therefore it is this parameter and the actual wall thickness that is specified for the simulations.

The simulations for both normal and maldeveloped placentas indicate that structural changes to the placental vessel wall properties have almost no effect on the RI's. This indicates that natural population variance at this level does not significantly alter the measured indices. Most structural changes to the walls of the placental vessels are found in association with IUGR and therefore abnormally developed placentas with elevated placental resistance. Simulations of

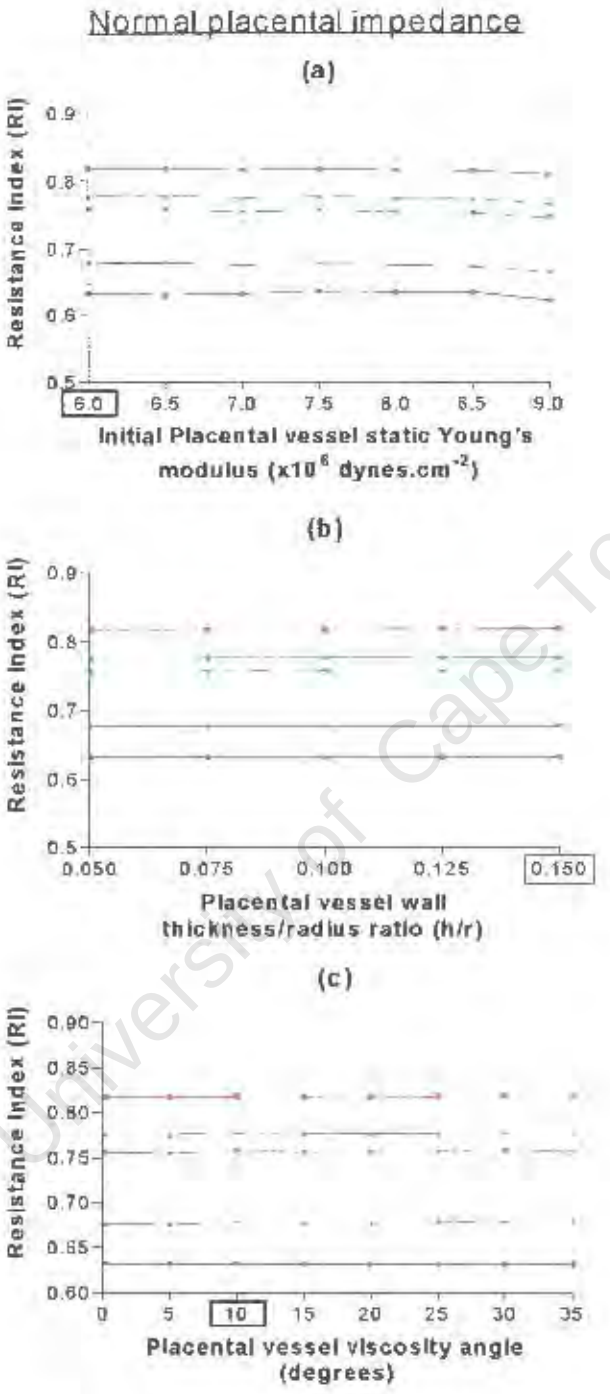

Figure 11.20: Simulated changes in RI in each of the arteries for changes in placental vessel wall properties: (a) for an increasing static Young's modulus; (b) for decreasing wall thickness to radius ratio and (c) for a changing viscoelastic angle, ϕ. Simulations are for a normally developed placenta. Reference values are indicated by the boxed numbers.

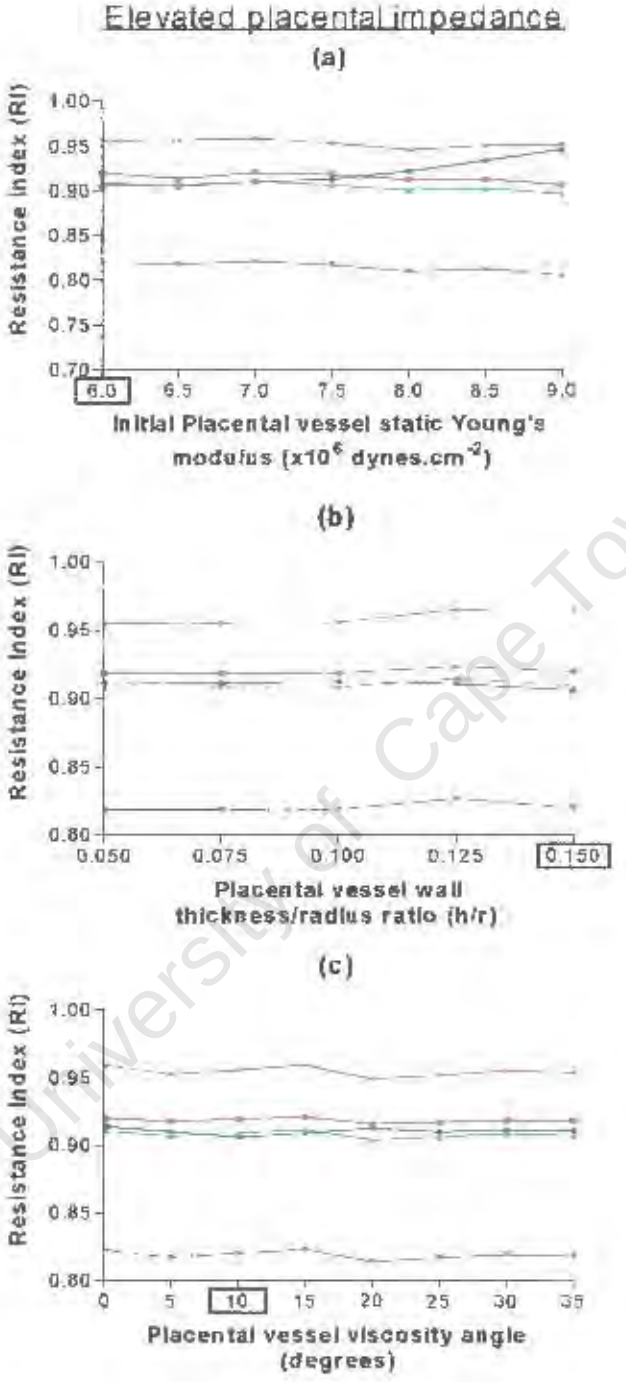

Figure 11.21: Simulated changes in RI in each of the arteries for changes in placental vessel wall properties; (a) for an increasing static Young's modulus; (b) for decreasing wall thickness to radius ratio and (c) for a changing viscoelastic angle, ϕ. Simulations are for a maldeveloped placenta. Reference values are indicated by the boxed numbers.

these scenarios again demonstrate that changes to the vessel wall properties result in very small changes to the measured resistance indices. This confirms the results of Mitra et al. (1997) who reported no correlation between the RI measured in the umbilical artery and wall thickness of the placental vessels.

11.12 Umbilical length

The mechanical consequences of an abnormally short or abnormally long umbilical cord are well known. Long umbilical cords predispose to cord entanglement or prolapse, whilst short cords predispose the foetus to rupture of the cord, failure to descend in labour and abruption of the placenta. Short cords are also associated with congenital foetal abnormalities (Naeye, 1985; Sherer and Anyaegbunam, 1997). A study performed by Naeye (1985) on 35 779 successful singleton pregnancies, demonstrated that within the normal foetal population, the umbilical cord length may vary by $\pm 21\%$ of the average length at a particular gestational age. No studies have been performed to investigate the effect of the umbilical arterial length on the Doppler indices. Given the considerable range of variation of cord length, it is necessary to determine whether cord length has any significant effect on the Doppler indices. Since the cord length cannot undergo acute changes, this is modelled as a chronic change. Here the increased resistance due to the increased cord length is compensated by a decreased placental resistance in order to maintain the placental flow. Similarly a decreased cord length would result in a placenta with a slightly higher resistance. As this is simulating a healthy foetus, the flow to the placenta and cord remains unchanged from nominal values. Figures (11.22 a and b) are the results of the model simulations for a healthy and diseased placenta respectively.

The results of figures (11.22 a and b) indicate that the effect of changes in umbilical cord length on the RI are similar for both a normal placenta and for a maldeveloped placenta. Shorter than average umbilical arteries tend to increase the RI's in every artery. However, the difference between indices from either end of the umbilical arteries are reduced. Increasing the length has the reverse effect. This is most likely due to the fact that in order to maintain the same proportion of flow to the placenta and cord, the placental resistance must increase for the case of short umbilical arteries and decrease for the case of long umbilical arteries. An elevated placental resistance was demonstrated to increase the Doppler indices and to decrease the differences in indices obtained at opposite ends of the umbilical arteries. At the extreme, for the healthy placenta, a change from 70cm to 20cm causes the RI at the placental and foetal ends of the umbilical arteries to change by 17% and 15% respectively. For the diseased placenta, the percentage change at the placental end is 26%, whilst at the foetal end this is 23%. Therefore the effect of umbilical length on the RI is more pronounced when placental resistance is elevated and for measurements obtained at the placental end of the umbilical artery. Thus, it is possible

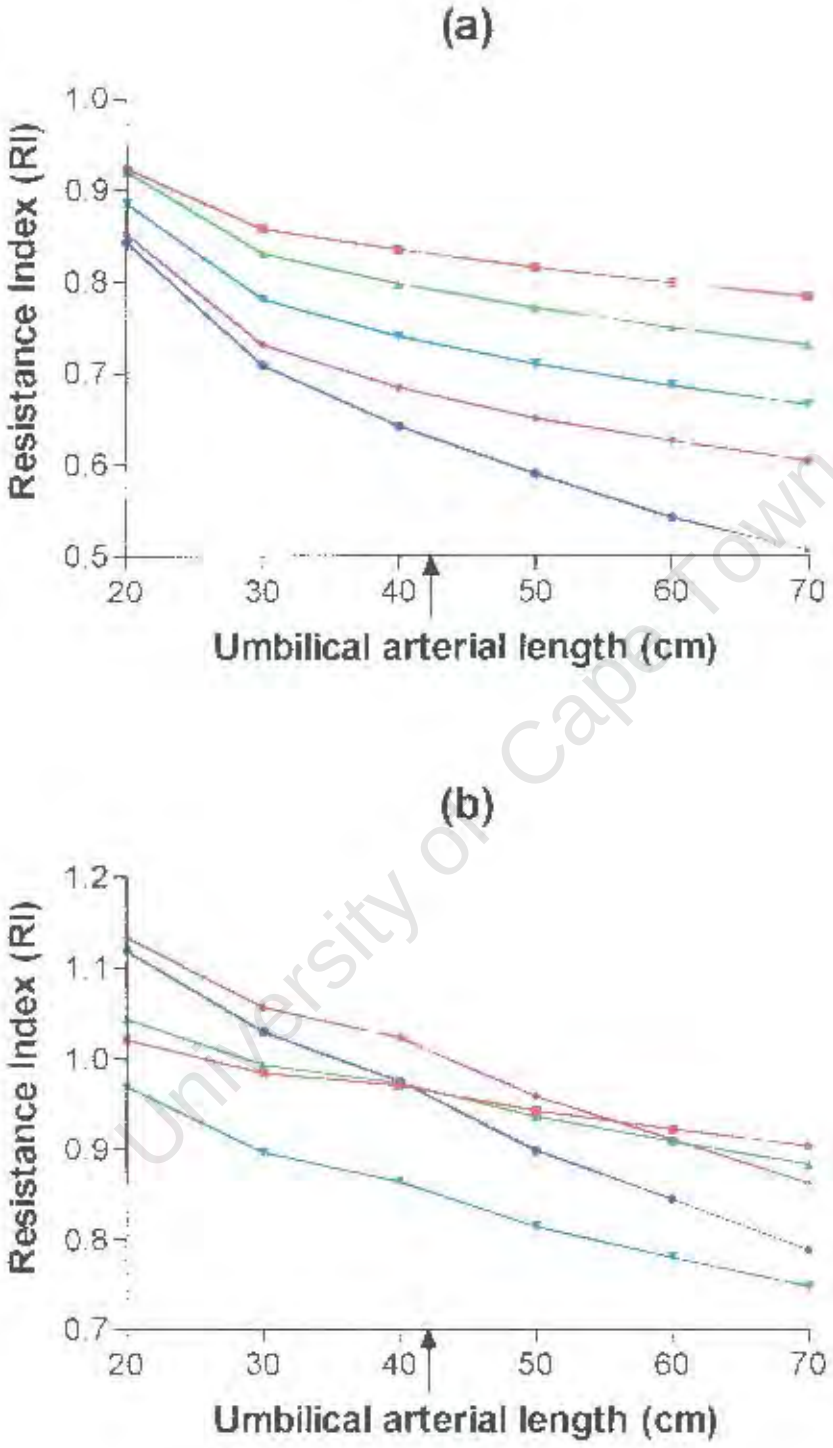

Figure 11.22: Simulated results in each artery of changes in RI versus umbilical arterial length, for (a) a healthy placenta and (b) a maldeveloped placenta. Reference values for umbilical arterial length are indicated by the arrows.

that unusually long umbilical arteries may result in a misinterpretation of the Doppler indices when placental resistance is increased.

11.13 Umbilical coiling

Simulations to assess the influence of the curvature of the umbilical arteries on the resistance or impedance to blood flow in the artery, and hence on the Doppler indices, is considered in a different manner to the simulations in the above sections. Equation (6.30) gave an expression for the ratio of flow in a curved tube to that in a straight tube assuming an identical imposed pressure gradient. This equation may be inverted to obtain the ratio of the resistance in a curved tube, relative to that in a straight tube and this is :

$$\frac{R_c}{R_s} = \left[\left(1 - \frac{0.18}{\left[1 + \left(\frac{35}{Dn} \right)^2 \right]^{1/2}} \right)^m + \left(1 + \frac{\lambda}{3} \right)^2 \frac{Dn}{88.33} \right]^{1/2} \tag{11.14}$$

In a similar manner, the ratio of the characteristic impedance in a curved tube, relative to that in a straight tube may be obtained and this is given by dividing equation (6.28) by equation (4.36) to obtain :

$$\frac{Z_{0c}}{Z_{0s}} = \pi (1 + mF_{10}) \left(1 / \left[\pi (1 + mF_{10}) + \frac{\lambda m a_0}{\alpha_0} \left[\begin{array}{c} -2a_0 \frac{J_1(\alpha_0)}{J_0(\alpha_0)} + \pi \left(\frac{1}{J_1(\alpha_0)} + \frac{a_0}{\alpha_0 J_0(\alpha_0)} \right) \times \\ (J_1(\alpha_0) \mathrm{H}_0(\alpha_0) - J_0(\alpha_0) \mathrm{H}_1(\alpha_0)) \end{array} \right] \right] \right) \tag{11.15}$$

Thus it is possible to determine the amount by which curvature alters the resistance or impedance of an artery without knowledge of the actual pressure gradients. Equation (11.14) is dependent upon λ and the Reynolds number $\mathrm{Re} = \frac{2\overline{m} a_0 \rho}{\mu}$ and equation (11.15) is dependent upon λ and α. It is therefore possible to obtain curves which demonstrate how the resistance and impedance in a curved relative to a straight artery vary with varying λ, Re and α. For the resistance to steady flow, the Reynolds number in the umbilical artery may vary up to about 300 and λ between 0.001 and 0.1. Thus it is easy to obtain a family of curves, as depicted in figure (11.23a), for the ratio of the resistance of curved to straight tubes versus the Reynolds number for coiling of $\lambda = 0.001, 0.01, 0.05$ and 0.1. In the umbilical artery α is usually around 2, although it is possible for small foetuses with abnormally low heart rates to have α values well below this. Thus it is possible to obtain a family of curves for both the magnitude and phase of the characteristic impedance in curved arteries to those in straight arteries versus α for $\lambda = 0.01, 0.05$ and 0.1 and this is depicted in figures (11.23 b and c) respectively.

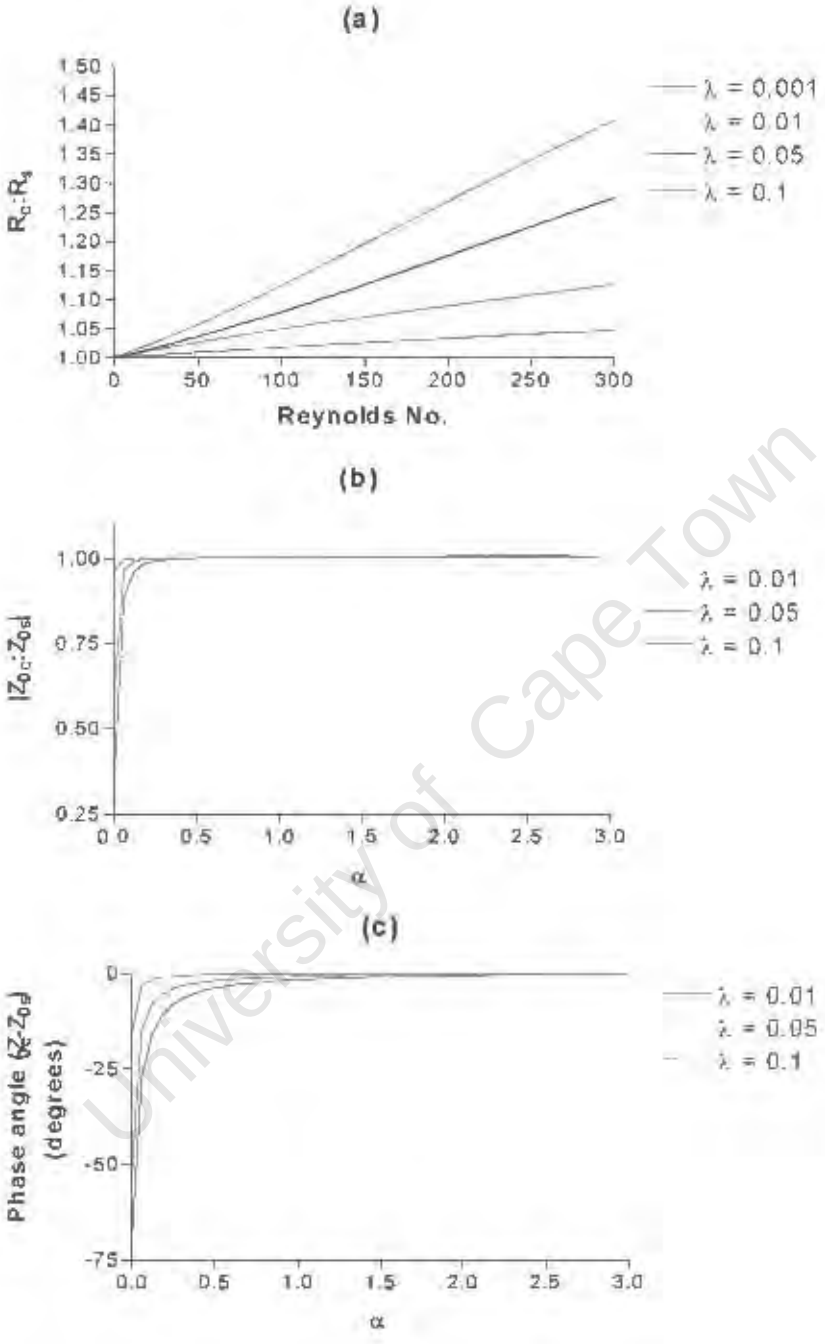

Figure 11.23: Family of curves for $\lambda = 0.001$ to 0.1 of the ratio of (a) the resistance, (b) the magnitude of the characteristic impedance and (c) the phase difference of the characteristic impedance in curved arteries to that in straight arteries. Figure (a) is plotted versus Reynolds number and figures (b) and (c) are plotted versus α.

Figure (11.23) indicates that the greatest effect of the coiling will be for values of $\lambda = 0.1$ and this value is approached in large foetuses with tightly coiled arteries. The effect of curvature on the steady resistance is most pronounced with increasing Reynolds number, which in turn will increase with increasing radius, increasing total cardiac output and decreasing viscosity. Both cardiac output and arterial radius increase with gestational age and therefore the effect of coiling is likely to become more prominent as the foetus ages. The effect of curvature on the characteristic impedance is far less significant, only becoming relevant at very low values of α, with the dominant effect being due to the change in phase angle. Low values of α are achieved for low values of heart rate, arterial radius and high values of viscosity. These values are likely to be encountered in a young foetus, with possible arterial constriction and one that is hypoxic and therefore has increased viscosity and decreased heart rate in response to the hypoxia. In both situations, increasing the coiling index increases λ. The equations governing the effect of coiling are independent of the downstream resistance and therefore no difference in results are expected for a given degree of development of the placenta.

Three scenarios were investigated. The first examines the effect of coiling on RI for a normal foetus at 28 weeks gestation, the second investigates a 40 week old foetus, where the effects of the steady resistance are expected to dominate and the third scenario examines a severely compromised 28 week old foetus, with an elevated viscosity ($\mu = 0.12$), a slightly decreased umbilical arterial radius ($a_0 = 0.1$) and a diminished heart rate (HR=100b.p.m). In this situation, the effect of the impedance at low frequencies is expected to dominate the results. Clearly this scenario is for an advanced state of distress, to illustrate the effect of coiling under these conditions. Figures (11.24 a - c) show the results of changes in resistance index in the arteries for changes in coiling index, where (a) is for scenario 1, (b) is for scenario 2 and (c) is for scenario 3.

Figures (11.24 a-c) indicate that the effect of increased coiling is to marginally increase the RI in the umbilical arteries. The greater the gestational age of the foetus, the greater the effect of coiling. This enhanced effect is primarily due to the increased mean flow component. A compromised foetus with very low values of α exhibits a very slight increase in RI due to increased coiling and this is primarily due to changes in the unsteady components. The most significant changes are to the indices measured in the umbilical arteries. A change in coiling index from 0.1 to 0.7 induces a corresponding change in the resistance index measured at the placental end of the umbilical artery of 2.26%, 8.4% and 3.7% for the respective situations of a healthy 28 week old foetus, a healthy 40 week old foetus and a compromised 28 week old foetus with a low value of α.

Degani et al. (1995) studied 45 healthy foetuses and found no correlation between the coiling index and the Doppler indices. The results of the above simulations support this finding, and

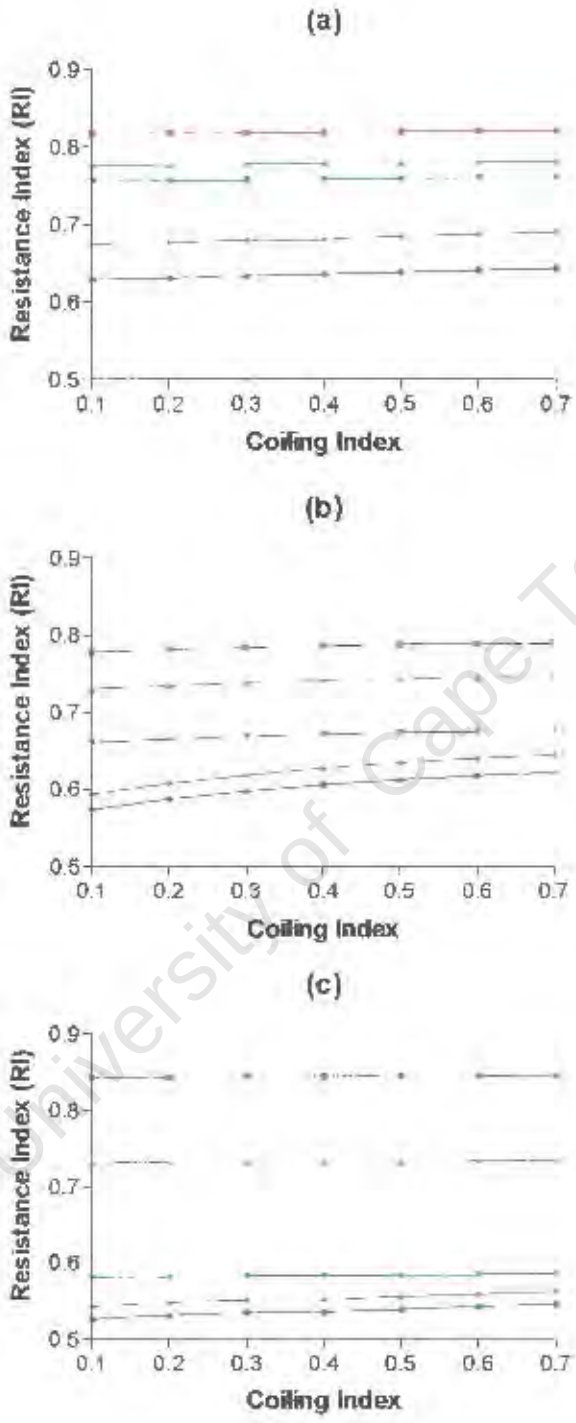

Figure 11.24: Simulated changes in resistance index for the model arteries versus changes in coiling index, where (a) is for a normal 28 week old foetus, (b) is for a normal foetus of 40 gestational weeks and (c) is for a compromised 28 week old foetus with increased viscosity, decreased heart rate and decreased umbilical arterial radius.

indicate that the increased resistance due to increased coiling only has a marginal effect on the flow waveform and hence the Doppler indices. However, Nishio et al. (1999), examined 8 growth retarded foetuses with hypercoiling and found that the RI in the umbilical artery in these cases is lower than that in normal foetuses. This finding may be interpreted by examination of the effect of coiling on venous return. Reynolds (1978) suggested that the vascular system of two coiled arteries wound around the vein possessed the basic elements of a pulsometer pumping system, whereby energy imparted by the arterial pulse augments venous return from the placenta to the foetus. Thus reduced cord coiling will result in a less efficient pumping system and therefore reduced venous return. This is most likely the mechanism that caused the observed foetal distress in the hypocoiled cords rather than the effect that coiling has on umbilical resistance. Nishio et al. (1999) found that all eight foetuses with hypercoiling had increased umbilical venous pulsation, further supporting the pulsometer theory. Upon examination of the placental vessels of the foetuses in their study, they found that the macroscopic and microscopic placental findings were normal, indicating no elevated placental resistance. They also speculated that the reduced resistance index in the umbilical artery may be attributed to an increase in the resistance of the artery. If the hypercoiling reduced the radius of the artery by constricting it in some manner, then this would support that finding.

11.14 Forward and reverse travelling waveforms

A particular advantage of a transmission line model is its ability to decompose flow waveforms into their constituent forward and retrograde components. It is possible to examine these components in each of the above simulations. However, it is more instructive to only examine the two scenarios that exert the greatest effect on the umbilical arterial Doppler indices. These are those of increased placental resistance and decreased umbilical radius. The purpose of this brief section is to illustrate the models capacity to further elucidate findings by investigating the forward and retrograde flow components, rather than performing a comprehensive study of these flow components in every possible situation. Graphs of the forward, reflected and total waveforms at either end of the umbilical artery are displayed, where the mean values of flow have been subtracted from the graphs. Figures (11.25 a and b), (11.26 a and b) and (11.27 a and b) respectively display the results of the simulations for a normal 28 week old foetus, a foetus with an acutely decreased umbilical arterial radius (from 0.15 cm to 0.1 cm, as obtained from simulating Adamson et al.'s experiment) and a foetus with a normal umbilical arterial radius but an elevated placental resistance due to a combination of increased branching angle and reduced vessel radii, such that the flow to the placenta is reduced by 60%.

The mean value of the umbilical flow waveform for a normal 28 week old foetus is 2.59cm^3/s,

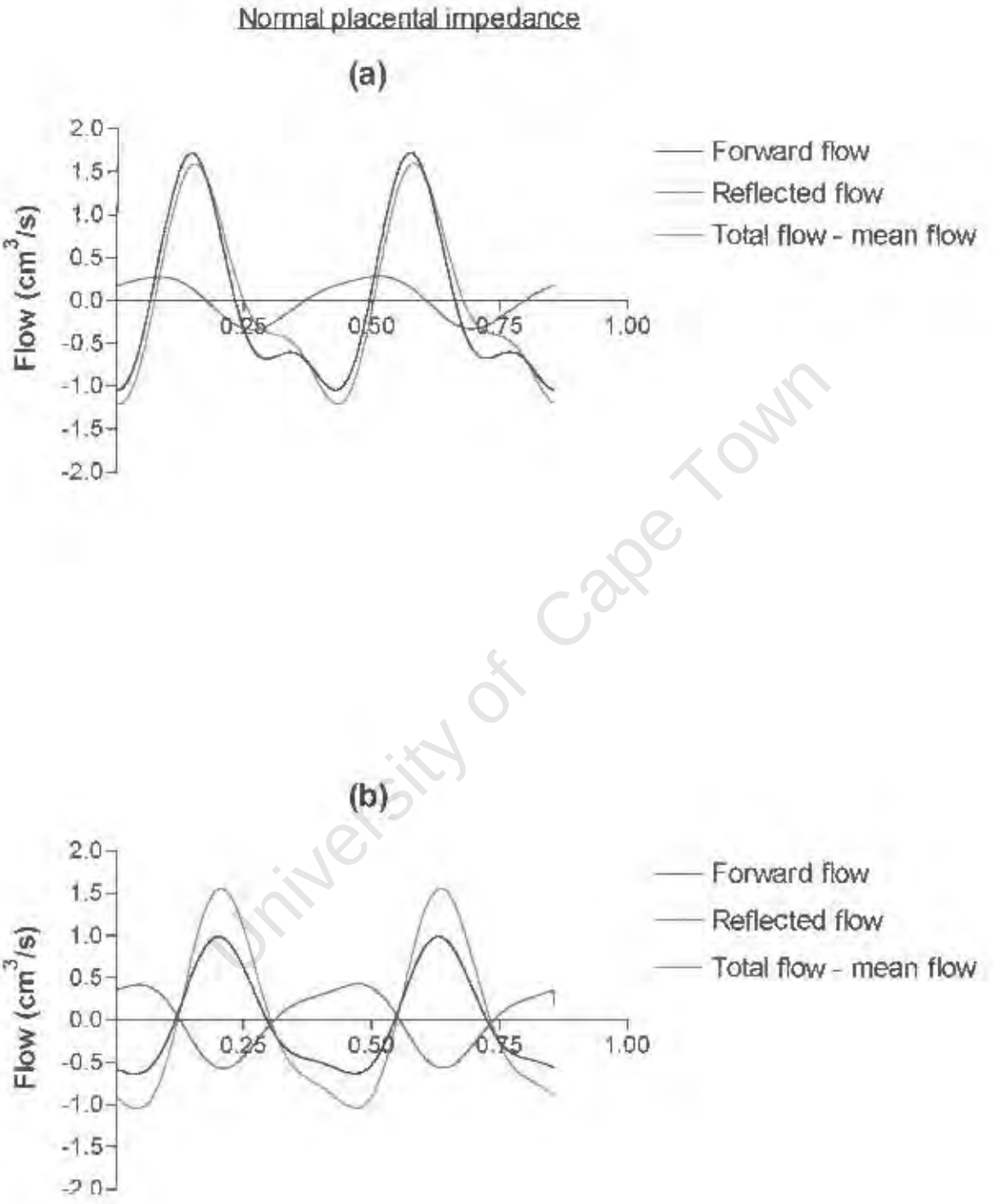

Figure 11.25: Forward, reflected and total flow velocity waveforms with the mean component subtracted for a healthy, 28 week old foetus. Waveforms are obtained at (a) the foetal end and (b) the placental end of the umbilical artery.

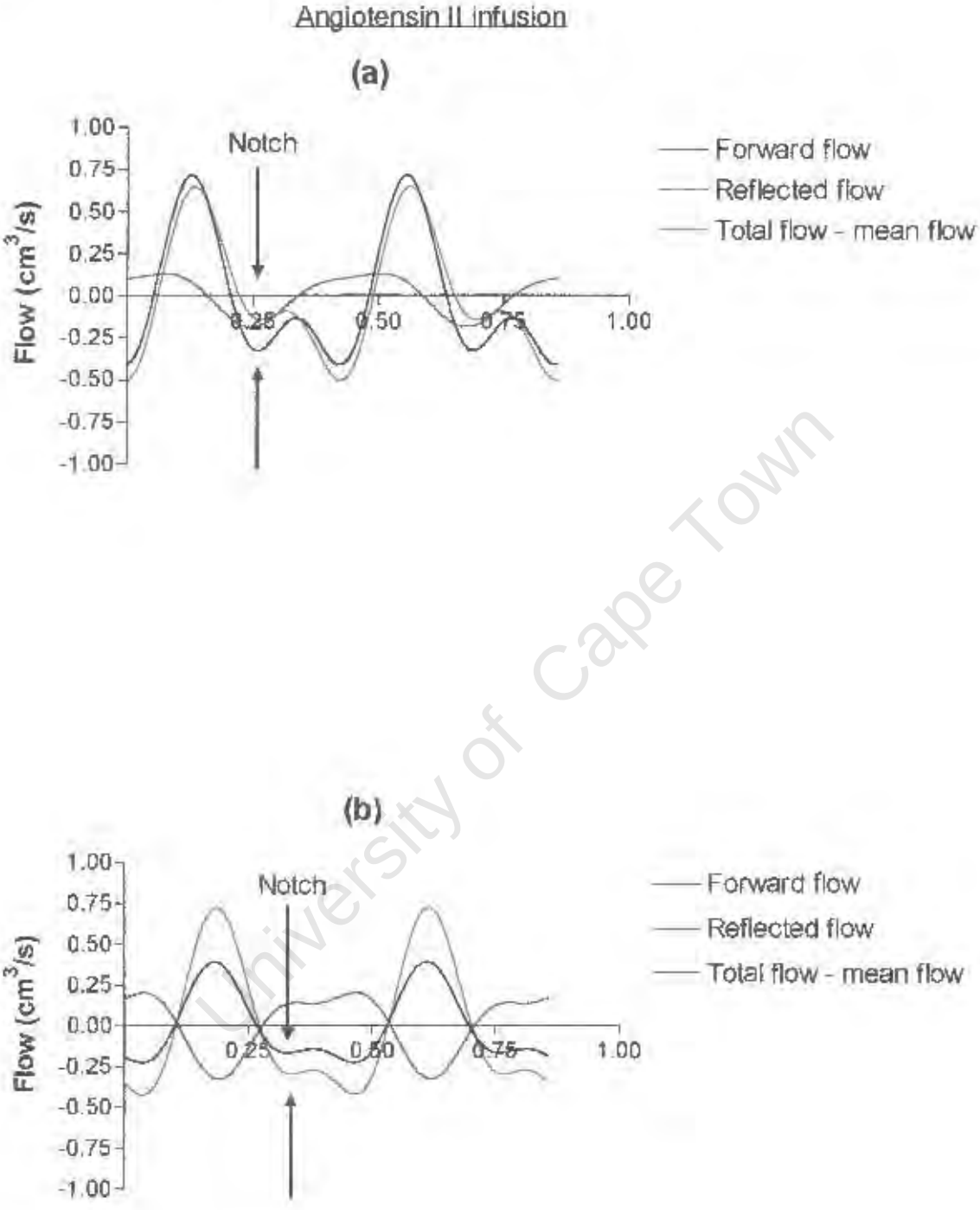

Figure 11.26: Forward, reflected and total flow velocity waveforms with the mean component subtracted for a 28 week old foetus with a reduced umbilical arterial radius due to angiotensin II infusion as per the experiments of Adamson et al. (1990). Waveforms are obtained at (a) the foetal end and (b) the placental end of the umbilical artery. The presence of a systolic notch in the total flow waveforms are indicated by the arrows.

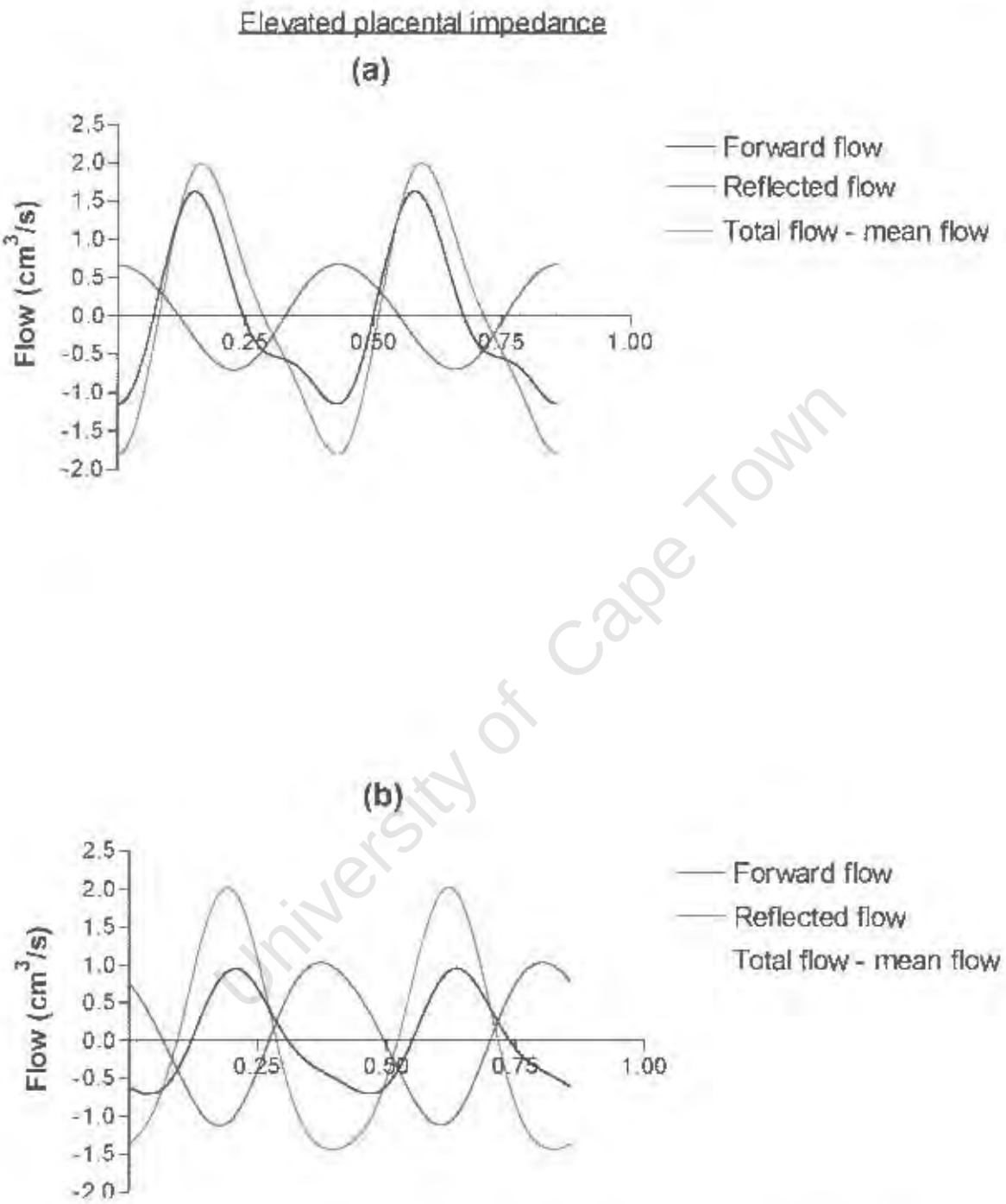

Figure 11.27: Forward, reflected and total flow velocity waveforms with the mean component subtracted for a 28 week old foetus with an elevated placental resistance due to a maldeveloped placenta. Waveforms are obtained at (a) the foetal end and (b) the placental end of the umbilical artery.

for a foetus with a restricted umbilical arterial radius it is 1.56cm^3/s and for a foetus with an elevated placental resistance it is 1.22cm^3/s. If the only change to the waveform were to its mean component, then decreasing the mean component would increase the resistance index. This may explained by considering a decrease in the mean component by a value of x. Then the RI changes from $(\max - \min)/\min$ to $(\max - x - (\min - x))/(\min - x) = (\max - \min)/(\min - x)$, which effectively reduces the denominator and thus increases the index. This partially explains the increase in index when placental resistance is elevated. However, when umbilical resistance is increased and therefore mean umbilical flow decreased, the opposite effect occurs. This may only be explained by considering the unsteady components of flow. Examination of figure (11.26 a and b) shows that the magnitudes of both forward and reflected components of flow are reduced to about 50% of their normal values and that their phases are unchanged. However, when the placental resistance is elevated, figure (11.27 a and b) demonstrates that the forward flow components remain mostly unchanged but that the reverse flow components are almost doubled in magnitude, so that at the placental end the reverse component is even slightly larger than the forward component. Their phase angles are slightly altered but not significantly so. As the forward and reverse flow components are almost 180° out of phase, subtracting the reflected waveform from the forward going waveform creates an additive effect, thereby further increasing the measured resistance index. The reflected component is created by the impedance mismatch between the umbilical artery and the placenta. The reflection coefficient is given by $\Gamma_t = (Z_{plac} - Z_{0umb})/(Z_{plac} + Z_{0umb})$. In the case of a decreased umbilical arterial radius, with a normal placenta, Z_{0umb} increases, which effectively decreases Γ_t. In the case of a maldeveloped placenta, Z_{0plac} increases whilst the umbilical artery remains unchanged. Thus Γ_t is increased, which increases the magnitude of the reflected waveform.

An interesting point to note is the appearance of the notch in the total flow waveform in figure (11.26 a and b) as marked by the arrows. This notch has been reported in clinical measurements of foetuses with umbilical cord abnormalities that resulted in reduced umbilical flow (Robinson et al. 1997; Jakobi et al. 1994) and may therefore be an indication of reduced umbilical arterial radius. This characteristic which has been verified using the model, may form the basis of clinical tests which can distinguish between the effects of placental insufficiency and umbilical radius reduction.

11.15 Discussion

This chapter sought to discover the primary determinants responsible for changes in Doppler indices in the foetal arteries through a number of carefully selected simulations. The purpose of this chapter was not to perform a comprehensive study of every possible variation that is known to occur in the foetal circulatory system or to reproduce the many animal experiments that have been conducted. Instead the intention was to focus on a number of simplified experiments that highlight important foetal states or changes so that the strengths of the foetal model may be efficiently demonstrated. These strengths lie in the ability of the foetal model to isolate the effects of individual parameters on the Doppler waveforms, whilst controlling the remaining parameters. A disadvantage with animal experimentation is that several modifications occur in response to a single interventional change and thus it may not always be possible to quantify the cumulative effects of these responses. A further advantage of the foetal model lies in the capacity to decompose the flow velocity waveforms into their constituent components.

The simulations conducted in this chapter may be summarised by separating the results into different categories based on observed effects to the Doppler indices measured in the umbilical arteries. If a 50% change in a particular parameter results in a change in index that is less than 10%, the index may be assumed to be stable for variations of that particular parameter. If the variations lie between 10% and 30%, the index may be classified as marginally sensitive to changes in those parameters and anything resulting in greater than a 30% variation is considered to be highly sensitive to those changes. Furthermore, a decrease in the parameter of interest can either increase or decrease the index in response. The last category of change is whether the difference between the Doppler indices measured at either end of the umbilical arteries increases or decreases when the parameter decreases and whether it becomes a negative value which implies that the placental end has a higher value than the foetal end. These results are reported for all the simulations and are generally divided into acute and chronic categories. As discussed earlier, acute changes are most commonly associated with interventional changes and chronic effects may be attributed to statistical variance or to chronic pathology. These results are summarised in table (11.2), where the symbols, L, M and H are used to denote the three categories of low change, medium change or high change. Each result is reported for a normal placenta and for a situation with chronic placental insufficiency (CPI). The symbol, $\uparrow$, is used to indicate an increase in RI for a decreasing parameter and $\downarrow$ is used to denote a decrease in RI for a decreasing parameter. Similar conventions are adopted to describe the effects on the differences to the indices measured at opposite ends of the umbilical arteries, where a $\longleftrightarrow$ denotes no effect on the differences. In this case a medium change is considered to be anything less than a 100% difference (for a 50% change in parameter) and a high change to be anything greater than a 100% difference. In some situations the differences may fluctuate slightly, however

if the overall variation is inconsistent and small this is regarded as no significant change at all.

The summary table indicates that the Doppler indices are most sensitive to changes to the heart rate, umbilical radius, umbilical length and to the placental resistance. Heart rate, umbilical arterial radius and length may vary within statistical limits for a given population group and thus it is important to consider a standardising correction to account for these differences. Although it has been well established that Doppler indices do vary with heart rate, many studies report that the change in index over the normal range (120-160 b.p.m) is low enough not to recommend corrections unless in the presence of foetal tachycardia (>160 b.p.m) or foetal bradycardia (<120 b.p.m) (Thompson et al. 1986, 1988; Gagnon et al. 1988; Kofinas et al. 1989). Over this range, the model shows a $\pm 10\%$ increase or decrease in the Doppler indices, regardless of placental impedance, and would thus agree with these findings. Furthermore, it is possible to obtain a measurement of the umbilical arterial radius with modern sonographic equipment and thus it is suggested that a study be conducted on normals to obtain regression curves so that future measurements may be standardised for variance in umbilical radius. For a 28 week old foetus, the umbilical arterial radius may statistically vary by ± 0.25mm from an average value of 1.5mm (Sherer and Anyaegbunam, 1997). Over this range, the model indicates that the Doppler indices may vary by approximately $\pm 20 - 25\%$. The recommendation is thus that Doppler indices should be standardised for umbilical arterial radius. Collins (1991) reports that it is possible to sonographically trace the umbilical cord length and therefore it is also possible to normalise measurements for this variable. Umbilical arterial length may statistically vary by ± 10cm for a 28 week old foetus (Naeye, 1985). The model shows that over this range of variation, the Doppler indices may vary by $\pm 8 - 10\%$ and thus it is probably not necessary to standardise for umbilical arterial length. However, it is possible that a particular foetus has an unusually long or short umbilical cord, or an unusually large or small umbilical artery or an unusually low or high heart rate and in these circumstances, standardisation for these variables would be important. Standardisation is commonly performed by conducting large clinical trials to obtain reference values and regression curves for the parameters that require standardisation. However, it is possible that the model may be utilised to provide multiple regression equations instead of conducting these trials. Of course, these results would have to be confirmed by clinical studies of foetal outcome before and after standardisation using the model regression values.

Previous works reported that the site of elevation of umbilical and placental resistance was consequential to a meaningful interpretation of measured Doppler indices (Adamson et al. 1990; Adamson, 1999). They reported that the Doppler indices were only sensitive to changes in placental resistance and not to umbilical resistance. However, these results were obtained experimentally by infusion of angiotensin II which has an effect on blood pressure, cardiac output and heart rate as well. Simulations with this model demonstrate that when these

parameters came into play in addition to a decreased umbilical arterial radius, the indices remained relatively stable for changes in umbilical radius. However, when these parameters were fixed and not allowed to vary, decreasing the umbilical radius produced a decrease in measured Doppler indices in the umbilical artery. In a clinical scenario, the umbilical radius may be constricted in a variety of ways (Benirschke, 1994). It is unclear whether these narrowings are due to primary anatomic abnormalities or are secondary to excessive movement by the foetus (Robinson et al. 1997). Clinical intervention may produce further arterial constrictions. Many of the narrowings encountered may not be associated with pressure and cardiac output increases or heart rate decreases and may therefore cause the Doppler indices to decrease. Should this take place in light of an elevated placental resistance, a severely compromised foetus may easily be mistaken for a normal foetus. It is possible that the presence of a systolic notch as indicated in figure (11.26) may be indicative of some problem with the umbilical artery and thus cautious interpretations are recommended when this is encountered.

Measurements of Doppler indices obtained from either end of the umbilical arteries may also help in the interpretation of the indices. In general, any change that results in a change in the wavespeed in the umbilical artery, will produce a change in the difference between the ends of the cord. Increasing the wave velocity will decreases the difference between the ends of the arteries and decreasing the wave velocity will increase these differences. As changes to the umbilical arterial wall structure often accompany cases of IUGR, it is likely that changes to the difference in indices measured at opposing ends of the arteries are indicative of foetal compromise. These differences should first be standardised for umbilical radius before further interpretations are made.

Examination of the reflection coefficient between the placental vascular bed and the umbilical artery proved useful to elucidate some of the simulated findings. Section (11.9) discussed how increasing the umbilical arterial resistance decreased the reflection coefficient and how increasing the placental resistance increased the coefficient. This explained how, given a decreased mean umbilical arterial flow, the Doppler indices either decreased or increased above the expected value due to the change in mean flow.

Simulation parameter (for a 50% decrease)	Sensitivity of index		Difference between ends	
	Normal placenta	CPI	Normal placenta	CPI
Acute placental insufficiency (API)	H↑	N/A	H↑	N/A
Chronic placental insufficiency (CPI)	H↑	N/A	M↑	N/A
Heart rate	H↑	H↑	⟷	⟷
Cardiac output (acute)	L↑	M↑	⟷	H↓
Cardiac output (chronic)	L↑	L↑	⟷	⟷
Blood pressure (acute)	L↓	L↓	⟷	⟷
Blood pressure (chronic)	L↓	L↓	⟷	⟷
Umbilical arterial elasticity	L↑	L↑	M↑	M↑
Umbilical arterial wall thickness	L↓	L↓	M↑	M↑
Whartons jelly	L↓	L↓	H↓	H↓
Umbilical arterial wall viscoelasticity	L↓	L↓	H↓	H↓
Placental vessel elasticity	L↑	L↑	⟷	H↑
Placental vessel wall thickness	L↓	L↓	⟷	⟷
Placental vessel wall viscoelasticity	L↑	L↑	⟷	⟷
Total foetal blood viscosity (acute)	M↑	M↑	⟷	⟷
Total foetal blood viscosity (chronic)	M↑	M↑	⟷	⟷
Acute redistribution	L↑	L↑	⟷	⟷
Umbilical radius (acute)	H↓	H↓	H↓	H↓
Umbilical radius (chronic)	H↓	H↓	H↓	H↓
Umbilical radius (sheep experiment)	M↓	N/A	H↓	N/A
Umbilical length	H↑	H↑	H↓	H↓
Coiling 28 weeks	L↓	N/A	⟷	N/A
Coiling 40 weeks	L↓	N/A	⟷	N/A
Coiling low alpha	L↓	N/A	⟷	N/A

Table 11.2: Summary of simulated changes in each variable listed under simulations. Changes are for the convention of decreasing values of the variable although in many cases the physiological response is to increase the parameter from its reference values. For index sensitivity, L denotes a low change (<10%), M a medium change (>10%, <30%) and H a high change (>30%). For the differences between the ends of the cord, a different scale is used and here M denotes a medium change (>10%, <100%) and H a high change (>100%). Anything less than 10% is insignificant and assumed to be equal. A ↓ symolises a decrease in index or difference in indices at either end of the cord, a ↑, an increase and ⟷ no change in differences. Simulations are for a normal placenta and for a situation of chronic placental insufficiency (CPI). Placental changes are for decreased flow to the placenta.

Chapter 12

Conclusions

12.1 Modelling methods

The theoretical foundation of the model is the equations which govern the relationship between the applied pressure and the resultant flow in an arterial segment. These equations describe the behaviour of the fundamental segments which are cascaded together using electrical transmission line analogies to form the complete foetal model. A review of the available models suggested that the two-dimensional, linear model's developed by Womersley, Dinnar and Atabek are the most appropriate for investigating the foetal circulatory system. These models were utilised to assess whether anisotropy, or different tethering models to account for the surrounding tissue, had any significant impact on Doppler indices. The necessity of such an investigation lies in the lack of quantitative data pertaining to these particular variables. If the model were to show that they have a pronounced effect, then further measurements to ascertain precise values of parameters governing these variables would be necessary. The results of the model indicate that neither anisotropy nor the specific choice of tethering model have any significant effect on the Doppler indices. Therefore, of the three basic models proposed, particular selection for use as a basic building block is essentially arbitary. For this model, the theory developed by Dinnar was selected as it best incorporates the effect of the surrounding tissue in an accurate but simple and quantitative manner. In addition, Dinnar's model agreed with clinical findings slightly better than the other models.

Exact solutions that account for the effect of both geometric and elastic tapering on arterial impedance and flow velocities were developed. It was demonstrated that arterial tapering in the foetal aorta does indeed influence the Doppler indices and therefore an accurate model should not neglect this tapering. An alternative procedure to include the influence of arterial tapering is to divide each tapered artery into a large number of smaller uniform segments and then to

cascade these segments together using transmission line equations. It was illustrated that as the number of segments (per arterial segment) approached 10-15, the exact and cascaded solutions converged to the same values and therefore either method of solution is acceptable. However, the segmented approach severely increases the overall simulation run time and is therefore less desirable. On this basis, the exact solution for tapering was used for all subsequent simulations and assessments. Radial taper has also been demonstrated to occur in the peripheral vascular networks and it is possible that elastic taper may also be present. The exact solution for the input impedance of a tapered arterial segment allows this effect to be incorporated into fractal models of these vascular beds. It was demonstrated that a network of tapered vessels produces results of greater accuracy compared with one where tapering is neglected. This accuracy is quantified by comparing simulated Doppler indices with measured ones for tapered and non-tapered models. In addition, the calculated terminal radii were determined for each model, for a given set of network parameters, and the tapered model exhibited more realistic values. The exact solutions for arterial tapering may be employed in any transmission line based, cardiovascular model and offers potential benefit beyond foetal investigations.

The umbilical arteries are coiled around the umbilical vein and thus it was necessary to develop a solution for the axial flow in curved arteries. Application of this solution is limited to situations of small values of the ratio of the radius to radius of curvature. This requirement is met in the specific case of the umbilical arteries and the development of these equations are a necessary requirement to investigate the effects on the Doppler indices of hyper or hypo-coiling of the umbilical arteries. These equations may also be utilised in other transmission line based cardiovascular models.

The peripheral vascular beds were all modelled as fractal networks of dichotomously branching vessels, where a reduced number of fractal parameters were used to specify the network structure. Previous foetal models often represented the peripheral vasculature with single lumped resistances. This approach is limited in the accuracy with which these beds could be represented. In addition, it would not give any insight into the interdependence of network morphology, input resistance and impedance. The peripheral network model developed in this thesis allows creates a link between the resistance and impedance, where a change in resistance due to a change in the morphology of the vascular network results in a corresponding change in impedance. This is significant for subsequent modelling scenarios, where specification of fractal parameters and input resistances determine both resultant network ultrastructure and input impedances. Acute changes may be modelled by maintaining the existing structure of the beds and constricting or dilating their individual radii. Chronic or long term changes may be modelled by specifying different morphological parameters.

The various building blocks of straight arterial segments, tapered segments, curved segments

and peripheral segments are all conveniently coded into easy to implement subroutines using Matlab™ with the Simulink™ interface. These building blocks are connected together using transmission line procedures. This results in a useful package of tools that form the theoretical foundation of foetal haemodynamic modelling.

Foetal growth results in decreasing peripheral resistance, increasing vessel dimensions and increasing number of vessels comprising the peripheral vascular networks. The rate of growth of each of the vascular compartments are different from one another and from the overall foetal growth rate. An accurate model of foetal growth that combines these factors was developed. The advantage of a valid model for all gestational ages is that assessment is possible at any age and that growth retardation may be simulated. The model was designed to be valid for a foetus between 28 weeks and term.

12.2 Simulations

Carefully selected simulations were conducted to assess the sensitivities of Doppler indices to relevant cardiovascular parameters. Where possible, all variables were held constant with the exception of the parameter being studied, which was varied over a physiologically relevant range. Simulations were conducted to assess the effects of statistical variance, acute and long term changes to individual parameters. These simulations demonstrated that the pulsatility and resistance indices are highly correlated and with the exception of heart rate, they both exhibit identical trends to variations in model parameters. The Doppler indices recorded in the umbilical arteries are the most sensitive to changing variables and therefore these arteries are the most frequent site of diagnostic measurements.

The simulations indicated that the most important determinants of variance in the Doppler indices are gross placental morphology, the umbilical arterial radius and length and heart rate. The indices were shown to be relatively insensitive to alterations in pressure, cardiac output, blood viscosity, acute blood flow redistribution, umbilical coiling and umbilical and placental arterial wall properties.

Changes to the gross placental morphology may arise in consequence of decreased or impaired placental growth or due to vasoconstriction or selective obliteration of placental arteries. Morphological changes to the placenta result in significantly elevated Doppler indices and the model indicates that the manner in which these changes are mediated does not significantly influence the results. Decreased growth is associated with an increased placental resistance. Hormonal vasoconstriction of the placental radii decreases the overall radii of the placental vessels. Increasing the branching angle, increases the degree of taper in the individual placental

vessels, effectively reducing the overall radii and decreasing the branching ratio, progressively reduces the overall radii. Thus any morphological change that results in an elevated placental resistance, is effectively brought about by a reduction in the overall radii of the placental vessels and therefore it may be concluded that so long as a reduction in the overall radii is present, the level at which this occurs is unimportant and the net effect is an increase in the Doppler indices.

The effects of changes to umbilical arterial radius are influenced by possible associated changes to mean arterial pressure, cardiac output, heart rate and blood flow redistribution. The degree of change to these parameters influences the degree with which the peripheral vasculature changes and therefore the Doppler indices. However, provided other cardiovascular parameters do not significantly vary from nominal values, the net effect of a decreasing umbilical radius is to decrease the Doppler indices.

Increasing the length of the umbilical artery and increasing the heart rate, both caused the Doppler indices to significantly decrease. The consequence of this is that it is possible for a foetus with a high placental impedance (which would normally be associated with high Doppler indices) to exhibit normal indices if that foetus were to have a high heart rate or a long or narrow umbilical artery or some combination of these factors. Therefore, it is necessary to account for these variables in order to obtain an accurate indication of placental compromise. Each of these variables has a normal range of variance, and the model showed that over this range, the foetal heart rate and the umbilical cord length would only change the indices by $\pm 10\%$ and thus standardisation for these variables may not be necessary. Over the normal range of variation for umbilical arterial radius, the Doppler indices may vary by as much as $\pm 25\%$ and thus it is essential to account for this radius prior to further interpretation of Doppler measurements. As it is possible for a normal foetus to have any of these variables exceeding the normal range, it would be of increased benefit to account for them.

The model therefore provides theoretical evidence that Doppler indices are not always reliable in the detection of foetal distress or growth restriction. It suggests that the primary utility of Doppler indices should be to reflect increases in placental resistance or impedance that may result from changes in gross placental morphology. However, caution is recommended when interpreting Doppler recordings, as the model shows that the presence of additional factors may mask placental compromise and could be responsible for reported normal Doppler findings in the case of severe growth retardation.

Pulsatility and resistance indices were demonstrated to decrease with advancing gestation. The model shows that this decrease may be attributed to decreasing peripheral resistances, increasing heart rate and increasing arterial dimensions. The increasing umbilical radius would tend to increase the indices, however it appears that this increase is less than the overall decrease

induced by the other factors. Simulations conducted at different gestational ages, between 28 weeks and term, indicated that, with the exception of umbilical coiling simulations, gestational age has little effect on overall trends of Doppler indices.

The model also shows how the measurement site along the cord affects the Doppler indices. In order to interpret the indices, the measurement site should be specified. In addition, the differences in index values from the ends of the cord may provide further information regarding foetal haemodynamics. The model showed that the difference in indices between opposite ends of the umbilical arteries were sensitive to changes in placental impedance, umbilical radius, umbilical length and umbilical wall properties. Thus any changes that alter the wavespeed along the umbilical arteries, the downstream reflection properties or the length a flow pulse travels along the arteries will influence the differences between waveforms obtained at opposite ends of the artery. Changes to the wavespeed usually arise as a result of structural changes to the arterial wall, which are frequently associated with adverse foetal conditions. Once the indices have been normalised (standardised) for foetal growth, umbilical arterial radius and length, the different locations along the cord may prove to be a reliable indicator of foetal risk, especially when used in conjunction with ordinary Doppler measurements. The model confirms the clinical finding that standardisation of measurement location is necessary when interpreting single measurements.

The model simulations had a systolic notch when the umbilical radius was significantly decreased and this has also been reported in isolated clinical situations. Therefore, it may be concluded that occurrences of a systolic notch in the umbilical arterial flow velocity waveforms, may be used to alert clinicians to potential changes in umbilical radii and thus reduce the possibility of incorrect interpretation of Doppler indices.

12.3 Recommendations for further research

12.3.1 Model

Examination of the forward and retrograde components of the flow waveforms indicated the shape of the reflected flow waveform in the umbilical artery is significantly influenced by the combination of downstream impedance and characteristic impedance within the umbilical artery itself. The ability to decompose actual clinically measured waveforms is currently limited as many of the documented techniques require both pressure and flow measurements (Pythoud et al. 1996; Li, 1986; Parker and Jones, 1990; Stergiopulos et al. 1993) . However, an interesting study conducted by Roffeh et al. (1996) applied cepstrum signal processing techniques designed to detect echoes in radar waveforms to decompose arterial pressure waveforms into

separate components. It may be possible to extend this technique for use with flow waveforms and therefore the model may be used to validate and test this technique and to determine the correlations of forward and reverse waveforms with cardiovascular parameters, thereby developing new diagnostic procedures. It is suggested that further research be conducted along these avenues.

It may be possible to configure the model to operate as an inverse model. Here, a select number of measurements may be acquired to ascertain the values of variables inaccessible to non-invasive measurements and future research should investigate this possibility. It may be possible to utilise the model as a clinical aid to account for variations in heart rate and umbilical arterial radius and length. In this case, the model would be configured using standard parameters at a known gestational age and then these three parameters would be clinically measured and entered into the model. The model would then output 'normal' ranges of indices for the given three parameters, with which the patient's results could be compared.

12.3.2 Clinical

The model suggested that it is necessary to standardise Doppler measurements for heart rate, umbilical arterial radius and length. Currently no large clinical trials have been conducted to correlate sonographical measurements of umbilical arterial radius and length with Doppler indices. It is submitted that, based on the findings of the model, this would be necessary in order to assess their clinical significance and to obtain regression curves so that subsequent measurements may be normalised.

As changes to umbilical radii may arise from a variety of causes, further investigation of the complete cardiovascular response to each of these causes is necessary in order to fully assess their effect on the Doppler indices. In addition, the incidence of a systolic notch as a consequence of reduced umbilical arterial radius requires further clinical investigation.

A comprehensive survey of the sensitivities of every Doppler index described in the literature to changing foetal parameters may be conducted and the model ought to be useful to test and derive variable specific indices that are highly sensitive to changes in one parameter but not to another. The model may be of further use to investigate the utility of multivariate diagnostics or to optimise a feature discovery process for subsequent neural network or pattern matching classifications.

Many further simulations are possible with the foetal model and these may be of increased benefit when utilised in conjunction with clinical trials or studies on animal models. It may also be possible to configure the model for further use as a teaching aid. It is hoped that this model will be the foundation for many new and exciting discoveries pertaining to the foetal

circulatory system and Doppler measurements thereof, eventually leading to improvement in clinical management of pregnancies.

References

[Abramowicz *et al.*(1989)] Abramowicz, J. S., Warsof, S. L., Arrington, J., and Levy, D. L. (1989). Doppler analysis of the umbilical artery. the importance of choosing the placental end of the cord. *J Ultrasound Med*, **8**, 219–221.

[Adamson(1999)] Adamson, S. (1999). Arterial pressure, vascular input impedance, and resistance as determinants of pulsatile blood flow in the umbilical artery. *Eur. J. Obstet. Gynecol.*, **84**, 119–125.

[Adamson and Langille(1992)] Adamson, S. and Langille, B. (1992). Factors determining aortic and umbilical blood flow pulsatility in fetal sheep. *Ultrasound in Med. & Biol.*, **18**, 255–266.

[Adamson *et al.*(1989)] Adamson, S., Morrow, R., Bull, S., and Langille, B. (1989). Vasomotor responses of the umbilical circulation in fetal sheep. *Am. J. Physiol. (Regulatory Integrative Comp. Physiol.)*, **256**, R1056–R1062.

[Adamson *et al.*(1990)] Adamson, S., Morrow, R., Langille, B., Bull, S., and Ritchie, J. (1990). Site-dependent effects of increases in placental vascular resistance on the umbilical arterial velocity waveform in fetal sheep. *Ultrasound in Med. & Biol.*, **16**, 19–27.

[Adamson *et al.*(1992)] Adamson, S., Whiteley, K., and Langille, B. (1992). Pulsatile pressure-flow relations and pulse-wave propagation in the umbilical circulation of fetal sheep. *Circ. Res.*, **70**, 761–772.

[Alfirevic and Neilson(1995)] Alfirevic, Z. and Neilson, J. P. (1995). Doppler ultrasonography in high-risk pregnancies: systematic review with meta-analysis. *Am J Obstet Gynecol*, **172**, 1379–1387.

[Alonso *et al.*(1989)] Alonso, J., Okai, T., Longo, L., and Gilbert, R. (1989). Cardiac function during long-term hypoxemia in fetal sheep. *Am. J. Physiol. (Heart Circ. Physiol.)*, **257**, H581–H589.

[Anderson(1992)] Anderson, D. (1992). Regulation of umbilical blood flow. chapter 68, pages 694–701. WB Saunders company,, Philadelphia, London, Tornonto, Montreal, Sydney, Tokyo.

[Anderson *et al.*(1986)] Anderson, P. A., Glick, K. L., Killam, A. P., and Mainwaring, R. D. (1986). The effect of heart rate on in utero left ventricular output in the fetal sheep. *J Physiol*, **372**, 557–573.

[A.P.(1980)] A.P., A. (1980). Multi-branched model of the human arterial system. *Med. Biol. Eng. Comput.*, **18**, 709–718.

[Atabek(1968)] Atabek, H. B. (1968). Wave propagation through a viscous fluid contained in a tethered initially stressed, orthotropic elastic fluid. *Biophys. J.*, **8**, 626–649.

[Atabek and Lew(1966)] Atabek, H. B. and Lew, H. S. (1966). Wave propagation through a viscous incompressible fluid contained in an initially stressed elastic tube. *Biophys. J.*, **6**, 481 – 503.

[Atalla *et al.*(1998)] Atalla, R. K., Abrams, K., Bell, S. C., and Taylor, D. J. (1998). Newborn acid-base status and umbilical cord morphology. *Obstet Gynecol*, **92**, 865–868.

[Austin and Seader(1973)] Austin, L. R. and Seader, J. D. (1973). Fully developed viscous flow in coiled circular pipes. *AIChE J.*, **19**, 85–94.

[Ball *et al.*(1994)] Ball, R., Parer, J., Caldwell, L., and Johnson, J. (1994). Regional blood flow and metabolism in ovine fetuses during severe cord occlusion. *Am. J. Obstet. Gynecol.*, **171**, 1549–1555.

[Barua(1963)] Barua, S. M. (1963). On secondary flow in stationary curved pipes. *J. Mech. Appl. Maths.*, **15**, 61–77.

[Beksac *et al.*(1996)] Beksac, M. S., Basaran, F., Eskiizmirliler, S., Erkmen, A. M., and Yorukan, S. (1996). A computerized diagnostic system for the interpretation of umbilical artery blood flow velocity waveforms. *Eur J Obstet Gynecol Reprod Biol*, **64**, 37–42.

[Belardinelli and Cavalcanti(1992)] Belardinelli, E. and Cavalcanti, S. (1992). Theoretical analysis of pressure pulse propagation in arterial vessels. *J Biomech*, **25**, 1337–1349.

[Benirschke(1994)] Benirschke, K. (1994). Obstetrically important lesions of the umbilical cord. *J Reprod Med.*, **39**(4), 262–272.

[Benirschke and Kaufmann(1990)] Benirschke, K. and Kaufmann, P. (1990). *Pathology of the Human Placenta*. Springer-Verlag, New York.

[Bennett(1994)] Bennett, S. (1994). Modeling methodology for vascular input impedance determination and interpretation. *J. Appl. Physiol.*, **76**, 455–484.

[Bennett *et al.*(1996)] Bennett, S. H., Goetzman, B. W., Milstein, J. M., and Pannu, J. S. (1996). Role of arterial design on pulse wave reflection in a fractal pulmonary network. *J Appl Physiol*, **80**, 1033–1056.

[Bergel(1961)] Bergel, D. (1961). The static elastic properties of the arterial wall. *J. Physiol.*, **156**, 445–457.

[Bergman and Ullberg(1998)] Bergman, D. and Ullberg, U. (1998). Scaling properties of the placenta's arterial tree. *J. Theor. Biol.*, **193**, 731–738.

[Bergqvist and Zetterstrom(1974)] Bergqvist, G. and Zetterstrom, R. (1974). Blood viscosity and peripheral circulation in newborn infants. a study on resting flow. *Acta Paediatr Scand*, **63**, 865–868.

[Bertelsen and Thorsen(1982)] Bertelsen, A. F. and Thorsen, L. K. (1982). An experimental investigation of oscillatory flow in pipe bends. *J. Fluid. Mech.*, **118**, 269–284.

[Block *et al.*(1984)] Block, B., Llanos, A., and Creasy, R. (1984). Responses of the growth-retarded fetus to acute hypoxemia. *Am. J. Obstet. Gynecol.*, **148**, 878–885.

[Block *et al.*(1989)] Block, B., Schlafer, D., Wentworth, R., Kreitzer, L., and Nathanielsz, P. (1989). Intrauterine growth retardation and the circulatory responses to acute hypoxemia in fetal sheep. *Am. J. Obstet. Gynecol.*, **161**, 1576–1579.

[Block *et al.*(1990a)] Block, B., Schlafer, D., Wentworth, R., Kreitzer, L., and Nathanielsz, P. (1990a). Intrauterine asphyxia and the breakdown of physiologic circulatory compensation in fetal sheep. *Am. J. Obstet. Gynecol.*, **162**, 1325–1331.

[Block *et al.*(1990b)] Block, B., Schlafer, D., Wentworth, R., Kreitzer, L., and Nathanielsz, P. (1990b). Regional blood flow distribution in fetal sheep with intrauterine growth retardation produced by decreased umbilical placental perfusion. *J. Dev. Physiol.*, **13**, 81–85.

[Bocking *et al.*(1988)] Bocking, A., Gagnon, R., White, S., Homan, J., Milne, K., and Richardson, B. (1988). Circulatory responses to prolonged hypoxemia in fetal sheep. *Am. J. Obstet. Gynecol.*, **159**, 1418–1424.

[Bracero *et al.*(1989)] Bracero, L. A., Beneck, D., Kirshenbaum, N., Peiffer, M., Stalter, P., and Schulman, H. (1989). Doppler velocimetry and placental disease. *Am J Obstet Gynecol*, **161**, 388–393.

[Brar *et al.*(1989)] Brar, H. S., Medearis, A. L., and Platt, L. D. (1989). Relationship of systolic/diastolic ratios from umbilical velocimetry to fetal heart rate. *Am J Obstet Gynecol*, **160**, 188–191.

[Brown(1996)] Brown, D. (1996). Input impedance and reflection coefficient in fractal-like models of asymmetrically branching complian tubes. *IEEE Trans. Biomed. Eng.*, **43**, 715–722.

[Bruch *et al.*(1997)] Bruch, J. F., Sibony, O., Benali, K., Challier, J. C., Blot, P., and Nessmann, C. (1997). Computerized microscope morphometry of umbilical vessels from pregnancies with intrauterine growth retardation and abnormal umbilical artery doppler. *Hum Pathol*, **28**, 1139–1145.

[Bruner *et al.*(1994)] Bruner, J. P., Sheppard, C. G., Reed, G. W., and Boehm, F. H. (1994). The umbilical artery doppler ultrasonographic gradient: confirmation, cause, and comparison of continuous-wave and duplex ultrasonographic pulsed-wave measurements. *J Perinatol*, **14**, 386–392.

[Campbell *et al.*(1990)] Campbell, K., Burattini, R., Bell, D., Kirkpatrick, R., and Knowlen, G. (1990). Time-domain formulation of asymmetric t-tube model of arterial system. *Amer. J. Physiol.*, **258**, H1761–H1774.

[Capper and Myers(2000)] Capper, W. and Myers, L. (2000). Gestational age dependency of umbilical flow waveforms: an investigation using a lumped parameter model. In *Paper 5293-97775 in the digest of papers from the 2000 World Congress on Medical Physics and Biomedical Engineering, and the 22nd annual International conference of the IEEE Engineering in Medicine and Biology Society*, Chicago Navy Pier.

[Caro *et al.*(1971)] Caro, C., Fitzgerald, J., and Schroter, R. (1971). Atheroma and arterial wall shear observation, correlation and proposal of a shear dependent mass transfer mechanism for atherogenes. *Proc. Royal Soc., London B*, **177**, 109–159.

[Chandran *et al.*(1974)] Chandran, K. B., Swanson, W. M., Ghista, D. N., and Yao, H. W. (1974). Oscillatory flow in thin-walled curved elastic tubes. *Ann Biomed. Eng.*, **2**, 392–412.

[Chandran *et al.*(1979)] Chandran, K. B., Hosey, R. R., Ghista, D. N., and Yao, V. W. (1979). Analysis of fully developed unsteady viscous flow in a curved elastic tube model to provide fluid mechanical data for some circulatory path-physiological situations and assist devices. *J. Biomech. Eng.*, **101**, 114 – 123.

[Chang *et al.*(1994)] Chang, K. C., Tseng, Y. Z., Lin, Y. J., Kuo, T. S., and Chen, H. I. (1994). Exponentially tapered t-tube model of systemic arterial system in dogs. *Med Eng Phys*, **16**, 370–378.

[Chang *et al.*(1995)] Chang, K. C., Tseng, Y. Z., Kuo, T. S., and Chen, H. I. (1995). Impedance and wave reflection in arterial system: simulation with geometrically tapered t-tubes. *Med Biol Eng Comput*, **33**, 652–660.

[Chang and Tarbell(1985)] Chang, L. J. and Tarbell, J. M. (1985). Numerical simulation of fully developed sinusoidal and pulsatile (physiological) flow in curved tubes. *J. Fluid. mech.*, **161**, 175–198.

[Chipman(1968)] Chipman, R. (1968). *Schaum's outline series. Theory and problems of transmission lines.* McGraw-Hill, New York, St. Louis, San Francisco, Toronto, Sydney.

[Clapp *et al.*(1988)] Clapp, J., Peress, N., Wesley, M., and Mann, L. (1988). Brain damage after intermittent partial cord occlusion in the chronically instrumented fetal lamb. *Am. J. Obstet. Gynecol.*, **159**, 504–509.

[Cohn *et al.*(1974)] Cohn, H., Sacks, E., Heymann, M., and Rudolph, A. (1974). Cardiovascular responses to hypoxemia and acidemia in fetal lambs. *Am. J. Obstet. Gynecol.*, **15**, 817–824.

[Cohn *et al.*(1980)] Cohn, H. E., Piasecki, G. J., and Jackson, B. T. (1980). The effect of fetal heart rate on cardiovascular function during hypoxemia. *Am J Obstet Gynecol*, **138**, 1190–1199.

[Collin(1966)] Collin, R. (1966). *Foundations for microwave engineering.* McGraw-Hill, New York, St. Louis, San Fransisco, London, Mexico, Panama, Sydney, Toronto.

[Collins(1991)] Collins, J. (1991). First report: Prenatal diagnosis of long cord. *Am. J. Obstet. Gynecol.*, **165**, 1901.

[Cox(1968)] Cox, R. H. (1968). Wave propagation through a newtonian fluid contained within a thick-walled, viscoelastic tube. *Biophys. J.*, **8**, 691–709.

[Dado *et al.*(1997)] Dado, G. M., Dobrin, P. B., and Mrkvicka, R. S. (1997). Venous flow through coiled and noncoiled umbilical cords. effects of external compression, twisting and longitudinal stretching. *J Reprod Med*, **42**, 576–580.

[Dawes(1968)] Dawes, G. (1968). *Foetal and neonatal physiology : a comparitave study of the changes at birth Foetal and neonatal physiology.* Year book, Chicago.

[Dawson *et al.*(1999)] Dawson, A., Krenz, G., Karau, K., Haworth, S., Hanger, C., and Linehan, J. (1999). Structure-function relationships in the pulmonary arterial tree. *J. Appl. Physiol.*, **86**, 569–583.

[De Muylder *et al.*(1984)] De Muylder, X., Fouron, J. C., Bard, H., Riopel, L., and Urfer, F. (1984). The difference between the systolic time intervals of the left and right ventricles during fetal life. *Am J Obstet Gynecol*, **149**, 737–740.

[Dean(1928)] Dean, W. (1928). The stream line motion of fluid in curved pipes. *Phil. Mag*, **5**, 673–693.

[Degani *et al.*(1995)] Degani, S., Lewinsky, R. M., Berger, H., and Spiegel, D. (1995). Sonographic estimation of umbilical coiling index and correlation with doppler flow characteristics. *Obstet Gynecol*, **86**, 990–993.

[Dennis(1977)] Dennis, J. (1977). Nonlinear least squares. In D. Jacobs, editor, *State of the art in numerical analysis*, pages 269–312. Academic press.

[Dinnar(1975)] Dinnar, U. (1975). The role of the surrounding tissue in the propagation of waves through the arterial system. *TIT J Life Sci*, **5**, 49–56.

[Dinnar(1981)] Dinnar, U. (1981). *Cardiovascular fluid dynamics.* CRC Press Inc., Boca Raton, Florida.

[Dombrowski *et al.*(1994)] Dombrowski, M. P., Berry, S. M., Hurd, W. W., Saleh, A. A., Chik, L., and Sokol, R. J. (1994). A gestational-age-independent model of birth weight based on placental size. *Biol Neonate*, **66**, 56–64.

[Dornan and Beattie(1992)] Dornan, J. and Beattie, B. (1992). Umbilical artery doppler ultrasonography as a screening tool. In J. M. Pearce, editor, *Doppler ultrasound in perinatal medicine*, chapter 5, pages 95–111. Oxford university press, Oxford New york Tokyo, 1st edition.

[Eik-Nes *et al.*(1982)] Eik-Nes, S. H., Marsal, K., Brubakk, A. O., Kristofferson, K., and Ulstein, M. (1982). Ultrasonic measurement of human fetal blood flow. *J Biomed Eng*, **4**, 28–36.

[Einav *et al.*(1988)] Einav, S., Aharoni, S., and Manoach, M. (1988). Exponentially tapered transmission line model of the arterial system. *IEEE Trans Biomed Eng*, **35**, 333–339.

[Ercal *et al.*(1996)] Ercal, T., Lacin, S., Altunyurt, S., Saygili, U., Cinar, O., and Mumcu, A. (1996). Umbilical coiling index: is it a marker for the foetus at risk? *Br J Clin Pract.*, **50**(5), 254–256.

[Erskine and Ritchie(1985)] Erskine, R. L. and Ritchie, J. W. (1985). Quantitative measurement of fetal blood flow using doppler ultrasound. *Br J Obstet Gynaecol*, **92**, 600–604.

[Evans(1962)] Evans, R. (1962). Pulsatile flow in vessels whose distensibility and size vary with site. *Phys. med. biol.*, **7**, 105–116.

[Fisk *et al.*(1988)] Fisk, N. M., MacLachlan, N., Ellis, C., Tannirandorn, Y., Tonge, H. M., and Rodeck, C. H. (1988). Absent end-diastolic flow in first trimester umbilical artery. *Lancet*, **2**, 1256–1257.

[FitzGerald and Drumm(1977)] FitzGerald, D. E. and Drumm, J. E. (1977). Non-invasive measurement of human fetal circulation using ultrasound: a new method. *Br Med J*, **2**, 1450–1451.

[FitzGerald *et al.*(1984)] FitzGerald, D. E., Stuart, B., Drumm, J. E., and Duignan, N. M. (1984). The assessment of the feto-placental circulation with continuous wave doppler ultrasound. *Ultrasound Med Biol*, **10**, 371–376.

[Fogliardi *et al.*(1997)] Fogliardi, R., Burattini, R., and Campbell, K. B. (1997). Identification and physiological relevance of an exponentially tapered tube model of canine descending aortic circulation. *Med Eng Phys*, **19**, 201–211.

[Forouzan *et al.*(1991)] Forouzan, I., Cohen, A. W., and Arger, P. (1991). Measurement of systolic-diastolic ratio in the umbilical artery by continuous-wave and pulsed-wave doppler ultrasound: comparison at different sites. *Obstet Gynecol*, **77**, 209–212.

[Fox(1978)] Fox, H. (1978). *Pathology of the Placenta*. W.B. Saunders Company Ltd, London.

[Frank(1899)] Frank, O. (1899). Die grundform des arteriellen pulses erste abhandlung. mathematische analyse. *Z. Biol.*, **37**, 483–526.

[Fry(1968)] Fry, D. (1968). Acute vascular endothelial changes associated with increased blood velocity gradients. *Circ. Res.*, **22**, 165–197.

[Fung(1997)] Fung, Y. (1997). *Biomechanics, circulation*. Springer-Verlag, New York, Berlin, Heidelberg, 2nd edition.

[Gagnon *et al.*(1988)] Gagnon, R., Morrow, R., Ritchie, K., Hunse, C., and Patrick, J. (1988). Umbilical and uterine artery blood flow velocities after vibratory acoustic stimulation. *Am J Obstet Gynecol*, **159**, 574–578.

[Gallivan *et al.*(1993)] Gallivan, S., Robson, S., Chang, T., Vaughan, J., and Spencer, J. (1993). An investigation of fetal growth using serial ultrasound data. *Ultrasound Obstet. Gynecol.*, **3**, 109–114.

[Gan and Yen(1994)] Gan, R. Z. and Yen, R. T. (1994). Vascular impedance analysis in dog lung with detailed morphometric and elasticity data. *J Appl Physiol*, **77**, 706–717.

[Gerrard and Taylor(1977)] Gerrard, J. H. and Taylor, L. A. (1977). Mathematical model representing blood flow in arteries. *Med Biol Eng Comput*, **15**, 611–617.

[Gilbert(1980)] Gilbert, R. (1980). Control of fetal cardiac output during changes in blood volume. *Am. J. Physiol. (Heart Circ. Physiol.)*, **238**, H80–H86.

[Gilbert(1982)] Gilbert, R. D. (1982). Effects of afterload and baroreceptors on cardiac function in fetal sheep. *J Dev Physiol*, **4**, 299–309.

[Giles and Trudinger(1986)] Giles, W. B. and Trudinger, B. J. (1986). Umbilical cord whole blood viscosity and the umbilical artery flow velocity time waveforms: a correlation. *Br J Obstet Gynaecol*, **93**, 466–470.

[Giles *et al.*(1985)] Giles, W. B., Trudinger, B. J., and Baird, P. J. (1985). Fetal umbilical artery flow velocity waveforms and placental resistance: pathological correlation. *Br J Obstet Gynaecol*, **92**, 31–38.

[Gill *et al.*(1981)] Gill, R. W., Trudinger, B. J., Garrett, W. J., Kossoff, G., and Warren, P. S. (1981). Fetal umbilical venous flow measured in utero by pulsed doppler and b-mode ultrasound. i. normal pregnancies. *Am J Obstet Gynecol*, **139**, 720–725.

[Giussani *et al.*(1997)] Giussani, D., Unno, N., Jenkins, S., Wentworth, R., Derks, J., Collins, J., and Nathanielsz, P. (1997). Dynamics of cardiovascular responses to repeated partial umbilical cord compression in late-gestation sheep fetus. *Am. J. Physiol. (Heart Circ. Physiol.)*, **273**, H2351–H2360.

[Glenny and Robertson(1990)] Glenny, R. and Robertson, H. (1990). Fractal properties of pulmonary blood flow: Characterization of spatial heterogeneity. *J. Appl. Physiol.*, **69**, 532–545.

[Goffinet *et al.*(1997)] Goffinet, F., Paris-Llado, J., Nisand, I., and Breart, G. (1997). Umbilical artery doppler velocimetry in unselected and low risk pregnancies: a review of randomised controlled trials. *Br J Obstet Gynaecol*, **104**, 425–430.

[Goodlin *et al.*(1972)] Goodlin, R. C., Girard, J., and Hollmen, A. (1972). Systolic time intervals in the fetus and neonate. *Obstet Gynecol*, **39**, 295–303.

[Gosling and King(1974)] Gosling, R. G. and King, D. H. (1974). Arterial assessment by doppler-shift ultrasound. *Proc R Soc Med*, **67**, 447–449.

[Gow and Taylor(1968)] Gow, B. S. and Taylor, M. G. (1968). Measurement of viscoelastic properties of arteries in the living dog. *Circ Res*, **23**, 111–122.

[Griffin *et al.*(1983)] Griffin, D., Cohen-Overbeek, T., and Campbell, S. (1983). Fetal and uteroplacental blood flow. *Clin. Obstet. Gynaecol.*, **10**(3), 565–602.

[Griffin *et al.*(1984)] Griffin, D., Bilardo, K., Masini, L., Diaz-Recasens, J., Pearce, J. M., Willson, K., and Campbell, S. (1984). Doppler blood flow waveforms in the descending thoracic aorta of the human fetus. *Br J Obstet Gynaecol*, **91**, 997–1006.

[Groenenberg *et al.*(1989)] Groenenberg, I. A., Wladimiroff, J. W., and Hop, W. C. (1989). Fetal cardiac and peripheral arterial flow velocity waveforms in intrauterine growth retardation. *Circulation*, **80**, 1711–1717.

[Guettouche *et al.*(1992)] Guettouche, A., Challier, J., Ito, Y., Papapanayotou, C., Y. Cherruault, Y., and Azancot-Benisty, A. (1992). Mathematical modeling of the human fetal arterial blood circulation. *International Journal of Biomedical Computing*, **31**, 127–139.

[Guiot *et al.*(1992)] Guiot, C., Pianta, P., and Todros, T. (1992). Modelling the feto-placental circulation: 1. a distributed network predicting umbilical haemodynamics throughout pregnancy. *Ultrasound in Med. & Biol.*, **18**, 535–544.

[Gunnarsson *et al.*(1998)] Gunnarsson, G., Gudmundsson, S., Hokegard, K., Stale, H., Kjellmer, I., Hafstrom, O., and Marsal, K. (1998). Cerebral doppler blood flow velocimetry and central hemodynamics in the ovine fetus during hypoxemia-acidemia. *J. Perinat. Med.*, **26**, 107–114.

[Hales(1733)] Hales, S. (1733). Statical essays: Containing haemastaticks. In *History of medicine series, Library of New York academy of medicine*. Hafner Publishing, New York.

[Hamakiotes and Berger(1988)] Hamakiotes, C. C. and Berger, S. A. (1988). Fully developed pulsatile flow in a curved pipe. *J. Fluid. mech.*, **195**, 23–55.

[Hamakiotes and Berger(1990)] Hamakiotes, C. C. and Berger, S. A. (1990). Periodic flows through curved tubes : The effect of the frequency parameter. *J. Fluid. mech.*, **210**, 353–370.

[Hamilton and Mossman(1972)] Hamilton, W. and Mossman, H. (1972). *Human Embryology: Prenatal Development of Form and Function*. Macmillan press, London.

[Harvey(1628)] Harvey, W. (1628). *De Motu Cordis*. William Fitzer.

[Hasaart *et al.*(1993)] Hasaart, T., Maulik, D., and Morrow, R. (1993). Validation of fetal flow velocimetry: A review of in vitro and in vivo modeling. *J. Maternal Fetal Invest*, **3**, 95–104.

[Hendricks *et al.*(1989)] Hendricks, S. K., Sorensen, T. K., Wang, K. Y., Bushnell, J. M., Seguin, E. M., and Zingheim, R. W. (1989). Doppler umbilical artery waveform indices–normal values from fourteen to forty-two weeks. *Am J Obstet Gynecol*, **161**, 761–765.

[Hill *et al.*(1995)] Hill, A., Surat, D., Cobbold, R., Mo, B. L. A., and Adamson, S. (1995). A wave transmission model of the umbilicoplacental circulation based on hemodynamic measurements in sheep. *Am. J. Physiol. (Regulatory Integrative Comp. Physiol.)*, **269**, R1267–R1278.

[Hitschold *et al.*(1993)] Hitschold, T., Weiss, E., Beck, T., Hunterfering, H., and Berle, P. (1993). Low target birth weight or growth retardation? umbilical doppler flow velocity waveforms and histometric analysis of fetoplacental vascular tree. *Am. J. Obstet. Gynecol.*, **168**, 1260–1264.

[Holt *et al.*(1981)] Holt, J. P., Rhode, E. A., Holt, W. W., and Kines, H. (1981). Geometric similarity of aorta, venae cavae, and certain of their branches in mammals. *Am J Physiol*, **241**, R100–R104.

[Horsfield(1978)] Horsfield, K. (1978). Morphometry of the small pulmonary arteries in man. *Circ Res*, **42**, 593–597.

[Huang *et al.*(1996)] Huang, W., Yen, R. T., McLaurine, M., and Bledsoe, G. (1996). Morphometry of the human pulmonary vasculature. *J Appl Physiol*, **81**, 2123–2133.

[Huikeshoven *et al.*(1980)] Huikeshoven, F., Coleman, T., and Jongsma, H. (1980). Mathematical model of the fetal cardiovascular system: The uncontrolled case. *Am. J. Physiol. (Regulatory Integrative Comp. Physiol.)*, **239**, R317–R325.

[Ito(1969)] Ito, H. (1969). Laminar flow in curved pipes. *Z. Angew. Math. Mech.*, **11**, 653–663.

[Itskovitz *et al.*(1983)] Itskovitz, J., LaGamma, E., and Rudolph, A. (1983). Heart rate and blood pressure responses to umbilical cord compression in fetal lambs with special reference to the mechanism of variable deceleration. *Am. J. Obstet. Gynecol.*, **147**, 451–457.

[Itskovitz *et al.*(1987)] Itskovitz, J., LaGamma, E., and Rudolph, A. (1987). Effects of cord compression on fetal blood flow distribution and o_2 delivery. *Am. J. Physiol. (Heart Circ. distribution and O_2 delivery)*, **252**, H100–H109.

[Iwamoto(1992)] Iwamoto, H. (1992). Endocrine regulation of the fetal circulation. chapter 62, pages 646–655. WB Saunders company, Philadelphia, London, Tornonto, Montreal, Sydney, Tokyo.

[Iwamoto and Rudolph(1981)] Iwamoto, H. S. and Rudolph, A. M. (1981). Effects of angiotensin ii on the blood flow and its distribution in fetal lambs. *Circ Res*, **48**, 183–189.

[Jackson *et al.*(1995)] Jackson, M., Walsh, A., Morrow, R., Mullen, J., Lye, S., and Ritchie, J. (1995). Reduced placental villous tree elaboration in small-for-gestational-age pregnancies: Relationship with umbilical artery doppler waveforms. *Am. J. Obstet. Gynecol.*, **172**, 518–525.

[Jacobs *et al.*(1988)] Jacobs, R., Robinson, J., Owens, J., Falconer, J., and Webster, M. (1988). The effect of prolonged hypobaric hypoxia on growth of fetal sheep. *J. Dev. Physiol.*, **10**, 97–112.

[Jager(1965)] Jager, G. (1965). *Electrical model of the human systemic arterial tree.* Ph.D. thesis, University of Utrecht.

[Jakobi *et al.*(1994)] Jakobi, P., Weiner, Z., and Goren, T. (1994). Systolic notch in umbilical artery flow velocity waveforms associated with a tight true knot of the cord. *J. Matern. Fetal Invest.*, **4**, 119.

[Jensen and Berger(1991)] Jensen, A. and Berger, R. (1991). Fetal circulatory responses to oxygen lack. *J. Dev. Phys.*, **16**, 181–207.

[Jensen *et al.*(1987)] Jensen, A., Hohmann, M., and Kunzel, W. (1987). Dynamic changes in organ blood flow and oxygen consumption during acute asphyxia in fetal sheep. *J. Develop. Physiol.*, **9**, 543–559.

[Jensen *et al.*(1999)] Jensen, A., Garnier, Y., and Berger, R. (1999). Dynamics of fetal circulatory responses to hypoxia and asphyxia. *Eur. J. Obs. & Gynecol.*, **84**, 155–172.

[Jiang *et al.*(1994)] Jiang, Z. L., Kassab, G. S., and Fung, Y. C. (1994). Diameter-defined strahler system and connectivity matrix of the pulmonary arterial tree. *J Appl Physiol*, **76**, 882–892.

[Joern *et al.*(1996)] Joern, H., Funk, A., Goetz, M., Kuehlwein, H., Klein, A., and Fendel, H. (1996). Development of quantitative doppler indices for uteroplacental and fetal blood flow during the third trimester. *Ultrasound Med Biol*, **22**, 823–835.

[John(2000)] John, L. R. (2000). *An inverse transmission line model of the lower limb arterial system.* Ph.D. thesis, University of Cape Town.

[Johnston *et al.*(1984)] Johnston, K. W., Kassam, M., Koers, J., Cobbold, R. S., and MacHattie, D. (1984). Comparative study of four methods for quantifying doppler ultrasound waveforms from the femoral artery. *Ultrasound Med Biol*, **10**, 1–12.

[Johnstone *et al.*(1993)] Johnstone, F. D., Prescott, R., Hoskins, P., Greer, I. A., McGlew, T., and Compton, M. (1993). The effect of introduction of umbilical doppler recordings to obstetric practice. *Br J Obstet Gynaecol*, **100**, 733–741.

[Jouppila and Kirkinen(1986)] Jouppila, P. and Kirkinen, P. (1986). Blood velocity waveforms of the fetal aorta in normal and hypertensive pregnancies. *Obstet Gynecol*, **67**, 856–860.

[Kamitomo *et al.*(1993)] Kamitomo, M., Alonso, J., Okai, T., Longo, L., and Gilbert, R. (1993). Effects of long-term, high-altitude hypoxemia on ovine fetal cardiac output and blood flow distribution. *Am. J. Obstet. Gynecol.*, **169**, 701–707.

[Kamitomo *et al.*(1994)] Kamitomo, M., Longo, L., and Gilbert, R. (1994). Cardiac function in fetal sheep during two weeks of hypoxemia. *Am. J. Physiol. (Regulatory Integrative Comp. Physiol.)*, **266**, R1778–R1785.

[Kay *et al.*(1989)] Kay, H. H., Carroll, B. A., Bowie, J. D., Killam, A. P., and Hertzberg, B. S. (1989). Nonuniformity of fetal umbilical systolic/diastolic ratios as determined with duplex doppler sonography. *J Ultrasound Med*, **8**, 417–420.

[Kenny *et al.*(1987)] Kenny, J., Plappert, T., Doubilet, P., Salzman, D., and Sutton, M. G. (1987). Effects of heart rate on ventricular size, stroke volume, and output in the normal human fetus: a prospective doppler echocardiographic study. *Circulation*, **76**, 52–58.

[Kenny *et al.*(1986)] Kenny, J. F., Plappert, T., Doubilet, P., Saltzman, D. H., Cartier, M., Zollars, L., Leatherman, G. F., and St John Sutton, M. G. (1986). Changes in intracardiac blood flow velocities and right and left ventricular stroke volumes with gestational age in the normal human fetus: a prospective doppler echocardiographic study. *Circulation*, **74**, 1208–1216.

[Kingdom *et al.*(1997)] Kingdom, J. C., Rodeck, C. H., and Kaufmann, P. (1997). Umbilical artery doppler–more harm than good? *Br J Obstet Gynaecol.*, **104**(4), 393–396.

[Kirkpatrick *et al.*(1976)] Kirkpatrick, S. E., Pitlick, P. T., Naliboff, J., and Friedman, W. F. (1976). Frank-starling relationship as an important determinant of fetal cardiac output. *Am J Physiol*, **231**, 495–500.

[Kitanaka *et al.*(1989)] Kitanaka, T., Alonso, J., Gilbert, R., Siu, B., Clemons, G., and Longo, L. (1989). Fetal responses to long-term hypoxemia in sheep. *Am. J. Physiol. (Regulatory Integrative Comp. Physiol.)*, **256**, R1348–R1354.

[Kleiner-Assaf *et al.*(1999)] Kleiner-Assaf, A., Jaffa, A., and Elad, D. (1999). Hemodynamic model for analysis of doppler ultrasound indexes of umbilical blood flow. *Am. J. Physiol. (Heart Circ. Physiol.)*, **276**, H2204–H2214.

[Klip *et al.*(1967)] Klip, W., van Loon, P., and Klip, D. (1967). Formulas for phase velocity and damping of longitudinal waves in thick-walled viscoelastic tubes. *J. applied physiol.*, **38**, 37–45.

[Kofinas *et al.*(1989)] Kofinas, A. D., Espeland, M., Swain, M., Penry, M., and Nelson, L. H. (1989). Correcting umbilical artery flow velocity waveforms for fetal heart rate is unnecessary. *Am J Obstet Gynecol*, **160**, 704–707.

[Krasney *et al.*(1984)] Krasney, J., McDonald, B., and Matalon, S. (1984). Regional circulatory responses to 96 hours of hypoxia in conscious sheep. *Resp. Phys.*, **57**, 73–88.

[Krebs *et al.*(1996)] Krebs, C., Macara, L., Leiser, R., Bowman, A., Greer, I., and Kingdom, J. (1996). Intrauterine growth restriction with absent end-diastolic flow velocity in the umbilical

artery is associated with maldevelopment of the placental terminal villous tree. *Am. J. Obstet. Gynecol.*, **175**, 1534–1542.

[Krenz *et al.*(1992)] Krenz, G., Linehan, J., and Dawson, C. (1992). A fractal continuum model of the pulmonary arterial tree. *J. Appl. Physiol.*, **72**, 2225–2237.

[Labarrere *et al.*(1985)] Labarrere, C., Sebastiani, M., Siminovich, M., Torassa, E., and Althabe, O. (1985). Absence of wharton's jelly around the umbilical arteries: an unusual cause of perinatal mortality. *Placenta*, **6**, 555–559.

[Lambert(1958)] Lambert, J. (1958). On the nonlinearities of fluid flow in nonrigid tubes. *J. Franklin institute*, **266**, 83–102.

[Laurin *et al.*(1987)] Laurin, J., Lingman, G., Marsal, K., and Persson, P. H. (1987). Fetal blood flow in pregnancies complicated by intrauterine growth retardation. *Obstet Gynecol*, **69**, 895–902.

[Li(1976)] Li, C. (1976). A note in comment on 'analysis of steady laminar flow of an incompressible fluid through curved pipes of small curvature'. *Trans. ASME I : J. Fluids Engng.*, **98**, 323–325.

[Li(1986)] Li, J. K. (1986). Time domain resolution of forward and reflected waves in the aorta. *IEEE Trans Biomed Eng*, **33**, 783–785.

[Ling and Atabek(1972)] Ling, S. and Atabek, H. (1972). A nonlinear analysis of pulsatile flow in arteries. *J. Fluid mech.*, **55**, 493–511.

[Ling *et al.*(1973)] Ling, S., Atabek, H., Letzing, W., and Patel, D. (1973). Nonlinear analysis of aortic flow in living dogs. *Circ. res.*, **33**, 198–212.

[Lingman and Marsal(1986)] Lingman, G. and Marsal, K. (1986). Fetal central blood circulation in the third trimester of normal pregnancy–a longitudinal study. ii. aortic blood velocity waveform. *Early Hum Dev*, **13**, 151–159.

[Luecke *et al.*(1995)] Luecke, R. H., Wosilait, W. D., and Young, J. F. (1995). Mathematical representation of organ growth in the human embryo/fetus. *Int J Biomed Comput*, **39**, 337–347.

[Lyne(1970)] Lyne, W. H. (1970). Unsteady viscous flow in a curved pipe. *J. Fluid. Mech.*, **45**, 13–31.

[Macara *et al.*(1995)] Macara, L., Kingdom, J., Bowman, A., Greer, I., and Kaufmann, P. (1995). Elaboration of stem villous vessels in growth restricted pregnancies with abnormal umbilical artery doppler waveforms. *Br. J. Obstet. Gynaecol.*, **102**, 807–812.

[Mackintosh and Walker(1973)] Mackintosh, T. F. and Walker, C. H. (1973). Blood viscosity in the newborn. *Arch Dis Child*, **48**, 547–553.

[Macpherson *et al.*(1984)] Macpherson, D. S., Evans, D. H., and Bell, P. R. (1984). Common femoral artery doppler wave-forms: a comparison of three methods of objective analysis with direct pressure measurements. *Br J Surg*, **71**, 46–49.

[Malcus *et al.*(1991)] Malcus, P., Andersson, J., Marsal, K., and Olofsson, P. A. (1991). Waveform pattern recognition–a new semiquantitative method for analysis of fetal aortic and umbilical artery blood flow velocity recorded by doppler ultrasound. *Ultrasound Med Biol*, **17**, 453–460.

[Manlapaz and Churchill(1980)] Manlapaz, R. L. and Churchill, S. W. (1980). Fully developed laminar flow in a helically coiled tube of finite pitch. *Chem. Eng. Commun.*, **7**, 57–78.

[Marsal *et al.*(1987)] Marsal, K., Laurin, J., Lindblad, A., and Lingman, G. (1987). Blood flow in the fetal descending aorta. *Semin Perinatol*, **11**, 322–334.

[Marsal *et al.*(1992)] Marsal, K., Nicolaides, K., Kaminpetros, P., and Hackett, G. (1992). The clinical value of waveforms from the descending aorta. In J. pearce, editor, *Doppler ultrasound in perinatal medicine*, chapter 13, pages 239–242. Oxford university press, Oxford, New York, Tokyo.

[Mazess(1965)] Mazess, R. B. (1965). Neonatal mortality and altitude in peru. *Am J Phys Anthropol*, **23**, 209–213.

[Mazumdar *et al.*(1991)] Mazumdar, J., Ang, K. C., and Soh, L. L. (1991). A mathematical study of non-newtonian blood flow through elastic arteries. *Australas Phys Eng Sci Med*, **14**, 65–73.

[McCowan *et al.*(1987)] McCowan, L. M., Mullen, B. M., and Ritchie, K. (1987). Umbilical artery flow velocity waveforms and the placental vascular bed. *Am J Obstet Gynecol*, **157**, 900–902.

[McCullough *et al.*(1977)] McCullough, R. E., Reeves, J. T., and Liljegren, R. L. (1977). Fetal growth retardation and increased infant mortility at high altitude. *Obstet Gynecol Surv*, **32**, 596–598.

[McDonald(1998)] McDonald, D. (1998). *McDonald's blood flow in arteries. Theoretical, experimental and clinical principles.* Arnold, London, Sydney, Auckland, 4th edition.

[McIlroy *et al.*(1986)] McIlroy, M. B., Seitz, W. S., and Targett, R. C. (1986). A transmission line model of the normal aorta and its branches. *Cardiovasc Res*, **20**, 581–587.

[McLachlan(1934)] McLachlan, N. (1934). *Bessel functions for engineers.* Oxford university press, London.

[McParland and Pearce(1988)] McParland, P. and Pearce, J. M. (1988). Doppler blood flow in pregnancy. *Placenta*, **9**, 427–450.

[Mead(1996)] Mead, M. (1996). The diagnosis of foetal distress: a challenge to midwives. *J Adv Nurs*, **23**, 975–983.

[Mehalek *et al.*(1989)] Mehalek, K. E., Rosenberg, J., Berkowitz, G. S., Chitkara, U., and Berkowitz, R. L. (1989). Umbilical and uterine artery flow velocity waveforms. effect of the sampling site on doppler ratios. *J Ultrasound Med*, **8**, 171–176.

[Menigault *et al.*(1998)] Menigault, E., Berson, M., Vieyres, P., Lepoivre, B., Pourcelot, D., and Pourcelot, L. (1998). Feto-maternal circulation: Mathematical model and comparison with doppler measurements. *Eur. J. Ultrasound*, **7**, 129–143.

[Milnor(1989)] Milnor, W. (1989). *Hemodynamics.* Williams and Wilkins, Baltimore, Hong Kong, London, Sydney, 2nd edition.

[Mires *et al.*(1987)] Mires, G., Dempster, J., Patel, N. B., and Crawford, J. W. (1987). The effect of fetal heart rate on umbilical artery flow velocity waveforms. *Br J Obstet Gynaecol*, **94**, 665–669.

[Mirsky(1968)] Mirsky, I. (1968). Wave propagation in a viscous fluid contained in an orthotropic elastic tube. *Biophys. J.*, **7**, 165–186.

[Mitra *et al.*(1997)] Mitra, S. C., Venkataseshan, V. S., von Hagen, S., Barton, P. T., Delshad, G., and Gil, J. (1997). Morphometric study of the placental vessels and its correlation with umbilical artery doppler flow. *Obstet Gynecol*, **89**, 238–241.

[Mo *et al.*(1988)] Mo, L., Bascom, P., Ritchie, K., and McCowan, L. (1988). A transmission line modelling approach to the interpretation of uterine doppler waveforms. *Ultrasound in Med. & Biol.*, **14**, 365–376.

[More(1977)] More, J. (1977). The levenberg-marquardt algorithm: Implementation and theory. In G. Watson, editor, *Numerical analysis*, volume 630 of *Lecture notes in mathematics*, pages 105–116. Springer Verlag.

[Morgan and Kiely(1955)] Morgan, G. and Kiely, J. (1955). Wave propagation in a viscous liquid contained in a flexible tube. *J. acoust. soc. am.*, **26**, 323–328.

[Morrow *et al.*(1990)] Morrow, R., Adamson, S., Bull, S., and Ritchie, J. (1990). Hypoxic acidemia, hyperviscosity, and maternal hypertension do not affect the umbilical arterial velocity waveform in fetal sheep. *Am J Obstet Gynecol.*, **163**, 1313–1320.

[Mulders *et al.*(1987)] Mulders, L. G., Wijn, P. F., Jongsma, H. W., and Hein, P. R. (1987). A comparative study of three indices of umbilical blood flow in relation to prediction of growth retardation. *J Perinat Med*, **15**, 3–12.

[Mullin and Greated(1980)] Mullin, T. and Greated, C. A. (1980). Oscillatory flow in curved pipes. part. *J. Fluid. Mech.*, **98**, 397–416.

[Murray(1926)] Murray, C. (1926). The physiological principle of minimum work. i. the vascular system and the cost of blood volume. *Proc. Natl Acad. Sci.*, **12**, 207–214.

[Myers and Capper(2001)] Myers, L. and Capper, W. (2001). Analytical solution for pulsatile axial flow velocity waveforms in curved elastic tubes. *IEEE Trans. Biomed. Eng.*, **48**(8), 864–873.

[Naeye(1985)] Naeye, R. L. (1985). Umbilical cord length: clinical significance. *J Pediatr*, **107**, 278–281.

[Nakamura and Sawada(1990)] Nakamura, M. and Sawada, T. (1990). Numerical study on the unsteady flow of non-newtonian fluid. *J Biomech Eng*, **112**, 100–103.

[Nishio *et al.*(1999)] Nishio, J., Nakai, Y., Mine, M., Imanaka, M., and Ogita, S. (1999). Characteristics of blood flow in intrauterine growth-restricted fetuses with hypercoiled cord. *Ultrasound Obstet Gynecol*, **13**, 171–175.

[Nordenvall *et al.*(1991)] Nordenvall, M., Laurin, U. U. A. G., Sandstedt, B., and Ulmsten, U. (1991). Placental morphology in relation to umbilical artery blood velocity waveforms. *Eur. J. Obstet. Gynecol. Reprod. Biol.*, **40**, 179–190.

[Parker and Jones(1990)] Parker, K. H. and Jones, C. J. (1990). Forward and backward running waves in the arteries: analysis using the method of characteristics. *J Biomech Eng*, **112**, 322–326.

[Patel and Fry(1966)] Patel, D. J. and Fry, D. L. (1966). Longitudinal tethering of arteries in dogs. *Circ Res*, **19**, 1011–1021.

[Patel *et al.*(1969)] Patel, D. J., Janicki, J. S., and Carew, T. E. (1969). Static anisotropic elastic properties of the aorta in living dogs. *Circ Res*, **25**, 765–779.

[Pattinson *et al.*(1989)] Pattinson, R. C., Theron, G. B., Thompson, M. L., and Lai Tung, M. (1989). Doppler ultrasonography of the fetoplacental circulation–normal reference values. *S Afr Med J*, **76**, 623–625.

[Pawlicka *et al.*(1999)] Pawlicka, E., Bankowski, E., and Jaworski, S. (1999). Elastin of the umbilical cord arteries and its alterations in eph gestosis (preeclampsia). *Biol Neonate*, **75**, 91–96.

[Pearce *et al.*(1988)] Pearce, J. M., Campbell, S., Cohen-Overbeek, T., Hackett, G., Hernandez, J., and Royston, J. P. (1988). References ranges and sources of variation for indices of pulsed doppler flow velocity waveforms from the uteroplacental and fetal circulation. *Br J Obstet Gynaecol*, **95**, 248–256.

[Pearson *et al.*(1994)] Pearson, A. C., Guo, R., Orsinelli, D. A., Binkley, P. F., and Pasierski, T. J. (1994). Transesophageal echocardiographic assessment of the effects of age, gender, and hypertension on thoracic aortic wall size, thickness, and stiffness. *Am Heart J*, **128**, 344–351.

[Peeters *et al.*(1979)] Peeters, L., Sheldon, R., Jones, M., Makowski, E., and Meschia, G. (1979). Blood flow to fetal organs as a function of arterial oxygen content. *Am. J. Obstet. Gynecol.*, **135**, 637–646.

[Pennati and Fumero(2000)] Pennati, G. and Fumero, R. (2000). Scaling approach to study the changes through the gestation of human fetal cardiac and circulatory behaviors. *Ann Biomed Eng*, **28**, 442–452.

[Pennati *et al.*(1997)] Pennati, G., Bellotti, M., and Fumero, R. (1997). Mathematical modelling of the human foetal cardiovascular system based on doppler ultrasound data. *Med. Eng. Phys.*, **19**, 327–335.

[Peterson *et al.*(1960)] Peterson, L., Jensen, R., and Parnell, J. (1960). Mechanical properties of arteries in vivo. *Circ. res.*, **8**, 622–639.

[Polianin and Zaitsev(1995)] Polianin, A. and Zaitsev, V. (1995). *Handbook of exact solutions for ordinary differential equations*. Boca Raton : CRC Press.

[Pourcelot(1974)] Pourcelot, L. (1974). Applications cliniques de l'examen doppler transcutane. In p. PERONNEAU, editor, *Velocimetric ultrasonor Doppler*, pages 213–40. inserm 7-11, PARIS.

[Press(1989)] Press, W. (1989). *Numerical recipes in Pascal : the art of scientific computing*. Cambridge University Press, New York.

[Pythoud *et al.*(1996)] Pythoud, F., Stergiopulos, N., and Meister, J. J. (1996). Separation of arterial pressure waves into their forward and backward running components. *J Biomech Eng*, **118**, 295–301.

[Rabadi *et al.*(1980)] Rabadi, N. J., Simon, H. A., and Chow, J. C. F. (1980). Numerical solution for fully developed, laminar pulsating flow in curved tubes. *Num. Heat Trans.*, **3**, 225–239.

[Rana *et al.*(1995)] Rana, J., Ebert, G. A., and Kappy, K. A. (1995). Adverse perinatal outcome in patients with an abnormal umbilical coiling index. *Obstet Gynecol*, **85**, 573–577.

[Reed *et al.*(1986)] Reed, K. L., Meijboom, E. J., Sahn, D. J., Scagnelli, S. A., Valdes-Cruz, L. M., and Shenker, L. (1986). Cardiac doppler flow velocities in human fetuses. *Circulation*, **73**, 41–46.

[Reed *et al.*(1987)] Reed, K. L., Anderson, C. F., and Shenker, L. (1987). Changes in intracardiac doppler blood flow velocities in fetuses with absent umbilical artery diastolic flow. *Am J Obstet Gynecol*, **157**, 774–779.

[Reuss and Rudolph(1980)] Reuss, M. L. and Rudolph, A. M. (1980). Distribution and recirculation of umbilical and systemic venous blood flow in fetal lambs during hypoxia. *J Dev Physiol*, **2**, 71–84.

[Reynolds(1978)] Reynolds, S. R. (1978). Mechanisms of placentofetal blood flow. *Obstet Gynecol*, **51**, 245–249.

[Richardson *et al.*(1996)] Richardson, B., Carmichael, L., Homan, J., Johnston, L., and Gagnon, R. (1996). Fetal cerebral, circulatory, and metabolic responses during heart rate decelerations with umbilical cord compression. *Am. J. Obstet. Gynecol.*, **175**, 929–936.

[Robinson *et al.*(1997)] Robinson, J. N., Abuhamad, A. Z., Sayed, A., and Evans, A. T. (1997). Umbilical artery doppler velocimetry waveform notching and umbilical cord abnormalities. *J Ultrasound Med*, **16**, 373–375.

[Roffeh *et al.*(1996)] Roffeh, Y., Einav, S., Liaw, J., Whiting, J., and Keren, G. (1996). Cepstrum analysis of reflected pressure waves in stenosed arteries. *Med Biol Eng Comput*, **34**, 175–180.

[Rudolph(1984)] Rudolph, A. (1984). *Congenital diseases of the heart : Clinical-physiologic considerations in diagnosis and management.* Year book, Chicago.

[Rudolph and Heymann(1974)] Rudolph, A. and Heymann, M. (1974). Fetal and neonatal circulation and respiration. *Ann Rev Physiol*, **19**, 187.

[Rudolph *et al.*(1971)] Rudolph, A., Heymann, M., Teramo, K., Barrett, C., and Raiha, N. (1971). Studies on the circulation of the previable human fetus. *Pediat Res*, **5**, 452–465.

[Rudolph(1985)] Rudolph, A. M. (1985). Distribution and regulation of blood flow in the fetal and neonatal lamb. *Circ Res*, **57**, 811–821.

[Sahn *et al.*(1980)] Sahn, D. J., Lange, L. W., Allen, H. D., Goldberg, S. J., Anderson, C., Giles, H., and Haber, K. (1980). Quantitative real-time cross-sectional echocardiography in the developing normal humam fetus and newborn. *Circulation*, **62**, 588–597.

[Sankaraiah and Rao(1973)] Sankaraiah, M. and Rao, Y. (1973). Analysis of steady laminar flow of an incompressible newtonian fluid through curved pipes of small curvature. *Trans. ASME I : J. Fluids Engng*, **95**, 75–80.

[Schwerdt and Constantinesco(1976)] Schwerdt, H. and Constantinesco, A. (1976). Periodic flow of a viscous fluid superposed on steady flow in an orthotropic initially stressed elastic tube. determination of fluid velocities and displacement components of the wall. *Biorheology*, **13**, 7–20.

[Sheldon *et al.*(1979)] Sheldon, R., Peeters, L., Jones, M., and Meschia, G. (1979). Redistribution of cardiac output and oxygen delivery in the hypoxemic fetal lamb. *A. J. Obstet. Gynecol.*, **135**, 1071–1078.

[Sherer and Manning(1999)] Sherer, D. and Manning, F. (1999). Prenatal ultrasonographic diagnosis of conditions associated with potential umbilical cord compression. *Am. J. Perinatology*, **16**, 445–458.

[Sherer and Anyaegbunam(1997)] Sherer, D. M. and Anyaegbunam, A. (1997). Prenatal ultrasonographic morphologic assessment of the umbilical cord: a review. part i. *Obstet Gynecol Surv*, **52**, 506–514.

[Sherriff *et al.*(1982)] Sherriff, S. B., Barber, D. C., Martin, T. R., and Lakeman, J. M. (1982). Use of principal component factor analysis in the detection of carotid artery disease from doppler ultrasound. *Med Biol Eng Comput*, **20**, 351–356.

[Simon *et al.*(1977)] Simon, H. A., Chang, M. H., and Chow, J. C. F. (1977). Heat transfer in curved tubes with pulsatile, fully developed, laminar flows. *J. Heat Trans*, **99**, 590–595.

[Skidmore and Woodcock(1978)] Skidmore, R. and Woodcock, J. P. (1978). Physiological significance of arterial models derived using transcutaneous ultrasonic flowmeters. *J Physiol.*, **227**, 29P–30P.

[Skidmore and Woodcock(1980a)] Skidmore, R. and Woodcock, J. P. (1980a). Physiological interpretation of doppler-shift waveforms–i. theoretical considerations. *Ultrasound Med Biol*, **6**, 7–10.

[Skidmore and Woodcock(1980b)] Skidmore, R. and Woodcock, J. P. (1980b). Physiological interpretation of doppler-shift waveforms–ii. validation of the laplace transform method for characterisation of the common femoral blood-velocity/time waveform. *Ultrasound Med Biol*, **6**, 219–225.

[Skidmore *et al.*(1980)] Skidmore, R., Woodcock, J. P., and Wells, P. N. (1980). Physiological interpretation of doppler-shift waveforms–iii. clinical results. *Ultrasound Med Biol*, **6**, 227–231.

[Skoll *et al.*(1997)] Skoll, M. A., Fouron, J. C., Sonesson, S. E., Nyctelius, H., Lessard, M., and Drblik, S. P. (1997). Doppler velocimetric indices from the abdominal and placental ends of the umbilical artery of growth-restricted fetuses. *J Clin Ultrasound*, **25**, 421–424.

[Smith(1975)] Smith, F. T. (1975). Pulsatile flow in curved pipes. *J. Fluid. mech*, **71**, 15–42.

[Sonesson *et al.*(1993)] Sonesson, S., Fouron, J., Drblik, S., Tawile, C., M, M. L., Skoll, A., Guertin, M., and Ducharme, G. (1993). Reference values for doppler velocimetric indices from the fetal and placental ends of the umbilical artery during normal pregnancy. *J Clin Ultrasound*, **21**(5), 317–324.

[Sparks and Cetin(1992)] Sparks, J. and Cetin, I. (1992). Intrauterine growth. In R. Polin and W. Fox, editors, *Fetal and neonatal physiology*, chapter 5, page 179. W.B. Saunders company, Philadelphia London Toronto Montreal Sydney Tojkyo.

[Steel *et al.*(1989)] Steel, S. A., Pearce, J. M., Nash, G., Christopher, B., Dormandy, J., and Bland, J. M. (1989). Correlation between doppler flow velocity waveforms and cord blood viscosity. *Br J Obstet Gynaecol*, **96**, 1168–1172.

[Stergiopulos *et al.*(1993)] Stergiopulos, N., Tardy, Y., and Meister, J. J. (1993). Nonlinear separation of forward and backward running waves in elastic conduits. *J Biomech*, **26**, 201–209.

[Stewart *et al.*(1990)] Stewart, P., Wladimiroff, J., and Stijnen, T. (1990). Blood flow velocity waveforms from the fetal external iliac artery as a measure of lower extremity vascular resistance. *Br J Obstet Gynaecol.*, **97**, 425–430.

[StJohnSutton *et al.*(1992)] StJohnSutton, M., Gill, T., and Plappert, T. (1992). Functional anatomic development in the fetal heart. In R. Pollin and W. Fox, editors, *Fetal and neonatal physiology*, chapter 58, pages 598–609. WB Saunders company,, Philadelphia, London, Tornonto, Montreal, Sydney, Tokyo.

[Streeter *et al.*(1963)] Streeter, V., Keitzer, W., and Bohr, D. (1963). Pulsatile pressure and flow through distensible vessels. *Circulation research*, **13**, 3–20.

[Strong Jr *et al.*(1994)] Strong Jr, T. H., Jarles, D. L., Vega, J. S., and Feldman, D. B. (1994). The umbilical coiling index. *Am J Obstet Gynecol*, **170**, 29–32.

[Struijk *et al.*(1992)] Struijk, P. C., Wladimiroff, J. W., Hop, W. C., and Simonazzi, E. (1992). Pulse pressure assessment in the human fetal descending aorta. *Ultrasound Med Biol*, **18**, 39–43.

[Stuart *et al.*(1980)] Stuart, B., Drumm, J., FitzGerald, D. E., and Duignan, N. M. (1980). Fetal blood velocity waveforms in normal pregnancy. *Br J Obstet Gynaecol*, **87**, 780–785.

[Sudo *et al.*(1992)] Sudo, K., Sumida, M., and Yamane, R. (1992). Secondary motion of fully developed oscillatory flow in a curved pipe. *J. Fluid. Mech.*, **237**, 189–208.

[Surat and Adamson(1996)] Surat, D. and Adamson, S. (1996). Downstream determinants of pulsatility of the mean velocity waveform in the umbilical artery as predicted by a computer model. *Ultrasound in Med. & Biol.*, **22**, 707–717.

[Szentkuti *et al.*(1995)] Szentkuti, A., Capper, W., Wright, A., Norman, K., and Odendaal, H. (1995). The high resistance state index: a new method to assess fetal compromise in absent end diastolic umbilical arterial flow. *J. Matern. Fetal Invest.*, **5**, 244–249.

[Takechi *et al.*(1993)] Takechi, K., Kuwabara, Y., and Mizuno, M. (1993). Ultrastructural and immunohistochemical studies of wharton's jelly umbilical cord cells. *Placenta*, **14**, 235–245.

[Tarbell and Samuels(1973)] Tarbell, J. M. and Samuels, M. R. (1973). Momentum and heat transfer in helical coils. *Chem. Engng J.*, **5**, 117–127.

[Taylor(1959)] Taylor, M. (1959). The influence of the anomalous viscosity of blood upon its oscillatory flow. *Phys. med. biol.*, **3**, 273–290.

[Taylor(1965)] Taylor, M. (1965). Wave travel in a non-uniform transmission line, in relation to pulses in arteries. *Phys. med. biol.*, **10**, 539–550.

[Taylor(1966)] Taylor, M. G. (1966). The input impedance of an assembly of randomly branching elastic tubes. *Biophys J*, **6**, 29–51.

[Theron and Thompson(1995)] Theron, G. B. and Thompson, M. L. (1995). A centile chart for birth weight for an urban population of the western cape. *S Afr Med J*, **85**, 1289–1292.

[Thompson and Stevens(1989)] Thompson, R. and Stevens, R. (1989). Mathematical model for interpretation of doppler velocity waveform indices. *Med. & Biol. Eng. & Comput.*, **27**, 269–276.

[Thompson and Trudinger(1990)] Thompson, R. and Trudinger, B. (1990). Doppler waveform pulsatility index and resistance pressure and flow in the umbilical placental circulation: An investigation using a mathematical model. *Ultrasound in Med. & Biol.*, **16**, 449–458.

[Thompson *et al.*(1986)] Thompson, R., Trudinger, B., and Cook, C. (1986). A comparison of doppler ultrasound waveform indices in the umbilical artery–i. indices derived from the maximum velocity waveform. *Ultrasound Med Biol.*, **12**, 835–844.

[Thompson *et al.*(1985)] Thompson, R. S., Trudinger, B. J., and Cook, C. M. (1985). Doppler ultrasound waveforms in the fetal umbilical artery: quantitative analysis technique. *Ultrasound Med Biol*, **11**, 707–718.

[Thompson *et al.*(1988)] Thompson, R. S., Trudinger, B. J., Cook, C. M., and Giles, W. B. (1988). Umbilical artery velocity waveforms: normal reference values for a/b ratio and pourcelot ratio. *Br J Obstet Gynaecol*, **95**, 589–591.

[Todros *et al.*(1992)] Todros, T., Guiot, C., and Pianta, P. (1992). Modelling the feto-placental circulation: 2. a continuous approach to explain normal and abnormal flow velocity waveforms in the umbilical arteries. *Ultrasound in Med. & Biol.*, **18**, 545–551.

[Todros *et al.*(1993)] Todros, T., Sciarrone, A., Pianta, P., and Guiot, C. (1993). Prediction of the umbilical artery flow velocity waveforms by modeling the feto-placental circulation. *J. Maternal-Fetal Invest.*, **3**(3), 178.

[Tonge *et al.*(1986)] Tonge, H. M., Wladimiroff, J. W., Noordam, M. J., and van Kooten, C. (1986). Blood flow velocity waveforms in the descending fetal aorta: comparison between normal and growth-retarded pregnancies. *Obstet Gynecol*, **67**, 851–855.

[Topakoglu(1967)] Topakoglu, H. (1967). Steady laminar flows of an incompressible viscous fluid in curved pipes. *J. Math. mech*, **16**, 1321–1328.

[Toubas *et al.*(1981)] Toubas, P., Silverman, N., Heymann, M., and Rudolph, A. (1981). Cardiovascular effects of acute hemorrhage in fetal lambs. *Am. J. Physiol (Heart Circ. Physiol.)*, **240**, H45–H48.

[Toy *et al.*(1985)] Toy, S. M., Melbin, J., and Noordergraaf, A. (1985). Reduced models of arterial systems. *IEEE Trans Biomed Eng*, **32**, 174–176.

[Trudinger *et al.*(1987)] Trudinger, B., Stevens, D., Connelly, A., Hales, J., Alexander, G., Bradley, L., Fawcett, A., and Thompson, R. (1987). Umbilical artery flow velocity waveform and placental resistance: The effects of embolization of the umbilical circulation. *Am. J. Obstet. Gynecol.*, **157**, 1443–1448.

[Truesdell and Adler(1970)] Truesdell, L. C. and Adler, R. J. (1970). Numerical treatment of fully developed laminar flow in helically coiled tubes. *AIChE J.*, **16**, 1010–1015.

[Tsangaris and Drikakis(1989)] Tsangaris, S. and Drikakis, D. (1989). Pulsating blood flow in an initially stressed, anisotropic elastic tube: linear approximation of pressure waves. *Med Biol Eng Comput*, **27**, 82–88.

[Van Den Wijngaard *et al.*(1988)] Van Den Wijngaard, J. A., Van Eyck, J., and Wladimiroff, J. W. (1988). The relationship between fetal heart rate and doppler blood flow velocity waveforms. *Ultrasound Med Biol*, **14**, 593–597.

[Van Lierde *et al.*(1984)] Van Lierde, M., Oberweis, D., and Thomas, K. (1984). Ultrasonic measurement of aortic and umbilical blood flow in the human fetus. *Obstet Gynecol*, **63**, 801–805.

[van Vugt *et al.*(1987)] van Vugt, J., Ruissen, C., Hoogland, H., and de Haan, J. (1987). Prospective study of velocity waveforms in the fetal descending thoracic and abdominal aorta in fetuses appropriate for gestational age and in growth-retarded fetuses. *Gynecol Obstet Invest.*, **24**(1), 14–22.

[VanDyke(1978)] VanDyke, M. (1978). Extended stokes series : Laminar flow through a loosely coiled pipe. *J. Fluid. Mech.*, **86**, 129–145.

[Veth(1976)] Veth, A. (1976). *Modelling the foetal circulation.* Ph.D. thesis, Free University, Amsterdam.

[Veth and van Bemmel(1978)] Veth, A. and van Bemmel, J. (1978). The role of the placental vascular bed in the fetal response to cord occlusion. In L. Longo and D. Reneau, editors, *Fetal and newborn cardiovascular physiology*, volume 1, pages 579–604. Garland, New York.

[Vieyres *et al.*(1991)] Vieyres, P., Durand, A., Patat, F., Descamps, P., Gregoire, J. M., Pourcelot, D., and Pourcelot, L. (1991). Influence of the measurement location on the resistance index in the umbilical arteries: a hemodynamic approach. *J Ultrasound Med*, **10**, 671–675.

[Wang and Tarbell(1992)] Wang, D. and Tarbell, J. (1992). Nonlinear analysis of flow in an elastic tube (artery): steady streaming effects. *J. Fluid mech.*, **239**, 341–358.

[Wang and Tarbell(1995)] Wang, D. M. and Tarbell, J. M. (1995). Nonlinear analysis of oscillatory flow, with a nonzero mean, in an elastic tube artery. *J Biomech Eng*, **117**, 127–135.

[Watson(1948)] Watson, G. (1948). *A treatise on the theory of bessel functions.* Cambridge university press, London, New York, Toronto, 2nd edition.

[Westerhof *et al.*(1969)] Westerhof, N., Frederik, B., Vries, C., and Noordegraaf, A. (1969). Analog studies of the human systemic arterial tree. *J. Biomech*, **2**, 121–143.

[Whirlow and Rouleau(1965)] Whirlow, D. K. and Rouleau, W. T. (1965). Periodic flow of a viscous liquid in a thick-walled elastic tube. *Bull Math Biophys*, **27**, 355–370.

[Wiener *et al.*(1966)] Wiener, F., Morkin, E., Skalak, R., and Fishman, A. (1966). Wave propagation in the pulmonary circulation. *Circ. Res.*, **19**, 834–850.

[Wiggert and Keitzer(1964)] Wiggert, D. and Keitzer, W. (1964). Pulsatile flow in cylindrical and tapered rubber tubing. *ASME paper no. 64 - WA/HUF-1.*

[Wigglesworth(1969)] Wigglesworth, J. (1969). Vascular anatomy of the human placenta and its significance for placental pathology. *J. Obstet. Gynaec. Brit. Cwlth.*, **76**, 979–989.

[Witzig(1914)] Witzig, K. (1914). Uber erzwungene wellenbewegungen zaher, inkompressibler flussigkeiten in elastichen rohern. *Inaug. diss. univ. bern. bern, wyss.*

[Wladimiroff *et al.*(1979)] Wladimiroff, J. W., Vosters, R., and Vletter, W. (1979). Ultrasonic measurement of fetal and neonatal ventricular dimensions. *Contrib Gynecol Obstet*, **6**, 109–114.

[Wolfson *et al.*(1977)] Wolfson, R. N., Zador, I. E., Pillay, S. K., Timor-tritsch, I. E., and Hertz, R. H. (1977). Antenatal investigation of human fetal systolic time intervals. *Am J Obstet Gynecol*, **129**, 203–207.

[Womersley(1955a)] Womersley, J. (1955a). Method for the calculation of velocity, rate of flow and viscous drag in arteries when the pressure gradient is known. *J. Physiol.*, **127**, 553–563.

[Womersley(1955b)] Womersley, J. (1955b). Oscillatory motion of a viscous liquid in a thin-walled elastic tube. i. the liinear approximation for long waves. *Phil. Mag.*, **46**, 199–221.

[Womersley(1957a)] Womersley, J. (1957a). The mathematical analysis of the arterial circulation in a state of oscillatory motion. *Wright air development center, technical report.*, pages WADC–TR56–614.

[Womersley(1957b)] Womersley, J. (1957b). Oscillatory flow in arteries: The reflection of the pulse wave at junctions and rigid inserts in the arterial system. *Phys. Med. Biol.*, **2**(178-187).

[Wosilait *et al.*(1992)] Wosilait, W. D., Luecke, R. H., and Young, J. F. (1992). A mathematical analysis of human embryonic and fetal growth data. *Growth Dev Aging*, **56**, 249–257.

[Yarlagadda *et al.*(1989)] Yarlagadda, P., Willoughby, L., and Maulik, D. (1989). Effect of fetal heart rate on umbilical arterial doppler indices. *J Ultrasound Med*, **8**, 215–218.

[Ye *et al.*(1993)] Ye, G. F., Moore, T. W., and Jaron, D. (1993). Incorporating vessel taper and compliance properties in navier-stokes based blood flow models. *Ann Biomed Eng*, **21**, 97–106.

[Zalosh and Nelson(1973)] Zalosh, R. G. and Nelson, W. (1973). Pulsating flow in a curved tube. *J. Fluid. Mech.*, **59**, 693–705.

[Zamir(1999)] Zamir, M. (1999). On fractal properties of arterial trees. *J. Theor. Biol*, **197**, 517–526.

[Zamir and Brown(1982)] Zamir, M. and Brown, N. (1982). Arterial branching in various parts of the cardiovascular system. *Am. J. Anat.*, **163**, 295–307.

[Zamir and Medeiros(1982)] Zamir, M. and Medeiros, J. (1982). Arterial branching in man and monkey. *J. Gen. Physiol.*, **79**, 353–360.

[Zamir *et al.*(1979)] Zamir, M., Medeiros, J., and Cunningham, T. (1979). Arterial bifurications in the human retina. *J. Gen. Physiol.*, **74**, 537–548.

[Zamir *et al.*(1983)] Zamir, M., Wrigley, S., and Langille, B. (1983). Arterial bifurications in the cardiovascular system of the rat. *J. Gen. Physiol.*, **81**, 325–335.

[Zapryanov and Matakiev(1980)] Zapryanov, Z. and Matakiev, V. (1980). An exact solution of the problem of unsteady fully-developed viscous flow in slightly curved porous tube. *Arch. Mech. (Poland)*, **32**, 461–474.

Appendix A

Equations for flow in curved elastic tubes

The governing equations for the fluid and tube motion, according to Chandran (1974), are :

Continuity equation :

$$\frac{\partial U}{\partial r'} + \frac{U}{r'} + \frac{1}{r'}\frac{\partial V}{\partial \psi} + \frac{U \sin\psi}{R + r' \sin\psi} + \frac{V \cos\psi}{R + r' \sin\psi} + \frac{1}{(R + r' \sin\psi)}\frac{\partial W}{\partial \theta} = 0 \qquad \text{(A.1)}$$

Momentum equations :

$$\rho\left\{\frac{\partial U}{\partial t} + U\frac{\partial U}{\partial r'} + \frac{V}{r'}\frac{\partial U}{\partial \psi} - \frac{V^2}{r'} + \frac{W}{R + r' \sin\psi}\frac{\partial U}{\partial \theta} - \frac{W^2 \sin\psi}{R + r' \sin\psi}\right\} =$$
$$-\frac{\partial P}{\partial r'} + \mu\left\{\frac{\partial^2 U}{\partial r'^2} + \frac{1}{r'}\frac{\partial U}{\partial r'} + \frac{1}{r'^2}\frac{\partial^2 U}{\partial \psi^2} + \frac{\sin\psi}{R + r' \sin\psi}\frac{\partial U}{\partial r'} + \frac{1}{(R + r' \sin\psi)^2}\frac{\partial^2 U}{\partial \theta^2} + \right.$$
$$\frac{\cos\psi}{r'(R + r' \sin\psi)}\frac{\partial U}{\partial \psi} - \frac{U}{r'^2} - \frac{U \sin^2\psi}{(R + r' \sin\psi)^2} - \frac{2}{r'^2}\frac{\partial V}{\partial \psi} - \frac{V \sin\psi \cos\psi}{(R + r' \sin\psi)^2}$$
$$\left. - \frac{V \cos\psi}{r'(R + r' \sin\psi)} - \frac{2 \sin\psi}{(R + r' \sin\psi)^2}\frac{\partial W}{\partial \theta}\right\} \qquad \text{(A.2)}$$

$$\rho\left\{\frac{\partial V}{\partial t} + U\frac{\partial V}{\partial r'} + \frac{UV}{r'} + \frac{V}{r'}\frac{\partial U}{\partial \psi} + \frac{W}{R + r' \sin\psi}\frac{\partial V}{\partial \theta} - \frac{W^2 \cos\psi}{R + r' \sin\psi}\right\} =$$
$$-\frac{1}{r'}\frac{\partial P}{\partial \psi} + \mu\left\{\frac{2}{r'^2}\frac{\partial^2 U}{\partial \psi^2} - \frac{U \sin\psi \cos\psi}{(R + r' \sin\psi)^2} + \frac{U \cos\psi}{r'(R + r' \sin\psi)} + \frac{\partial^2 V}{\partial r'^2} + \frac{1}{r'}\frac{\partial V}{\partial r'} + \right.$$
$$\frac{1}{r'^2}\frac{\partial^2 V}{\partial \psi^2} + \frac{\sin\psi}{R + r' \sin\psi}\frac{\partial V}{\partial r'} + \frac{1}{(R + r' \sin\psi)^2}\frac{\partial V}{\partial \theta^2} + \frac{\cos\psi}{r'(R + r' \sin\psi)}\frac{\partial V}{\partial \psi} - \frac{V}{r'^2} -$$
$$\left. \frac{V \cos^2\psi}{(R + r' \sin\psi)^2} - \frac{2 \cos\psi}{(R + r' \sin\psi)^2}\frac{\partial W}{\partial \theta}\right\} \qquad \text{(A.3)}$$

$$\rho\left\{\frac{\partial W}{\partial t}+U\frac{\partial W}{\partial r'}+\frac{V}{r'}\frac{\partial W}{\partial \psi}+\frac{UW\sin\psi}{R+r'\sin\psi}+\frac{VW\cos\psi}{R+r'\sin\psi}+\frac{W}{R+r'\sin\psi}\frac{\partial W}{\partial \theta}\right\}=$$
$$-\frac{1}{(R+r'\sin\psi)}\frac{\partial P}{\partial\theta}+\mu\left\{\frac{2\sin\psi}{(R+r'\sin\psi)^2}\frac{\partial U}{\partial\theta}+\frac{2\cos\psi}{(R+r'\sin\psi)^2}\frac{\partial V}{\partial\theta}+\frac{\partial^2 W}{\partial r'^2}+\frac{1}{r'}\frac{\partial W}{\partial r'}+\right.$$
$$\left.\frac{1}{r'^2}\frac{\partial^2 W}{\partial\psi^2}+\frac{\sin\psi}{R+r'\sin\psi}\frac{\partial W}{\partial r'}+\frac{1}{(R+r'\sin\psi)^2}\frac{\partial^2 W}{\partial\theta^2}+\frac{\cos\psi}{r'(R+r'\sin\psi)}\frac{\partial W}{\partial\psi}-\frac{W}{(R+r'\sin\psi)^2}\right\} \tag{A.4}$$

In the above, W is the axial (θ) velocity, U is the radial (r') velocity and V is the tangential (ψ) velocity. The axial pressure gradient is $\frac{\partial P}{\partial\theta}$ and is assumed independent of r', θ and ψ in fully developed flow. μ is the viscosity and ρ the density.

The equations of motion for the tube wall are :

$$\rho_t h_t\frac{\partial^2\eta}{\partial t^2}=\left[P-2\mu\frac{\partial U}{\partial r'}\right]_{r'=a}-\left[\frac{h_t E}{R+a\sin\psi}\right]\left[\frac{1}{(1-\sigma^2)}\right]\left[\frac{\left(\eta\sin\psi+\xi\cos\psi+\frac{\partial\zeta}{\partial\theta}\right)}{R+a\sin\psi}+\right.$$
$$\left.\sigma\left(\frac{\eta}{a}+\frac{1}{a}\frac{\partial\zeta}{\partial\psi}\right)\right]-\left[\frac{h_t E}{a(1-\sigma^2)}\right]\left[\frac{\eta}{a}+\frac{1}{a}\frac{\partial\xi}{\partial\psi}+\frac{\sigma\left(\eta\sin\psi+\xi\cos\psi+\frac{\partial\zeta}{\partial\theta}\right)}{R+a\sin\psi}\right] \tag{A.5}$$

$$\rho_t h_t\frac{\partial^2\xi}{\partial t^2}=-\mu\left[\frac{1}{r'}\frac{\partial U}{\partial\psi}-\frac{V}{r'}+\frac{\partial V}{\partial r'}\right]_{r'=a}+\frac{h_t E}{a(1-\sigma^2)}\left[\frac{1}{a}\frac{\partial\eta}{\partial\psi}+\frac{1}{a}\frac{\partial^2\xi}{\partial\psi^2}\right]+$$
$$\left[\frac{\sigma h_t E}{a(1-\sigma^2)}\right]\left[\frac{\eta\cos\psi+\sin\psi\frac{\partial\eta}{\partial\psi}+\frac{\partial\xi}{\partial\psi}\cos\psi-\xi\sin\psi+\frac{\partial^2\zeta}{\partial\psi\partial\theta}}{R+a\sin\psi}-\right.$$
$$\left.\frac{a\left(\eta\sin\psi+\xi\cos\psi+\frac{\partial\zeta}{\partial\theta}\right)\cos\psi}{(R+a\sin\psi)^2}\right]+\left[\frac{h_t G}{R+a\sin\psi}\right]\times\left[\frac{1}{a}\frac{\partial^2\zeta}{\partial\theta\partial\psi}+\frac{1}{R+a\sin\psi}\left(\frac{\partial^2\zeta}{\partial\theta^2}-\frac{\partial\zeta}{\partial\theta}\right)\cos\psi\right] \tag{A.6}$$

$$\{M_0+\rho_t h_t\}\frac{\partial^2\zeta}{\partial t^2}+k_s\zeta=-\mu\left[\frac{1}{R+a\sin\psi}\frac{\partial U}{\partial\theta}-\frac{W\sin\psi}{R+a\sin\psi}+\frac{\partial W}{\partial r'}\right]_{r'=a}+\left[\frac{h_t}{R+a\sin\psi}\right]\left[\frac{E}{1-\sigma^2}\right]\times$$
$$\left[\frac{\frac{\partial\eta}{\partial\theta}\sin\psi+\frac{\partial\xi}{\partial\theta}\cos\psi+\frac{\partial^2\zeta}{\partial\theta^2}}{R+a\sin\psi}+\frac{\sigma}{a}\left(\frac{\partial\eta}{\partial\theta}+\frac{\partial^2\zeta}{\partial\psi\partial\theta}\right)\right]+\frac{hG}{a}\left[\frac{1}{a}\frac{\partial^2\zeta}{\partial\psi^2}+\frac{\left(\frac{\partial^2\zeta}{\partial\psi\partial\theta}+\zeta\sin\psi-\cos\psi\frac{\partial\zeta}{\partial\psi}\right)}{R+a\sin\psi}\right]-$$
$$\frac{hG}{a}\frac{\left(\frac{\partial\zeta}{\partial\theta}-\zeta\cos\psi\right)a\cos\psi}{(R+a\sin\psi)^2} \tag{A.7}$$

In these equations a is the undisturbed radius of the tube, h_t is the tube thickness, η, ζ and ξ are the r', ψ and θ tube displacement components respectively. E is the modulus of elasticity, σ is Poisson's ratio, k_s is the spring constant and ρ_t is the density of the tube material.

Chandran performed an order of magnitude study to eliminate the nonlinear terms. The quasi-linearized and simplified equations for the fluid are :

Continuity equation :

$$\frac{\partial U}{\partial r'} + \frac{U}{r'} + \frac{1}{r'}\frac{\partial V}{\partial \psi} + \frac{U \sin\psi}{R + r' \sin\psi} + \frac{V \cos\psi}{R + r' \sin\psi} + \frac{1}{(1 + r'/R \sin\psi)}\frac{\partial W}{\partial \theta} = 0 \tag{A.8}$$

Momentum equations :

$$\frac{\partial U}{\partial t} - \frac{W^2 \sin\psi}{R + r' \sin\psi} = -\frac{1}{\rho}\frac{\partial P}{\partial r'} + \nu \left\{ \frac{\partial^2 U}{\partial r'^2} + \frac{1}{r'}\frac{\partial U}{\partial r'} + \frac{1}{r'^2}\frac{\partial^2 U}{\partial \psi^2} - \frac{V \cos\psi}{r'(R + r' \sin\psi)} - \frac{2 \sin\psi}{(R + r' \sin\psi)^2}\frac{\partial W}{\partial \theta} + \frac{\sin\psi}{R + r' \sin\psi}\frac{\partial U}{\partial r'} + \frac{\cos\psi}{r'(R + r' \sin\psi)}\frac{\partial U}{\partial \psi} - \frac{U}{r'^2} - \frac{2}{r'^2}\frac{\partial V}{\partial \psi} \right\} \tag{A.9}$$

$$\frac{\partial V}{\partial t} - \frac{W^2 \cos\psi}{R + r' \sin\psi} = -\frac{1}{\rho}\frac{1}{r'}\frac{\partial P}{\partial \psi} + \nu \left\{ \frac{\partial^2 V}{\partial r'^2} + \frac{1}{r'}\frac{\partial V}{\partial r'} + \frac{2}{r'^2}\frac{\partial^2 U}{\partial \psi^2} + \frac{U \cos\psi}{r'(R + r' \sin\psi)} + \frac{\sin\psi}{R + r' \sin\psi}\frac{\partial V}{\partial r'} + \frac{\cos\psi}{r'(R + r' \sin\psi)}\frac{\partial V}{\partial \psi} + \frac{1}{r'^2}\frac{\partial^2 V}{\partial \psi^2} - \frac{V}{r'^2} \right\} \tag{A.10}$$

$$\frac{\partial W}{\partial t} = -\frac{1}{\rho}\frac{1}{(1 + r'/R \sin\psi)}\frac{\partial P}{\partial \theta} + \nu \left\{ \frac{\partial^2 W}{\partial r'^2} + \frac{1}{r'}\frac{\partial W}{\partial r'} + \frac{1}{r'^2}\frac{\partial^2 W}{\partial \psi^2} + \frac{\sin\psi}{R + r' \sin\psi}\frac{\partial W}{\partial r'} + \frac{\cos\psi}{r'(R + r' \sin\psi)}\frac{\partial W}{\partial \psi} \right\} \tag{A.11}$$

For the tube equations, Morgan and Kiely (1955) showed in an order of magnitude study that the inertial stress terms may be neglected for small values of h_t/a and a/l. Where l is the wavelength.

Appendix B

Struve's function

Struve's function may be determined according to

$$\mathrm{H}_{v}(z)=\sum_{r=0}^{\infty}(-1)^{r}\frac{\left(\frac{1}{2}z\right)^{v+2r+1}}{\Gamma\left(r+\frac{3}{2}\right)\Gamma\left(v+r+\frac{3}{2}\right)} \tag{B.1}$$

For small v and z these usually converge quite rapidly.

$\Gamma(x)$ is the Gamma function and is

$$\Gamma(x)=\int_{0}^{\infty}t^{x-1}e^{-t}dt \tag{B.2}$$

This may be evaluated easily for the Struve function, using the formula

$$\Gamma\left(x+\frac{1}{2}\right)=\frac{1\cdot 3\cdot 5\cdots(2x-1)}{2^{x}}\sqrt{\pi} \tag{B.3}$$

where x is an integer.

Appendix C

Modified Bessel functions of complex argument and order

The modified Bessel function of the first kind of order v and argument z is given by :

$$I_v(z) = \sum_{r=0}^{\infty} \frac{\left(\frac{1}{2}z\right)^{v+2r}}{r!\Gamma(v+r+1)} \tag{C.1}$$

where both v and z may be complex variables. $\Gamma(x)$ is the Gamma function and for complex variables may be evaluated using

$$\frac{1}{\Gamma(x)} = xe^{\gamma x} \prod_{m=1}^{\infty} \left(\left(1+\frac{x}{m}\right)e^{-x/m}\right) \tag{C.2}$$

where $\gamma = 0.5772156649$ and is the Euler constant.

However, this requires a very large number of product terms to converge and a far more efficient means of evaluating the Gamma function was provided by Lanczos (Press et al. 1989) and is :

$$\Gamma(x+1) = \left(x+m+\frac{1}{2}\right)^{x+\frac{1}{2}} e^{-\left(x+m+\frac{1}{2}\right)}\sqrt{2\pi}\left(c_0 + \frac{c_1}{x+1} + \frac{c_2}{x+2} + \cdots + \frac{c_N}{x+N} + \epsilon\right) \tag{C.3}$$

For $m = 5$ and $N = 6$, the error is smaller than $|\epsilon| < 2 \times 10^{-10}$.

Here $c_0 = 1$, $c_1 = 76.18009173$, $c_2 = 24.01409822$, $c_3 = -1.231739516$, $c_4 = 0.120858003 \times 10^{-2}$ and $c_5 = -0.536382 \times 10^{-5}$.

Appendix D

Matlab^{TM} and Simulink^{TM} code

The Simulink^{TM} interface allowed basic model building blocks to be developed and graphically pieced together to construct the complete foetal model. The graphical flow diagram used in Simulink^{TM} to represent the overall foetal model and each component of this model will be presented in this Appendix. Subsequently, the Matlab^{TM} routines that contain the algorithms that link the Simulink^{TM} blocks together will be presented. Physical and anatomic variables are entered in the *physical properties* blocks of each arterial block. Further variables are entered via the main Matlab routine which first initialises variables and then calls the Simulink programme. A simple Simulink *to workspace* block may be placed at any point in each of the arterial blocks to send parameters to the main routine for subsequent processing. These *to workspace* blocks have not been included in the layouts depicted in this Appendix as they were included in the model when necessary to obatin relevant parameters (e.g. input impedance) and then removed. The model routines as presented here are for the healthy foetus and subsequent alterations to the code were necessary in order to simulate any pathalogical changes. These alterations will be discussed at the end of the Appendix, once the Matlab m files have been presented.

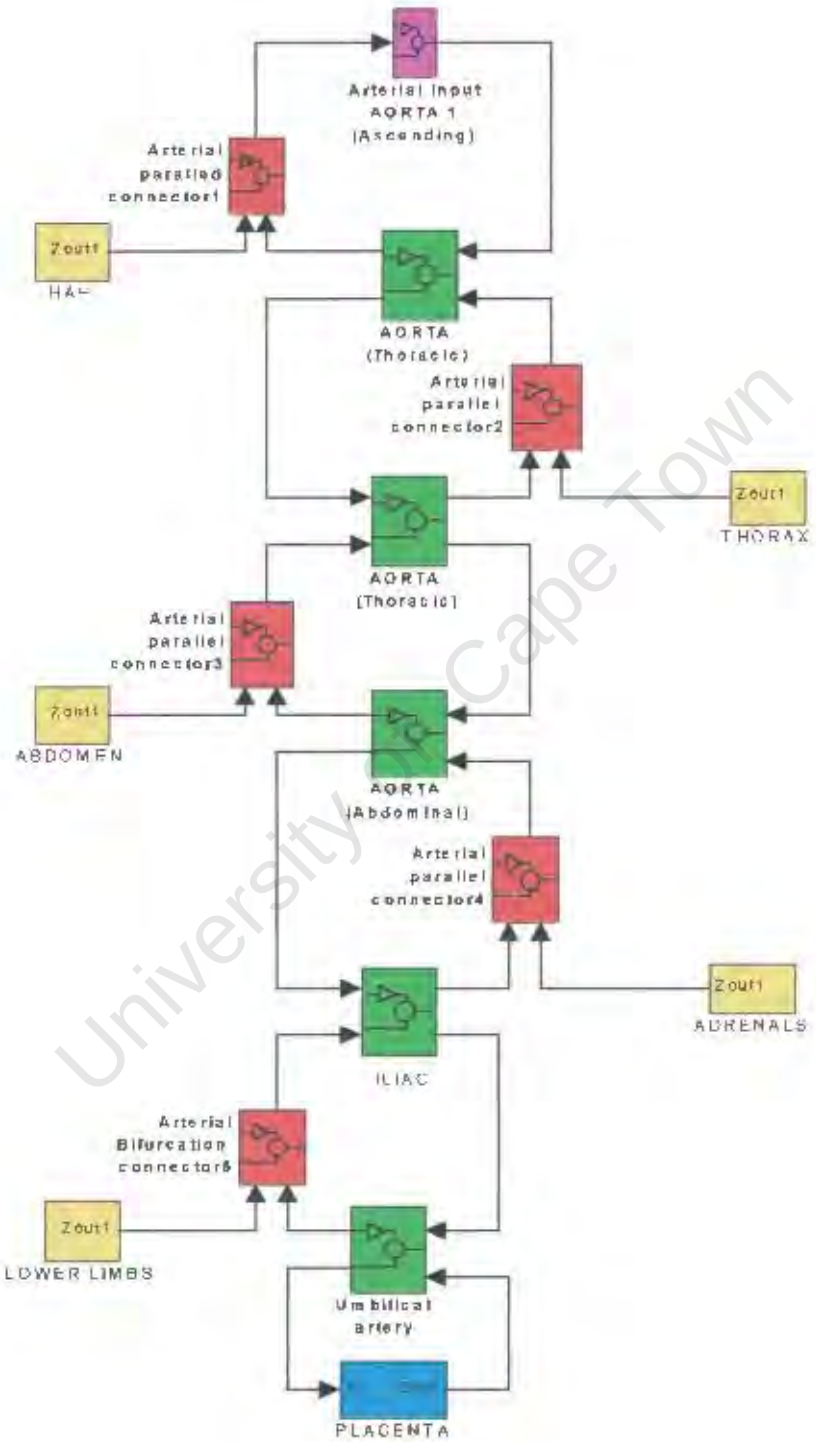

Figure D.1: Simulink system diagram of foetal model.

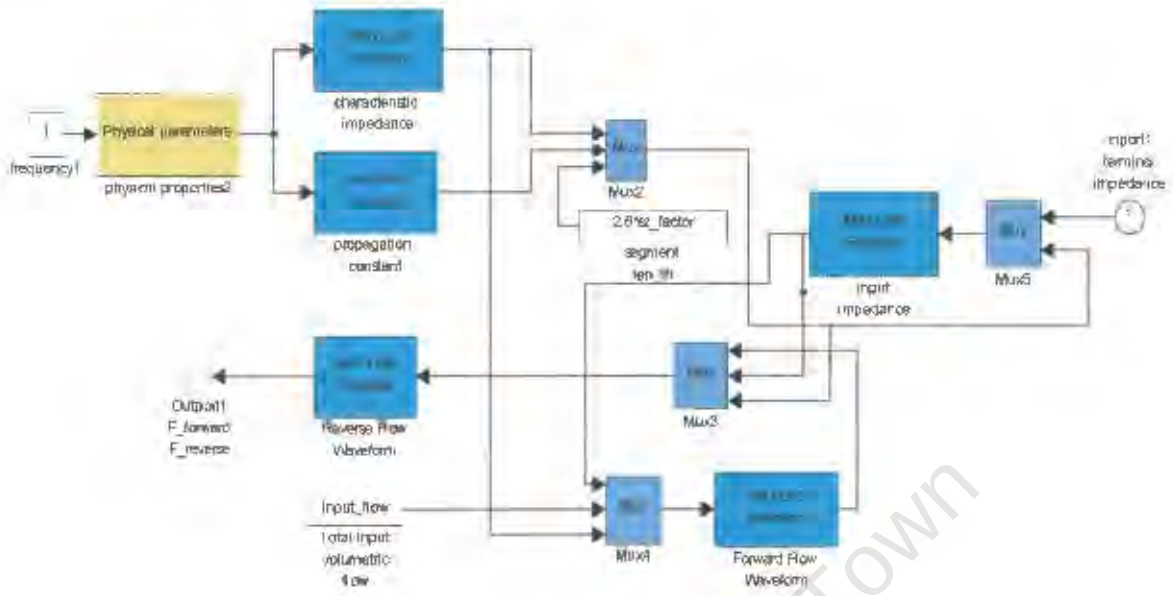

Figure D.2: Arterial Input : Ascending aorta. 1 input (input flow from the heart). 1 output (forward and reverse flow waveforms at terminal end of artery)

D.0.3 Matlab^{TM} code for simulink blocks

Function for calculating the characteristic impedance or steady flow resistance

of a non-tapered and non-coiled arterial segment **function z0 = Z_0(u);** % Transmission line model building block Z_0 characteristic Impedance

```
%
% z0 = Z_0(u);
%
% Takes the simulink vector u consisting of :
% c (complex wave speed), m (model factor) and r (arterial radius)
%Calculates either the steady flow resistance or the characteristic impedance
% of the arterial segment
global omega rho mu mu;
c = u(1);
m = u(2);
r = u(3);
if (omega == 0),
 z0 = 8*mu/pi/r^4;
else
 F10 = F_10(omega, mu, r);
 z0 = rho*c/(1+m*F10)/(pi*r^2);
end
```

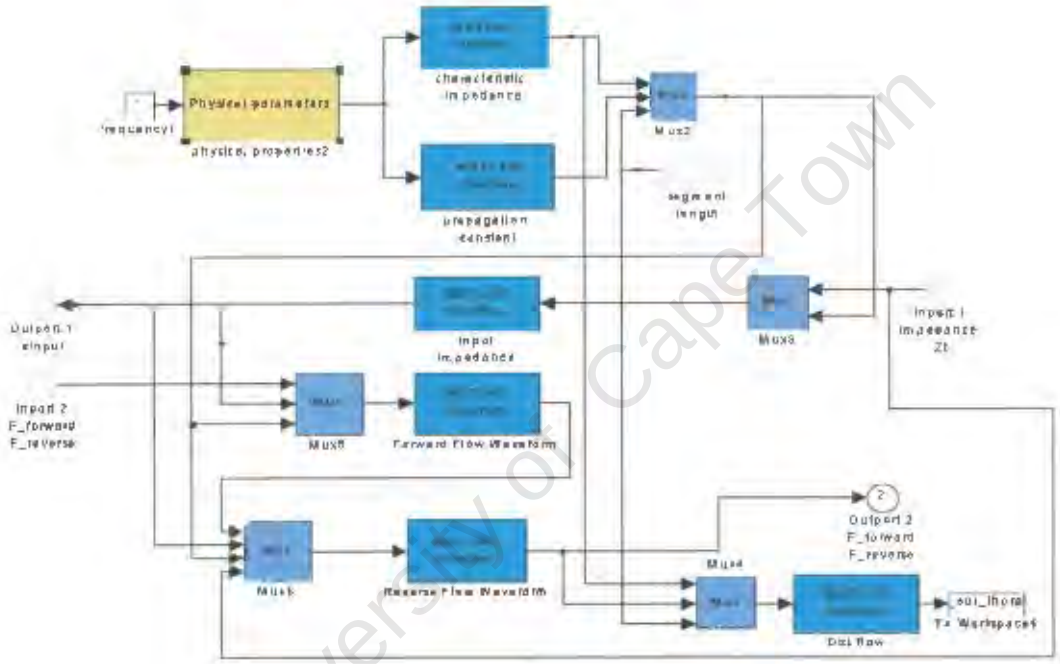

Figure D.3: Tapered arterial segment. 2 inputs (forward and reverse waveform from proximal segment and terminal impedance from distal segment). 2 outputs (Input impedance of segment and forward and reverse waveforms at terminal end of segment).

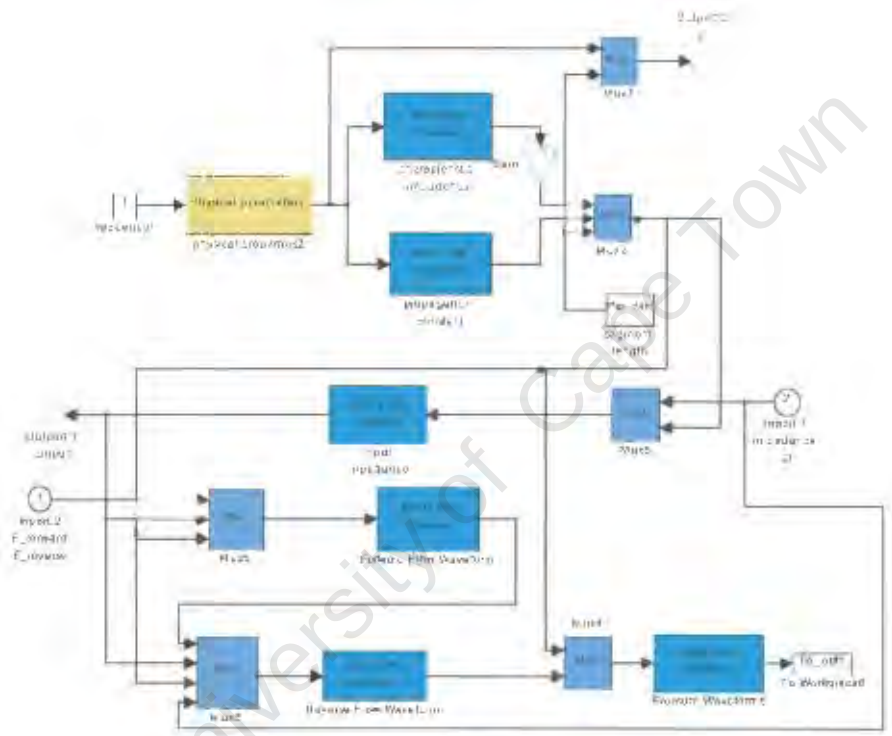

Figure D.4: Umbilical arteries : 2 inputs (forward and reverse waveforms of proximal segment and terminal impedance of distal segment). 2 outputs : Input impedance of segment and radius and length variables to send to placenta)

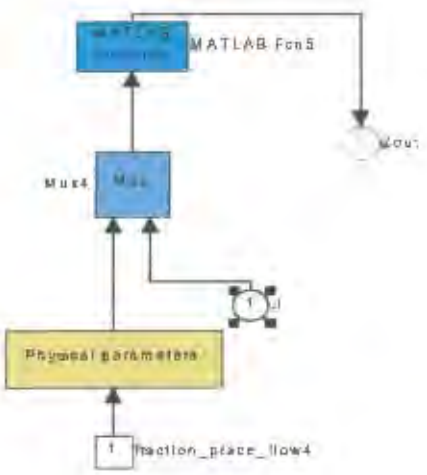

Figure D.5: Placenta. 1 Input. (radius and length of umbilical arteries). 1 Output (input impedance of placenta).

Figure D.6: Peripheral arterial network block : 1 output (input impedance of the network).

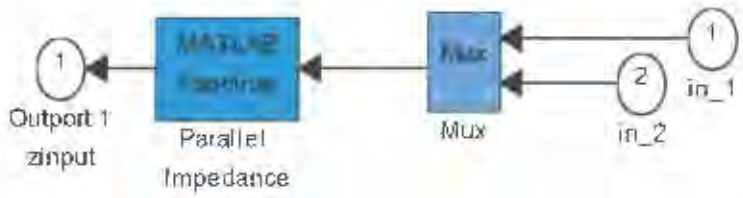

Figure D.7: Parallel connector. 2 inputs (impedances from two downstream sources), 1 output (combined parallel impedance of the two inputs)

Function for calculating the characteristic impedance or steady flow resistance
and characteristic impedance tapering constant for a non-coiled tapered arterial segment

```
function [z0] = Z_0_taper(u);
% Transmission line model building block Z_0_taper = characteristic Impedance
%
% z0] = Z_0_taper(u);
%
% Takes a simulink vector u, consisting of :
% ci (initial complex wavespeed), mi (initial model factor), ci (initial complex wavespeed),
% cf (final complex wavespeed), mf (final model factor), cf (final complex wavespeed),
% len (length of arterial segment)
% includes DC tapering by first working out the tapering constant from the
% start and finish radii
% For oscillatory tapering, instead of returning Z0, the tapering constant and the initial Z0 are
% returned so that Z0 may be calculated at any point
global omega rho nu mu;
ci = u(1);
mi = u(2);
ri = u(3);
cf = u(4);
mf = u(5);
rf = u(6);
len = u(7);
if (omega == 0),
 p = -log(rf/ri)/len;
 if p == 0,
 z0 = [8*mu/pi/ri^4*len 0];
 else z0 = [2*mu/pi*(exp(4*p*len)-1)/ri^4/p 0];
 end

else
 F10i = F_10(omega, nu, ri);
 F10f = F_10(omega, nu, rf);
```

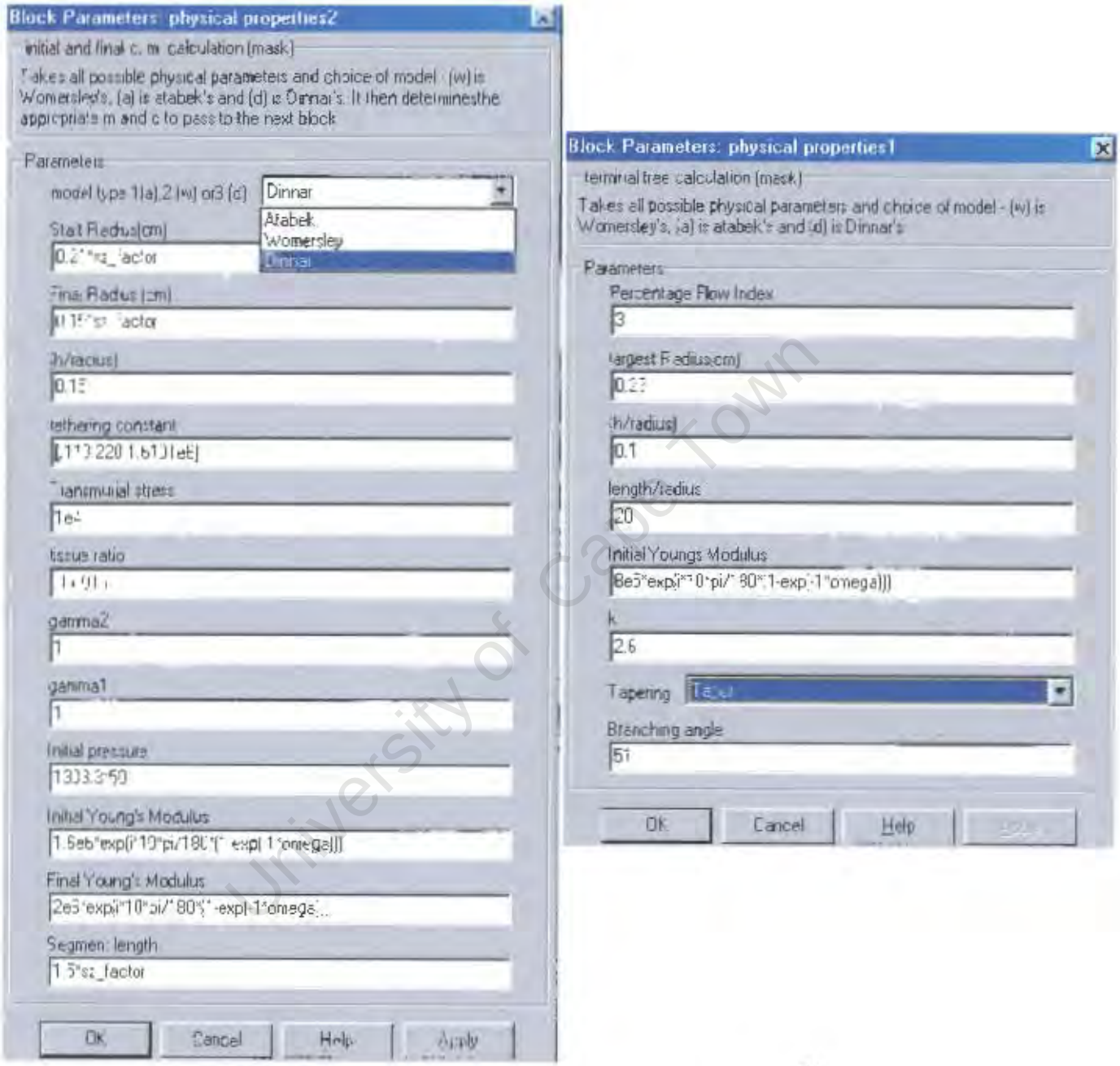

Figure D.8: Drop down menus for *physical parameters* blocks. (a) menu for a tapered arterial segment. The non-tapered segments are identical except they do not have space for the final radius and Young's modulus. (b) menu for a peripheral arterial tree.

```
z0 = rho*ci/(1+mi*F10i)/(pi*ri^2); % initial Z0
z0f = rho*cf/(1+mf*F10f)/(pi*rf^2); % final Z0

% Fit an exponential to the initial and final Z0
k = log(z0f/z0)/len;
z0 = [z0 k];
end
```

Function for calculating the characteristic impedance or steady flow resistance for a non-tapered, coiled arterial segment (umbilical artery)

```
function z0 = Z_0_umb(u);
% Transmission line model building block Z_0_umb = umbilical arterial characteristic Impedance
%
% ZL = Z_L(omega, r, nu, rho,m)
%
% Takes the simulink vector u consisting of :
% c (complex wave speed), m (model factor) and r (arterial radius)
% also uses the global variable wmean as an estimate for the mean flow for the Dean no.
% Calculates either the steady flow resistance or the characteristic impedance
% of the coiled arterial segment
global omega rho nu mu wmean sz_factor tmp_var
c = u(1);
m = u(2);
r = u(3);
Rc = r + .2*sz_factor; % adjust umbilical vein radius for growth as well
coilingindex = 0.25;
h = 1/coilingindex; % pitch
R = Rc*(1+(h/2/pi/r)^2); % effective radius of curvature
lambda = r/R;
if (omega == 0),
 Dn = 2*r*wmean/mu*rho*sqrt(lambda); % Dean number
 if Dn < 20,
 mm = 2;
 elseif Dn > 40,
 mm = 0;
 else mm = 1;
 end

 fc = 1/sqrt(1-.18/sqrt(1+(35/Dn)^2)^mm+(1+lambda/3)^2*Dn/88.33);
 z0 = 8*mu/pi/r^4/fc; % adjust z0 for curvature
else
 F10 = F_10(omega, nu, r);
 z0 = rho*c/(1+m*F10)/(pi*r^2);
 % adjust for curvature
 alpha0 = sqrt(i^3*r.^2.*omega/nu);
 z0 = rho*c/r^2/(pi*(1+m*F10)+r/R*m*r/alpha0*(-2*r/pi*besselj(1,alpha0)/besselj(0,alpha0) +
...
```

```
 (1/besselj(1,alpha0)+r/alpha0/besselj(0,alpha0))*...
 (besselj(1,alpha0)*struveh(0,alpha0)-besselj(0,alpha0)*struveh(1,alpha0))));
end
```

Function to calculate Struve's function for use with Z_0_umb

```
function out = struveh(v,z)
% Function to calculate Struve polynomials of order order v and argument z
%
% out = struveh(v,z)
r = [0:1:100];
if size(z) == [1 1],
 sumz = ((-1).^r).*((0.5*z).^(v+2*r+1))./(gamma(r+3/2).*gamma(v+r+3/2));
 out = sum(sumz);
else
 for a = 1:length(z),
 sumz = ((-1).^r).*((0.5*z(a)).^(v+2*r+1))./(gamma(r+3/2).*gamma(v+r+3/2));
 out(a) = sum(sumz);
 end
end
```

Function for calculating the propagation constant of a non-tapered arterial segment

```
function gamma = prop_const(u);
% Transmission line model building block prop_const = complex propagation constant
%
% gamma = prop_const(u);
%
% Takes simulink vector u consisting of :
% c (complex wave speed), m (m value from flow model), r (radius of segment)
% Returns the complex propagation constant for the vessel segment
global omega;
c = u(1);
m = u(2);
r = u(3);
if (omega == 0),
 gamma = 0;
else
 gamma = i*omega/c;
end
```

Function for calculating the propagation constant of a tapered arterial segment

```
function [gamma] = prop_const_taper(u);
% Transmission line model building block prop_const = complex propagation constant
%
% [gamma, q] = prop_const_taper(u);
%
% Uses omega (frequency) and c (model dependent wave speed)
```

```
% Returns the complex initial propagation constant for the tapered vessel segment
% as well as the tapering constant, q
global omega;
ci = u(1);
mi = u(2);
ri = u(3);
cf = u(4);
mf = u(5);
rf = u(6);
len = u(7);
if (omega == 0),
 gamma = [0 0];
else
 gamma = i*omega/ci;
 gammaf = i*omega/cf;

 % Fit an exponential to the initial and final gamma
 q = -log(gammaf/gamma)/len;
 gamma = [gamma q];
end
```

Function for calculating the input resistance or impedance of a non-tapered arterial segment

```
function zin = sim_inp_imped(u);
% Transmission line model building block Zin = Input Impedance
%
% zin = sim_inp_imped(u);
%
% Uses the simulink vector u, consisting of :
% Zt (Terminal inpedance from next block), Z0 (characteristic impedance),
% gamma (complex propagation constant) and l (vessel segment length)
% Returns the input impedance or resistance for the vessel segment
global omega mu;
Zt = u(1);
z0 = u(2);
gamma = u(3);
l = u(4);
if (omega == 0),
 zin = z0*l + Zt;
else
 zin = Zin(Zt,z0,gamma,l);
end
```

Function called by sim_inp_imped to calculate the actual impedances

```
function inp_imp = Zin(Zt,Z0,gamma,l);
% Transmission line model building block Zin = input impedance
%
```

```
% inp_imp = Zin(Zt, Z0, gamma, l);
%
% Takes Zt (terminal resistance), Z0 (characteristic impedance), gamma
% (propagation constant) and l (vessel length) as input parameters
% Returns The input impedance (Zin)
global omega
if omega == 0,
 inp_imp = Zt + Z0*l;
else
 inp_imp = Z0*( (Zt+Z0)*exp(gamma*l) + (Zt-Z0)*exp(-gamma*l) )/...
 ( (Zt+Z0)*exp(gamma*l) - (Zt-Z0)*exp(-gamma*l) );
end
```

Function for calculating the inpute resistance or impedance of a tapered arterial segment

```
function [zinoutput] = sim_inp_imped_taper(u);
% Transmission line model building block Zin = Input Impedance
%
% zinoutput = sim_inp_imped_taper(u);
%
% Uses the simulink vector u, consisting of :
% Zt (Terminal inpedance from next block), Z0 (characteristic impedance),
% k (characteristic impedance tapering constant), gamma (complex propagation constant),
% q (propagation constant tapering constant) and l (vessel segment length)
% Returns the input resistance or impedance for the tapered vessel segment
% as well as the constant xi for the unsteady harmonics - this is passed along
% to save computation time by not having to recalculate the bessel functions
global omega mu;
Zt = u(1);
z0 = u(2);
k = u(3);
gamma = u(4);
q = u(5);
l = u(6);
if (omega == 0),
 zin = z0 + Zt;
 xi = 1;
else
 z0f = z0*exp(k*l);
 % determine terminal reflection coefficient
 rhot = (Zt - z0f)/(Zt + z0f);
 h = k;
 bk1 = besselkc(.5*(h+q)/q,gamma/q*exp(-q*l));
 bk2 = besselkc(.5*(h+3*q)/q,gamma/q*exp(-q*l));
 bi1 = besselic(.5*(h+q)/q,gamma/q*exp(-q*l));
 bi2 = besselic(.5*(h+3*q)/q,gamma/q*exp(-q*l));

 bk3 = besselkc(.5*(h+q)/q,gamma/q);
 bk4 = besselkc(.5*(h+3*q)/q,gamma/q);
```

```
bi3 = besselic(.5*(h+q)/q,gamma/q);
bi4 = besselic(.5*(h+3*q)/q,gamma/q);
xi = -((-Zt*gamma + z0*exp(l*(h+q))*(h+q))*bk1 - z0*gamma*exp(l*h)*bk2)/...
((-Zt*gamma + z0*exp(l*(h+q))*(h+q))*bi1 + z0*gamma*exp(l*h)*bi2);


zin = z0/gamma*(h+q+gamma*(xi*bi4-bk4)/(xi*bi3+bk3));
abs(zin);
end
zinoutput(1) = zin;
zinoutput(2) = xi;
```

Function for calculating the forward flow waveform of the ascending aorta input

```
function fflow = f_flow(u);
% Transmission line model building block f_flow = forward flow waveform
%
% [fflow] = f_flow(u);
%
% For use with the initial arterial input into the aorta. Takes the simulink vector u consisting of :
% zin (input resistance or impedance), Tflow (total flow waveform) and z0 (characteristic impedance)
% Calculates the source reflection coefficient and thus
% Returns the forward flow waveform
global omega;
zin = u(1);
Tflow = u(2); % Total flow
z0 = u(3);
rho_s = (zin-z0)/(zin+z0);
fflow = Tflow/(1-rho_s);
if (omega == 0)
 fflow = [Tflow];
end
```

Function for calculating the forward flow waveform of a tapered arterial segment

```
function fflow = f_flow1_taper(u);
% Transmission line model building block f_flow1_taper = forward flow waveform for tapered arter-
ies
%
% [fflow1] = f_flow1_taper(u);
%
% For use with the tapered arteries. Takes the simulink vector u consisting of :
% ff (forward pressure waveform), fr (reverse pressure waveform), zin (input impedance),
% zeta (tapering input impedance constant), z0 (initial characteristic impedance),
% k (characteristic impedance tapering const), gamma ( initial propagation constant),
% q (propagation constant tapering constant), l (arterial length)
%
% Calculates the source reflection coefficient and thus
% Returns The forward flow waveform
% Differs to f_flow in that this must first combine the forward and reflected waves
```

```
% from the previous block into a total waveform
global omega;
ff = u(1);
fr = u(2);
zin = u(3);
zeta = u(4);
z0 = u(5);
k = u(6);
gamma = u(7);
q = u(8);
l = u(9);
% determine source reflection coefficient
rho_s = (zin-z0)/(zin+z0);
Tpres = ff+fr;
fpres = Tpres/(1+rho_s);
fflow = fpres/z0;
if (omega == 0)
 % here fr is actually the pressure at the terminal end of the previous artery
 fflow = [fr/zin];
end
```

Function for calculating the forward flow waveform of a non-tapered arterial segment

```
function fflow = f_flow1_umb(u);
% Transmission line model building block f_flow1_umb = forward flow waveform in umbilical artery
%
% fflow = f_flow1_umb(u);
%
% For use with the umbilical artery. Takes the simulink vector u consisting of :
% ff (forward pressure waveform), fr (reverse pressure waveform), zin (input impedance)
% z0 (characteristic impedance)
%
% Calculates the source reflection coefficient and thus
% Returns The forward flow waveform
% Differs to f_flow in that this must first combine the forward and reflected waves
% from the previous block into a total waveform
global omega;
ff = u(1);
fr = u(2);
zin = u(3);
z0 = u(4);
rho_s = (zin-z0)/(zin+z0);
Tpres = ff+fr;
fpres = Tpres/(1+rho_s);
fflow = fpres/z0;
if (omega == 0)
 fflow = [fr/zin];
end
```

Function for calculating the reverse flow waveform of a non-tapered arterial segment

```
function rfflow = r_flow(u);
% Transmission line model building block r_flow = reverse flow waveform
%
% rfflow = r_flow(u);
%
% Takes a simulink vecotr, u, consiting of :
% fflow (forward flow waveform), z0 (characteristic impedance),
% gamma (complex propagation constant), l (vessel segment length)
% Calculates the reverse flow waveform at the source and
% Returns the forward flow and reverse flow waveforms at the terminal end of the segment
% as a vector [fflow, rflow]
global omega;
fflow = u(1);
zin = u(2);
z0 = u(3);
gamma = u(4);
l = u(5);
if (omega == 0),
 % The final DC vector is [flow at terminal end; pressure at terminal end]
 pres_in = fflow*zin;
 pres_term = pres_in - fflow*z0*l;
 rfflow = [fflow pres_term];
else
 rho_s = (zin-z0)./(zin+z0);
 rflow = rho_s.*fflow;
 % refer to terminal end
 rfflow(1) = fflow*exp(-gamma*l)*z0;
 rfflow(2) = rflow*exp(gamma*l)*z0;
end
```

Function for calculating the reverse flow waveform of a tapered arterial segment

```
function rfflow = r_flow_taper(u);
% Transmission line model building block r_flow_taper = reverse flow waveform
%
% rfflow = r_flow_taper(u);
%
% Takes the simulink vector, u, consiting of :
% fflow (forward flow waveform), zin (input impedance), xi (tapering input impedance factor),
% z0 (characteristic impedance), k (characteristic impedance tapering constant),
% gamma (complex propagation constant), q (propagation constant tapering consatnt),
% l (vessel segment length), Zt (terminal impedance)
% Calculates the reverse flow waveform at the source and
% Returns the forward flow and reverse flow waveforms at the terminal end of the segment
% as a vector [fflow, rflow]
global omega;
fflow = u(1);
zin = u(2);
```

```
xi = u(3);
z0 = u(4);
k = u(5);
gamma = u(6);
q = u(7);
l = u(8);
Zt = u(9);
if (omega == 0),
 % The final DC vecotr is [flow at terminal end; pressure at terminal end]
 pres_in = fflow*zin;
 pres_term = pres_in - fflow*z0;
 rfflow = [fflow pres_term];
else
 z0f = z0*exp(k*l);
 % determine source reflection coefficient
 rho_s = (zin-z0)/(zin+z0);
 rflow = rho_s.*fflow;

 Qs = fflow - rflow; % total flow at the source end

 % split back into forward and reverse adjusted pressures at terminal end

 h = k;
if (h<1e-10)&(q<1e-10),
 rho_s = (zin-z0)./(zin+z0);
 rflow = rho_s.*fflow;

 % refer to terminal end
 rfflow(1) = fflow*exp(-gamma*l)*z0;
 rfflow(2) = rflow*exp(gamma*l)*z0;
else
 b1 = gamma./q.*exp(-q.*l);
 bi1 = besselic(.5*(h+q)/q,b1);
 bk1 = besselkc(.5*(h+q)/q,b1);
 b2 = gamma./q;
 bi2 = besselic(.5*(h+q)/q,b2);
 bk2 = besselkc(.5*(h+q)/q,b2);
 fl = xi*bi1+bk1;
 f0 = xi*bi2+bk2;
 Qtaper = exp(log(Qs) - 1/2*(h+q) + log(fl)-log(f0));
 rhot = (Zt-z0f)/(Zt+z0f);
 fflow = Qtaper/(1-rhot);
 rflow = fflow - Qtaper;

 rfflow(1) = fflow*z0f;
 rfflow(2) = rflow*z0f;
end
```

```
end
```

Function to calculate c and m for Atabek's model

```
function [c,m] = cmatabek(omega, r, nu, rho, E, h, sigma, gam1, gam2, M, P0,
Tt);
% Transmission line model building block cmatabek = wave speed and model coefficient using
% Atabek's tethered model
%
% [c,m] = cmatabek(omega, r, nu, rho, E, h, sigma, gam1, gam2, M, P0, Tt);
%
% Takes omega (frequency), r (vessel radius), nu (kinematic viscosity), rho (density),
% E (Youngs modulus - theta component), h (wall thickness),
% sigma (Poisson's ratio - theta component), gam1(Et/Etheta),
% gam2 (sigmat/sigmatheta) - gams represent the degree of anisotropy,
% M (a three element vector for the tethering spring constant), P0 (inital inflated pressure),
% Tt (initial longitudinal stress)
% Returns the wave speed according to Atabek's tethered model
c0 = sqrt(E*h/2/r/rho); % Moens-Koertweg wave speed
% adjust for thick walled models
if h/r > 0.1,
 b = (h/r+1)*r;
 c0 = sqrt(E*(b^2-r^2)/3/b^2/rho);
end
F10 = F_10(omega, nu, r);
M0 = M(1);
Cl = M(2);
Kl = M(3);
alpha = sqrt(r.^2.*omega/nu);
M = M0/r/rho;
mu = rho*nu;
C = Cl*r/mu;
K = Kl*r^3*rho/mu^2;
k = M-i*C/alpha^2-K/alpha^4;
T0 = P0*r;
tau0 = T0/(E*h/(1-gam2*sigma)); % tau_theta
taut = Tt/(E*h/(1-gam2*sigma^2)); % tau_t
A = 4*(1-F10)*(gam1*(1-tau0)-gam2*sigma*(gam1*sigma+taut-tau0))/(1-gam2*sigma^2)^2;
B = 2/(1-gam2*sigma^2)*(-k*(1-F10)*(1-tau0)+F10*((gam1+gam2)*sigma+taut-.5*tau0-.5)-2*gam1);

C = (2*k+F10);
c = sqrt( c0^2*2*A/(-B + sqrt(B^2-4*A*C)) );
m = ((2*gam2*sigma - (1-tau0))*c0^2/c^2 + 1 - gam2*sigma^2)/...
 (((1-tau0)*F10 - 2*gam2*sigma)*c0^2/c^2);
```

Function to calculate c and m for Womersley's model

```
function [c,m] = cmwomersley(omega, r, nu, rho, E, h, sigma);
% Transmission line model building block cmwomersley = wave speed and
```

```
% model coefficient using Womersleys model
%
% [c,m] = cmwomersley(omega, r, nu, rho, E, h, sigma);
%
% Takes omega (frequency), r (vessel radius), nu (kinematic viscosity), rho (density),
% E Youngs modulus, h (wall thickness) and sigma (Poisson's ratio)
% Returns the wave speed according to Womersley's untethered model
F10 = F_10(omega, nu, r);
c0 = sqrt(E*h/2/r/rho); % Moens-Koertweg wave speed
k = h/r*(1-3.66^2/omega^2); % set frequency of elastic constraint equal to frequency of first harmonic
% adjust for thick walled model
if k > 0.1,
 b = (k+1)*r;
 c0 = sqrt(E*(b^2-r^2)/3/b^2/rho);
end
A = 4*(1-F10);
B = -2*k*(1-F10) + F10*(4*sigma-1) - 4;
C = (2*k+F10)*(1-sigma^2);
c = sqrt( c0^2*2*A/(-B + sqrt(B^2-4*A*C)) );
B = E/(1-sigma^2);
gamma = omega/c;
x = B*k*gamma^2/rho/omega^2;
m = (2-(1-2*sigma)*x)/(x*(F10 - 2*sigma));
```

Function to calculate c and m for Dinnar's model

```
function [c,m,fval,exitflag,output] = cmdinnar(omega, r, nu, rho, E, h, sigma, g);
% Transmission line model building block cmdinnar = wave speed and model coefficient using
% Dinnar's numerical model accounting for the effect of surrounding tissue
%
% c = cmdinnar(omega, r, nu, rho, E, h, sigma, g);
%
% Takes omega (frequency), r (vessel radius), nu (kinematic viscosity), rho (density),
% E (Youngs modulus in wall), h (wall thickness), sigma (Poisson's ratio),
% g (ratio of Lame's constant in tissue to that in wall)
% Returns the wave speed and model coefficient according to Dinnar's numerical model
 alpha = (r*sqrt(omega/nu));
 F10 = F_10(omega, nu, r);
 c0 = sqrt(E*h/2/rho/r);
 mu = nu*rho;

 B2 = 0.36746;
 Z = (g-1)/(g+1);
 R2 = r+h;
 R1 = r;
```

```
S = R1/R2;
F20 = (1-F10)/F10;
H = mu*omega/(E/2/(1+sigma));
RR = 1/S^2-1;
Q = B2+i+1/pi*log(alpha*H/4/S^2);

% Set up options for Levenberg-marquadt solution
options = optimset('fminsearch');
options = optimset(options,'MaxFunEvals','1000*numberOfVariables');
options = optimset(options,'MaxIter','10000*numberOfVariables');
options = optimset(options,'Display','off');

% determine initial guess based on Womersley's solution
cw = cmwomersley(omega, r, nu, rho, E, h, sigma);
Winit = omega*nu/H/cw^2;
Winitr = real(Winit);
Winiti = imag(Winit);
% Winitr = 1; % alternative initial guess if solution doesnt converge
% Winiti = 1;
% fminsearch is a Matlab function that performs the required iteration by calling Dinnar which contains the function
% to be minimised
[W,fval,exitflag,output] = fminsearch('dinnar',[Winitr Winiti],options,alpha,F10,RR,mu,nu,omega,h,E,sigma,g);

c = sqrt(omega*nu/H/(W(1)+i*W(2)));
W = W(1)+i*W(2);
c = c0/sqrt(3*W*(1-S)/2/S);
x = real(c0/c);
y = -imag(c0/c);
x1 = real(c0/cw);
y1 = -imag(c0/cw);
% Sometimes the solution was unstable and in this situation it is re-evaluated the initial guesses set to [1 1]
if exp(-2*pi*y/x) > 1,
[W,fval,exitflag,output] = fminsearch('dinnar',[1 1],options,alpha,F10,RR,mu,nu,omega,h,E,sigma,g);

W = W(1)+i*W(2);
c = c0/sqrt(3*W*(1-S)/2/S);
x = real(c0/c);
y = -imag(c0/c);
end
exp(-[2*pi*y/x 2*pi*y1/x1]);
kd = h/r;
H = (1+2*kd)/(1-F10) - 1;
G = (5/4 - sigma)/(1-F10) + kd + sigma - 1/4;
x = (G+sqrt(G^2-H*(1-sigma^2)))/(1-sigma^2);
m = (2/x + 2*sigma - 1)/(F10 - 2*sigma);
```

Function called by Dinnar's model to perform the necessary iterations

```
function out = dinnar(W1,alpha,F10,RR,mu,nu,omega,h,E,sigma,g);
% Function that requires minimisation for solution of Dinnar's model
%
% out = dinnar(W1,alpha,F10,RR,mu,nu,omega,h,E,sigma,g);
%
% Takes W1 (vector of real and imaginary solutions to minimise the function), alpha (frequency constant), F10,
% mu (viscosity), nu (kinematic viscosity), omega (frequency), h (wall thickness), E (viscoelastic modulus in wall),
% sigma (Poisson's ratio), g (ratio of Lame's constant in tissue to that in wall)
% Returns the value of the function to be minimised
W = W1(1)+i*W1(2);
B2 = 0.36746;
Z = (g-1)/(g+1);
S = sqrt(1/(1+RR));
F20 = (1-F10)/F10;
H = mu*omega/(E/2/(1+sigma));
R = RR;
Q = B2+i+1/pi*log(alpha*H/4/S^2);
P = 1-F20*(1-Z*S^2)-W*F20*(1+Z*S^2);
out = (Z*S^2/P-1)*Q + (Z*S^2/P-1)*(1/pi*(W-1)*log(W-1)) + ...
 R*1/pi*(W-1/g)*log(W-1/g)+(Z*S^2/P-1-R)*1/pi*W*log(W) + ...
 i*R/g+Z*S^2/P*2/pi*log(S);
out = abs(real(out));
```

Function to determinethe frequently used constant F10

```
function out = F_10(omega, nu, r)
% Transmission line model building block F_10 = Womersley model constant
%
% out = F_10(omega, nu, r);
%
% Takes omega (frequency), nu (kinematic viscosity) and r (vessel radius)
% Returns the constant F10
alpha0 = sqrt(i^3*r.^2.*omega/nu);
out = 2*besselj(1,alpha0)./alpha0./besselj(0,alpha0);
```

Function to combine two arterial impedances in parallel

```
function Zeq = parallel_imp(u);
% Transmission line model building block Zeq = parallel_imp(u);
%
% Zeq = parallel_imp(u);
%
% This function calculates the equivalent input impedance at
% a transmission line bifurcation given the input impedance at
% both branch lines.
```

```
z1 = u(1);
z2 = u(2);
Zeq = (z1*z2)/(z1+z2);
```

Function for simulink model to call either of the three fundamental models

```
function [c,m] = get_model(mod_type,rad,hhr,M,Tt,g,gam2,gam1,P0,Ymod);
% Transmission line model building block - takes physical parameters and type of model
% and returns c and m for the appropriate model
%
% [c,m] = get_model(mod_type,rad,hhr,M,Tt,g,gam2,gam1,P0,Ymod);
%
% mod_type is either 'w', 'a' or 'd' depending on which model is being used
% Womersley's, Atabek's or Dinnar's
global omega rho nu sigma
h = rad*hhr;
Ymod = Ymod;
if (omega == 0),
 c = 0;
 m = 0;
else
 switch mod_type
 case 2
 [c,m] = cmwomersley(omega, rad, nu, rho, Ymod, h, sigma);
 case 1
 [c,m] = cmatabek(omega, rad, nu, rho, Ymod, h, sigma, gam1, gam2, M, P0, Tt);
 case 3
 [c,m] = cmdinnar(omega, rad, nu, rho, Ymod, h, sigma, g);
 end
end
```

Function to pass the input variables from the physical parameters block into the simulink variable u for a non-tapered arterial segment

```
function paramout = mvals(c,m,rad)
% Transmission line model building block - mvals : converts to single width output
%
% paramout = mvals(c,m,rad)
%
% Takes c and m for the given model and the artery radius and converts this to a
% vector [c,m,r] for use with simulink model
 paramout(1,1) = c;
 paramout(2,1) = m;
 paramout(3,1) = rad;
```

Function to pass the input variables from the physical parameters block into the simulink variable u for a tapered arterial segment

```
function paramout = mvals_taper1(ci,mi,radi,cf,mf,radf,len)
% Transmission line model building block - mvals : converts to single width output
```

```
%
% paramout = mvals_taper1(ci,mi,radi,cf,mf,rad_f,len)
%
% Takes c and m for the given model and the artery radius and converts this to a
% vector {ci,mi,ri,cf,mf,rf,len} for use with simulink model
% includes initial and final c,m and radius for tapering
 paramout(1,1) = ci;
 paramout(2,1) = mi;
 paramout(3,1) = radi;
 paramout(4,1) = cf;
 paramout(5,1) = mf;
 paramout(6,1) = radf;
 paramout(7,1) = len;
```

Function to calculate the modified Bessel function of the first kind of complex order and argument

```
function out = besselic(v,z)
% Modified bessel function of the first kind and of complex order.
% Note the built in Matlab function besseli cannot handle complex orders
%
% takes order (v) and argument (z)
load factr % mat file with variable rfact containing a vector of values of r!
for k=0:15, % may have to set this higher to converge but generally converges for most applications
at this value
 % computation speed is decreased for higher values
 tmpc(k+1) = (.5*z).^(v+2*k)./(r(k+1).*gammacomplex(v+k+1));
end
out = sum(tmpc);
```

Function to calculate the modified Bessel function of the 2nd kind of complex order and argument

```
function out = besselkc(v,z)
% Modified bessel function of the second kind and of complex order.
% Note the built in Matlab function besseli cannot handle complex orders.
%
% takes order (v) and argument (z)
out = .5*pi*(besselic(-v,z)-besselic(v,z))./sin(v*pi);
```

Function to calculate the complex gamma function for use with the Bessel functions

```
function out = gammacomplex(z);
% evaluates the gamma function for a complex argument
% for use with besselic
%
% out = gammacomplex(z);
stp = 2.50662827465;
```

```
z = z-1;
tmp = z+5.5;
tmp = (z+0.5)*log(tmp)-tmp;
ser = 1+76.18009173/(z+1)-86.50532033/(z+2)+24.01409822/(z+3)-1.231739516/(z+4)+...
 0.120858003e-2/(z+5)-0.536382e-5/(z+6);
gammaln1 = tmp+log(stp*ser);
out = exp(gammaln1);
```

Function to calculate the input flow from the heart

```
function [flthrt,sp] = heart_i2(W,HR,CVO,samples);
% Function : Approximates the blood flow pulse in the proximal aorta.
%
% [flthrt,sp] = heart_i2(W,HR,CVO,samples);
%
% arguments - W = pulse width in s
% HR = Heart Rate
% CVO = cardiovascular output
% samples = no. of points for heart pulse
delay = 0; % the start of each waveform may be delayed slightly
T = 60/HR; % period of waveform in s
s = 4; % W/s is the duration of the upstroke
g = 2; % W/g-W/s is the duration of the steady top part
% The peak of the waveform is calculated
k = CVO/HR/W*2*g*s/(g*s+s-g);
%t = total time of pulse
t = linspace(0,T,samples);
% t1=number of points for upstroke
t1 = round(W/s*samples/T);
% t2 = number of points for top
t2 = round((W/g-W/s)*samples/T)+t1;
% t3 = number of points for down stroke
t3 = round((W-W/g)*samples/T)+t2;
hrt = zeros(size(t));
d = delay;
% upstroke
hrt(d+1:d+t1) = s*k/W*t(d+1:d+t1); % straight line y=mx+c
% top
hrt(d+t1+1:d+t2) = k*ones(t2-t1,1);
% downstroke
hrt(d+t2+1:d+t3) = -k*t(d+t2+1:d+t3)/(W-W/g)+k/(1-1/g);
% *******end waveform, upstroke, top, downstoke

% The following copies the 256 point input waveform
% 4 times to create a series of 4 input heart beats
% each one lasting a time equivalent to "sample" points
for i=1:samples
hrt(i+1*samples)=hrt(i);
hrt(i+2*samples)=hrt(i);
```

```
hrt(i+3*samples)=hrt(i);
end
% butter(n,wn) calculatess coefficients for nth order butterworth filter
% wn=cutoff freq, 0,<wn<1 where wn=1 corresponds to 0.5 of sampling rate
fflt = 5; % previously a paramter that was passed
[b,a] = butter(2,1/fflt); % filter order 2, cutoff freq=(1/fflt)*nyquist_freq
flthrt = filtfilt(b,a,hrt);
sp = fft(flthrt,4*samples); % fft done on series of 4 input waveforms
 % so that T is 4*larger, and the frequency
 % resolution = 1/T is finer. This is
 % done instead of zero padding which would
 % have the same effect
```

File containing constants for blood properties

```
% file containing constants for blood properties
 mu = 0.06; % blood viscosity in units of dynes.s/cm^2
 rho = 1.06; % blood density units of g/cm^3

 nu = mu/rho; % kinematic viscosity

 sigma = 0.5; % Poison ratio defining relationship between strain in x and y directions

% constants for heart
sys_t=0.18; % 0.18 systolic time, set as constant=180ms, used to calculate
 % fl_wdth, which is in points, relative to "samples"
 % all pressures are relative to central venous pressure
cent_v_p=4; % central venous pressure is usually around 4mmHg,
 % and does not change, Itskovitz 87, table 1
```

Function to display flow waveforms for use with tapered arterial segments

```
function fl_out = flow_disp_taper(u);
% function for use with transmission line models to return values from simulink code to the
% main routine for subsequent display. For use with tapered arterial segments.
% Takes as input argument the simulink vector u which consistis of :
% z0 (initial characteristic impedance), k (characteristic impedance tapering constant),
% fpres (forward pressure waveform), rpres (reverse pressure waveform), l (arterial length).
%
% Obtains the forward and reverse flows at the terminal end of the arterial
% segment and sends it to the main program
global omega;
z0 = u(1);
k = u(2);
fpres = u(3);
rpres = u(4);
l = u(5);
if (omega == 0),
 fl_out = [fpres 0];
```

```
else
 z0f = z0*exp(k*l);
 fl_out = [fpres/z0f rpres/z0f];
end
```

Function to display forward and reverse waveforms at any point on the umbilical artery

```
function frpress = fr_press(u);
% Transmission line model building block fr_press = forward and reverse pressure waveforms for the
% umbilical artery
%
% frpress = fr_press(u);
%
% Takes simulink vector u consisting of :
% z0 (characteristic impedance), gamma (complex propagation constant), l (vessel segment length),
% fpres (forward pressure), rpres (reverse pressure),
% Calculates the forward and reverse flow waveform at the terminal ends and
% Returns the forward and reverse flow and forward and reverse pressure waveforms
% at the terminal end of the segment as well as gamma and l
% as a vector [fflow, rflow, fpres, rpres, gamma, l]
global omega;
z0 = u(1);
gamma = u(2);
l = u(3);
fpres = u(4);
rpres = u(5);
if (omega == 0),
 % fpres is the flow waveform and rpres is the pressure waveform at the source end
 frpress = [fpres 0 rpres 0 gamma l];
 else
 frpress = [fpres/z0, rpres/z0, fpres, rpres, gamma, l];
end
```

Function to determine the placental input resistance and impedance for a given set of morphological parameters. This function requires adaptation by uncommenting various sections depending on the simulation required

```
function zout = term_treePt(u);
% Transmission line model building block term_treePt = terminal placental impedance
%
% zout = term_treePt(u);
%
% Takes the simulink vector, u, consisting of :
% r0 (initial tree radius), rn, rn1 (for use with earlier version - no longer used),
% dhdr1 (h/r ratio), E0 (initial Young's modulus), k1 (branching ratio), dldr1 (length-radius ratio),
% taper (1 = tapering, 2 = no tapering), theta (branching angle),
% perctg_flow_index (index into percentage flow vector - 2 for the placenta),
% ctmp (complex wave speed of umb artery), mtmp (m factor of umb artery),
%rad_cord (radius of umb artery),
```

```
% l_cord (length of umb artery)
%
% Returns The input impedance of the placenta(Zin)
% (special changes required for placental distributed flow)
global omega per_flow nu rho sigma mu term_tree_vec redist_flag redist_flag1 ...
 sz_factor_plac sz_factor tmp_var dldr_factor r0new
r0 = abs(u(1)*sz_factor);  % multiply by sz_factor for growth
rn = u(2);
rn1 = u(3);
dhdr1 = u(4);
E0 = u(5);
k1 = u(6);
dldr1 = u(7)*dldr_factor;
taper = u(8);
theta = u(9);
perctg_flow_index = u(10);
ctmp = u(11);
mtmp = u(12);
rad_cord = u(13);
l_cord = real(u(14));
pr_ave = per_flow(10);
CO = per_flow(8);
CO28 = per_flow(12); % reference CO
percentage = per_flow(perctg_flow_index);
% load reference values for rad and len of umb artery
l_cord_ref = 43*sz_factor;
rad_cord_ref = 0.15*sz_factor;
r_cord_new = 8*mu*l_cord/pi/rad_cord^4/2; % NB to divide by 2 for 2 arteries in parallel
r_cord_old = 8*mu*l_cord_ref/pi/rad_cord_ref^4/2;
r_cord_new/r_cord_old
inpll = 4; % no of placental trees in parallel
% a number of scenarios are commented out for use with various pathology simulations
% as is the code is for a normal placenta
 % this section of code is for Adamson's experiment of a reduced umb rad
 % here the distribution matrix is reworked and mean arterial pressure altered
%if redist_flag ~= 5,
 r_placenta = abs(1333.3*pr_ave/((CO/60)*percentage/100)-r_cord_old);
 r_required = r_placenta*inpll;
% y = abs(CO/60*pr_ave*1333.3/(percentage/100*CO/60)/((100-percentage)/...
% 100*CO/60*(r_cord_new+r_placenta)+pr_ave*1333.3));
% z = (1-percentage/100*y)/(1-percentage/100);

% per_flow(10) = pr_ave*z
% per_flow(2:6) = per_flow(2:6)*1*z;
% per_flow(2) = percentage*y;
% per_flow(1) = 100 - sum(per_flow(2:6));
% per_flow(1:6)
% sum(per_flow(1:6))
```

```
% redist_flag = 5;
% (r_cord_new+r_placenta)/(r_cord_old+r_placenta)
%end
% r_placenta2 and r_placental may be altered depending on whether reference values
% are used or not.
r_placenta2 = 1333.3*pr_ave/((CO28/60)*25/100)-r_cord_new;
r_required2 = r_placenta2*inpll;
r_placenta1 = 1333.3*60/((CO28/60)*25/100)-r_cord_old;
r_required1 = r_placenta1*inpll;
% iterate to determine the number of layers, branching assymetry and length-radius ratio
if (omega == 0),

 % check if flow to the placenta has been reduced (embolisation)
 % uncomment this section of code if a reduction of placental flow takes place
% if ((abs(percentage - 25) ~= 0)&(redist_flag1 ~= 1)),

 % redistribute the difference - 50 % to head and heart 20 % to adrenals, 20 % to legs and
% 10% to abdomen
% redist = 25 - percentage;
% per_flow(1:6)=[[27+0.6*redist,percentage,15+0.125*redist,7.7+0.125*redist,0.3+.025*redist,25+.125*redist]'

% per_flow(1:6)=per_flow(1:6) + [0.6*redist,0,0.125*redist,0.125*redist,.025*redist,.125*redist]
% redist_flag1 = 1;

% end
% this section of code is for an altered umbilical arterial radius but for constant pressure
% if (abs(r_cord_new) ~= abs(r_cord_old))&(redist_flag ~=3),
% redist_flag
% r_placenta_old = 1333.3*pr_ave/((CO/60)*redist/100)-r_cord_old;
% r_plac_cord = r_placenta_old + r_cord_new;
 % total new flow to placenta and cord
% flow_plac_cord = 1333.3*pr_ave/r_plac_cord;
% frac_flow_plac_cord = abs(flow_plac_cord/(CO/60)*100); % expressed as a fraction

 % now redistribute the difference - 50 % to head and heart 20 % to adrenals, 20 % to legs and
 % 10% to abdomen
% redist = abs(redist - frac_flow_plac_cord);
 % per_flow(1:6)=[[27+0.6*redist,25,15+0.125*redist,7.7+.125*redist,0.3+.025*redist,25+.125*redist]'];

% per_flow(1:6)=per_flow(1:6) + [0.6*redist,0,0.125*redist,0.125*redist,.025*redist,.125*redist];
% per_flow(2) = frac_flow_plac_cord;
% redist_flag = 3;
% end
% if redist_flag == 3,
% r_required = r_required1;
% end
 zout = (r_required + 1e-20*i)/inpll;
```

```
% function to calculate the number of levels of branching - note that dependent
% upon which experiment is being conducted either of r_required, r_required1 or
% r_required2 may be used
% if viscosity changes, mu must be set to mu_ref (0.06)
ntree = ncalct(abs(r_required1),taper,theta,dldr1, r0, mu, k1);

% uncomment to display the number of levels of branching and terminal radius of the placenta
%['Placenta' ' ' num2str(ntree,4) ' ' num2str(r0/((2^(1/k1))^ntree)*1e6,4)]
%term_tree_vec(perctg_flow_index) = ntree;

else
 if r0new ~= 0,
 r0 = r0new;
 end

% store the number of levels of branching in theterm_tree_vec
ntree = term_tree_vec(perctg_flow_index);
% set delta - the fraction of the original number of levels of branching for the
% reduced placental flow experiments
delta = 1;
% uncomment as required - find_theta solves for the new theta so that delta*ntree levels of branching
% are achieved
% for a required resistance as set by the parameters in r_required2
% find_k is similar but uses r_required and delta*ntree (may be used in conjunction with find_theta)
% find_epsilon is for arterial vasoconstriction - a new value of r0 is calculated to obtain the resistance
% according to the parameters in r_required (may set to r_required1 or r-required2 as desired)
%theta = find_theta(r_required2,delta,ntree,r0, dldr1, k1, taper);
%k1 = find_k(r_required,delta,ntree,r0, dldr1, theta, taper);
%epsilon = abs(find_epsilon(r_required,theta,delta*ntree,r0, dldr1, k1, taper));
%r0 = epsilon*r0;
% determine the impedance using the given morphology parameters
[tmp1,zout] = frac_tree4(theta,delta*ntree,r0, dldr1, abs(k1), taper, E0, dhdr1);
% divide by the number of trees in parallel
zout = zout/inpll;
end
```

Function to find new branching angle for a specified level of branhcing

```
function theta = find_theta(r_required,delta,ntree,r0, dldr, k1, taper);
% function to calculate the new branching angle theta for a change in placental morphology
%
% [theta] = find_theta(r_required,delta,ntree,r0, dldr, k1, taper);
%
% this function determines how theta must change to match the desired resistance
% takes as arguments r_required (target input resistance), delta (fraction of levels of branching),
% ntree (old number of levels of branching), r0 (initial tree radius),
% dldr (ratio of length to radius constant), k1 (branching ratio) ,
% taper (=1 for no tapering, 2 for tapering)
```

```
% returns the new theta for given input resistance and new level of branching
global mu
n = delta*ntree;
k = (2)^(1/k1);
A = 8*mu*dldr*k^3*(k^(3*n)*2^(-n)-1)/(r0^3*(k^3-2)*pi*log(2/k^2));
x = (k^4*A/(abs(r_required)+A))^(1/4);
theta = acos(x/2)*180/pi;
```

Function to find new branching ratio for a specified level of branhcing

```
function k = find_k(r_required,delta,ntree,r0, dldr, theta, taper);
% function to calculate the parameter new k for a change in placental morphology
%
% [k] = find_k(r_required,delta,ntree,r0, dldr, theta, taper)
%
% this function determines how k must change to match the desired resistance
% takes as arguments r_required (target input resistance), delta (fraction of levels of branching),
% ntree (old number of levels of branching), r0 (initial tree radius),
% dldr (ratio of length to radius constant), theta (branching angle),
% taper (=1 for no tapering, 2 for tapering)
% returns the new k for given input resistance and new level of branching
global mu
n = delta*ntree;
% uses built in function to solve via iterative process
options = optimset('fsolve');
options = optimset(options,'Display','off');
options = optimset(options,'LevenbergMarquardt','on');
options = optimset(options,'LargeScale','on');
k = fsolve('solverk',k,options,r_required,n,r0,dldr,theta);
```

Function for use with find_k - to perform the necessary iteration for minimisation

```
function out = solverk(K,r_required,n,r0,dldr,theta);
% function for use with solve_k to iterate to minimse
global mu
k = (2).^(1./K);
rat = sin(pi/180*(180-2*theta))/sin(pi/180*theta);
rn = r0*(1./k).^n;
B = 4*mu*dldr/pi/rat^4*(rat^4-k.^4)./log(.5*k.^2);
R0 = B./rn^3*(k.^3)*(2^(-n) - k.^(-3*n))./(k.^3-2);
R0 = 2*R0;
out = r_required - R0;
```

Function to find new radius ratio for a specified input resistance (peripheral vasoconstriction or dilation)

```
function epsilon = find_epsilon(r_required,theta,ntree,r0, dldr, k1, taper);
% function to calculate epsilon, where rad_new = epsilon*rad_old
%
% [epsilon] = find_epsilon(r_required,theta,ntree,r0, dldr, k1, taper);
```

```
%
% i.e. for situations where the resistance of the vascular tree changes due to a changing radius only
% this function determines how the radius must change to match the desired resistance
% takes as arguments r_required (target input resistance), theta (branching angle),
% ntree (number of levels of branching), r0 (initial radius), dldr (ratio of length to radius constant),
% k1 (branching ratio), taper (=1 for no taperin, 2 for tapering)
global mu
n = ntree;
k = (2)^(1/k1);
rat = sin(pi/180*(180-2*theta))/sin(pi/180*theta);
rn = r0*(1/k)^n;
B = 4*mu*dldr/pi/rat^4*(rat^4-k^4)/log(.5*k^2);
epsilon = (-2*B*k^(3*n)*k^3*(k^(-3*n)-2^(-n))/(r0^3*r_required*(k^3-2)))^(1/4);
```

Function to calculate peripheral network input resistance and impedance for a specified set of morphological parameters

function [R0, AC] = frac_tree4(theta, nn, r0, dldr, K, taper, E0, dhdr)

```
% Transmission line model building block ftree = fractal terminal tree resistance and impedance
%
% [R0, AC] = frac_tree4(theta, nn, r0, dldr, K, taper, E0, dhdr)
%
% Takes theta (branching angle), nn (number of levels of branching), r0 (initial vessel radius),
% dldr (length to radius ratio), K (branching ratio), taper (=1 for no taperin, 2 for tapering),
% E0 (initial viscoelastic modulus), dhdr (ratio of wall thickness to radius)
% Calculates the resistance and impedance of the peripheral neworks using either the tapered or
% untapered model.
% returns R0 (resistance) and AC (frequency dependent impedance)
global omega rho sigma nu mu sz_factor
switch taper
 case 1 % No taper

% input resistance
nn = (nn);
k = (2)^(1/K);
rn = r0*(1/k)^nn;
B = 8*mu*dldr/pi;
R0 = B/rn^3*(k^3)*(2^(-nn) - k^(-3*nn))/(k^3-2);
R0 = 2*R0;
% work out vectors for z0 and gamma
g = .1+.01*i;
for loop1 = 1:round(nn),
 % select the model for use by uncommenting the desired model
 % [c0,m0] = cmdinnar(omega, r0*(1/k)^(loop1-1), nu, rho, E0*(3-2*exp(-5*(loop1-1)/nn))^2,...
 % dhdr*r0*(1/k)^(loop1-1), sigma, g);
 % [c0,m0] = cmwomersley(omega, r0*(1/k)^(loop1-1), nu, rho, E0*(3-2*exp(-5*(loop1-1)/nn))^2,...
 %dhdr*r0*(1/k)^(loop1-1), sigma);
 [c0,m0] = cmatabek(omega, r0*(1/k)^(loop1-1), nu, rho, E0*(3-2*exp(-5*(loop1-1)/nn))^2, ...
```

```
 dhdr*r0*(1/k)^(loop1-1), sigma, 1, 1, [.113 220 1.6101e6], 0, 0);
 Z0vec(loop1) = rho*c0/(1+m0*F_10(omega, nu, r0*(1/k)^(loop1-1)))/pi/(r0*(1/k)^(loop1-1))^2;
 gamvec(loop1) = i*omega/c0;
end
% calculate the impedance
% multiply gamma by l
gamvec = gamvec.*dldr.*r0.*(1/k).^([0:1:round(nn)-1]);
Zt = 8*mu*dldr*rn/pi/rn^4;
for loop1 = round(nn):-1:1,
 AC = Z0vec(loop1)/2*( (Zt + Z0vec(loop1))*exp(gamvec(loop1)) + ...
 (Zt - Z0vec(loop1))*exp(-gamvec(loop1)) )/...
 ( (Zt + Z0vec(loop1))*exp(gamvec(loop1)) - ...
 (Zt - Z0vec(loop1))*exp(-gamvec(loop1)) );
 Zt = AC;
end
AC = AC*2;
otherwise

% tapered solution
nn = (nn);
k = (2)^(1/K);
rn = r0*(1/k)^nn;
rat = sin(pi/180*(180-2*theta))/sin(pi/180*theta);
B = 4*mu*dldr/pi/rat^4*(rat^4-k^4)/log(.5*k^2);
R0 = B/rn^3*(k^3)*(2^(-nn) - k^(-3*nn))/(k^3-2);
R0 = 2*R0;
% work out vectors for z0 and gamma
g = .1+.01*i;
for loop1 = 1:round(nn),
 % select the model for use by uncommenting the desired model
 % [c0,m0] = cmdinnar(omega, r0*(1/k)^loop1, nu, rho, E0*(3-2*exp(-5*loop1/nn))^2,...
 % dhdr*r0*(1/k)^loop1, sigma, g);
 % [c0,m0] = cmwomersley(omega, r0*(1/k)^(loop1-1), nu, rho, E0*(3-2*exp(-5*(loop1-1)/nn))^2,...
 % dhdr*r0*(1/k)^(loop1-1), sigma);
 [c0,m0] = cmatabek(omega, r0*(1/k)^(loop1-1), nu, rho, E0*(3-2*exp(-5*(loop1-1)/nn))^2, ...
 dhdr*r0*(1/k)^(loop1-1), sigma, 1, 1, [.113 220 1.6101e6], 0, 0);
 Z0vec(loop1) = rho*c0/(1+m0*F_10(omega, nu, r0*(1/k)^(loop1-1)))/pi/(r0*(1/k)^(loop1-1))^2;
 gamvec(loop1) = i*omega/c0;

% [c0f,m0f] = cmwomersley(omega, r0*(1/k)^(loop1)*rat, nu, rho, E0*(3-2*exp(-5*(loop1)/nn))^2,
dhdr*r0*(1/k)^(loop1)*rat, sigma);
 [c0f,m0f] = cmatabek(omega, r0*(1/k)^(loop1), nu, rho, E0*(3-2*exp(-5*(loop1)/nn))^2, ...
 dhdr*r0*(1/k)^(loop1), sigma, 1, 1, [.113 220 1.6101e6], 0, 0);
 Z0vecf(loop1) = rho*c0f/(1+m0f*F_10(omega, nu, r0*(1/k)^(loop1)))/pi/(r0*(1/k)^(loop1))^2;
 gamvecf(loop1) = i*omega/c0f;

 lvec(loop1) = r0*(1/k)^(loop1-1);
end
```

```
% calculate the h and q tapering constants at each generation
hvec = 1./lvec.*log(Z0vecf./Z0vec);
qvec = -1./lvec.*log(gamvecf./gamvec);
% calculate the impedance
Zt = 8*mu*dldr*rn/pi/rn^4;
for loop1 = round(nn)-1:-1:1,
 gamma = gamvec(loop1);
 q = qvec(loop1);
 h = hvec(loop1);
 l = lvec(loop1);
 z0 = Z0vec(loop1);

 bk1 = besselkc(.5*(h+q)/q,gamma/q*exp(-q*l));
 bk2 = besselkc(.5*(h+3*q)/q,gamma/q*exp(-q*l));
 bi1 = besselic(.5*(h+q)/q,gamma/q*exp(-q*l));
 bi2 = besselic(.5*(h+3*q)/q,gamma/q*exp(-q*l));
 bk3 = besselkc(.5*(h+q)/q,gamma/q);
 bk4 = besselkc(.5*(h+3*q)/q,gamma/q);
 bi3 = besselic(.5*(h+q)/q,gamma/q);
 bi4 = besselic(.5*(h+3*q)/q,gamma/q);
 xi = -((-Zt*gamma + z0*exp(l*(h+q))*(h+q))*bk1 - z0*gamma*exp(l*h)*bk2)/...
 ((-Zt*gamma + z0*exp(l*(h+q))*(h+q))*bi1 + z0*gamma*exp(l*h)*bi2);

 AC = 1/2*z0/gamma*(h+q+gamma*(xi*bi4-bk4)/(xi*bi3+bk3));
 Zt = AC;
end
AC = AC*2;
end
```

Function to calculate the number of levels of branching of a peripheral tree for a specified input resistance and set of morphological parameters

```
function [ntree] = ncalct(Rr,taper,theta,dldr, r0, mu, K)
% Transmission line model building block ncalct = determines numer of levels for the terminal tree
%
% [ntree] = ncalct(Rr,taper,theta,dldr, r0, mu, K)
%
% Iterative routine
% Takes Rr (Required DC resistance), taper (=1 for no tapering, 2 otherwise),
% theta (branching angle), dldr (ratio of length to radius), r0 (radius of initial branch),
% mu (viscosity), K (branching ratio)
% Return n - the number of branches required to give resistance Rr
k = (2)^(1/K);
if (taper == 1), % No tapering
 B = 8*mu*dldr/pi;
else
 rat = sin(pi/180*(180-2*theta))/sin(pi/180*theta);
 B = 4*mu*dldr/pi/rat^4*(rat^4-k^4)/log(.5*k^2);
```

```
end
ntree = log(2*B.*(k.^3./(Rr.*r0.^3.*k.^3 - 2.*Rr.*r0.^3 + 2*B.*k.^3)))./log(2./k.^3);

Function to determine peripheral input resistances and impedances for
a given set of morphological parameters. This function requires adaptation
by uncommenting various sections depending on the simulation required.

function zout = term_treet(u);
% Transmission line model building block term_treet = terminal tree impedance
%
% zout = term_treet(u);
%
% Takes the simulink vector, u, consisting of :
% perctg_flow_index (index into percentage flow vector (1-6 depending on peripheral bed)),
% r0 (initial tree radius), rn (for use with earlier version - no longer used),
% dhdr (h/r ratio), dldr (length-radius ratio), E (initial Young's modulus), k (branching ratio),
% taper (1 = tapering, 2 = no tapering), theta (branching angle),
%
% Returns The input impedance of the peripheral bed (Zin)
% (special changes required for distributed flow)
global omega per_flow nu rho sigma mu term_tree_vec redist_flag sz_factor
% calculate the required DC resistance for the terminal tree
perctg_flow_index = u(1);
r0 = abs(u(2)*sz_factor); % multiply by sz_factor for growth
rn = u(3);
dhdr = u(4);
dldr = u(5);
E = u(6);
k = u(7);
taper = u(8);
theta = u(9);
pr_ave = per_flow(10);
CO = per_flow(8);
per_flow_ctrl(1:11)= [[27,25,15,7.7,0.3,25,0,500,140,60,0]']; % control values
name_vec = {'HAH', 'Plac', 'Thorax', 'Abdomen', 'Adrenals', 'lower limbs'};
CO28 = per_flow(12); % reference value
percentage_ctrl = per_flow_ctrl(perctg_flow_index); % reference values
percentage = per_flow(perctg_flow_index);
% dpeneds on which simulation is being conducted - may alter these for reference values
r_required = 1333.3*pr_ave/((CO/60)*percentage/100);
r_required1 = 1333.3*60/((CO28/60)*percentage_ctrl/100);
if (omega == 0),
 zout = (r_required+1e-20*i);
 ntree = ncalct(abs(r_required),taper,theta,dldr, r0, 0.06, k);

 % uncomment to display the number of levels of branching and terminal radii
 [name_vec{perctg_flow_index} ' ' num2str(ntree,4) ' ' num2str(r0/((2^(1/k))^ntree)*1e6,4)];
 term_tree_vec(perctg_flow_index) = ntree;
```

```
else
 ntree = term_tree_vec(perctg_flow_index);
 % uncomment for vasoconstriction or dilation simulations
% epsilon = abs(find_epsilon(r_required1,theta,ntree,r0, dldr, k, taper));
% r0 = epsilon*r0;
 [tmp1,zout] = frac_tree4(theta,ntree,r0, dldr, k, taper, E, dhdr);
 zout = zout;
end
```

Function to pass the input variables from the physical parameters block into the simulink variable u for a peripheral tree network

```
function paramout = mval_tree(perctg_flow_index,r0,rn,dhdr,dldr,E,k,Ba,nn)
% Transmission line model building block - mval_tree : converts to single width output
%
% paramout = mval_tree((perctg_flow_index,mod_type,r0,rn,dhdr,g,M,E)
%
% Takes physical parameters for tree evaluation converts this to a
% single vector for use with simulink model
 paramout(1,1) = perctg_flow_index;
 paramout(2,1) = r0;
 paramout(3,1) = rn;
 paramout(4,1) = dhdr;
 paramout(5,1) = dldr;
 paramout(6,1) = E;
 paramout(7,1) = k;
 paramout(8,1) = Ba;
 paramout(9,1) = nn;
```

Function to pass the input variables from the physical parameters block into the simulink variable u for the placenta tree network

```
function paramout = mval_treePt(r0,rn, rn1,dhdr,E,k,k1a,Ba,Ba1,perctg_flow_index)

% Transmission line model building block - mval_treeP : converts to single width output
%
% paramout = mval_treePt(frac_plac_flow,perctg_flow_index,mod_type,r0,rn,dhdr,g,M,E)
%
% Takes physical parameters for tree evaluation converts this to a
% single vector for use with simulink model
% (special version for placental distributed flow)
paramout(1,1) = r0;
paramout(2,1) = rn;
paramout(3,1) = rn1;
paramout(4,1) = dhdr;
paramout(5,1) = E;
paramout(6,1) = k;
paramout(7,1) = k1a;
paramout(8,1) = Ba;
paramout(9,1) = Ba1;
```

```
paramout(10,1) = perctg_flow_index;
```

Main programme to run simulations. Type sim_foetus1. Variables may be changed in this programme for different experiments and for different measurement outputs

```
% Main program to begin simulation of transmission line, simulink foetal model
% (sim_foetus1) - type indmat to get indice matrix - see the end of file
% define global variables to be used by the programme here :
global sz_factor
global omega
global Input_flow
global per_flow
global nu
global rho
global sigma
global mu
global wmean
global term_tree_vec
global redist_flag
global redist_flag1
global sz_factor_plac
global tmp_var
global tmp_varc
global dldr_factor
global r0new
% Run constants to set up the constants used
constant
% set gestational age of simulation
GA = 28; % must always be 28
gatest = 28; % age of simulation
% growth factors
grow_taper
dldr_factor = mm(gatest-23,:);
% Determine the size factor
p=[-0.073745,9.95,-226.24,1443]; % taken from reference, pg 15 and converted for GA in weeks,
 % accurate from 17-40 weeks

mass=polyval(p,gatest); % calculates the value of the polynomilal at GA
 % mass=-0.073*GA^3+9.95*GA^2-226*GA+1443
mass28 = polyval(p,GA);
sz_factor=(polyval(p,gatest)/mass28)^(1/3); % cube root of mass at GA/mass at 28wks
 % note sz_factor=1 at 28 weeks

weeks = [24 25 26 27 28 29 30 31 32 33 34 35 36 37 38 39 40 41 42 43];
 % assume that fetal mass is proportional to volume
 % also, all the cardi-vasc outputs set up by
 % distrb are in ml/min/kg so we must multiply
 % by the mass (sz_factor^3) to get true cvo.
```

```
% Work out the percentage flow matrix

 per_flow(1:11)= [[27,25,15,7.7,0.3,25,0,500,140,60,0]']; % control values
 % [[hah,pla,thr,abd,adr,lg1,lg2,cvo,HR,art_pres,ven_pres]'];

 % These may be altered for various simulations
% note that umbilical venous pressure set to zero, should be about 12mmHg
% note that cardiac output=500ml/min/kg, flow to placenta=120ml/min/kg=25%
% flow to lungs=15%, flow to kidneys=8%, legs=12.5% each, head and heart=27%
% check if per_flow has changed from reference values
redist_flag = 0;
redist_flag1 = 0;
load ref_vals
CO28 = 500*mass28/1000; % ref val
per_flow(12) = CO28;
% modify the CO according to the Gestational Age
per_flow(8)=per_flow(8)*mass/1000;
 % to vary the cardiac
 % output from measured value,
 % note length^3=volume assumed
 % proptional to flow.


% Obtain the input waveform

samples = 256;
CO = per_flow(8);
HR = per_flow(9);
period = 60/HR;
% heart_i2 generates an input waveform (flow_in) and its spectrum (fl_in_sp)
% the input waveform (samples) is duplicated 4 times to improve frequency
% resolution (fundamental=1/T) where T = period of 4 waveforms. If samples=256
% fft will yield 1024 frequency bins, bottom 512 repeated as complex conjugate in
% the upper bins. A transfer function (for each point)is generated for each freq of interest,
% and multiplied by input spectrum to obtain the otput spectrum, from
% which time waveform is calculated using inverse fft
%[flow_in,fl_in_sp] = heart_i1(samples,fl_sys,fl_wdth,HR);
[flow_in,fl_in_sp] = heart_i2(sys_t,HR,CO,samples);
fl_in_sp = fl_in_sp./(samples*4);
ki = 1;
df = HR/(4*60); % this is the fundamental frequency, ie lowest possible
 % (resolution) and all others are multiples of this
 % the 4 is because each cycle is repeated 4 times
 % if HR=140 then df=0.58Hz
low_freq = df;
up_freq = 6; %6 upper frequency, note increasing the range above 10Hz makes no difference
```

```
omega = 0;
% initialise output variables for flow, pressure and impedances
% these may be added to or adapted if further measurement points are desired
flow_f = zeros(1,samples*4);
flow_r = zeros(1,samples*4);
pres_f = zeros(1,samples*4);
pres_r = zeros(1,samples*4);
temp_f = zeros(1,samples*4);
temp_r = zeros(1,samples*4);
impedHah = zeros(1,samples*4);
impedThorax = zeros(1,samples*4);
impedAbdomen = zeros(1,samples*4);
impedAdrenals = zeros(1,samples*4);
impedLegs = zeros(1,samples*4);
impedPlac = zeros(1,samples*4);
impedUmb = zeros(1,samples*4);
z0umbout = zeros(1,samples*4);
impedThor = zeros(1,samples*4);
sz_factor = sz_factor + 1e-40*i;
for Hz=low_freq:df:up_freq, % increments of df Hz; Range 0-up_freq (Hz)
 % altogether 10/0.58=18 points

Input_flow = fl_in_sp(ki);
if ki == 1,
 Input_flow =Input_flow +1e-20*i;
end
% Iterate for curvature on steady flow
% asume an initial mean flow velocity equal to that in the straight tube
if omega == 0,
 rumb = .15;
 wmean = CO/HR*per_flow(2)/100/pi/rumb^2; % percentage CO to cord and placenta

 % use foetal_taper2d for Dinnar's model, foetal_taper2a for Atabek's and foetal_taper2w
 % for Womersley's
 y = sim('foetal_taper2d',[1 1]);
 wmean_new = flo_out1(1)/pi/rumb^2;
 while abs(wmean-wmean_new)/wmean > 1e-4,
 wmean = wmean_new;
 y = sim('foetal_taper2d',[1 1]);
 wmean_new = flo_out1(1)/pi/rumb^2;
 end
else
 y = sim('foetal_taper2d',[1 1]);
end
% total flow = forward flow - reverse flow
% obtain output variables
flo_f_sp1(ki) = flo_out1(1);
flo_r_sp1(ki) = flo_out1(2);
```

```
pre_f_sp1(ki) = flo_out1(3);
pre_r_sp1(ki) = flo_out1(4);
gamm1(ki) = flo_out1(5);
ll1(ki) = flo_out1(6);
flo_f_sp(ki) = flo_out_thoracic1(1);
flo_r_sp(ki) = flo_out_thoracic1(2);
pre_f_sp(ki) = flo_out_abdominal(1);
pre_r_sp(ki) = flo_out_abdominal(2);
tmp_f_sp(ki) = flo_out_iliac(1);
tmp_r_sp(ki) = flo_out_iliac(2);
impedHah1(ki) = impedHah;
impedThorax1(ki) = impedThorax;
impedAbdomen1(ki) = impedAbdomen;
impedAdrenals1(ki) = impedAdrenals;
impedLegs1(ki) = impedLegs;
impedPlac1(ki) = impedPlac;
impedUmb1(ki) = impedUmb(1);
z0umbout1(ki) = z0umbout(1);
%impedThor(ki) = thor_imp(1);
cc1(ki) = cmr1(1);
mm1(ki) = cmr1(2);
rr1(ki) = cmr1(3);
om1(ki) = omega;
ki = ki+1;
omega = 2*pi*Hz;
end;
% determine flow at all points along the umbilical cord
% flow is recorded in a nxmxp matrix
% the forward flows for the :
% thoracic flow is flow_f, the abdominal flow is pres_f, the ilical flow is temp_f
% the umbilical flow at the foetal end is Qf(1,:) and at the placental end is Qf(43,:) (adjust for cord length)
% the reverse flows are the same but with r . i.e. the total flow at the foetal end of the umbilical artery is
% Qf(1,:)-Qr(1,:) etc.
% these variables may be adapted for varying measurement points
clear Q_f1 Q_r1 Qf1 Qr1
F101 = F_10(om1, nu, rr1);
R = 100;
alpha01 = sqrt(i^3*rr1.^2.*om1/nu);
ll1(1) = floor(ll1(1));
for ln = 0:ll1(1),
 qs1 = mm1.*rr1(1)./alpha01.*(-2*rr1(1)/pi.*besselj(1,alpha01)./besselj(0,alpha01) + ...
 (1./besselj(1,alpha01)+rr1(1)./alpha01./besselj(0,alpha01)).*...
 (besselj(1,alpha01).*struveh(0,alpha01)-besselj(0,alpha01).*struveh(1,alpha01)));
 Q_f1(ll1(1)-ln+1,:) = pre_f_sp1./rho./cc1.*(1+mm1.*F101)*pi*rr1(1)^2.*exp(gamm1*ln);
 Q_r1(ll1(1)-ln+1,:) = pre_r_sp1./rho./cc1.*(1+mm1.*F101)*pi*rr1(1)^2.*exp(-gamm1*ln);
end
```

```
%imped_p = imped_p*1024;
%imped_p = real(ifft(imped_p));
[lenumb,hgkug] = size(Qf);
mid = round(lenumb/1.3);
thor1 = (flow_f-flow_r)./max(flow_f-flow_r);
abdo1 = (pres_f-pres_r)./max(pres_f-pres_r);
ilia1 = (temp_f-temp_r)./max(temp_f-temp_r);
fend1 = (Qf(1,:)-Qr(1,:))./max(Qf(1,:)-Qr(1,:));
midu1 = (Qf(mid,:)-Qr(mid,:))./max(Qf(mid,:)-Qr(mid,:));
pend1 = (Qf(lenumb,:)-Qr(lenumb,:))./max(Qf(lenumb,:)-Qr(lenumb,:));
% indice matrix for 9 different indices
% The resistance index at each point in the arteries is given by indmat(:,2) and the
% pulsatility index by indmat(:,1)
% the arteries are ordered according to :thoracic, abdominal, iliac, foetal end, palcental end
indmat = [pii(thor1) ri(thor1) ab(thor1) hwi(thor1) pli(thor1) acs(thor1) arw(thor1) ups(thor1)
hwi1(thor1); ...
 pii(abdo1) ri(abdo1) ab(abdo1) hwi(abdo1) pli(abdo1) acs(abdo1) arw(abdo1) ups(abdo1) hwi1(abdo1);
...
 pii(ilia1) ri(ilia1) ab(ilia1) hwi(ilia1) pli(ilia1) acs(ilia1) arw(ilia1) ups(ilia1) hwi1(ilia1); ...
 pii(fend1) ri(fend1) ab(fend1) hwi(fend1) pli(fend1) acs(fend1) arw(fend1) ups(fend1) hwi1(fend1);
...
 pii(midu1) ri(midu1) ab(midu1) hwi(midu1) pli(midu1) acs(midu1) arw(midu1) ups(midu1) hwi1(midu1);
...
 pii(pend1) ri(pend1) ab(pend1) hwi(pend1) pli(pend1) acs(pend1) arw(pend1) ups(pend1) hwi1(pend1)];

flow_f = flow_f(1:512);
flow_r = flow_r(1:512);
pres_f = pres_f(1:512);
pres_r = pres_r(1:512);
temp_f = temp_f(1:512);
temp_r = temp_r(1:512);
```

```
% check if flow to the placenta has been reduced (embolisation)
% uncomment this section of code if a reduction of placental flow takes place
% if ((abs(percentage - 25) ~= 0)&(redist_flag1 ~= 1)),

% redistribute the difference -
% redist = 25 - percentage;
% per_flow(1:6)=per_flow(1:6) + [0.6*redist,0,0.125*redist,0.125*redist,.025*redist,.125*redist]
% redist_flag1 = 1;
% end
```

This sets the redist_flag to one so that this is only done once (remember mean vlaues are iterated for curvature until convergence)

this alters the redistribution matrix - the simulink code is set to begin with the placenta.

the function term_treePt1 has three versions for the required resistance of the placental bed. These are of the form :

```
r_placenta = 1333.3*pr_ave/((CO/60)*percentage/100)-r_cord_new;
r_placenta1 = 1333.3*60/((CO28/60)*25/100)-r_cord_old;
```

Here r_placenta is set with the new values and r_placenta1 with the old values. The desired resistance is that of r_placenta, however, assume that vasconstriction takes place. The ncalct (the function that determines the number of levels) must be set with r_placenta1 as the number of levels of branching were set prior to any change. The function find_epsilon will be set with r_placenta so that epsilon may be solved for to determine the new radius so that the actual resistance r_placenta is achieved. (remember r0_new = epsilon*r0_old). Similar set-ups must be conducted depending on the changes required and for each change the code must be carefully checked as there are no generic ways of doing this.

Corresponding changes must be made to the function term_treet for the other peripheral networks. Certain experiments such as Adamson's angiotensinII infusion experiment have a separate section of code that must be uncommented. However, in this case it is important to remember to comment out the normal umbilical vasoconstriction section of code.

Three models are included - foetal_taper2d, foetal_taper2a and foetal_taper2w and these must be changed in the main code depending on whether Dinnar's, Atabek's or Womersley's code are being used respectively.

As a final note, the functions used to calculate the modified Bessel functions of the first and second kind, for tapered arterial segments, require iteration until convergence. The number of iterations is set to be quite low and in most cases this is acceptable. On rare circumstances the model code causes an error and in these cases, it is necessary to increase the number of iterations, which unfortunately significnatly slows down the code run time. A diskette is included with the Matlab^{TM} m-files. These are for version 5.22, release II and requires the simulink, signal processing and optimisation toolboxes.